Antagonism of the Integrated Stress Response By Tick-Borne Encephalitis Virus

Thesis

Antagonism of the Integrated Stress Response by Tick-Borne Encephalitis Virus

Laís Nascimento Alves

A thesis submitted in fulfillment of the requirements of the Faculty of Life Sciences of the Open University for the degree of Doctor of Philosophy

&

International Centre for Genetic Engineering and Biotechnology (ICGEB)

Director of Studies: Alessandro Marcello, PhD

External Supervisor: Paolo Maiuri, PhD

Trieste, Italy

April 2022

ABSTRACT

Flaviviruses are a large family of viruses of increasing importance for human health. The host response to infection is critical to determine the outcome of the disease, particularly at early stages. In addition, they are known to rearrange the endoplasmic reticulum (ER) membrane to form characteristic replication vesicles. Membrane rearrangements and accumulation of viral proteins in the ER during replication lead to the activation of diverse cellular stress responses.

The integrated stress response (ISR) is a cellular program to restore homeostasis after exposure to different stresses, including viral infection. It can reversibly stall protein translation through phosphorylation of the translation initiation factor 2α (eIF2α). The direct effect is the formation of cytoplasmic structures called stress granules (SG), clusters of stalled mRNA, initiation factors, and RNA-binding proteins. SG have also been proposed to signal innate immune responses and are directly targeted by several viral proteins. The kinetic of the unfolded protein response (UPR) and ISR activation following Tick-Borne Encephalitis Virus (TBEV) infection have been described by our group (Carletti and Zakaria et al., 2019). Both occur early upon infection, before activation of interferon β (IFNβ) and interferon-stimulated genes (ISG). However, few SG are observed at late stages. Stimulation of infected cells with an activator of the UPR induces an earlier and stronger innate response and formation of SG.

Further, analysis of the kinases that induce eIF2α phosphorylation by the generation of knocked-down cells showed that late formation of the TBEV-induced functional SG is PERK independent but PKR dependent. These observations indicate that the UPR response *per se* cannot induce SG during TBEV infection. Interestingly, PKR activation is concomitant with IFNβ induction and requires unmasking and detection of viral RNA intermediates. Furthermore, it was also found that the NS4B and NS5 proteins of TBEV can inhibit PKR activation after Poly(I:C) transfection and thus prevent SG formation. Finally, cells deficient in SG formation showed a modest increase in viral replication and a lower level of IFNβ mRNA.

To conclude, I have defined the most relevant kinase involved in SG formation following TBEV infection and identified NS4B and NS5 as viral factors involved in the modulation of this pathway.

"*A te che sei il mio grande amore*
Ed il mio amore grande
A te che hai preso la mia vita
E ne hai fatto molto di più

A te che sei, semplicemente sei
Sostanza dei giorni miei
Sostanza dei sogni miei"

A te - Jovanotti

To my mom (*in memoriam*)

ACKNOWLEDGEMENTS

To my supervisor Dr. Alessandro Marcello, for accepting me to be part of his wonderful research team. It has been a rewarding experience learning about flaviviruses and molecular biology, and I feel truly grateful for the scientific opportunities and healthy environment Alessandro has offered throughout my doctoral studies. Thank you for always being sincere about my performance, challenging me to think more critically, and helping me complete my graduate program.

I am grateful to Dr. Paolo Maiuri, my second supervisor, for excellent ideas, critical analysis, brainstorming and interesting discussion sessions.

I am equally thankful to all the members of Molecular Virology Lab. Tea Carletti for training me in laboratory skills and for excellent support with experiments and life. To current and past colleagues from the lab - Erick Mora-Cárdenas, Chiara Aloise, Rafaela Milan Bonotto, Federica Dattola, Pamela Martinez, Chiara Kalebic, Emanuele Orsini, Denis Rajnovic, Monica Poggianella, Amedeo Bonetti - who have made my everyday research much more colorful and enjoyable.

I appreciate and am pretty thankful for the ICGEB units installed to support the fellows. Special thanks to Barbara Argenti, Tiziana Feriani, and Sandra Nigris for their excellent efforts in performing their tasks.

To my PhD defense examiners Dr. Nicolas Locker and Dr. Marco Baralle who have taken their time to read my thesis and offer insightful comments.

To Sally Flores, one of the most gifted individuals I have ever known. She has never failed to amaze me with her courage, patience and kindness. To Nema Dajic, thank you for the time spent together, the constant support and encouragement during this adventure. To all Fabio Severo crew: Nicola Papale, Elisabetta Sergi, Aline Viol, Luka Giga, Nancy Reis, Frederico Alabarse and Irina Guldt. To the gifts I received from the mountains: Aris, Michela and Tea. Thank you all for the memories we share!

To Rebeca Fuzinatto and Ivica Dimkic. Thank you for the delightful moments, the laughs, and the trips!

To my previous mentors Dr. Carlos Eduardo Bonacossa, Dr. Sotiris Missailidis, Dr. Claudia Lage and Dr. Marcia Arissawa, who nurtured scientific curiosity and passion in me, and paved the way for my higher education abroad. I am deeply thankful.

Most importantly, to my beloved family and friends, whom I have not physically seen since the beginning of my studies due to the SARS-CoV2 pandemic restrictions. They share my ups and downs regardless of our distance and continue to inspire me and believe in me. They have made everything possible. For that, I am forever grateful.

Last but not least, to my little niece who I haven't met yet but has already a home in my heart. Ana, nossa família me ensinou que trabalho duro e perseverança fazem alcançar conquistas honestas. Espero que quando você cresça seja tão orgulhosa o quanto eu sou da nossa história.

TABLE OF CONTENTS

LIST OF FIGURES

LIST OF TABLES

LIST OF ABBREVIATIONS AND ACRONYMS

DENV	Dengue virus
DNA	Deoxyribonucleic acid
eIF2α	Eukaryotic initiation factor 2α
E	Envelope protein
ER	Endoplasmic reticulum
HCV	Hepatitis C virus
IFNβ	Interferon β
ISG	Interferon-stimulated gene
ISR	Integrated stress response
NS	Non-structural protein
PAMP	Pathogen-associated molecular patterns
PERK	Protein kinase RNA-like ER kinase
PIC	Poly(I:C)
PKR	Protein kinase RNA-activated
PRR	Pattern recognition receptors
RIG-I	Retinoic acid-inducible gene I
RNA	Ribonucleic acid
RV	Replication vesicle
SG	Stress granule
TBEV	Tick-borne encephalitis virus
UPR	Unfolded protein response
WNV	West Nile virus
ZIKV	Zika virus

PART I

1. INTRODUCTION

1.1. Flaviviruses

The *Flaviviridae* family comprise enveloped, positive single-stranded RNA viruses that share similarities in morphology, genome organization and replication strategy. The genus called *Flavivirus*, within this family, consists in more than 70 viruses that can be transmitted to humans through arthropod vectors bite (Figure 1). It includes mosquito-borne viruses like Yellow Fever virus (YFV), Dengue virus (DENV), Japanese Encephalitis virus (JEV), West Nile virus (WNV) and Zika virus (ZIKV), and tick-borne viruses such as Langat virus (LGTV) and Tick-Borne Encephalitis virus (TBEV) (Dobler, 2010; Grabowski et al., 2016; K. L. Mansfield et al., 2009; Neyts et al., 1999).

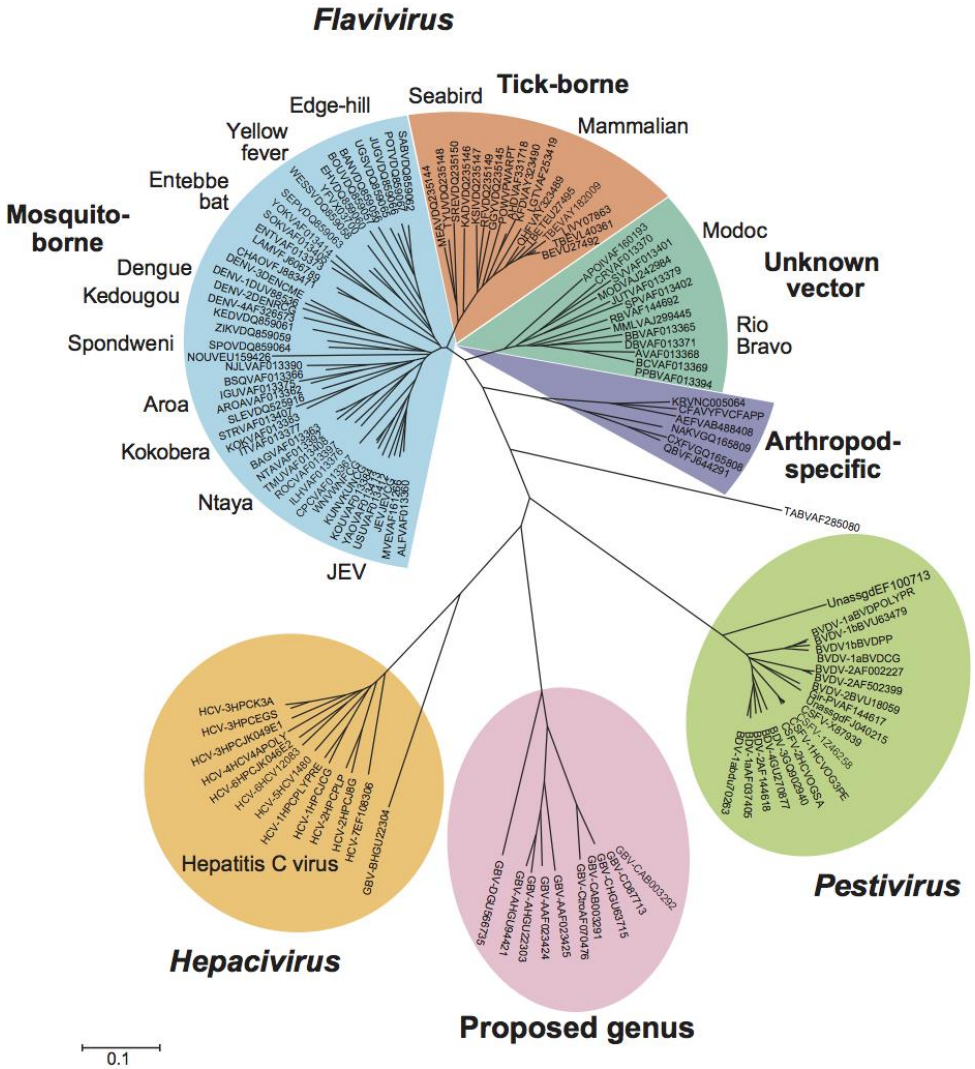

Figure 1. The *Flaviviridae* family. Phylogeny of the conserved sequences in the RNA-dependent RNA polymerase of classified members of the family *Flaviviridae* (ICTV, 2011).

Many factors such as urbanization, globalization and bird migration can lead to the spread of viruses to new geographic areas (J. S. Mackenzie et al., 2004). Many *Flaviviruses* can cause a variety of diseases in humans, including encephalitis and hemorrhagic fever (Gould & Solomon, 2008). For example, ZIKV infection of pregnant women has been reported to be associated with microcephaly in fetuses (Brady et al., 2019; Cugola et al., 2016).

1.1.1. Tick-Borne Encephalitis Virus

TBEV can cause the tick-borne encephalitis disease (TBE) and the number of cases is increasing over the years around Europe (ECDC, 2021). This is influenced by several socioeconomic, behavioral, and ecological factors (Donoso Mantke et al., 2008; Randolph, 2008). The risk of contracting TBEV increases with a lifestyle that involves recreational or occupational outdoor activities where ticks are abundant (Donoso Mantke et al., 2008; Randolph, 2008; Šumilo et al., 2008). As TBEV is mostly transmitted to humans via bites of TBEV infected ticks, yearly incidence of TBE is highly dependent on tick activity. In Europe, TBEV is transmitted to humans primarily by *Ixodes ricinus* tick species, particularly during the nymph and adult stage (Figure 2) (K. L. Mansfield et al., 2009). TBEV persistence in tick populations is highly dependent on co-feeding of larvae and nymphs on small rodents, where the virus can be passed between the ticks (Randolph et al., 1999). Humans are entirely accidental and dead-end hosts and do not contribute to TBEV persistence within the tick populations (Ličková et al., 2021) (Figure 2). In rare occasions, TBEV can also be transmitted via the ingestion of contaminated milk from an infected animal (Süss, 2011) (Figure 2).

TBE is typically a biphasic disease with a mild febrile illness during the first phase, and moderate to severe neurological manifestations during the second phase (Bogovic & Strle, 2015). Although TBEV primarily targets neurons in the central nervous system, other cell types can be infected (Gelpi et al., 2005, 2006). For example, cells residing in the skin have been shown to be susceptible to TBEV, potentially facilitating the spread of TBEV to peripheral tissues via the lymphatic system early after the tick bite (Labuda et al., 1996; Thangamani et al., 2017). As most patients experience only mild symptoms at the first stage, they typically do not seek medical care. It is believed that TBEV enters the central nervous system during this phase and many potential mechanisms of TBEV entry have been proposed, as reviewed by (Maximova & Pletnev, 2018).

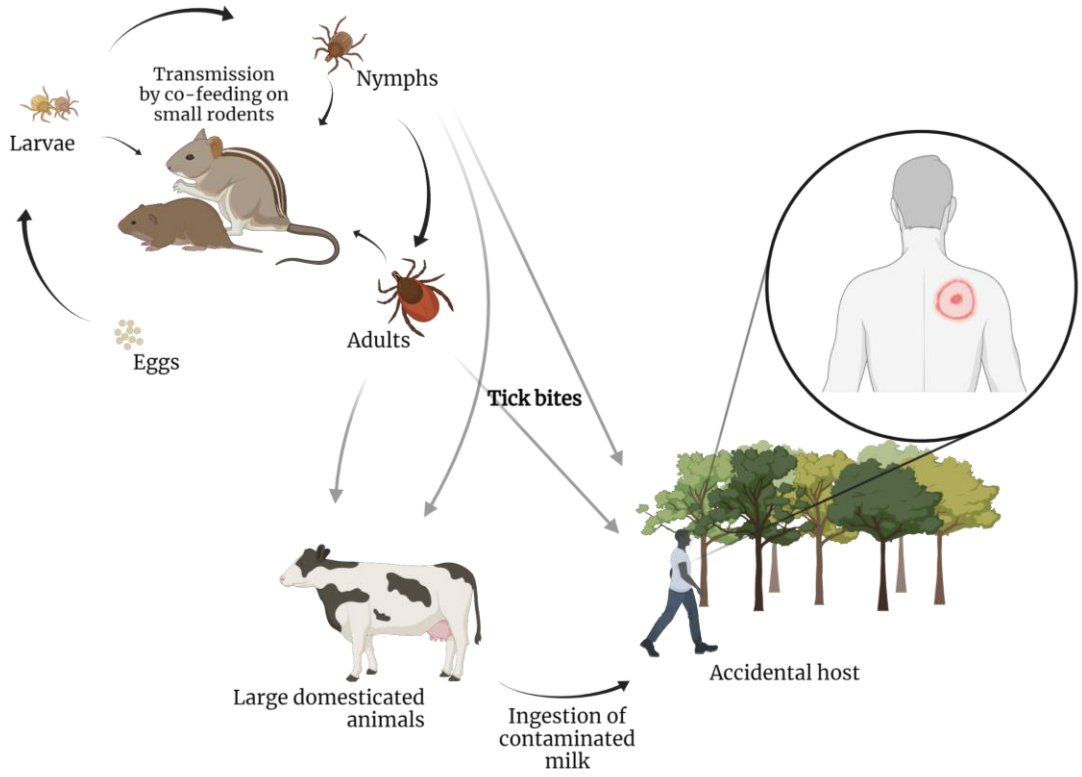

Figure 2. TBEV transmission cycle. The life cycle of ticks and the TBEV transmission routes within the tick population, animals, and humans. Created with BioRender.com

TBE is endemic in Europe and Asia and different virus strains are spread across the two continents. In Europe, the annual notification rate is around 0.7 cases per 100,000 people, with the highest incidence in Lithuania (around 25 cases per 100,000 population) followed by the Czech Republic (around 7 cases per 100,000 population) (ECDC, 2021). Five subtypes of TBEV are known: the European, the Siberian, the Far Eastern, the Baikalian and the Himalayan, that are classified based on the amino acid sequence of the envelope protein (Abdiyeva et al., 2020; Dai et al., 2018; Demina et al., 2010; Tkachev et al., 2017). The European TBEV subtype causes the disease with low mortality, and the most recent Europe-wide report estimated the case-fatality in TBE patients to be 0.7% (ECDC, 2021). In Italy, the incidence of TBE is confined to the North-Eastern (autonomous provinces of Trento and Bolzano, and the regions of Veneto, and Friuli-Venezia-Giulia (Rezza et al., 2015; Riccò et al., 2020).

The low incidence in Europe may be explained by the availability of a TBE vaccine (Heinz et al., 2013). The vaccine's efficiency is highlighted by a successful national immunization program in Austria, that was initiated in 1981 and reduced the incidence of TBE to around

one-fifth compared to pre-vaccination era (Heinz et al., 2007; Kunz, 2003). In Europe, there are two available TBE vaccines: FSME-Immun (Pfizer) based on the Neudörfl TBEV strain and Encepur (GSK) based on the K23 TBEV strain (Amicizia et al., 2013). These are formaldehyde inactivated whole-virus vaccines with alum adjuvant and comparable dosing and administration schedules. The conventional immunization schedule for TBE vaccination consists of a primary immunization with three doses within a one-year period, followed by booster doses every 3 to 5 years (Amicizia et al., 2013).

Unlike the yellow fever vaccine, which provides a lifelong immunity to the YFV (WHO, 2015), the TBE vaccine must be frequently readministered to maintain protection, although in some cases antibody persistence has been shown to last for up to 10 years after booster vaccination (Konior et al., 2017). Even though TBE vaccine is immunogenic in the majority of individuals and leads to seroconversion (Demicheli et al., 2009), vaccination breakthroughs have been reported, a phenomenon particularly common in older individuals (Andersson et al., 2010; Hansson et al., 2020; Lotrič-Furlan et al., 2017).

1.1.2. Flavivirus life cycle

1.1.2.1. Entry

Mature virions are small, with around 50 nm of diameter and their surface contains two proteins: E (envelope) and M (membrane). E glycoprotein is the main antigenic determinant and mediates binding of the virus to the host membrane receptor and fusion during virus entry (Billoir et al., 2000; Daep et al., 2014).

The entry of *Flavivirus* to cells occurs through receptor-mediated endocytosis (Lindenbach & Rice, 2003). Previous studies have reported that glycosaminoglycans serve as attachment factors for several *Flaviviruses* in different cell types (H.-L. Chen et al., 2010; Y. Chen et al., 1997; Germi et al., 2002; Kozlovskaya et al., 2010; E. Lee & Lobigs, 2008; Mandl et al., 2001). In the case TBEV, the heparan sulfate was reported to be the main receptor to mediate viral entry (Kroschewski et al., 2003). *Flaviviruses* enter host cells by clathrin-dependent endocytosis (Chu & Ng, 2004; Nawa et al., 2003; Ng & Lau, 1988; van der Schaar et al., 2008) in which clathrin coated pits on the plasma membrane invaginate to form clathrin-coated vesicles inside the cell. The clathrin coat dissociates, and the virus-containing vesicle is transported within the cytoplasm and fused with other vesicles to form an early endosome (Smit et al., 2011; van der Schaar et al., 2008). Viruses subsequently traffic to a pre-lysosomal endocytic compartment where low pH induces fusion between virus and host cell membranes to release the viral nucleocapsid (Smit et al., 2011).

1.1.2.2. Genome structure

Flavivirus genome consists of a single, positive-strand RNA of approximately 11 kb. Unlike cellular messenger RNA (mRNA), *Flavivirus* genomes lack the 3' polyadenylate tail (Wengler et al., 1978). The genome encodes a long open reading frame flanked by 5' noncoding region (NCR) or untranslated region (UTR) and a 3' NCR (or 3' UTR) (Markoff, 2003) (Figure 3). The 3' NCR is relatively longer than the 5' NCR and shows a significant heterogeneity in length and sequence even among closely related strains (Gritsun & Gould, 2006a, 2006b, 2007). Both the 5' and 3' NCR can be divided into a highly conserved core element (C5' and C3', respectively) and a variable part (V5'and V3', respectively) (Gritsun & Gould, 2006a, 2007; Wallner et al., 1995). Deletions on the C3' NCR were shown to produce attenuated TBEV mutants that cannot revert to wild-type sequence, whereas viruses with removed V3' NCR retain levels of infectivity compared to wild type viruses (Mandl et al., 1998).

Although there is a lack of sequence conservation at the 5' NCR, common secondary structures in the region called 5'-stem loop was been shown to be conserved among Flaviviruses (Brett D. Lindenbach Heinz-J & C. Rice, 2007). The 3' NCR is not polyadenylated however it forms a loop structure. This secondary structure induces the formation of a subgenomic flavivirus RNA (sfRNA) through degradation by the cellular 5′-3′ exoribonuclease XRN1. This process leads to cytosolic accumulation of 0.3 to 0.5 kb nuclease-resistant sfRNA that were reported to regulate multiple cellular pathways to facilitate Flaviviral pathogenicity in mosquito and mammalian cells (Eiermann et al., 2020; Manokaran et al., 2015; J. P. Mansfield et al., 1997; Pijlman et al., 2008).

The 5´ and 3´ NCR contain complementary sequences that help genomic cyclization through long distance base pairing to form a panhandle structure. The sequences and organization of flavivirus 5´- and 3´NCRs differ between the mosquito-borne, tick-borne, and no-known-vector viruses. However, several conserved regions, RNA secondary structures, and sequence repeats are common among flaviviruses, and the 5´- and 3´NCRs are important for replication, translation initiation, and packaging of the viral RNA (Chiu et al., 2005; Holden & Harris, 2004; Markoff, 2003).

1.1.2.3.Translation and polyprotein processing

The translation is performed by the host cell machinery and produces a single large polyprotein with approximately 3,400 amino acids. This precursor is a multi-transmembrane domain protein and it is located on the membrane of the endoplasmic reticulum (ER). The

polyprotein is co- and post-translationally cleaved by cellular and viral proteases into three structural proteins named capsid (C), envelope (E) and pre-membrane (prM), and seven non-structural proteins named non-structural protein 1 (NS1), NS2A, NS2B, NS3, NS4A, NS4B, NS5 that are involved in viral replication, virus assembly and immune response evasion (Kuno et al., 1998; Saiz et al., 2016) (Figure 3).

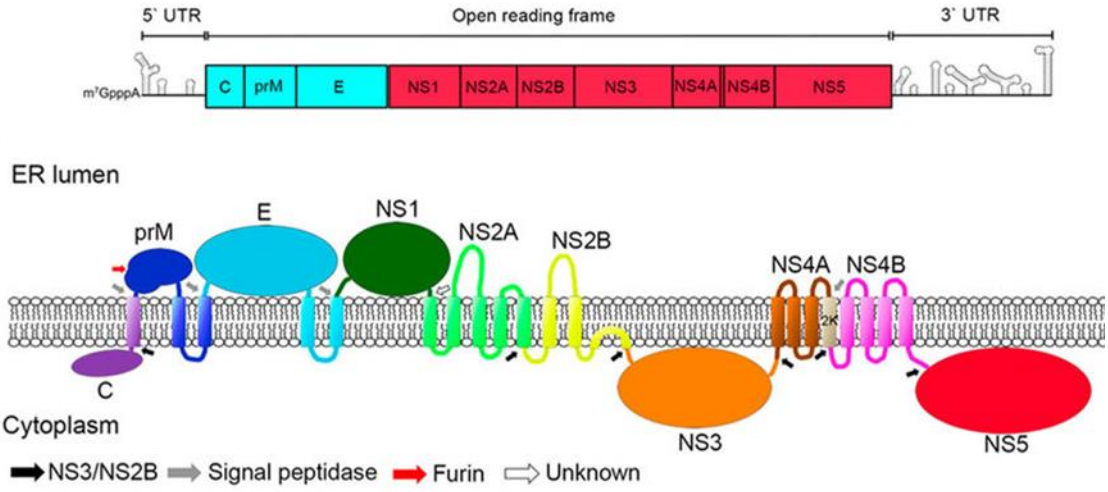

Figure 3. Schematic diagram of Flavivirus polyprotein organization and processing. Top panel: representation of the Flavivirus genome with approximately 11 kb. Simplified open reading frame showing RNA secondary and tertiary structures within the non-coding regions (NCR) is indicated. Bottom panel: schematic representation of the organization of structural and nonstructural proteins in the endoplasmic reticulum (ER) membrane predicted from biochemical and cellular analyses, which is then processed by cellular and viral proteases, indicated by arrows. Adapted from (Barrows et al., 2018).

1.1.2.3.1. Structural proteins

Capsid protein

Small (approximately 11 kDa) dimeric cytosolic Flaviviral protein that is translated at the N-terminus of the polyprotein. It has four structurally conserved α-helices and an internal hydrophobic domain that presumably interacts with viral membranes while the other side interacts with the viral RNA. Maturation to a soluble protein happens after cleavage from the prM signal sequence by the viral encoded NS3/2B protease (Murray et al., 2008).

prM glycoprotein

This is an approximately 26 kDa glycoprotein which is the precursor of the membrane (M) protein. It folds rapidly and acts as the chaperone of the Envelope by assisting in the proper folding and secretion of the E protein. The prM protein has been implicated, together with several host factors in the Flavivivirus life cycle, in virus entry, secretion and egress from the cell. The dissociation of its pr peptide by furin yields mature virions (Duan et al., 2008; Murray et al., 2008).

Envelope glycoprotein

The envelope (E) is a protein of approximately 53 kDa and the major surface glycoprotein in Flaviviruses. The E protein induces a protective immune response and the domain III of this protein is the target of neutralizing antibodies. Its major function in the flaviviral life cycle is mediating binding of the virus to the host receptors and the fusion of the virus onto the host cell membrane. The proper folding and secretion as well as its stability in low pH conditions depend on its co-expression with the prM protein (Bollati et al., 2010; Duan et al., 2008; Heinz et al., 1991).

1.1.2.3.2. Non-structural proteins

NS1 glycoprotein

The flavivirus NS1 is a highly conserved glycoprotein, approximately 46 to 55 kDa depending on its glycosylation status. It contains two or three N-linked glycosylation sites. It is localized in the ER lumen by a signal sequence located at the C-terminus of the E protein. NS1 is thought to be involved in the viral RNA replication process and the development of disease. NS1 is considered a major viral immunogen and found in the blood during early stages of infection as a viral marker of infection (Avirutnan et al., 2007; Murray et al., 2008). I was reported that NS1 of all DENV serotype can induce dysfunctions of the endothelial barrier, causing increased permeability and leading to vascular leak. It was also shown in the same work that this effect could be inhibited by treatment with anti-NS1 mouse serum or monoclonal antibody against NS1 (Beatty et al., 2015).

NS2A

This is an approximately 22 kDa, hydrophobic membrane non-structural protein that is a product of the processing of the NS2 portion of the flaviviral polyprotein. The actual function of NS2A is not entirely known but has been suggested to function as a scaffold protein that

organizes the replication complex (Barrows et al., 2018). It has been suggested that NS2A, alone or in complex with NS3, may be involved in genome transport (Apte-Sengupta et al., 2014). Moreover, the NS2A protein of DENV has been shown to assist on viral RNA encapsulation and virion formation (Muñoz-Jordán et al., 2003).

NS2B

A small membrane associated protein of approximately 14 kDa. Its main known function is to serve as a cofactor of the viral protease NS3 forming the NS3/2B complex. This interaction between the two proteins is essential for optimal protease activity during infection. The cofactor activity of NS2B is encoded in a conserved hydrophilic region of 40 residues flanked by hydrophobic regions that mediate membrane association, suggesting a possible role of the protein in modulation of membrane permeability during infection (Brett D. Lindenbach Heinz-J & C. Rice, 2007). NS2B of JEV and DENV have been shown to be associated with lipid rafts, a feature which makes them possess membrane-destabilizing properties (García Cordero et al., 2014; Gopala Reddy et al., 2018). NS2B of JEV has been shown to contribute to replication and virion assembly through interaction with NS2A, and its transmembrane domains playing a fundamental role in both (X.-D. Li et al., 2016).

NS3

This is a multifunctional, modular protein of approximately 70 kDa involved in processing of the polyprotein and in viral RNA replication. NS3 serves as the viral protease in the complex NS2B by processing the precursor polyprotein and therefore in the maturation of viral proteins. It harbors an NTPase-dependent RNA helicase activity in its C-terminus that may play a role in genome replication and vRNA synthesis (Barrows et al., 2018; K. Li et al., 2014). The C-terminal portion of NS3 shows significant homology with members of the DEAD box family of RNA helicases and its activity is believed to be involved in RNA synthesis by unraveling the secondary structures present at the 3‘UTR of the Flavivirus genomes, to facilitate polymerase processivity during elongation, or to separate double-stranded RNA (dsRNA) intermediates generated during viral (Brett D. Lindenbach Heinz-J & C. Rice, 2007; Warrener et al., 1993).

NS4A

It is a small (approximately 16 kDa), hydrophobic transmembrane protein and one of the products of the processing and cleavage of the NS4 portion of the polyprotein that yields NS4A and NS4B proteins. The two proteins are linked by a fragment of approximately 23

amino acids that form the 2K-linker peptide. NS4A has been suggested to be a major driver of ER rearrangements in DENV infection (Miller et al., 2007) where the replication factories are assembled, and has a role in replication (Lindenbach & Rice, 1999). NS4A may also help in the organization of luminal, transmembrane and cytoplasmic components of replication complexes (RC) (Barrows et al., 2018). It is believed that NS4A of WNV facilitates the formation of RC by recruiting both viral and host cell proteins to cholesterol-rich microdomains within the ER to ease RC biogenesis (Mikulasova et al., 2021).

NS4B

This is a transmembrane protein of approximately 27 kDa linked to NS4A by the 2K-linker peptide. The linker specifically leads NS4B into the ER membrane where it has been shown to localize at sites of replication as well as in the nucleus (Barrows et al., 2018). It has also been shown to interact with NS3 suggesting an interaction with the replication complexes, and probably has a role in replication. NS4B has also been implicated in ER rearrangements induced by WNV infection (Kaufusi et al., 2014). It was recently reported a pan-serotype DENV inhibitor that targets the NS4B-NS3 interaction. It was reported to be remarkably efficient and binds with great affinity to DENV NS4B with very low cytotoxicity and high barrier for viral resistance (Kaptein et al., 2021).

NS5

This is the largest (around 103 kDa), most conserved multifunctional protein that is indispensable in viral replication. It contains at its C-terminal the RNA dependent RNA polymerase and a methyltransferase at its N-terminus that catalyzes the methylation in the genome capping process (Bollati et al., 2010; Murray et al., 2008). These processes are suggested to be vital for viral genome replication in complex with NS3 (Barrows et al., 2018) as well as viral genome stability (Murray et al., 2008) and are therefore central to the regulation and coupling of RNA synthesis and virion morphogenesis. In addition, NS5 has been proposed as IFN antagonist. A study on DENV, TBEV and JEV demonstrated that NS5 antagonizes IFN signaling by hindering the Janus kinase (JAK)-signal transducer and activator of transcription (STAT) transduction pathway (Ashour et al., 2009; Best et al., 2005; R.-J. Lin et al., 2006).

1.1.2.4. RNA replication and membrane rearrangements

During replication of the genomic RNA, the viral RNA-dependent RNA polymerase (RdRP) NS5 synthesizes a negative-strand RNA, which serves as a template for the synthesis of

additional positive-strand RNA; this process is typically marked by the production and accumulation of dsRNA (Apte-Sengupta et al., 2014; Paul & Bartenschlager, 2015). The newly synthesized positive-strands can be subsequently used for several purposes: for further translation of viral proteins, for the synthesis of new negative-strand RNA, or to be incorporated into new viral particles.

Flavivirus replication occurs in close association with virus-induced vesicles that are membrane invaginations of the rough ER. The replication vesicles (RV) serve as physical support where the replication complexes are anchored for the coordinated accumulation of components required for efficient replication (Gopal et al., 2022; Miorin et al., 2012). Moreover, RV ensure minimal or no exposure of viral nucleic acids to the host immune system by shielding the viral genome from cellular pattern-recognition receptors and nucleases. The actual mechanism of membrane remodeling is still unknown (J. M. Mackenzie & Westaway, 2001; Miorin et al., 2012; Overby et al., 2010; Rajah et al., 2020). These invaginations of ER membranes retain an open connection to the surrounding cytoplasm via pores that are possibly required for importing host factors and nucleotides necessary for RNA replication and the export of new viral genomes (Miorin et al., 2013; Welsch et al., 2009).

Studies show strong involvement of viral proteins, such as NS4A and NS4B, in remodeling of membranes in DENV, WNV and ZIKV infections (Kaufusi et al., 2014; D. L. Lin et al., 2019; Miller et al., 2006). The oligomerization of NS4A and its interaction with NS4B may be the sustenance force to membrane rearrangements (Miller et al., 2006; Stern et al., 2013; Zou, Xie, et al., 2015). It has been suggested that DENV NS4B is N-glycosylated at residues 58 and 62 and can be found in glycosylated and unglycosylated forms during infection. Mutation on the glycosylation sites lead to instability of RV and lower viral replication (Gopal et al., 2022).

However, it has also been suggested that additional viral proteins may also play a role in the rearrangements that are induced in the morphogenesis of RV. One such protein may be NS1 that has been shown to dimerize and bind to and remodel membranes in vitro (Akey et al., 2014) and it likely interacts with the NS4A-NS4B complex (Lindenbach & Rice, 1999; Youn et al., 2012). In addition, there is a possibility that NS2A might also be involved in the induction of flavivirus replication organelles (Y. S. Chang et al., 1999; Kümmerer & Rice, 2002; Xie et al., 2015).

A recent publication demonstrated that a human cell line stably expressing the TBEV non-structural proteins (except for NS5) can trigger an ER dilation with the formation of peculiar invaginations resembling RV in size and shape. This indicates NSP alone can induce the morphological changes observed during infection without the presence of viral RNA replication (Yau et al., 2019).

1.1.2.5. Assembly and budding

The process of replication is closely related and somewhat intertwined with that of virus assembly both spatially and temporally. Additionally, it has been suggested that only actively replicated RNA gets packaged and this plays a role in the infectivity of the virus (Khromykh et al., 2001). The RNA genome is packaged by the Capsid protein in nucleocapsids on the cytoplasmic side of the ER membrane, a process coordinated with the viral envelope assembly that is acquired by budding of the nucleocapsid into the ER. Nucleocapsids are then transported into the lumen of the endoplasmic reticulum at the replication vesicle pore during formation of the prM-E lipid envelope (Roby et al., 2012).

1.1.2.6. Maturation and virion release

Assembled, immature virions are trafficked to the Trans-Golgi Network (TGN) where they undergo reversible conformational changes due to the low pH rendering them accessible to furin, a cellular protease abundant in the TGN and responsible for the proteolytic cleavage of the prM and the ultimate dissociation of its pr peptide. This event is the hallmark of virion maturation and marker for infection-competent virions. Mature virions finally bud out of the cell by exocytosis (I.-M. Yu et al., 2008). Only properly cleaved progeny virions, with a nucleocapsid containing a full genome copy can successfully infect other cells in proceeding rounds of infection (Barrows et al., 2018; Roby et al., 2012) (Figure 4).

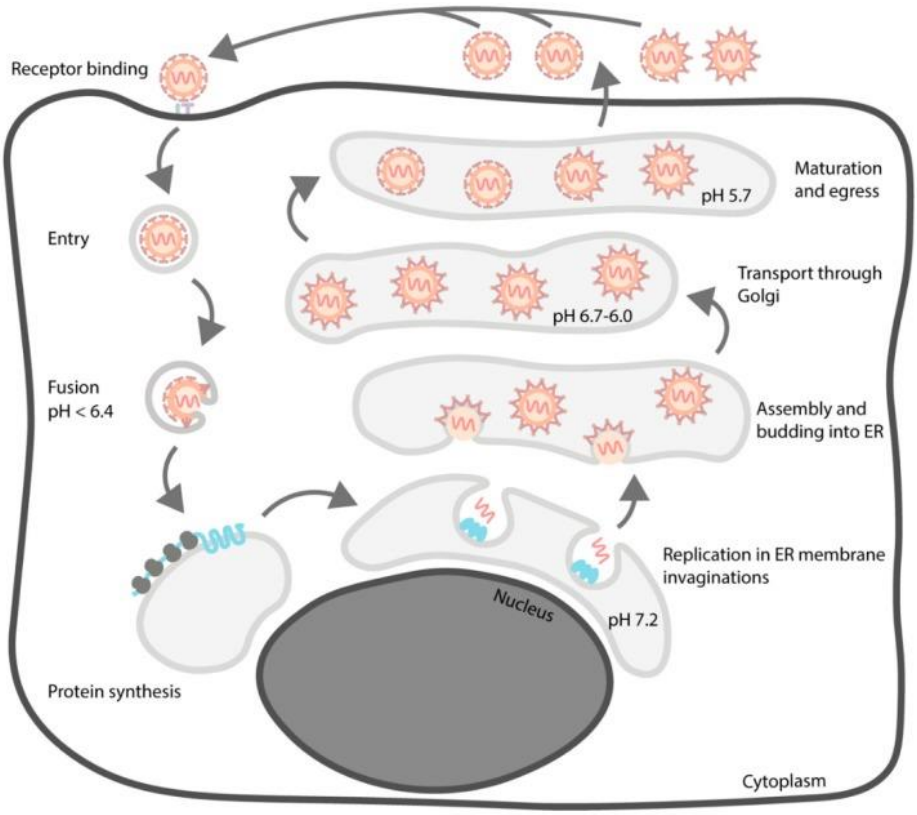

Figure 4. Flavivirus life cycle, an overview. The virus attaches to the host cell receptor and is internalized by receptor-mediated endocytosis and trafficked to early endosomes. Low pH in the endosome induces fusion between the virus and the host membrane resulting in genome release. Following, the viral RNA is translated into a single polyprotein that is cleaved by viral and host proteases before commencing the replication process. Packaging of newly synthesized RNA genomes occurs on the surface of the ER, and viral assembly initiates when the nucleocapsid buds into the ER. The immature virions further are transported to the trans-Golgi, where Furin-mediated cleavage of prM to M generates mature infectious particles that are released by exocytosis. Adapted from (Pulkkinen et al., 2018).

1.2. Interaction of Flavivirus with cellular antiviral systems

To control and defend against viruses, host cells are equipped with an elaborate network of antiviral pathways. Not surprisingly, flaviviruses have evolved ways to evade and modulate these cellular defenses.

1.2.1. The interferon response

The interferon (IFN) system consists of a family of autocrine and paracrine proteins that stimulate a network of signaling cascades that confer crucial protection for infected cells. Thus far, the immunological functions of IFNs are not only implicated in regulation of innate antiviral defenses, but also regulation of adaptive immunity as well as cancer progression (reviewed in (Borden et al., 2007)).

1.2.1.1. Types of interferon

Thus far, three types of IFNs have been identified: Type-I, -II, and -III (Figure 5). In humans, Type-I IFNs include IFN-α, -β, -ε, -κ, and –ω, which interact with IFN receptor 1 (IFNAR1) and IFNAR2; Type-II IFN only consists of IFN-γ, which binds to IFN-γ receptor 1 (I FNGR1) and IFNGR2; and Type III IFNs are the four isoforms of IFN-λ, whose cognate receptors are IFN-λ receptor 1 (IFNLR1) and interleukin 10 receptor 2 (IL10R2) (Borden et al., 2007) (Figure 5).

Despite sharing similar signaling molecules, different IFNs play distinctive roles in regulating resistance to infections. For instance, Type-I IFNs are produced by diverse cell types including immune cells, fibroblasts, endothelial cells and epithelial cells and they are thought to provide the first line of defense against a wide range of viral infections by activating the production of antiviral molecules (Borden et al., 2007). In contrast, Type-II IFNs are secreted from a subset of immune cells including T lymphocytes, macrophages and natural killer cells (Saha et al., 2010). Their main function is to activate and recruit leukocytes to sites of infection and promote clearance of intracellular pathogens such as viruses (Saha et al., 2010). The receptors for Type-III IFNs are largely confined to cells of the epithelial origin including respiratory, intestinal, and reproductive tract epithelial cells (Bayer et al., 2016; Sommereyns et al., 2008), suggesting that the Type-III IFN response is important for limiting viral infections in anatomical compartments lined with mucosal barriers.

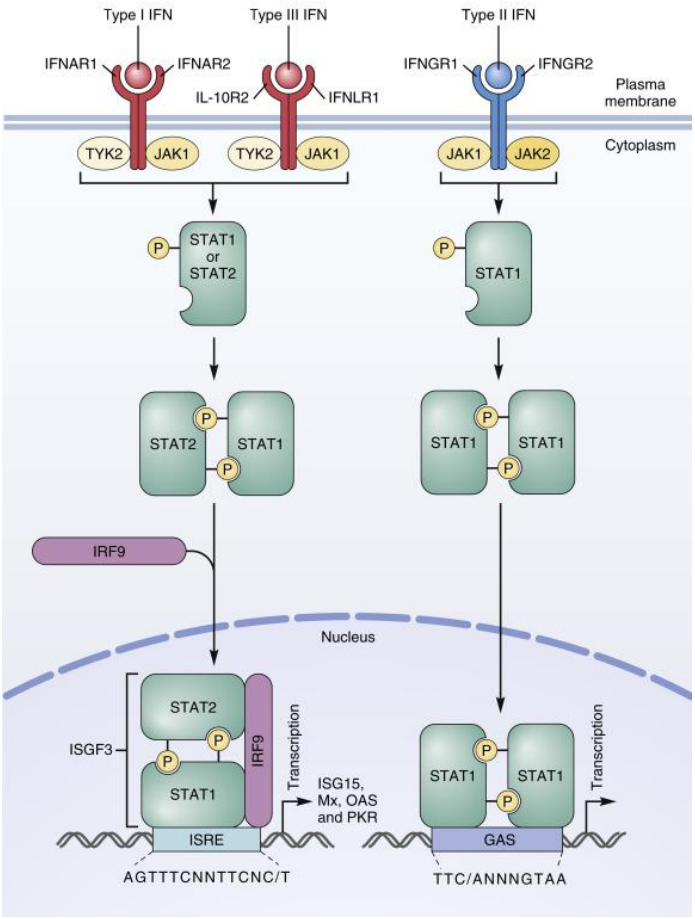

Figure 5. The Type I, II, and III interferon signaling pathways. The IFN system includes three types of IFN: Type-I (e.g., IFN-α and –β), Type-II (IFN-γ and –ω) and Type-III (IFN-λ1, 2, 3 and 4). IFN signaling is initiated upon binding of IFNs to their cognate receptors. Specifically, Type-I IFNs bind to IFN-α receptor 1 (IFNAR1) and IFNAR2; Type-II IFNs bind to IFN-γ receptor 1 (I FNGR1) and IFNGR2; and Type III IFNs bind to IFN-λ receptor 1 (IFNLR1) and interleukin 10 receptor 2 (IL10R2). This leads to activating phosphorylation of the JAK kinase family (JAK1 and TYK2), which phosphorylate the downstream transcription factors STAT1 (signal transducer and activator of transcription protein 1) and STAT2. During Type-I and –III IFN response, activated STAT1 and STAT2 dimerize and form a complex with the transcriptional activator IRF9 (IFN-regulatory factor 9), with which they stimulate the expression of IFN-stimulated genes (ISGs) through the ISRE (IFN-stimulated response element) promoter. During Type-II IFN response, phospho-STAT1 form a homodimer, which translocates into the nucleus to promote transcription of ISGs through the GAS (IFN-gamma-activated sequence) promoter. Production of diverse ISGs confers protection and resistance to viral infections through their specific functions in limiting viral entry, replication as well as spread. Adapted from (Sadler & Williams, 2008).

1.2.1.2. The IFN intrinsic response

The IFN response is composed of two phases: an initial induction stage where detection of pathogens activates the expression and release of IFNs (intrinsic response); and a downstream signaling stage where binding of IFNs to their cognate receptors triggers the production of a wide range of antiviral molecules. Consequently, through the release of IFNs, an infected cell can "signal" its neighbors to generate an effective antiviral state against a wide range of pathogens (Borden et al., 2007; A. J. Lee & Ashkar, 2018).

Several pathogen pattern recognition receptors (PRRs) have been identified in detecting flavivirus-specific pathogen-associated molecular patterns (PAMPs), although their effectiveness in inducing an antiviral response varies depending on the cell type and virus. Three types of RNA sensors recognize distinct non-self RNA structures of flaviviruses: the Toll-like receptor (TLR) family (TLR3 and TLR7), the retinoic acid inducible gene (RIG-I)-like receptor (RLR) family (RIG-I and melanoma differentiation-antigen 5 (MDA5)) and the dsRNA-activated protein kinase PKR (Diamond & Gale, 2012; Ye et al., 2013).

TLR3 and TLR7, which are present mainly in endosomes, dsRNA and single-stranded RNA (ssRNA) of viral origin, respectively (H. Kato et al., 2011). RIG-I and MDA5 are cytosolic RNA helicases (H. Kato et al., 2011). RIG-I recognizes structures within the 5′ triphosphate termini of dsRNA, as well as short dsRNA and uridine (U)- or adenosine (A)-rich viral RNA motifs (Anchisi et al., 2015; H. Kato et al., 2011; Schuberth-Wagner et al., 2015). Similarly, MDA5 binds long dsRNA and AU-rich viral RNAs (H. Kato et al., 2011; Runge et al., 2014). PKR is both a cytosolic PRR that detects viral dsRNA and an ISG capable of controlling viral replication by blocking translation of viral genome (Diamond & Gale, 2012). The PRR function of PKR is activated upon binding to viral dsRNA, which leads to its dimerization and subsequent autophosphorylation. Precisely how PKR mediates IFN induction is unclear, but it has been proposed to facilitate activation of IRF3 by interacting and possibly facilitating RLR-signaling (Pham et al., 2016). However, the role of PKR in IFN induction during flavivirus infection remains controversial. While activation of this kinase induces production of IFNs against WNV infection (Diamond & Gale, 2012), studies of DENV suggest that it is dispensable for IFN-mediated inhibition of viral replication (Diamond & Harris, 2001).

1.2.1.3. Antagonism of the IFN signaling by Flavivirus

To ensure productive infections, flaviviruses have evolved strategies to evade the host cell immunity. They can, for example, evade or delay detection by PRRs. For instance, as

mentioned before, flavivirus replication takes place within an almost completely closed ER membrane invaginations (Miorin et al., 2012; Overby et al., 2010; Welsch et al., 2009). This membrane rearrangement is thought to provide a factory for genome replication and virion assembly (Welsch et al., 2009), but it may also protect the replication intermediates from detection by the cellular RNA sensors RLRs and PKR, thereby delaying activation of the antiviral response (den Boon & Ahlquist, 2010; Miorin et al., 2012; Overby et al., 2010). In addition, as demonstrated by WNV, flavivirus NS5 methylates the viral genome 5′-cap. This avoids recognition by MDA5 and therefore prevents the induction of MDA5-mediated antiviral signaling (Szretter et al., 2012; Züst et al., 2011).

Flaviviruses can also directly interfere with signal transduction initiated from PRRs to suppress transcription of IFNs. For example, WNV NS1 blocks TLR3-induced transcription of IFN-β and IL-6 (Wilson et al., 2008) while expression of the viral protein NS2A attenuates production of IFN-α/β through a yet unknown mechanism (W. J. Liu et al., 2004). NS4B of both DENV and WNV inhibits activation of IRF3 and thereby reduces the expression of IFN-β (Dalrymple et al., 2015). In human cells, the PRR-signaling adaptor molecule STING is cleaved by DENV protease NS3/2B, thus disrupting IFN production (Aguirre et al., 2012; Rodriguez-Madoz et al., 2010; C.-Y. Yu et al., 2012). In addition, DENV NS4A interacts with the RLR-signaling adaptor protein MAVS and prevents it from interacting with RIG-I (He et al., 2016). Viral RNA can also antagonize IFN responses as well. The sfRNA of DENV was shown to blunt RIG-I-mediated IFN induction by binding to and destabilizing Tripartite motif-containing protein 25 (TRIM25), a positive regulator of RIG-I (Manokaran et al., 2015).

Apart from blocking the expression of IFNs, flaviviruses can also hinder the IFNR-initiated signaling pathways. For example, WNV infection results in depletion of IFNAR1 through a non-canonical protein degradation pathway that may be mediated by viral non-structural proteins (Evans et al., 2011). Since STAT1 and STAT2 are essential to produce ISGs, a common scheme employed by flaviviruses is to interfere with their activation. For example, the non-structural proteins have been shown to prevent phosphorylation of STAT1 and/or STAT2 during infection of WNV (Guo et al., 2005; W. J. Liu et al., 2004; Muñoz-Jordán et al., 2005), DENV (Munoz-Jordan et al., 2003), JEV (Lin et al., 2006), YFV (Muñoz-Jordán et al., 2005) and TBEV (Best et al., 2005; Werme et al., 2008). In addition, DENV NS5 targets STAT2 for proteasomal degradation(Ashour et al., 2009; Morrison et al., 2013). Although many of these findings require further validation in more physiologically relevant

systems (such as in primary cells), they have revealed several attractive candidates for novel antiviral therapeutics.

1.2.2. Stress responses

1.2.2.1. Unfolded protein response

The ER quality control system ensures that only correctly folded proteins leave the ER via the secretory pathway, with ER resident chaperones aiding and monitoring nascent protein maturation (Braakman & Bulleid, 2011; Ellgaard & Helenius, 2003). There are two main chaperone families responsible for protein folding in the ER: the lectin chaperones, which interact with unfolded glycoproteins, and the binding immunoglobulin protein (BiP, also known as GRP78 or HSPA5) that belongs to the heat shock protein (HSP) 70 family and recognizes both, non-glycosylated and glycosylated proteins (Braakman & Bulleid, 2011; Zhu & Lee, 2015).

Several intrinsic (such as a mutations control) and extrinsic (such as viral infection) events can disrupt the ER protein-folding environment. An imbalanced load of proteins folding in the ER and exceeding its capacity is referred to as ER stress, which results in the accumulation of unfolded and misfolded proteins in the ER lumen (Rao & Bredesen, 2004). To prevent undergoing apoptotic cell death and to overcome the ER stress condition, cells trigger an adaptive response that has evolved to respond to accumulated misfolded proteins in the ER called unfolded protein response (UPR). The UPR reorganizes a cell's transcriptional and translational program, aiming to resolve protein-folding stress and to restore cellular homeostasis (Hetz et al., 2020). First, mRNA translation is transiently attenuated to prevent the accumulation of more unfolded proteins. Second, the translation of new proteins is decreased by degradation of ER membrane-associated mRNAs. Third, the protein folding capacity as well as ER-associated degradation (ERAD) capacity are increased by transcriptional upregulation of ER chaperones and ERAD components. Fourth, if homeostasis cannot be restored, the terminal UPR is induced, resulting in apoptosis to remove damaged cells and protect the organism (Hetz, 2012; Hetz et al., 2020) (Figure 6).

The three main UPR signaling pathways are initiated by three ER transmembrane stress sensors: inositol-requiring enzyme 1 (IRE1), protein kinase R-like ER kinase (PERK) and activating transcription factor 6 (ATF6). The ER stress sensors consist of a luminal domain that senses misfolded proteins, a transmembrane domain that anchors the sensors in the membrane and a cytosolic domain that transmits signals to the nucleus (Johnston & McCormick, 2019) (Figure 6). Normally, BiP is bound to the transmembrane ER stress

transducers blocking their activation (Hetz et al., 2020). Moreover, the UPR can be chemically activated by several compounds, such as tunicamycin (TM) that disrupts protein maturation by blocking N-linked glycosylation (Azim & Surani, 1979; Hakulinen et al., 2017; Yoo et al., 2018).

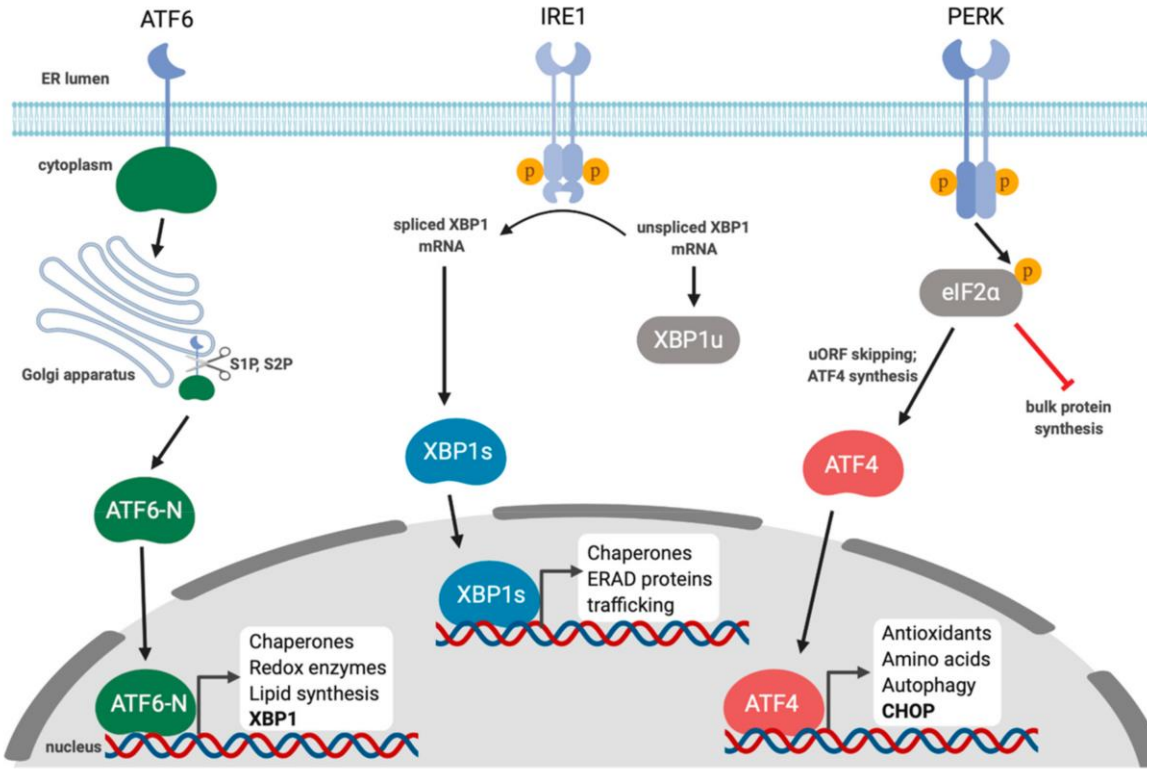

Figure 6. The unfolded protein response in a nutshell. Following BiP dissociation, ATF6 is transported to the Golgi where the proteases S1P and S2P remove the luminal and the transmembrane domain, respectively. The resulting N-terminal fragment is a DNA-binding protein that translocates to the nucleus where it activates the transcription of UPR target genes. IRE1, on the other hand, oligomerize after BiP dissociation and transphosphorylate other IRE1 molecules in the complex. Activated IRE1 performs a non-conventional cytoplasmic splicing, excising a 26-nucleotide sequence from the X-box-binding protein 1(XBP1) mRNA. This splicing event causes a shift in the reading frame of XBP1 mRNA generating a new longer protein called XBP1 spliced form (XBP1s). Once translated, XBP1s translocates to the nucleus where it binds to UPR elements (UPRE) on the promoter of several UPR target genes. Dissociation of BiP from PERK initiates its transphosphorylation, promoting PERK oligomerization. The kinase domain of PERK phosphorylates the α subunit of the eukaryotic translation initiation factor-2 (eIF2α) at Ser51, causing a global inhibition of translation, thus reducing also the amount of newly synthesized proteins. Some mRNAs that contain an internal ribosome entry site

(IRES) sequence in the 5' untraslated regions bypass the P-eIF2α translational block. The most common is the transcription factor ATF4 which activates the transcription of pro-survival genes as well as pro-apoptotic genes such as CHOP. Additionally, ATF4 is a co-factor to GADD34, whose role is to dephosphorylate eIF2α reversing protein synthesis attenuation with a negative feedback mechanism. Adapted from (Johnston & McCormick, 2019).

1.2.1.1.1. UPR activation during Flavivirus infection

Viruses have evolved multiple mechanisms to manipulate the UPR, either to favor their replication or to avoid detrimental effects by certain UPR pathways.

For example, DENV infections showed a time-dependent activation of all three UPR pathways. During early time points PERK activation led to eIF2α phosphorylation which was rapidly reversed. Phosphorylation of eIF2α was reversed upon DENV infection even in the presence of the potent ER stress inducer thapsigargin. At mid and late stage in the replication cycle, the IRE1 and ATF6 pathways were activated, respectively. Additionally, PERK-/- knockout MEFs showed higher DENV titers, illustrating the antiviral role of PERK. DENV infection of IRE1-/- knockout MEFs yielded significantly lower infectious viral titers, implying a pro-viral role of the IRE1 pathway for DENV replication (Peña & Harris, 2011). Although ATF6 was activated and translocated to the nucleus upon DENV infection, an ATF6-/- knockout did not affect viral titers (Peña & Harris, 2011; Umareddy et al., 2007). A comparison of DENV-1 and DENV-2 revealed a serotype-specific activation of UPR pathways with different intensities. DENV-1 induced GADD34 more strongly than DENV2, whereas DENV-2 led to a slightly higher phosphorylation of eIF2α and to higher expression levels of XBP1s than DENV-1 (Umareddy et al., 2007).

In the case of WNV, activation of IRE1 was demonstrated by XBP1 mRNA splicing (Ambrose & Mackenzie, 2011). Moreover, the small hydrophobic proteins NS4A and NS4B enhance XBP1 splicing with undetectable unspliced XBP1 in transfected cells (Ambrose & Mackenzie, 2011). WNV infection of XBP1-/- MEFs showed no difference in viral RNA, protein or infectious virus compared to WT cells, suggesting that IRE1 signaling is dispensable for WNV replication (Ambrose & Mackenzie, 2013). Furthermore, WNV infection of ATF6-/- knockout MEFs resulted in reduced secretion of virions, implying a pro-viral role for WNV replication (Ambrose & Mackenzie, 2013). Infected ATF6-/- cells showed an increase in PERK-related factors with higher phosphorylation of eIF2α and

upregulated CHOP activity, suggesting that ATF6 may dampen PERK signaling (Ambrose & Mackenzie, 2013).

Our laboratory has extensively studied the UPR and its interplay with innate immunity to TBEV infection. After identifying that the IFN response is delayed during TBEV infection (Miorin et al., 2012), we showed with a transcriptome analysis that UPR is among the earlier responses activated during TBEV infection, before the IFN response. ATF6 and PERK and IRE1 are all active at early time points, but cells with IRE1 silenced produce higher titers of TBEV. Moreover, pre-activation of UPR with tunicamycin or thapsigargin leads to increased antiviral state in TBEV-infected cells. Therefore, UPR is believed to destabilize the viral replication vesicles in the ER membrane and expose dsRNA which, coupled with PRR-mediated intrinsic innate immunity, lead to IFNβ response (Carletti et al., 2019).

1.2.2.2. Integrated stress response

The integrated stress response (ISR) is a cellular program that can be activated to restore homeostasis after cellular exposure to different types of stress, such as viral infection. It can reversibly stall protein translation through phosphorylation of the α unit of the translation initiation factor eIF2 (eIF2α) at serine 51. The direct effect of eIF2α phosphorylation is the formation of membraneless structures called stress granules (SG), which are clusters of stalled mRNA, translation initiation factors and RNA binding proteins (Costa-Mattioli & Walter, 2020). eIF2α phosphorylation can be performed by four different kinases that are activated by various sources of stress: PERK, a transmembrane protein that is activated by ER stress; general control non-derepressible 2 (GCN2), senses low amino acids levels by binding to uncharged tRNAs; heme-regulated inhibitor (HRI), is mainly expressed in erythrocytes and is activated by heme deficiency; and PKR which is ubiquitously expressed and activated by sensing dsRNA. Upon activation, all four kinases phosphorylate eIF2α leading to inhibition of mRNA translation and stress granules formation (Figure 7) (Harding et al., 2003; Ron, 2002). A common characteristic among the ISR members is that they are activated by stress-induced dimerization and autophosphorylation (Donnelly et al., 2013).

Upon ISR activation and formation of SGs, the translation of most cellular mRNAs is inhibited; nevertheless, selective translation of transcripts such as the ones for ATF4, pro-apoptotic C/EBP homologous protein (CHOP) and DNA damage inducible 34 (GADD34) is promoted (Pakos-Zebrucka et al., 2016). ATF4 is the main effector of the ISR and its translation is regulated by two upstream open reading frames (uORF) (Costa-Mattioli & Walter, 2020). uORF1 is the favorable element that induces ribosome scanning and initiation

of translation at next coding regions, whereas uORF2 is an inhibitory element that negatively regulates ATF4 expression. In non-stressed cells, ribosome scanning starts preferentially downstream of uORF1 and initiates translation at uORF2, inducing ribosome dissociation from ATF4 mRNA and thus preventing ATF4 translation. In ER stress conditions, protein synthesis is attenuated increasing the availability of ribosomes. This allows the translation of ATF4 mRNA at the alternative downstream coding region leading to increased ATF4 protein synthesis. ATF4 then induces expression of proteins like CHOP and ATF3 (Harding et al., 2003; Pakos-Zebrucka et al., 2016; Wek et al., 2006).

GADD34 mediates the dephosphorylation of eIF2α through protein phosphatase 1 (PP1), whose catalytic subunit is recruited to eIF2α. In non-stressed cells, the constitutive repressor of eIF2α phosphorylation (CReP), a regulatory subunit of PP1, maintains low levels of eIF2α phosphorylation (Jousse et al., 2003), especially at the ER (Kastan et al., 2020). Under stress conditions, GADD34 is both transcriptionally and translationally upregulated to antagonize eIF2α phosphorylation and translational arrest initiated by the ISR (Connor et al., 2001; Kojima et al., 2003; Novoa et al., 2001). Furthermore, viruses such as ZIKV (Amorim et al., 2017) and infectious bronchitis virus (IBV) (Wang et al., 2009) have been reported to modulate this negative feedback loop to escape the host antiviral response.

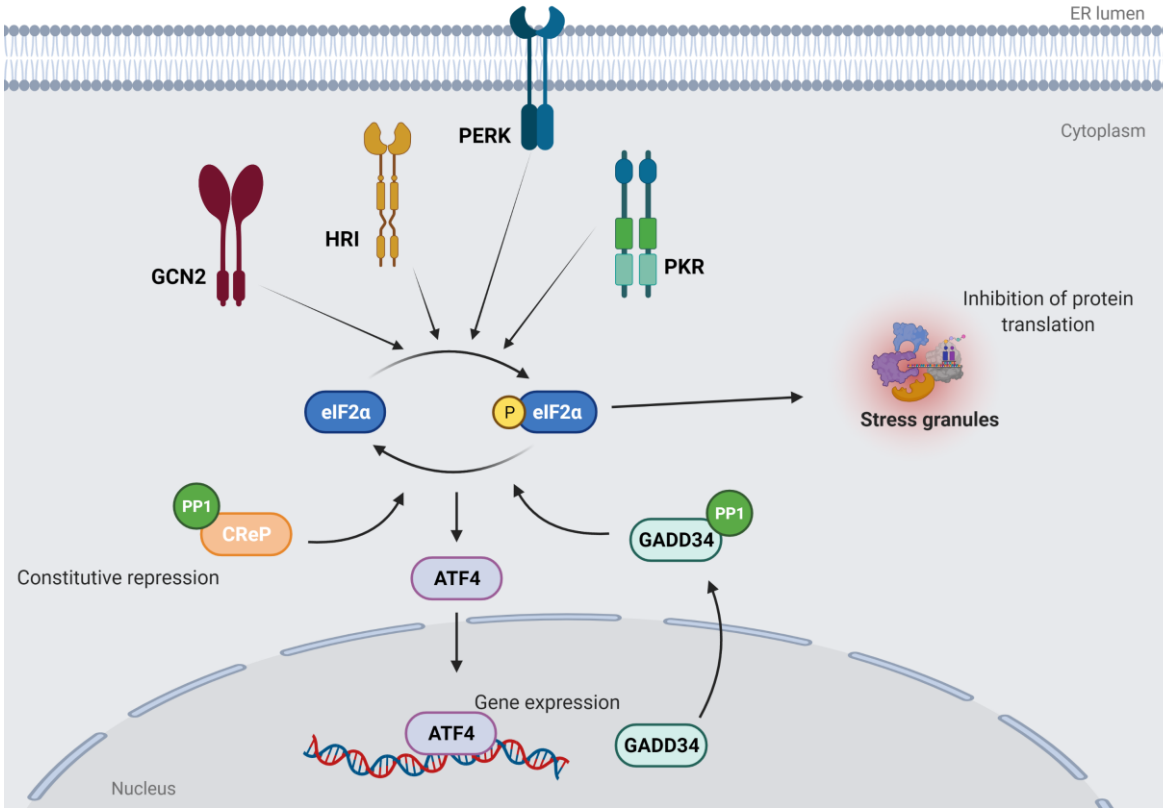

Figure 7. The integrated stress response. eIF2α phosphorylation occurs via 4 kinases: Protein kinase RNA-activated (PKR), in response to foreign dsRNA, Protein kinase RNA-

like endoplasmic reticulum kinase (PERK), in response to ER stress, general control non-derepressible 2 (GCN2), in response to nutrient deprivation, and heme-regulated inhibitor (HRI) in response to heme deficiency in erythroid cells. Constitutive repressor of eIF2α phosphorylation (CreP) is expressed and maintains low levels of phosphorylated eIF2α. Under stress conditions the phosphorylation of eIF2α leads to an inhibition of the vast majority of translation with the exception of a subset of gene necessary for cell survival and response to stress, such as the ATF4 gene. Phosphorylation of eIF2α results in protein translation inhibition, ultimately leading to SG formation. Created with BioRender.com

1.2.2.2.1. GCN2

GCN2 responds to nutritional deprivation and is the only eIF2α kinase conserved among virtually all eukaryotes. The mechanism of activation during amino acid depletion involves the binding of accumulating uncharged tRNAs in the cytoplasm to a region of GCN2. GCN2 binding to uncharged tRNA ultimately triggers a conformational change that relieves inhibitory interactions within the protein kinase domain, resulting in autophosphorylation in the activation loop of the enzyme. GCN2 can also be activated by glucose deprivation and exposure to high salt, and stresses not directly related to nutrients, such as UV irradiation and anti-cancer drugs (P. Zhang et al., 2002).

1.2.2.2.2. HRI

HRI is mainly expressed in erythroid cells, red blood cell precursors, and is activated by heme deficiency, protecting cells from toxic globin aggregates (A. P. Han et al., 2001). It transitions between an inactive, heme-bound, dimeric form stabilized by disulfide bonds, and an active dimer stabilized by non-covalent interaction, promoting autophosphorylation and kinase activity in the absence of heme (Chefalo et al., 1998; Rafie-Kolpin et al., 2000).

1.2.2.2.3. PERK

As discussed before, PERK is an ER transmembrane protein that contains a regulatory region that resides in the lumen of the ER and a cytosolic eIF2α kinase domain. PERK is a member of the ISR for being a eIF2α kinase, and at the same time is also a member of UPR for being the ER resident that reduces the influx of nascent proteins into the ER. Activation of PERK during ER stress is believed to occur in along with the other UPR sensors, but the timing or duration of each may be different. Misfolded proteins that accumulate in the ER lumen compete with PERK for BiP binding, which triggers the release of the ER chaperone, thus leading to PERK oligomerization which facilitates PERK autophosphorylation and enhanced phosphorylated eIF2α (Z.-W. Liu et al., 2013; Rozpedek et al., 2015).

1.2.2.2.4. PKR

PKR is a component of the antiviral pathway and is activated by binding of dsRNA to its N-terminal moiety and is important for limiting viral replication during infection. Its kinase activity is also dependent on dimerization and autophosphorylation of its C-terminal kinase domain (Kaufman, 1999). A minimal dsRNA length of 30 bp is required for PKR activation, however short stem loop RNAs containing flanking single stranded tails are capable of activating PKR. As mentioned before, dsRNA is produced as an intermediate of viral replication and recognized as non-self molecule by the host cell through sensors like PKR (Kaufman, 1999; Williams, 1999).

As illustrated in Figure 8, the PKR protein has a closed conformation when inactive, and its activation happens in several steps. Initially, dsRNA binds to one of the two double-stranded RNA binding motifs (DRBM), which leads to the first conformational change. The second step is dimerization, and the third, phosphorylation due to the proximity of the kinase domains (Cesaro et al., 2021; Mayo et al., 2019).

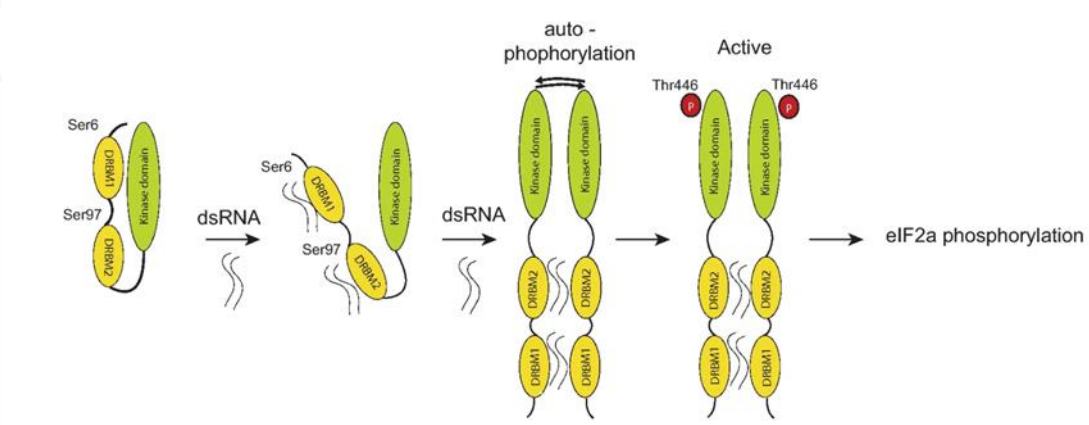

Figure 8. PKR activation. Adapted from Cesaro et al., 2021

1.2.2.2.4.1. Viral evasion from PKR signaling

Viruses whose propagation is inhibited by PKR often develop methods to inhibit activation of this kinase. Many strategies exploited by viruses have been reported: dsRNA sequestration, masking, or degradation, PKR degradation, inhibition of PKR dimerization and phosphorylation, and PKR direct inhibition by interaction of viral RNA or proteins (Cesaro & Michiels, 2021).

For example, the Middle East respiratory coronavirus 4a protein was reported to sequester dsRNA to inhibit formation of PKR-dependent SG. Mutation on the dsRNA binding motif of 4a protein was sufficient to neutralize its antagonistic function (Rabouw et al., 2016). Similarly, the NS1 protein of Influenza B virus was also shown to compete with PKR for dsRNA binding via its N-terminal domain, while its C-terminal domain could silence IFN response (Dauber et al., 2006). Interestingly, it was demonstrated recently that the endonuclease activity of the nsp15 protein of Infectious Bronchitis Virus and of avian coronavirus can degrade dsRNA and prevent PKR activation (B. Gao et al., 2021; Zhao et al., 2021).

Some viral proteins were shown to directly bind PKR through and block its dimerization or autophosphorylation, such as the nucleoprotein (N) of Respiratory syncytial virus (Groskreutz et al., 2010) and the ORF57 from Kaposi's sarcoma-associated herpes virus (Sharma et al., 2017). Moreover, although the NS5A of hepatitis C can bind the dimerization domain of PKR (Gale et al., 1997, 1998), no evidence was provided if PKR activity is inhibited by NS5A during HCV infection (Dabo & Meurs, 2012). Recently it was described that the newly emerged SARS-CoV-2, the pandemic pathogen responsible for the current state of a global health emergency, can also interfere with the PKR response to promote replication. Zheng and colleagues discovered that the nucleocapsid (N) protein block PKR phosphorylation during SARS-CoV-2 infection (Zheng et al., 2021).

1.2.2.2.5. Stress granules

SG are cytoplasmic membraneless granules formed in response to multiple types of stress. The most fully characterized pathway for stress granule formation involves phosphorylation of eIF2α, leading to accumulation of stalled translation pre-initiation complexes.

For protein synthesis in normal conditions the so-called ternary complex (eIF2/GTP/ $tRNA_i^{Met}$) delivers initiator $tRNA_i^{Met}$ to the 40S ribosomal subunit, forming a 43S pre-initiation complex (preIC). The eIF4F complex (eIF4E, eIF4A, and eIF4G) binds together with eIF4B to the 5′ cap of the mRNA. The eIF4F-bound mRNA associates with the 43S preIC, and then scans to the AUG start codon, where 48S PIC formation occurs (Figure 9) (Panas et al., 2016). This process depends on the exchange of GDP to GTP mediated by eIF2 mediated by eIF2B. Upon ISR activation, ternary complex depletion occurs by mechanistic impairment of interaction between the α subunit of eIF2 and eIF2B, promoting assembly of a noncanonical preIC unable to deliver of initiator $tRNA_i^{Met}$, which results in a reduction of protein synthesis in stressed cells (Panas et al., 2016; Potter & Parker, 2016).

SG are composed of stable protein cores that contain a large set of RNA-binding proteins, poly-adenylated mRNA, stalled translation initiation factors, heat shock proteins, DEAD-box proteins, RNA helicases, and many other proteins, some of which remain to be verified (Jain et al., 2016). Ras-GTPase activating binding protein 1 (G3BP1) and its isoform G3BP2, Caprin1, T-cell internal antigen 1 (TIA-1), and TIA-1-related protein (TIA/R) are believed to be key nucleators of SG assembly (Gilks et al., 2004; Kedersha et al., 2016; Tourrière et al., 2003; Tsai et al., 2016). Furthermore, SG cores has a dynamic shell with weak interactions between proteins and RNA (Han et al., 2012; Kato et al., 2012; Weber & Brangwynne, 2012).

SG formation can also occur via eIF2α-independent pathways such as cleavage the of eIF4G or inhibition of eIF4E proteins. Upon stress resolution and reinitiation of translation SG disassemble (Aulas et al., 2017).

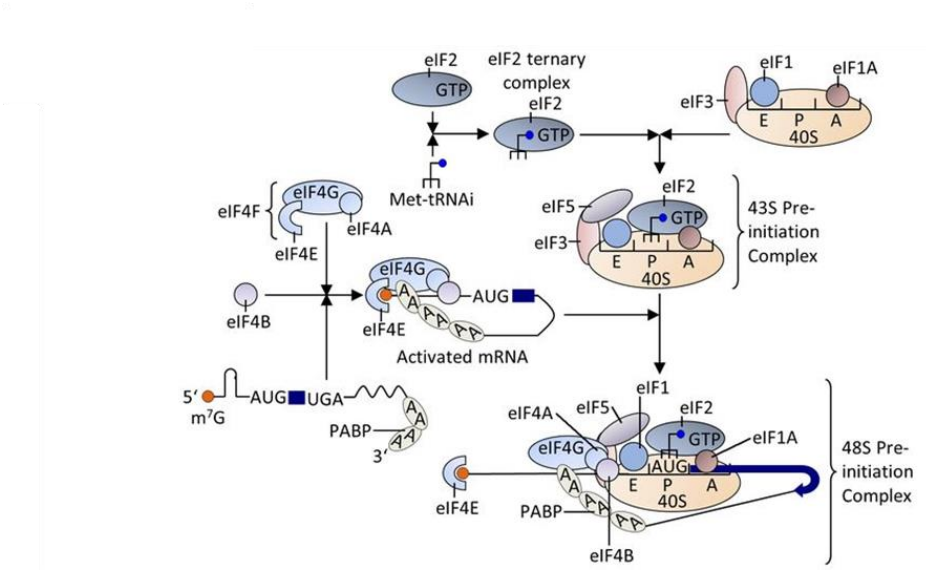

Figure 9. Conventional translation initiation in eukaryotes. Simplified cartoon of cap-dependent translation initiation. Outlined are the steps of preinitiation complex (preIC) assembly, mRNA scanning, AUG codon recognition and 60S ribosomal subunit joining. The main participants of the translation initiation are indicated. Adapted from (Panas et al., 2016)

1.2.2.2.5.1. Stress granules assembly

SG are formed by liquid-liquid phase separation (LLPS), in which dispersed proteins and protein-bound RNA condensate in droplet-like structures in the cytoplasm (Brangwynne et al., 2009). After detection of stress and initial stimulus, there is the release of mRNA from polysomes and a subsequent increase on the amount of free mRNA in the cytoplasm. The

increase in mRNA concentration is detected by G3BP1, which activates SG assembly by LLPS (Guillén-Boixet et al., 2020; P. Yang et al., 2020).

G3BP1 is the central hub for the SG network. It contains an internal RNA recognition motif (RRM) domain for protein-RNA interaction, as well as a nuclear transport factor 2 (NTF2)-like domain for protein-protein interaction (Guillén-Boixet et al., 2020; Tourrière et al., 2003). G3BP1 mutants lacking the NTF2-like domain fail to form SG, suggesting that the role of the NTF2-like domain in undergoing intra- and inter-molecular interactions is critical to SG formation. In addition, diffuse cytoplasmic G3BP1 contains a constitutively phosphorylated serine residue at position 149 at resting states (Tourrière et al., 2003). During cellular stress, S149 is dephosphorylated, inducing a conformational change that permits protein aggregation in a fashion like that of prion aggregation. A constitutively phosphorylated mutant form of G3BP1 (S149E) acts as a dominant inhibitor against SG formation (Tourrière et al., 2003). Therefore, G3BP1 is shown to play a particularly significant role in SG formation and function.

The differences in how individual SG components contribute to SG formation and function is not fully understood. Purification and RNA-Seq analysis of SG cores showed that different SG could have diverse proteomes (Jain et al., 2016). It was previously shown, for example, that the Ubiquitin associated protein 2-like (UBAP2L) forms distinct cores from G3BP1, and it was suggested that cores with different components might coexist inside the same SG. Authors also suggest that UBAP2L is an important SG nucleator and acts upstream of G3BP1 (Cirillo et al., 2020). Furthermore, the SG-associated protein Caprin-1 can bind to NTF2-domain of G3BP1, thereby assisting in G3BP1-dependent condensation and promoting SG (Kedersha et al., 2016; Solomon et al., 2007). Interestingly, overexpression of Caprin-1 alone induces the formation of type SG, resulting in global inhibition of protein synthesis. Solomon et al. suggested that the ability of Caprin-1 or G3BP-1 to form SG do not depend on each other (Solomon et al., 2007).

The SG formation route can vary, and this can classify them into three subtypes (type I, type II type III) (Advani & Ivanov, 2020; Ivanov et al., 2019; Riggs et al., 2020). Type I) form in response to oxidative stress, ER stress, and viral infection; depend on phosphorylation of eIF2α, and require G3BP1 and 48S preinitiation complexes. Type II) assemble and can stall translation independent of eIF2α phosphorylation. These SG can form with eIF4F inhibitors treatment via inactivation of eIF4A. Type III) typically lack eIFs, appear in response to glucose starvation, sodium selenite, nitric oxide, and UV (Advani & Ivanov, 2020; Aulas et al., 2018). It indicates that SG may sequester specific proteins, altering the dynamics of

cytosolic proteins, which in turn could change the course of signaling cascades in the cytoplasm (Riggs et al., 2020). Moreover, dysregulation and aberrant accumulation of SG are demonstrated to be a contributing factor to cytotoxicity, which are increasingly associated with neuropathology, such as amyotrophic lateral sclerosis (ALS) (Wolozin & Ivanov, 2019).

Recently, the study of the clinical relevance of SG persistence took a significant turn. The principal role of mitochondria is to break down blocks of fat called fatty acids (FA) and other molecules to release energy that powers many processes in cells in a pathway called fatty acid β-oxidation (FAO) (Nowinski et al., 2020). Some pathological conditions may cause nutrient deprivation and starvation, and the cell needs to reorganize endogenous substrates to keep the intracellular energy at safe levels, and FA may be mobilized from the mitochondria to other organelles as energy supply (Nowinski et al., 2020; Zeidler et al., 2017). Long-term chronic nutrient starvation is a known trigger for SG, which induces the assembly of SG with specific components mediated by the mammalian target of rapamycin (mTOR) pathway (Buchan et al., 2011; Reineke et al., 2018). Amen & Kaganovich reported that SG can regulate metabolic remodeling by interacting with the mitochondria during starvation stress. They showed that SG formation leads to a downregulation of FAO through the regulation of the mitochondrial voltage-dependent anion channels (VDAC), which import fatty acids to the mitochondria. The following decrease in FAO during chronic starvation reduces oxidative damage and rations FAs for longer use (Amen & Kaganovich, 2021). Failure to form SG, either caused by the genetic deletion of SG components or an ALS-associated mutation, means inability to downregulate FAO (Amen & Kaganovich, 2021; Reineke & Neilson, 2019; Wolozin & Ivanov, 2019).

1.2.2.2.5.2. Stress granules disassembly

Less is known about the disassembly of SG, compared to SG assembly. Disassembly of SG has been shown to correlate with recovery in cellular protein synthesis and may involve dissociation of SG contents and/or release of mRNA from granules to resume translation (Buchan & Parker, 2009; Hofmann et al., 2021). Drugs that stabilize polysomes such as cycloheximide and emetine lead to SG disassembly (Anderson & Kedersha, 2006; Kedersha et al., 2000).

Several RNA-binding proteins have been implicated in promoting SG disassembly, including Staufen and Grb7. Over-expression of Staufen can inhibit SG assembly possibly by stabilizing mRNA-polysome interaction (Thomas et al., 2009), while phosphorylation of

Grb7 is required to weaken its interaction with HuR, TIA-1 and certain mRNAs from SG (Tsai et al., 2008). Moreover, while Caprin-1 binds to G3BP1 to assist on SG condensation, a protein called Ubiquitin Specific Peptidase 10 (USP10) competes for the same binding site and this interaction induces SG disassembly (Kedersha et al., 2016; Sanders et al., 2020).

Furthermore, SG disassembly has also been shown to occur via autophagy in a process referred to as granulophagy (Buchan et al., 2013). The targeting of SG to the autophagic pathway depends on the function of p97, an AAA ATPase also known as valosin-containing protein (VCP). In fact, SG clearance is reduced by autophagy inhibition, and depletion or mutations in VCP (Buchan et al., 2013). Unc-51 like autophagy activating kinase 1 (ULK1) and ULK2 have been shown to mediate SG clearance through activation of VCP (B. Wang et al., 2019).

It has also been recently described that ubiquitylation may also play a pivotal role in SG disassembly. Proteins marked with K48 ubiquitin chains are typically targeted to proteolytic degradation, whereas other chains, such as K63, mediate a non-proteolytic signaling functions to induce the extraction of proteins from complexes. VCP has an essential role in both cases by extracting ubiquitylated proteins from membranes, chromatin, or protein complexes (Maxwell et al., 2021). Using a model of heat-induced SG, Gwon and colleagues showed that VCP labels G3BP1 with a K63 polyubiquitylation chain which mediates its removal from SG cores and ultimately leads to granule disassembly (Gwon et al., 2021).

1.2.2.2.5.3. Stress granules and Flaviviruses

Several viruses can manipulate the SG components and regulate their formation, as this could be disadvantageous, for RNA viruses for example, that use the cellular translation machinery for their own replication. It is known that some viruses can induce the formation of SG, for instance, Respiratory Syncytial virus (RSV), whereas other viruses, for example, West Nile virus (WNV) and Rotavirus among others, do not induce SG formation (Emara & Brinton, 2007; Lindquist et al., 2010).

Because the translation is a critical first step in the Flavivirus life cycle, the formation of type I SG may represent an immediate obstacle to infection. For this reason, during infection with different Flaviviruses, such as WNV, Dengue virus (DENV), and Japanese Encephalitis virus (JEV), SG are blocked and treatment of virus-infected cells with arsenite fails to induce SG through HRI kinase (Basu et al., 2017; Emara & Brinton, 2007; Katoh et al., 2013; Roth et al., 2017). Although WNV, DENV, and JEV belong to the same Flavivirus genus, each virus employs a particular mechanism to block the SG assembly. For instance, natural WNV

infection does not induce SG, but chimeras produce high levels of viral replication and induce SG through activation of PKR by the detecting exposed dsRNA replication intermediates, which results in phosphorylation of eIF2α, stalling of translation initiation, and formation of stress granules. The inhibition of SG might involve non-structural proteins such NS4B and NS5 (Courtney et al., 2012; Elbahesh et al., 2011a; Emara & Brinton, 2007). G3BP1, G3BP2, and Caprin1 can stimulate translation of interferon-stimulated genes (ISGs) to fight DENV infection, and the virus has evolved mechanism to escape their action by targeting with non-coding viral RNA (Bidet et al., 2014; Ward et al., 2011).

Similar to DENV and WNV, ZIKV was shown to limit the assembly of SG (Amorim et al., 2017; Hou et al., 2017). In particular, Hou et al. described that transfection Flag-tagged NS3 and NS4A repress translation, and the formation of SG is restricted when Flag-tagged capsid, NS3, NS2B-3, and NS4A proteins were individually expressed (Hou et al., 2017). Amorim et al. additionally demonstrated that ZIKV escapes the antiviral stress response by increasing the rate of eIF2α dephosphorylation during infection (Amorim et al., 2017).

These studies provide insight into how SG assembly is inhibited during Flavivirus infection, however it is reasonable to consider that stress granules may play a role for the cells during infection and that its specific role or function has yet to be well defined.

It has been demonstrated that during WNV and DENV infection, both TIA-1 and TIAR are sequestered at viral replication sites and thus SG formation is reduced, suggesting that these viruses interfere with SG formation by altering the cellular localization of SG proteins (Emara & Brinton, 2007). Furthermore, a study shows that JEV core protein recruits several SG-associated proteins, including G3BP1 and USP10, through interaction with Caprin-1, another RNA binding protein recruited during SG formation (Katoh et al., 2013). In the same study, it was demonstrated that JEV carrying a mutated core protein incapable of binding to Caprin1 exhibited lower propagation in vitro and lower pathogenicity in mice than the wild-type JEV, suggesting that the core protein activity on SG inhibition is essential to antagonize host defense (Katoh et al., 2013). Altogether these results suggest a common strategy of Flaviviruses to prevent the inhibition of viral mRNA translation and to enhance RNA synthesis by modulating the SG response. We demonstrated previously that TIA-1 and TIAR proteins are recruited to the sites of TBEV replication, bind the viral RNA and inhibit its replication. We also showed that TBEV can trigger the formation of SG containing other SG markers as G3BP, eIF3 and eIF4B (Albornoz et al., 2014).

Previous studies performed in our lab (Miorin et al., 2012, 2013) as well as by Overby *et al.* (Overby et al., 2010) have demonstrated that the IFN response to TBEV infection is delayed. Miorin and colleagues showed that the innate response to TBEV is RIG-I dependent and that its agonists are present in infected cells as early as 8 hpi. It has been proposed that the dsRNA of TBEV is retained into ER-derived vesicles, to protect it from cell surveillance. Another key observation is the fact that the start of SG formation is concomitant with the beginning of IFN mRNA detection, and both events are induced earlier with UPR pre-activation (data not published).

1.2.2.2.5.4. Antiviral stress granules

In the context of IFN signaling, SG are believed to function as antiviral hubs, serving as platforms for the recruitment of signaling molecules and coordinating signaling events (Onomoto et al., 2012).

Depending on the virus and the host cell, different patterns of SG formation can be observed during infection: stable SG formation, no SG formation, transient SG formation and oscillating SG formation (Eiermann et al., 2020; Onomoto et al., 2014; Ruggieri et al., 2012). The antiviral nature of SG can be demonstrated by depleting viral mechanisms that antagonize SG this response. For example, the NS1 protein of Influenza A virus (IAV) was shown to inhibit SG formation by blocking PKR activation (Onomoto et al., 2012). When IAV NS1 was removed (IAVΔNS1), the interaction with PKR was lost and led to the formation of SG. Onomoto and colleagues also demonstrated that the antiviral proteins RIG-I, MDA5, PKR, 2′–5′ oligoadenylate synthetase (OAS), and RNase L localize to IAVΔNS1-induced SG, along with viral RNA. Moreover, they showed that SG inhibition during IAVΔNS1 infection, by silencing the G3BP1 protein, reduce the expression of IFN-β. A similar behavior was also observed upon infection with encephalomyocarditis virus (EMCV), and Sindbis virus (SINV). In these models, the inhibition of SG formation led to a marked decrease of IFN production and higher viral replication. Taken together, these data led Onomoto and colleagues to hypothesize that the redistribution of antiviral molecules to SG facilitate signaling, and SG acts as a platform for viral RNA identification and activation of IFN response. They called it antiviral SG (avSG) (Onomoto et al., 2012).

Few studies suggest, however, that SG might not be necessary for the IFN response upon virus infection. It was shown that infection with a mutant mengovirus induces formation of SG with colocalization of MDA5, and these were dispensable for IFN production (Langereis et al., 2013). In that study, the presence of viral RNA was not detected inside SG, which

could indicate that avSG depend on both antiviral proteins and accumulation of viral RNA to be functional

Other foci have been described to resemble avSG's function in helping to mount an antiviral response. RNase L is an IFN-induced endoribonuclease able to cleave both viral and cellular RNAs. The cleavage products are detected by PRR to amplify the IFN response (Silverman, 2007). Interestingly, RNase L has recently been demonstrated to modulate translation in regardless of the PKR > p-eIF2α > SG axis (Burke et al., 2020), and its activity has been related to the formation of specific SG-like punctate membraneless organelles called RNase L-bodies (RLB) that do not require G3BP1 for condensation (Burke et al., 2020; Manivannan et al., 2020). Moreover, a recent study showed the pivotal role of RNase L in avSG in coordinating ligands with its respective receptors to ensure effective response during viral infections (Manivannan et al., 2020).

Although there are still discussions about whether SG assist on the host response as a platform for IFN induction, an increasing number of studies suggests the significance of SG for antiviral responses. (Eiermann et al., 2020). In line with this hypothesis, most viruses appear to inhibit SG formation through numerous strategies for the evasion of host antiviral responses (White & Lloyd, 2012).

2.MATERIALS AND METHODS

2.1. Materials

2.1.1. Cells

Mammalian

- U2OS: Human osteosarcoma;
    - U2OS_shPERK: produced in this work; U2OS transduced with a lentivirus carrying shPERK
    - U2OS_shPKR: produced in this work; U2OS transduced with a lentivirus carrying shPKR
    - U2OS_Scramble: produced in this work; U2OS transduced with a lentivirus carrying shScramble
    - U2OS_PKR: produced in this work; U2OS transduced with a lentivirus carrying human PKR
    - U2OS_ΔΔG3BP: Kindly donated by Dr Nicolas Locker
- Vero E6: African green monkey kidney;
- HEK 293T: Human embryonic kidney, mut SV40 large T antigen.
- MRC-5: Human lung fibroblasts
- SK-N-SH: Human neuroblastoma

Bacteria

- XL10-Gold Ultracompetent Cells (Stratagene - cat.num. 200315). Genotype: Tetr Δ(mcrA)183 Δ(mcrCB-hsdSMR-mrr)173 endA1 supE44 thi-1recA1 gyrA96 relA1 lac Hte [F′ proAB lacIqZΔM15 Tn10 (Tetr) Amy (Kanr)].

- MAX Efficiency DH5α Competent Cells (Invitrogen – cat. num. 18258012 Genotype: F- Φ80lacZΔM15 Δ(lacZYA-argF) U169 recA1 endA1 hsdR17 (rk-, mk+) phoA supE44 λ-thi-1 gyrA96 relA1

2.1.2. Media

Mammalian

• DMEM complete medium: Dulbecco's Modified Eagle Medium (Gibco - cat.num. 31885-023) supplemented with 10% fetal bovine serum (FBS) (Euroclone - cat.num. ECS0180L). For selection of stable cell lines, Puromycin Dihydrochloride (Invitrogen – A1113803) was added at a concentration of 1 μg/mL.

• OptiMEM: Reduced-Serum Medium (Gibco - cat.num 31985-070)

• Cryo medium: for long-term storage cells were frozen at -80 °C in 90% FBS, 10% DMSO.

Bacteria

Luria-Bertani (LB) Medium: 10 g bacto-trypton, 5 g bacto-yeast extract, 10 g NaCl per 1 liter medium. Ampicillin was added at a concentration of 100 μg/ml. For hardening 1.5 % agar-agar was added to the liquid medium.

2.1.3. Antibodies

Primary antibodies

Target	Species	Source	Catalog number	Dilution
eIF3η	Goat	Santa Cruz	sc-16377	IF 1:100
eIF4B	Rabbit	Abcam	ab68474	IF 1:100
G3BP	Mouse	BD Transduction Labs	611126	IF 1:100
TBEV E	Rabbit	Produced by Gianmarco Corazza	Produced *in house*	IF 1:100 WB 1:1000
PERK	Rabbit	Santa Cruz	sc-13073	WB 1:500
PKR	Mouse	Santa Cruz	sc-6282	WB 1:200
p-PKR	Rabbit	Abcam	ab32036	WB 1:1000
β-Actin/HRP	Mouse	Sigma	A3854	WB 1:50000
dsRNA J2	Mouse	SciCom	10010500	IF 1:200
Puromycin	Mouse	EMD Millipore	MABE343	IF 1:200
FLAG	Mouse	Sigma	F1804	IF 1:500 WB 1:5000
p-eIF2α	Rabbit	Cell Signalling	9721S	WB 1:500
eIF2α	Rabbit	Santa Cruz	sc-11386	WB 1:100

Table 1. Primary antibodies used in this study

Secondary antibodies

Donkey, anti-goat IgG, Alexa Fluor 594; 1:500 for IF (Molecular Probes cat.num. A11058)

Donkey, anti-mouse IgG, Alexa Fluor 488; 1:500 for IF (Molecular Probes cat.num. A21202)

Donkey anti-mouse IgG, Alexa Fluor 594; 1:500 for IF (Molecular Probes cat.num. A21203)

Donkey, anti-rabbit IgG, Alexa Fluor 488; 1:500 for IF (Molecular Probes cat.num. A21206)

Donkey anti-rabbit IgG, Alexa Fluor 594; 1:500 for IF Molecular Probes cat.num. A21207)

Goat polyclonal, anti-mouse immunoglobulins/HRP; 1:10000 for WB (DakoCytomation cat.num. P0447)

Goat polyclonal, anti-rabbit immunoglobulins/HRP; 1:10000 for WB (DakoCytomation cat.num. P0448)

2.1.4. Vectors

Plasmid	**Relevant characteristics**	**Source**	**Catalog number**
psPAX2	Packaging Vector	Addgene	12260
pMDG.2	Encodes VSV-G Envelope protein	Addgene	12259
pLVTHM	Lentivector expressing GFP	Addgene	12247
pWPI_PURO	Lentivector with empty backbone and puromycin resistance gene	Addgene	12254
shPERK	Encodes short hairpin sequence to halt PERK protein expression	Produced by Tea Carletti	
shPKR	Encodes short hairpin sequence to halt PKR protein expression		
shScramble	Encodes a non specific short hairpin sequence		
pWPI_PURO-PKR	Lentivector expressing human PKR	Porduced in this study	
pEGFP	Encodes the enhanced green fluorescence protein	BD Biosciences Clontech	6084-1
pl.18 TBE Hy NS1 3xFlag	Encodes Flag-tagged TBE non-structural protein 1	Kindly provided by Dr Anna K. Överby	
pl.18 TBE Hy NS2A 3xFlag	Encodes Flag-tagged TBE non-structural protein 2A		
pl.18 TBE Hy NS2B 3xFlag	Encodes Flag-tagged TBE non-structural protein 2B		
pl.18 TBE Hy NS3 3xFlag	Encodes Flag-tagged TBE non-structural protein 3		

pl.18 TBE Hy NS4A 3xFlag	Encodes Flag-tagged TBE non-structural protein 4A	
pl.18 TBE Hy NS4B 3xFlag	Encodes Flag-tagged TBE non-structural protein 4B	
pl.18 TBE Hy NS5 3xFlag	Encodes Flag-tagged TBE non-structural protein 5	

Table 2. Plasmids used in this study

2.1.5. Primers

Name	**Sequence 5' to 3'**
TBEV 5'NCR Fw	GCGTTTGCTTCGGA
TBEV 5'NCR Rv	CTCTTTCGACACTCGTCGAGG
IFNβ Fw	AGGACAGGATGAACTTTGAC
IFNβ Rv	TGATAGACATTAGCCAGGAG
β-Actin Fw	CATGTGCAAGGCCGGCTTCG
β-Actin Rv	GAAGGTGTGGTGCCAGATTT
PKR cloning Fw	TTGGCGCGCCATGGCTGGTGATCTTTC
PKR cloning Rv	AGATACGCGTCTAACATGTGTGTCGTTC

Table 3. Primers used in this study. The restriction sites are indicated in sublined text.

2.1.6. Solutions and Buffers

- 1X PBS

  In 800 mL of distilled water, the following were added; 8 g of NaCl, 0.2 g of KCl, 1.44 g of Na_2HPO_4, 0.24 g of KH_2PO_4. pH adjusted to 7.4 and distilled water was added to bring solution to volume of 1 liter.

- 2X HBS

  In water, 42 mM HEPES (Sigma-Aldrich cat. num. H4034-100G), 274 mM NaCl, 1.5 mM $Na_2HPO_4 \cdot 12H_2O$, 15 mM D-glucose and pH adjusted to 7.0 (final volume: 1 liter)

- 5X TBE

  54 g Tris base (Invitrogen cat.num. 15504-020), 27.5 g Boric acid (Sigma-Aldrich cat.num. 31146), 20 mL 0.5 M EDTA (Sigma-Aldrich cat.num. E5134-1KG) and distilled water to final volume of 1 liter

- 3.7 % Paraformaldehyde (PFA)

  5mL of 37% PFA: 1.85 g of PFA powder, reagent grade crystalline (Sigma-Aldrich cat. num. P6148-500G) dissolved in 5 mL of distilled water, 10µl 10 M KOH. 37% PFA was diluted in 2X PHEM buffer (18.14g PIPES (ChemCruz cat.num. sc-216099); 6.5 g HEPES; 3.8 g EGTA; 0.99 g MgSO4; pH adjusted to 7.0 with 10 M KOH) to produce 3.7 % PFA.

- 2% high viscosity carboxymethylcellulose sodium salt (CMC)

  Sterile 20 g CMC powder (Sigma-Aldrich cat. num. C5013-500G) was dissolved in 1 liter of 1X PBS

- 1% Crystal violet solution

  1L; 10 g Crystal violet powder (Sigma- Aldrich cat.num. C6158-50G), 200 mL PBS and 800 mL Methanol (Sigma-Aldrich cat.num. 32213-2.5L-M)

- SDS electrophoresis buffer (10X)

  30.2 g Tris, 188 g Glycine (Sigma-Aldrich 33226-1KG), 50 mL 10 % SDS (Sigma-Aldrich L5750-500G), add water to 1 liter

- 10X Transfer Buffer

  30.3 g Tris, 144 g Glycine, add water to 1 liter

  - 1X Transfer buffer: 100 mL 10X Transfer Buffer, 200 mL Methanol and 700 mL water

- 10X TBS

  60 g Tris, 2 g KCl, 80 g NaCl, pH adjusted to 8.5 with 37% HCl, add water to 1L

  - 1X TBS-T: 100 mL 10X TBS, 900 mL water, 1 mL Tween-20 (Sigma-Aldrich P2287)

2.1.7. DNA and protein ladders

• PageRuler Plus Prestained Protein Ladder, Thermo Scientific cat.num.26619

• 1kb DNA ladder (100µg/mL), Promega cat.num. G571A (DNA ladder supplied with Blue/Orange 6X Loading dye, Promega cat.num. G190A)

2.2. Methods

2.2.1. Mammalian cell culture

Adherent mammalian cells were cultivated with DMEM supplemented with 10% FBS. Monolayers of cells were grown at 37 °C, 5 % CO_2 in DMEM complete medium. When needed, cells were passaged with 0.05 % trypsin + 0.02 % EDTA and seeded at the appropriate dilution. Passaging and experiments were performed with monolayer around 75 % confluent. Cell culture was done in aseptic conditions, cells were routinely screened for Mycoplasma contamination and new cell stocks were revived at regular intervals.

2.2.2. Plasmid construction

The sequence of human PKR protein was isolated from cDNA sample of U2OS cells. The PCR amplification reaction was performed using the specific cloning primers described in Table 3 and the high fidelity PrimeSTAR® GXL DNA Polymerase kit (Takara, cat.num. R050A) according to manufacture's instructions, under the following thermal cycling conditions: 98 °C 2min, - 98 °C 10sec, 55 °C 15sec, 68 °C 2min for 30 cycles -, and 72 °C 5min. The PCR product was purified using the NucleoSpin Gel and PCR clean-up kit (Macherey-Nagel cat.num. 740609.250). Further, the pWPI_PURO cloning plasmid and the insert were double digested with AscI and MluI restriction enzymes. After purification, the digested PCR product was ligated overnight at 16°C with gentle agitation using T4 DNA Ligase enzyme (New England Biolabs - cat.num M0202S) into the linearized pWPI-PURO vector a 1:5 molar ratio.

At every step, the size and integrity of both linearized vector and PCR product were analyzed by separating the DNA in 1 % Agarose gel for 45 minutes at 90V. Gel preparation: UltraPure™ Agarose powder (Invitrogen cat.num. 16500-500) melted in 0.5X TBE buffer and mixed with 250 ng/mL of Ethidium Bromide. Agarose gels were visualized using the UVIdoc HD2 gel documentation system (UVITEC Cambridge).

2.2.3. Plasmid transformation

XL10-Gold or DH5α chemo-competent cells were used for transformation of all plasmids in this study. Cells were incubated with the plasmids on ice for 30 min. They were then heat-shocked at 42°C for 45 seconds, moved immediately to ice for 2 minutes followed by addition of LB medium without antibiotics. Cells were then incubated at 37°C for 1 hour with agitation, then were plated onto LB agar with the required antibiotic. They were grown

overnight at 37 °C. On the next day, colonies were picked and pre-inoculated into 5 ml of LB medium containing the required antibiotic.

2.2.4. Plasmid DNA extraction

After approximately 16 hours cell growth, plasmid DNA was extracted using NucleoSpin Plasmid (Macherey-Nagel cat.num.1801/003) for minipreps or NucleoBond Xtra Midi (Macherey-Nagel cat. num. 1803/009) for midipreps. Extracted DNA was authenticated by restriction endonuclease digestion and sequencing. Restriction endonucleases and their specific buffers were purchased from New England Biolabs (NEB).

2.2.5. Plasmid transfection

Lipofectamine LTX transfection

Plasmids were transfected into U2OS cells using Lipofectamine™ LTX Reagent with PLUS™ Reagent (Invitrogen cat.num. 15338-100) according to a standard, optimized protocol. Transfection was done using reduced serum medium (Opti-MEM) and further grown in DMEM supplemented with 10% FBS.

Calcium Phosphate transfection

Transfections for luciferase reporter assay were performed in HEK293T cells using a standard, optimized protocol. Transfection was done in DMEM supplemented with 10% FBS and further incubated at 37°C, 5% CO_2 until sample collection.

2.2.6. Production of infectious Lentiviral particles

Lentiviral (LV) particles were produced in HEK293T cells using calcium phosphate transfection method. The following mix was prepared:

- 5 µg expression plasmid,
- 3.75 µg psPAX2 packaging plasmid
- 1.25 µg pMD2.G envelope plasmid
- 50 µL of sterile 2.5 M $CaCl_2$ was added to each tube.
- Sterile H_2O to 500 µL final volume

This mixture was incubated for 5 min at room temperature and then added dropwise to 500 µL sterile 2X HBS by gently vortexing and incubated at room temperature for 20 min. The transfection mixture was then added dropwise to the cells and incubated for ~16h. In sequence, the media was changed to remove the transfection reagents and replaced with fresh complete media. Cells were then incubated at 37 °C, 5% CO_2 for 24 h. The following day, media containing the lentiviral particles were collected and centrifuged at 2250 rpm for 10 min at 4 °C to pellet any HEK-293T cells that were accidentally collected during harvesting. The supernatant was filtered with 0.45 µm sterile filters. The filtered lentiviral stocks were aliquoted and stored at -80 °C.

2.2.6.1. Flow cytometry analysis

Transfection efficiency was evaluated by flow cytometry using pLVTHM-expresing LV. Cell monolayers were treated with 10 mM of EDTA in PBS to prepare single-cell suspensions. Cells were then washed twice with PBS, resuspended with 500 µL of PBS and immediately analyzed by flow cytometry with a FACS Calibur machine (Becton Dickinson) and the Cell Quest Pro software. Appropriate controls were employed every time with untreated cells.

2.2.7. Transduction of target cells with clarified *Lentiviruses*

To produce stable cell lines with silenced target proteins, $3x10^5$ U2OS cells were prepared in 1 mL together with 1 mL of LV suspension + 6 mL of complete medium. The mixture was plated in 10 cm dishes and incubated at 37 °C. One day after, medium was replaced with fresh complete medium to remove excess of reagents, and on the next day, complete medium containing 1 µg/mL of puromycin was added to start selection. A control plate of not transduced cells was also subjected to puromycin treatment as an indicator of the selection status. Silencing efficiency was evaluated by WB analyses.

2.2.8. TBEV infection of cells

Virus stock preparation

Neudoerfl strain of TBEV was used for all experiments reported herein. Viral stocks were prepared by infection of Vero cells at multiplicity of infection of 0.1. After observation of cytopathic effects (CPE), the supernatant was collected, clarified by centrifugation, supplemented with 20 % FBS, and stored in aliquots at -80°C. Viral titres were determined by using a plaque-forming assay.

Cell infection and tunicamycin treatment

When performing infection experiments, cells are seeded in a 12 well plate at an appropriate confluence. After 24 hours, cells are infected at multiplicity of infection (MOI) of 1 by incubating with 500 µl of virus stock properly diluted in serum-free medium, or with 500 µl of only serum-free medium (mock infection). After 1 hour incubation at 37 °C, cells are washed once with 1X PBS and overlayed with 1 mL of DMEM supplemented with 4 % heat-inactivated FBS (heat-inactivation: 56 °C for 30min) and 0.1 µg/ml of Tunicamycin (Sigma-Aldrich cat. num. T7765-1MG), or only DMEM with heat-inactiveted FBS (mock treatment). The moment in which the virus suspension is replaced with complete medium is considered time zero, 0 hpi, and subsequent hours of incubation are counted from this initial point. Supernatants were collected for plaque assay, and cells were then fixed with 3.7 % PFA for immunofluorescence (IF), or harvested for western blot (WB) or quantitative reverse transcription PCR (qRT-PCR) analyses at desired time points, as described in the scheme in Figure 10.

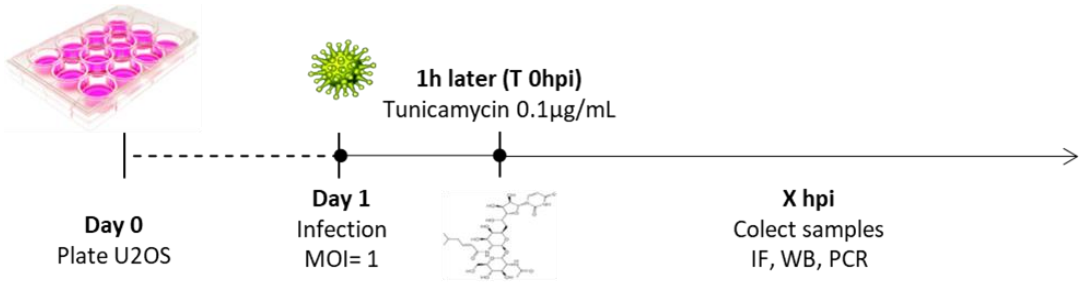

Figure 10. Workflow of experiments with infected cells.

2.2.9. Plaque assay

Vero cells ($1x10^5$) were seeded into 24-well plates in order to be 100% confluent the second day. Cells were infected the day after with a 10-fold serial dilution of TBEV supernant in a total volume of 200 µL of serum-free medium. After 1 hour incubation at 37 °C with 5% CO_2, the inoculum was removed and 1 mL overlay containing 1 volume of 2% CMC to 1 volume of DMEM supplemented with 4 % heat-inactivated FBS was added. The plates were incubated for 5 days before fixation with 3.7 % PFA dissolved in PHEM buffer. Infected cells were stained with 1% crystal violet solution. After 20 minutes the staining solution was removed and cells were washed 3-4 times with water. Viral titres were determined by counting number of plaques formed and dividing it by volume of infection multiplied for the dilution factor.

$$PFU/mL = \frac{\#plaques\ counted}{vol.infection\ x\ dil.factor}$$

2.2.10 Cell lysis

Depending on the type of analysis to be performed, cells were lysed in one of the following lysis buffers:

• Laemmli Buffer (LB) (50 mM Tris-Cl pH 6.8, 2% SDS, 10% glycerol, 100 mM DTT, 0.1% bromophenol blue - Bio-Rad cat.num. 161-0404)

• RIPA buffer (50 mM Tris-Cl pH 7.5, 150 mM NaCl, 1% NP-40, 0.1% SDS, 1mM EDTA, 1mM EGTA, 1mM PMSF, 0.5% Sodium deoxycholate (Sigma-Aldrich cat.num. D6750-100G) and Proteinase Inhibitors Cocktail (Roche - 11836170001) and Phosphatase Inhibitors: Sodium Fluoride (Riedel-deHaën 30105) and Sodium Orthovanadate (Sigma-Aldrich S6508-10G 028K0117)

2.2.11. SDS-PAGE and western blot analysis

Whole cell lysates were collected with RIPA buffer and resolved in a 10 % SDS–PolyAcrylamide Gel Electrophoresis (SDS-PAGE). Initially, the protein lysates were diluted in LB boiled at 95 °C for 10 min, and centrifuged for 1min at RT at 1000 g. Subsequently, denaturated proteins were loaded into the polyacrylamide gel. The run was performed in

SDS electrophoresis buffer (25 mM Tris, 190 mM glycine, 0.1 % SDS), at 90 V into the stacking gel and later at 120 V into the resolving gel.

After electrophoresis, proteins were transferred onto a nitrocellulose membrane (GE Healthcare - 10600015), blocked for 1 hour with 5 % non-fat milk or, in case of phosphorylated proteins, 5 % bovine serum albumin (BSA, Roche – cat.num 10735078001) solutions in TBS with 0,1 % of Tween-20 (TBST) followed by an overnight incubation with the appropriate primary antibodies diluted in 5% milk or 5 % BSA in TBST at 4 °C. After three washes with TBST secondary antibodies conjugated with HRP were diluted in 5% milk and incubated for 1 hour. Blots were developed using Immobilon Western Chemiluminescent HRP Substrate (Merck Millipore – WBKLS0500) according to the manufacturer's instructions.

2.2.12. Real-time quantitative reverse transcription PCR

Total cellular RNA was extracted by using TRiFast II (EuroClone cat.num. EMR517100) according to the manufacturer's instructions, treated with DNase I (Life Technologies – cat.num 18060-015) and then quantified. 500 ng of extracted RNA was used as a template to synthesize cDNA using 150 ng Random Primers (Life Technologies – cat.num 8190-011) and M-MLV Reverse Transcriptase (Life Technologies – cat.num 28025-013) according to manufacturer's protocol. Quantitative Real-time PCR (qRT-PCR) using KAPA SYBR FAST qPCR Master Mix (KapaBiosystem - cat. num. KK4607) was performed from cDNA samples. Signals of IFNβ mRNA or viral RNAs were normalized to the β-Actin mRNA signal. The sequences of oligonucleotides used for this analysis are reported in Table 3 Amplification and detection were carried out on a CFX96 Real Time System (Bio-Rad).

2.2.13. Streptolysin O permeabilization

Permeabilization with streptolysin O (SLO) was performed as described by Overby *et al*, 2010 (Overby et al., 2010). Briefly, cells were plated on coverslips and treated as desired. Then washed with ice cold permeabilization buffer (P-buffer) (125 mM K Acetate, 25 mM Hepes pH 7.2, 10 mM Glucose, 2.5 mM Mg Acetate, 10 mM NaCl, 1.8 mM $CaCl_2$, 5 mM EGTA). Cells were then permeabilized with P-buffer and 1 U/mL SLO (30 ng/mL) for 15 min on ice. The excess of SLO was washed away with P-buffer. Following, pre-warmed P-buffer at 37 °C was added and cells were incubated for 5 min at 37 °C. Finally, cells were

washed once with PBS and fixed with 3.7 % PFA. A scheme of SLO permeabilization is shown in Figure 11.

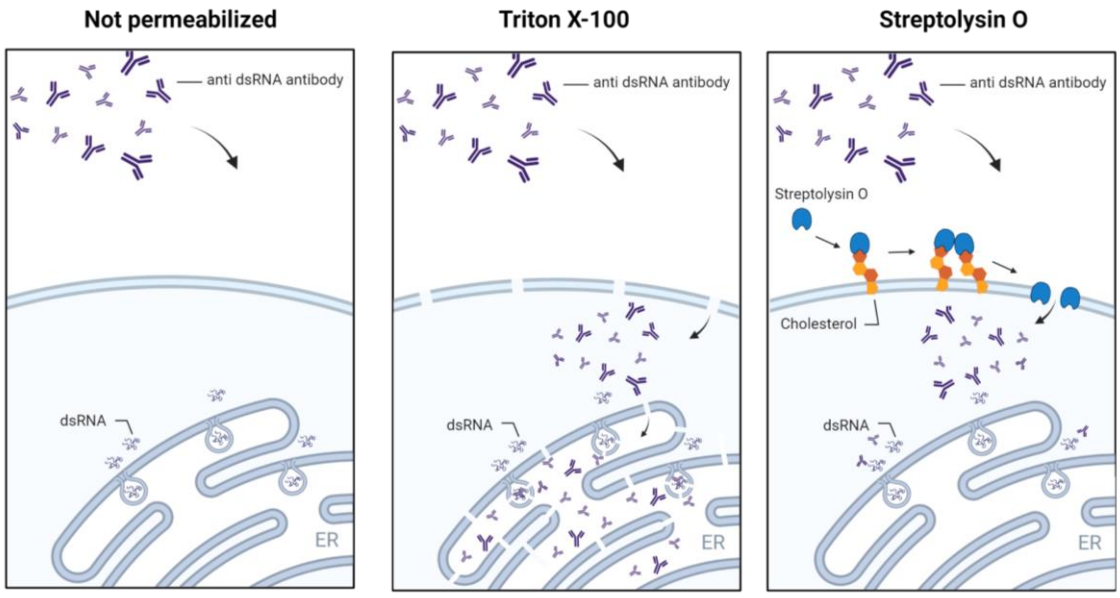

Figure 11. Graphic scheme of permeabilization methods. The specific antibody targeting dsRNA is not able to enter cells that have not been permeabilized. In cells permeabilized with the detergent triton x-100, all the membranes are permeabilized, including those of the ER and replication vesicles, making it possible to stain the dsRNA everywhere. While, with the selective plasma permeabilization with SLO, that binds to cholesterol on the cell surface and oligomearizes to form pores, dsRNA can only be stained on the cytoplasm. Created with BioRender.com

2.2.14. Indirect immunofluorescence assay

Cells were seeded onto 15x15mm glass coverslips in 12-well plates. After desired treatment, cells were washed once with PBS and fixed in 3.7 % PFA in PHEM buffer solution for 20 minutes at room temperature. Thereafter, cells were washed three times with PBS followed by and incubation of 5 minutes with 100 mM Glycine in PBS in order to saturate excesses of PFA and to stop the fixation reaction. Cells were permeabilized for 5 minutes with 0.1 % Triton X-100 in PBS and washed three times, 5 min each. Before incubation with antibodies, a blocking step was performed at 37°C for 30 minutes with 1 % BSA and 0.1 % Tween in PBS. Antibodies were diluted to the desired concentration in blocking solution to prevent unspecific binding. The coverslips were inverted onto 50 µL drops of primary antibody and incubated overnight at 4 °C in a humidified container. After incubation, coverslips were

positioned back into plate wells and rinsed three times with PBS + 0.1 % Tween 20 and incubated with secondary antibodies for 1 hour at 37°C. coverslips were finally washed three times with washing solution and mounted on slides using 5 µL of Fluoro-Gel II mounting medium with DAPI.

2.2.15. Imaging of fixed cells

Fluorescent images of fixed cells were captured with the Carl Zeiss LSM880 laser scanning confocal microscope. The pinhole of the microscope was adjusted to get an optical slice of less than 1.0 µm for any wavelength acquired. The fluorophore AlexaFluor 488 was excited with 488 nm line of the Argon Laser, while the fluorophore AlexaFluor 594 was excited with the HeNe Laser 543 nm. Their emissions were collected using the appropriate filters. For statistical purposes, 200±10 cells were counted for each condition.
Cells with the desired phenotype were counted using the ImageJ software, and its Cell Counter plug-in. The results are presented in percentage. In case the case of analysing the mean fluorescence intensity (MFI) of a specific channel, the cellular area was selected manually and the average of the fluorescence intensity values was obtained and used to perform statistical analysis.

2.2.16. Figures and statistical analysis

Three independent experiments in duplicate repeats were conducted unless indicated otherwise. GraphPad Prism 7 was used to generate graphs and perform all statistical analyses. Mean values are shown with standard deviation and p-values, measured with an unpaired two-tailed t-test or one-way ANOVA as indicated in figure legends. Significant p-values are denoted by asterisks ($p \leq 0.05$ = *; significant, $p \leq 0.01$=**; highly significant and $p \leq 0.001$ =***; extremely significant). Where asterisks are missing the differences are not significant.

3. RESULTS

Our laboratory has studied before the profiling of UPR activation following TBEV infection (Carletti and Zakaria et al., 2019). Between 8 and 16 hours post-infection (hpi) in U2OS cells, a particular time window was observed when TBEV sustainably replicates but the host interferon β (IFNβ) response is not yet active. The original hypothesis was that the virus somehow hides itself, impairing the antiviral response. In fact, TBEV replicates within invaginations of the endoplasmic reticulum (ER) membrane called replication vesicles (Miorin et al., 2012). Further, a transcriptome analysis led us to focus on the unfolded protein response (UPR), suggesting that it might be a very early cellular response to infection that primes cells for the innate response. The critical observation is that the UPR is active before the IFNβ response, and its pre-activation with tunicamycin (TM), a commonly used UPR inducer that inhibits protein N-linked glycosylation, leads to an earlier and increased IFNβ response and to TBEV inhibition. Our results also indicate that the pattern recognition receptors (PRR) RIG-I is required in synergy with UPR for a complete and more potent antiviral response from 16 hpi (Carletti and Zakaria et al., 2019).

Finally, we also demonstrated that TBEV induces the formation of stress granules (SG) (Albornoz et al., 2014) and that this response temporally correlates with the innate antiviral response induced by ER stress (data not published). Therefore, the current project investigates this phenomenon in detail to understand whether there is a causal link between SG induction and cell-intrinsic innate responses.

3.1. TBEV infection induces stress granule formation in a small number of infected cells

Cells maintain a stable internal environment conducive to vital biochemical processes while counteracting endogenous and environmental stresses. Examples of cellular stresses include hypoxia, heat shock, oxidative stress, starvation, and viral infection. Failure to cope with internal and external stresses can lead to metabolic dysregulation, genetic instability, and cell death. As a result, understanding how stress-response mechanisms orchestrate provides the fundamental knowledge required to understand the development and pathogenesis of a diseases.

As previously demonstrated, TBEV infection induces SG formation in the host cells; however, a quantitative analysis of the phenotype has not yet been performed. To this purpose, U2OS cells were TBEV-infected at an MOI of 1, treated with TM, and fixed for immunofluorescence analysis (IF) at 24 hpi. IF was performed using anti-TBEV as a marker

for infection and anti-G3BP and anti-eIF3η antibodies to stain SG. In addition, DAPI is used to stain the nucleus (Figure 12A).

200±10 cells for each condition were acquired at the confocal microscope, infected cells and infected cells with SG were manually counted using the ImageJ software. In Figure 12B, it is possible to observe that the percentage of infected cells is 100 % at 24 hpi (white bars), but with TM treatment (black bars), there is a 60 % decrease in the number of infected cells, consistent with previous observations. On the other hand, as shown in the graph of Figure 12C, about 5 % of the infected cells showed SG, while when TBEV-infected cells are treated with TM, the percentages of cells containing SG are significantly higher, around 15 %, even though the amount of infected cells is abundantly reduced. The results are comparable for both SG markers.

Finally, it is possible to observe that TM treatment not only induces a higher percentage of infected cells with SG at late time points, but it also allows earlier detection of this phenotype. In fact, as shown in the time course analysis of Figure 12D, SG formation start from 8 hpi in cells that are both TBEV infected and UPR active.

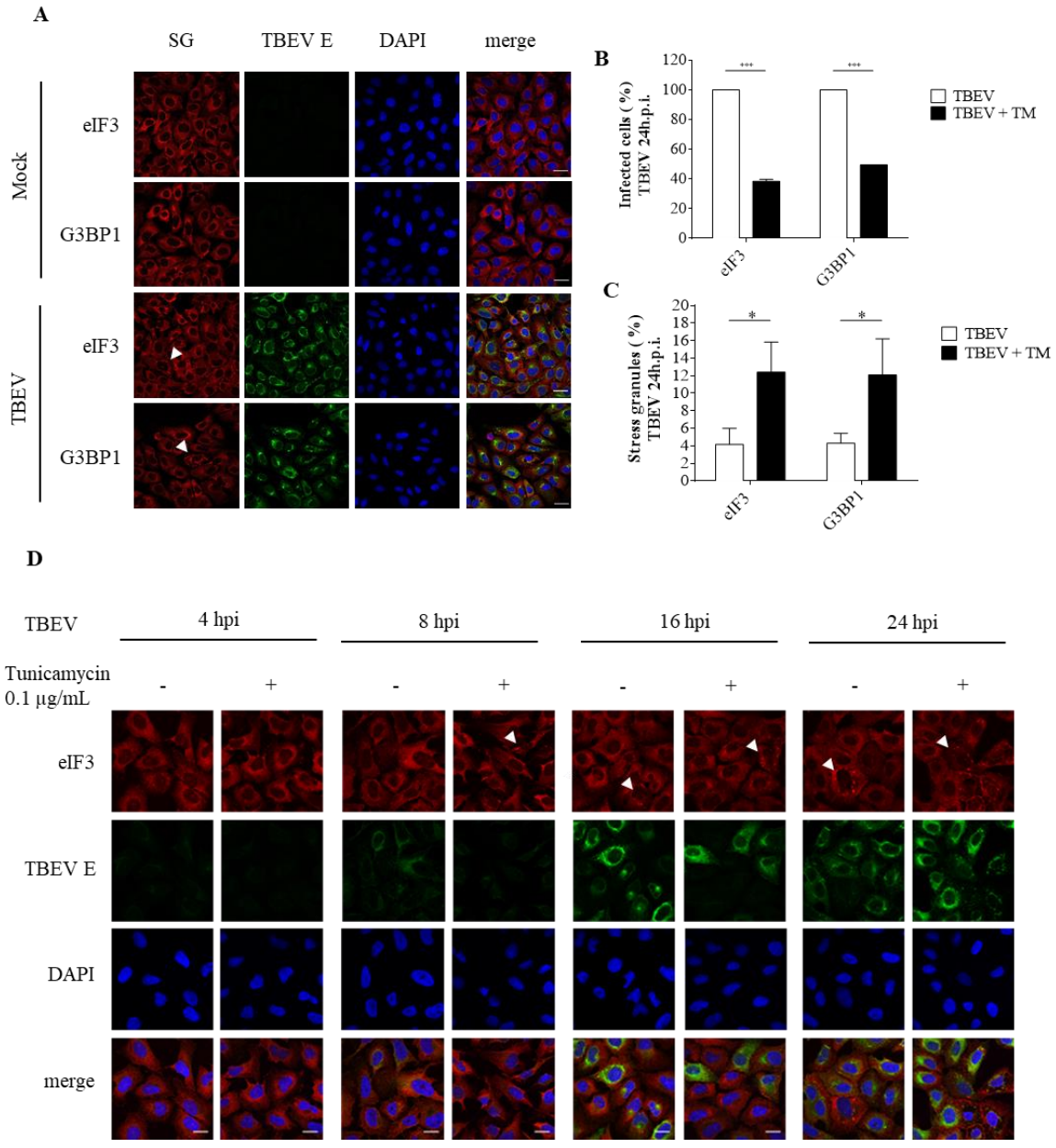

Figure 12. Stress granules are formed upon TBEV infection. U2OS cells were infected with the TBEV Neudoerfl strain at an MOI of 1 and treated with 0.1 µg/mL TM for 24 hours. Mock treatments were conducted in parallel for both conditions. A) Representative immunofluorescence pictures of U2OS infected cells stained with anti-TBEV antibody and anti-eIF3 or anti-G3BP as markers for SG; white stars indicate cells with stress granules. The graphs show the quantification of TBEV replication (B) and SG (C) stained for eIF3 or G3BP proteins. D) Timepoint analysis of SG formation upon TBEV infection, using eIF3 as marker for SG and TBEV E as marker for infection; white arrows indicate cells with stress granules. For statistical purposes, 200±10 cells were counted. Scale bars represent 30 µm. *p≤0.05, ***p≤0.001 unpaired, student's t-test

The TBEV has a tropism for brain cells which has been shown to have a differential innate immune response that leaves the tissue more susceptible to infection (Fares et al., 2020). SG formation was hence monitored by confocal microscopy in the SK-N-SH (neuroblastoma) cells, but also in MRC-5 (lung fibroblasts) and in primary human fibroblasts freshly harvested from the skin and adipose tissues (kindly provided by the Cardiovascular Biology Laboratory in ICGEB), using U2OS as control. This approach was chosen in order to confirm that the SG phenotype is TBEV-specific and common to different cell lines. Cells were infected at an MOI of 1 and collected for IF analysis at 24 hpi. SG were identified by staining for G3BP, and TBEV-infected cells were identified by staining the viral E protein.

The immunofluorescence shows that all the cell types studied can be infected with TBEV and, except fat tissue, can form SG (Figure 13A). However, quantification of the confocal images indicates that the primary cells are more resistant to the virus infection, showing only 20 % of cells infected while the cell lines are 100 % infected (Figure 13B). Moreover, similar results were obtained for SG formation in all the cells, in which few G3BP-positive SG are present in the cytoplasm of the infected cells analyzed (Figure 13C). The percentage of infected cells containing SG is very low, about 5 %, for every type of cell used in this experiment, except for MRC-5 that shows around 10 % of infected cells with SG.

These observations indicated that TBEV induces a meager percentage of SG in different cell types, and it would be interesting to individuate which process the virus uses to achieve so. Moreover, it also demonstrates that U2OS, the cell line selected to conduct this study, is an excellent model to study the SG response upon TBEV infection.

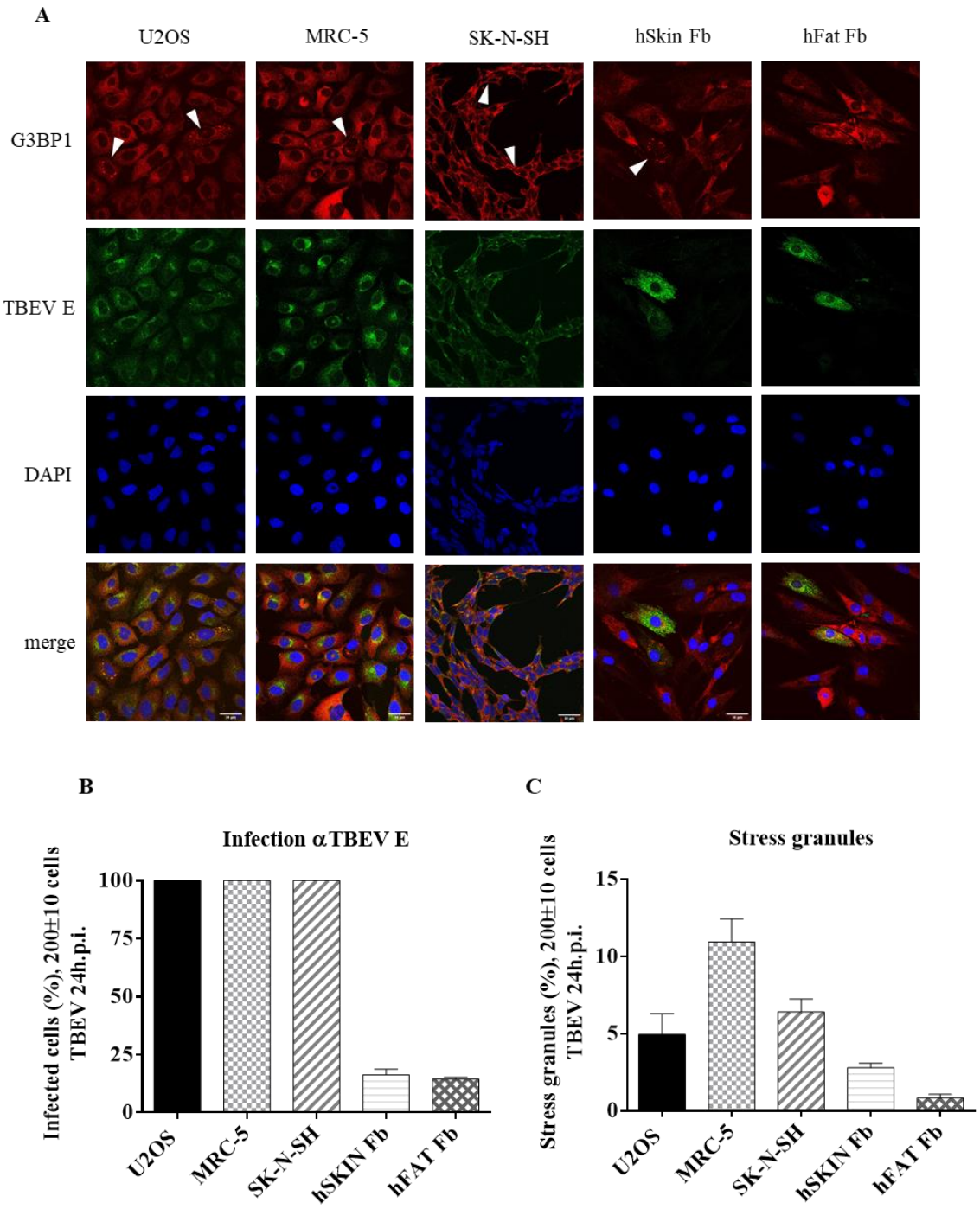

Figure 13. TBEV prevents SG formation in different cell types. Different cell types, indicated in the top row, were infected with TBEV at an MOI of 1. Twenty-four hours post-infection, cells were fixed, permeabilized and analyzed with IF. TBEV-infected cells were detected with α-TBEV E antibody (green) and SG were detected with α-G3BP antibody (red). A) Representative immunofluorescence images of infected cells. White arrows highlight SG-positive cells. Scale bars represent 30 µm. B) Quantification of infected cells. C) Quantification of G3BP-containing SG within infected cells.

3.2.TBEV significantly interferes with PIC-induced SG assembly

Several members of the Flaviviridae family can modulate SG formation to maintain the cell favorable to replication. As a second step to understand how TBEV infection affects the stress granule response, it was investigated whether TBEV can interfere with the SG assembly in fully infected cells. U2OS cells were infected with TBEV and treated at 24 hpi with 1 mM of sodium arsenite (ARS) for 30 min, transfected with 500 ng of poly(I:C) (PIC) for 4 hours using Lipofectamine LTX or treated with 10 µM of thapsigargin (Tg) for 1 hour to induce cellular stress and phosphorylation of eIF2α. Sodium arsenite induces oxidative stress that leads to HRI activation, poly(I:C) is a dsRNA analog that mimics the replication intermediates and activates PKR, whereas thapsigargin inhibits ER Ca2+-dependent ATPase which leads to ER stress and PERK activation. SG assembly was accessed by indirect immunofluorescence of G3BP, and infected cells were identified by staining the E protein.

Immunofluorescence analysis shows that a considerable amount of cells display SG when whichever kinase is stimulated, and when the cells are infected, it is possible to qualitatively conclude that there is some level of impairment on the number of cells with SG (Figure 14A). Therefore, the next step was to quantify the number of cells with SG. In the absence of treatment, mock-infected (black bars) and TBEV-infected cells (gray bars) formed SG at a rate of 0% and 5%, respectively, as observed before. On the other hand, ARS, PIC, and Tg treatments of mock-infected cells induce SG assembly abundantly, between 60 and 100 %. In the graph of Figure 8B, the percentages of infected cells with SG normalized to those found in mock-infected cells are reported. TBEV inhibited about 20 % of SG formation when induced by ARS and Tg, while it significantly inhibited 40% of PIC-stimulated SG formation (Figure 14B). The current results demonstrate that TBEV can inhibit SG assembly, especially those PKR-dependent.

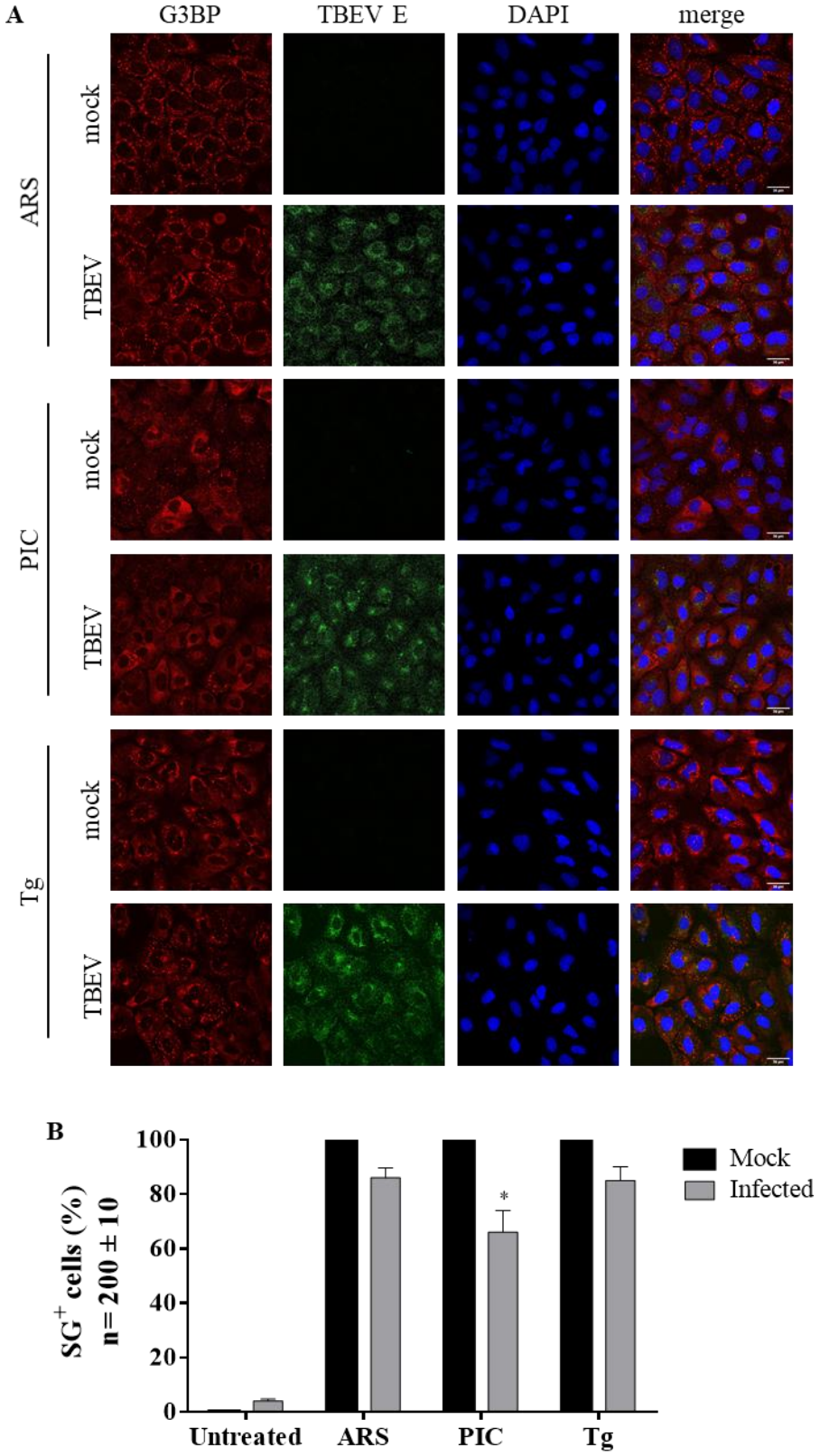

Figure 14. TBEV inhibits stress granules assembly. U2OS cells were infected with TBEV at an MOI of 1. Twenty-four hours post-infection, cells were treated with ARS, PIC or Tg for SG stimulation. Cells were then fixed, permeabilized, and immunostained for IF analysis with α-TBEV E (green) and α-G3BP (red) antibodies. A) Representative immunofluorescence images. B) Quantification of cells with SG. For statistical purposes, 200±10 cells were counted. Scale bars represent 30 µm. *p≤0.05, unpaired, student's t-test.

3.3.Stress granules formation after TBEV infection is PKR-dependent

Gene silencing was used to study whether SG formation upon TBEV infection was explicitly dependent on one of the two ISR kinases that seem to be more involved with cellular response against *Flavivirus* infection, PERK, and PKR. The technique selected was genome integration of a short hairpin sequence designed to interfere with mRNA translation using vectors based on *Lentiviruses*. U2OS cells stably interfering with the expression of PERK (U2OS_shPERK) and PKR (U2OS_shPKR), and control with non-target short hairpins (U2OS_shSCR) were produced as described in the methods session. After puromycin selection was complete, knockdown was confirmed by western blot (Figure 15A and 15B), with β-Actin as the loading control.

Cells were plated onto coverslips, infected with TBEV at an MOI of 1, treated with TM and processed for IF using anti-E and eIF3 antibodies at 24 hpi. Confocal images were acquired, and the phenotypes were quantified manually using the ImageJ software. Figure 15C shows the percentage of infected cells (white bars) and cells infected and treated with tunicamycin (black bars). It is possible to observe that all the cell lines studied have the same pattern of infection at late time points. The ability of those cells to form SG was also analyzed. The U2OS_shPERK shows percentages of infected cells with SG comparable to those observed in U2OS_shSCR, with and without TM treatment. In contrast, there were no SG observed in TBEV-infected U2OS_shPKR cells. When UPR is pre-activated with tunicamycin, there is a low percentage of SG positive cells also in U2OS_shPKR sample which could be related to PERK activity (Figure 15D). This result indicates that the PKR protein is indispensable for SG formation after TBEV infection.

The proteins knockdown does not affect viral replication - which demonstrates that PERK and PKR are not indispensable for TBEV replication - as shown with plaque assay (Figure 15E), nor levels of viral RNA analyzed by RT-qPCR (Figure 15F). Further, a functional analysis demonstrates the inability of knocked-down cell lines to produce SG stimulated by specific inducers. Monolayers of U2OS_shPERK, U2OS_shPKR, and U2OS_SCR were treated with ARS 1mM in cell culture medium for 30 minutes, transfected with 500 ng of PIC using Lipofectamine LTX for 4 hours or treated with 10 µM of Tg in culture medium for 1 hour. Cells were then PFA fixed, immunostained using antibodies against G3BP, and analyzed with the confocal microscope. As shown in Figure 10G, the cells that were not treated with inducers (mock) did not form SG, while arsenite treatment stimulated SG

formation in all three cell lines at a frequency of 100 %. Impairment on the percentage of SG-positive cells was observed when treating a cell line with a kinase inducer for which the cell had been knocked-down. Therefore, U2OS_shPKR has a low percentage of cells with SG when treated with PIC, U2OS_shPERK when treated with Tg, and finally, U2OS_shSCR shows a good response to all stimuli. All together these results indicate that the proteins knockdown is specific and efficient, and that the induction of SG upon TBEV infection is PKR dependent.

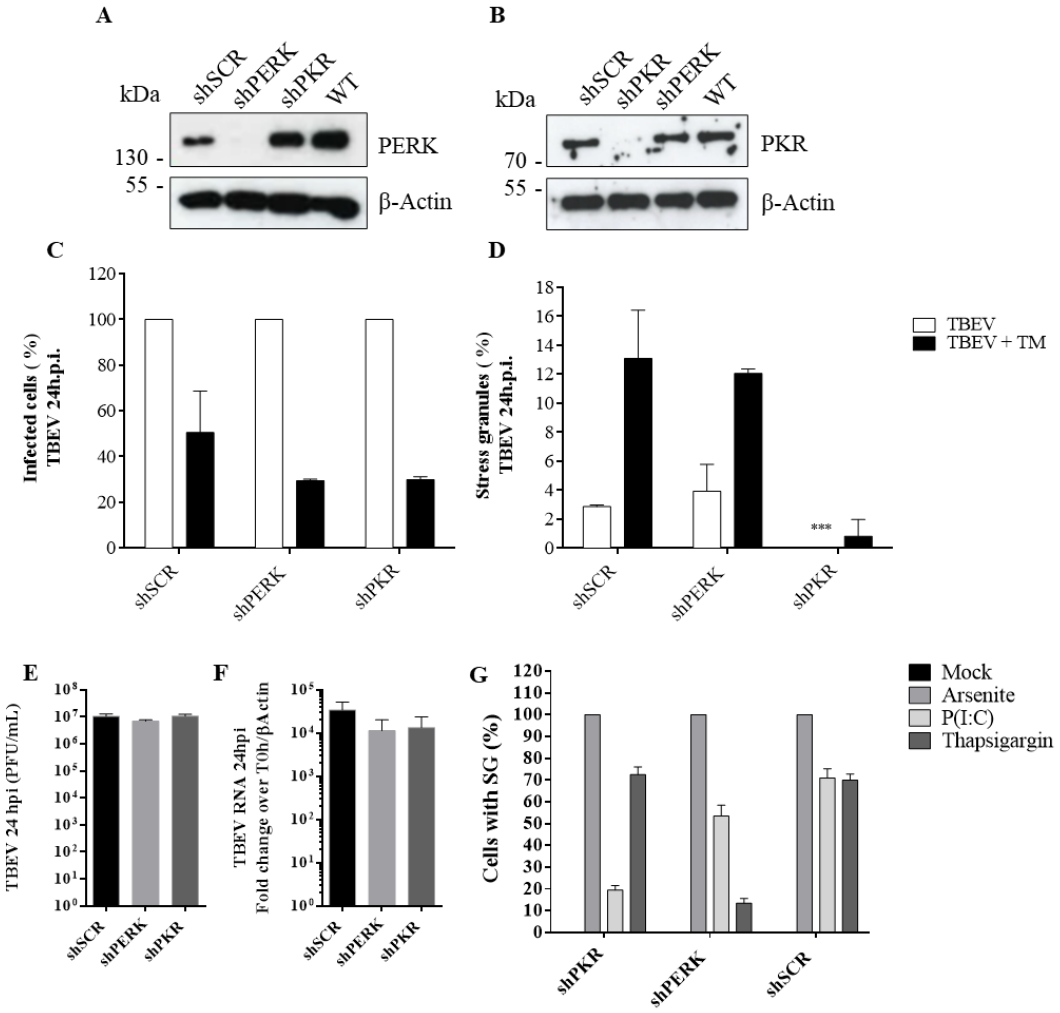

Figure 15. Stress granules formation in TBEV-infected cells is PKR dependent. U2OS cells were knocked-down for PERK and PKR proteins. The upper images show western blot analysis of KD cells for A) PERK and B) PKR. Cells were infected with TBEV at an MOI of 1 and treated with 0.1 µg/mL of tunicamycin, with appropriate controls, as indicated. C) Percentage of knocked-down cells infected with TBEV and treated with TM. D) Percentage of infected cells with eIF3 containing SG. Viral replication was analyzed by both E) plaque assay and F) qPCR. G) Functional analysis of SG formation using different inducers. For statistical purposes, 200±10 cells were counted. ***$p \leq 0.001$ unpaired, student's t-test.

3.4. Single-cell analysis shows that viral dsRNA is released from replication vesicles to form PKR-dependent stress granules

In virtually every case studied to date, the activation of PKR in virus-infected cells is associated with the induction of an antiviral state (Garaigorta & Chisari, 2009). For that reason, many viruses have evolved molecular mechanisms to prevent PKR activation, presumably to inhibit the type I interferon response or to ensure host translation machinery remains sufficiently active for the synthesis of viral proteins. Strategies to prevent PKR activation often include expressing viral proteins that interact directly with PKR or bind and sequester dsRNA, and activating host proteins that inhibit or counteract PKR activation (García et al., 2007).

The previous observations support the hypothesis that dsRNA is released from replication vesicles, activates PKR, and starts the downstream cascade. Therefore, it was decided to use selective plasma permeabilization with streptolysin O (SLO) to test the hypothesis. SLO is a bacterial toxin that binds to cholesterol on the surface of mammalian cells, where it oligomerizes to form large pores in the plasma membrane (Walev et al., 2001). The aim was to avoid permeabilization of the ER membrane so that detection of dsRNA replication intermediates in the cytoplasm would indicate release of PKR substrates from replication vesicles (termed unmasking). Moreover, a higher dsRNA unmasking would be expected in TM-treated cells, in line with previous observations showing that UPR pre-activation promotes earlier antiviral responses.

U2OS cells were plated, infected, and TM-treated as previously described. After 8 or 16 hpi, cells were either fixed with PFA and permeabilized with 0.1 % Triton X-100 (TRI) in PBS, which permeabilizes all cellular membranes, or permeabilized with SLO at a final concentration of 1 U/mL and then fixed with PFA. SG were stained with anti-eIF3 antibody, and replication intermediates were stained with the J2 anti-dsRNA antibody. The time-points mentioned above were selected considering that it was already established that cells with SG start appearing from 16 hpi upon TBEV infection and that at 8 hpi there is no formation of SG (Figure 12D).

As controls of the experiment, no specific signal for dsRNA was detected in mock-infected cells, while not permeabilized cells showed a faint signal in only few cells for the cytoplasmic marker eIF3 (Figure 16). In contrast, the dsRNA signal was detected in all slides with cells infected with TBEV, regardless of the permeabilization method. Furthermore, in every condition, all cells permeabilized with SLO or TRI presented a signal for eIF3 (Figure

16). It indicates that SLO is efficient in permeabilizing the plasma membrane and that any substrate available in the cytoplasm should be detected by their respective specific antibodies.

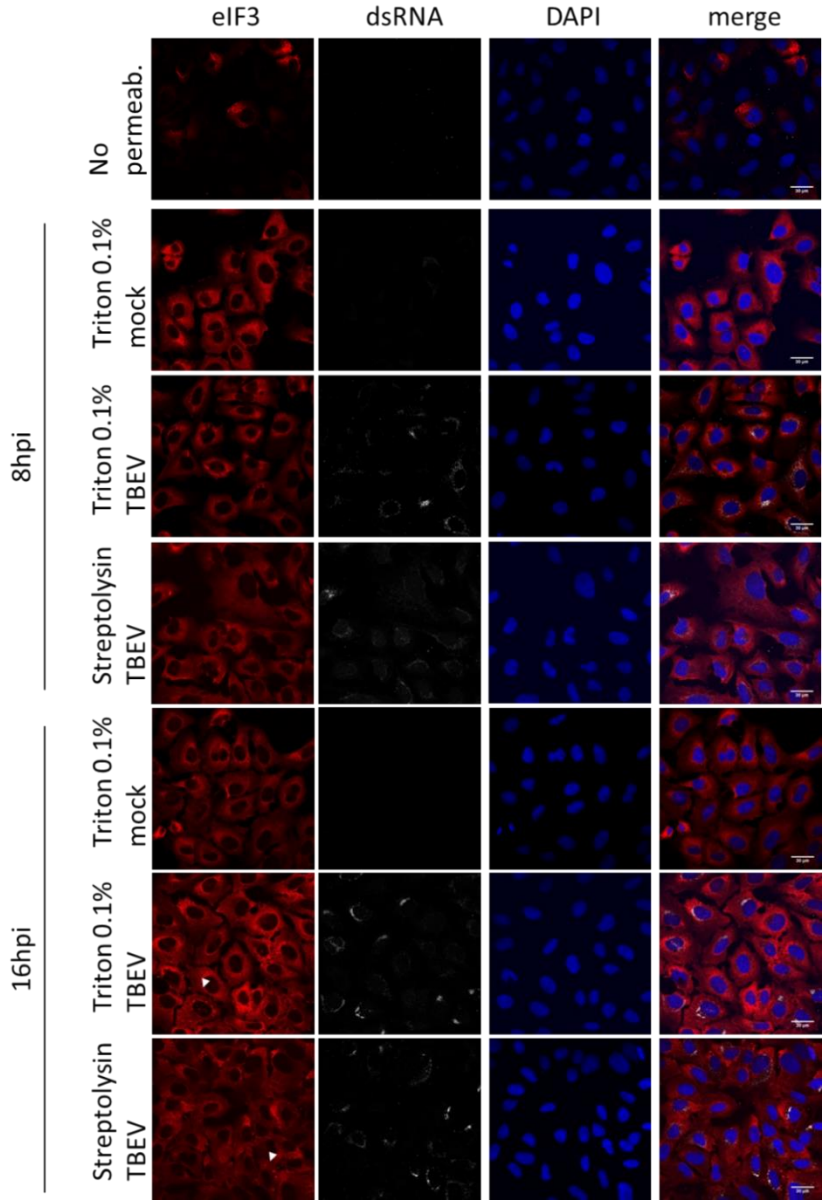

Figure 16. Subcellular localization of viral dsRNA. Cells were infected with TBEV (MOI 1) or left uninfected (mock) and, at the indicated times, were treated either with 0.1% triton X-100, or with SLO at a final concentration of 1 U/mL. Cells were then prepared for immunodetection of eIF3 (located in the cytoplasm and SG marker) and dsRNA (located in or outside the ER and infection marker); nuclei are shown in blue with DAPI staining. A control of not permeabilized mock cells is shown in the first line. White arrows indicate stress granules. Scale bars represent 30 µm.

Multiple confocal images were acquired for each condition, and quantification of the dsRNA mean fluorescence intensity (MFI) in individual cell cytoplasm was accessed using ImageJ software. In order to effectively measure such a subtle thing as fluorescence intensity difference, the same acquisition parameters were used during microscopy analysis for slides of different groups with the same time point. Cells with dsRNA MFI higher than the average value of the background signal found in mock cells (respective to each condition) were considered infected.

Permeabilization with TRI showed a higher percentage of infected cells when compared to SLO-permeabilized cells. For example, at 8 hpi, TRI-permeabilization of TBEV-infected cells showed 53% of infection, against 39% on SLO- permeabilized cells (Figure 17A and 17B). Similarly, at 16 hpi, the percentages of infected cells were 91% and 63%, with TRI and SLO, respectively (Figure 17C and 17D). This difference is expected since TRI reveals the whole amount of dsRNA produced as replication intermediates while SLO makes detectable only those released in the cytoplasm. Figure 17E shows an example of an analysis of confocal images, with ImageJ as describe in materials and methods.

Finally, a statistical analysis of the dsRNA MFI values was performed. Normalizing the values found in SLO-permeabilized samples with those found in TRI-permeabilized helped to understand the difference between the conditions to measure the amount of dsRNA released in the SLO-permeabilized cells. The following equation was applied:

$$\text{Unmasking } \% = \frac{1 - (\text{SLO MFI} - \text{TRI MFI})}{(\text{mock MFI} - \text{TRI MFI}) \acute{} 100}$$

The values found in the TRI permeabilization conditions were considered 100 %, and the percentages found in SLO permeabilization conditions represented the amount of dsRNA in the cytoplasm. The frequency of unmasking in cells infected at 8 hpi is around 10 %, which is the condition where there is no formation of TBEV-induced SG. Interestingly, the values found in cells infected and TM-treated at 8hpi are the same as those without TM treatment. Thus, it could indicate no unmasking happens at 8 hpi, and another eIF2α kinase forms the SG observed with TM treatment (Figure 17F). On the other hand, at 16 hpi the unmasking is higher than at 8 hpi, around 35 %, and this process is even more evident when UPR is pre-activated, reaching 55 % (Figure 17F). These observations indicate that after 16 hours of

infection an appreciable amount of viral dsRNA released from replication vesicles reach the cytoplasm to activate PKR, and there seems to be a threshold, which is not reached at 8 hpi, that determines the formation of these PKR-dependent SG. Important to mention that the time in which the dsRNA is unmasked coincide with the time of IFNβ induction (previous work).

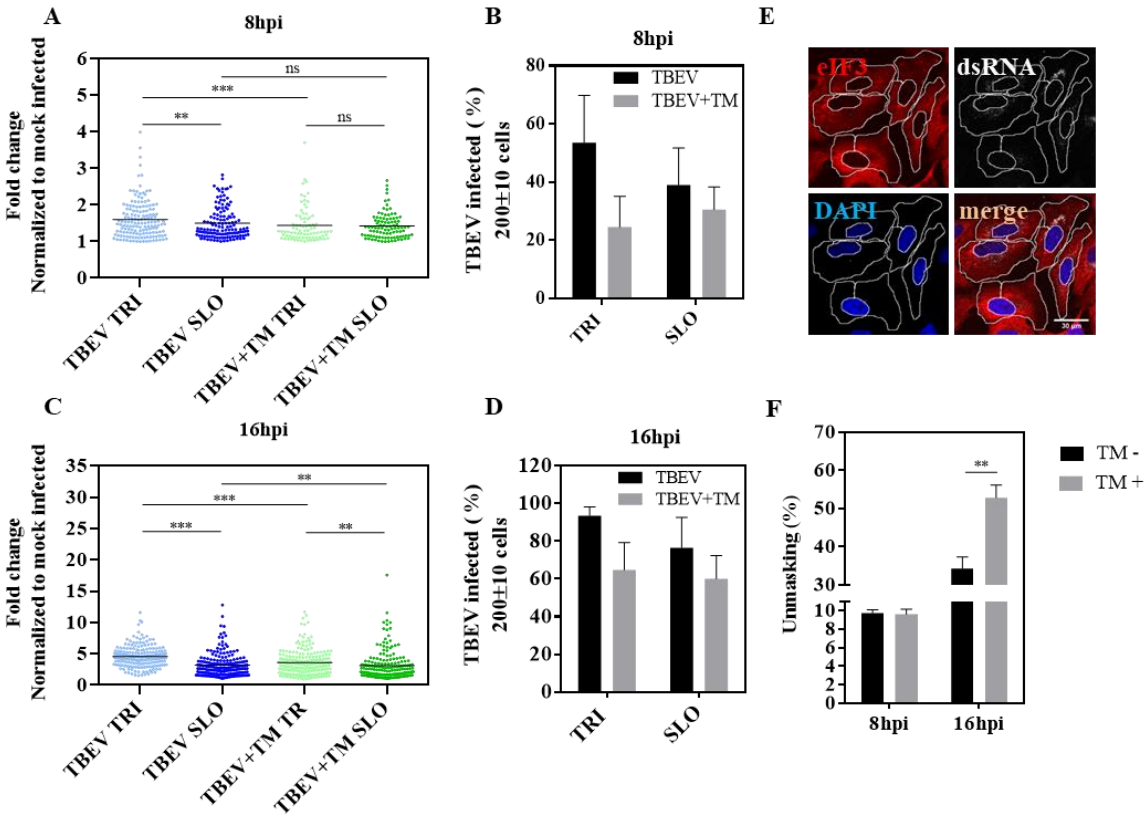

Figure 17. Single-cell analysis shows that dsRNA is released from replication vesicles starting at 16hpi. TBEV-infected U2OS cells were either permeabilized with triton x-100 or SLO. Cells were then fixed and treated for immunofluorescence analysis to detect dsRNA (to detect replication intermediates) and eIF3 (to delimitate the cytoplasm) signals. Dot plot of dsRNA fluorescence intensity of individual cells obtained by analyzing confocal images using ImageJ software are shown for 8 hpi (A) and 16 hpi (C); the average values are displayed in B) 8 hpi and D) 16 hpi. E) Example of the IF images used for quantification showing the areas manually chosen for the measurements. F) Amount of dsRNA intermediates released in the cytoplasm in SLO-permeabilized cells in comparison to TRI. **p≤0.01, ***p≤0.001 unpaired, student's t-test.

3.4.1. TBEV suppresses PKR mediated SG formation

Using the single-cell analysis approach also allowed understanding the profile of individual cells with stress granules. As mentioned before, there is no SG formation in infected cells at 8hpi, but when UPR is pre-activated with tunicamycin, SG are detected at this time point. Surprisingly, even if we determined that TBEV-induced SG are PKR dependent (Figure 10D), this kinase's substrate is not available for recognition in TM-treated cells at 8hpi (Figure 12F), suggesting the involvement of another kinase or that the technique is not sufficiently sensitive to detect subtle changes at 8 hpi.

By analyzing the dsRNA fluorescence intensity only in cells with SG it is possible to observe that 90 % of the cells with SG at 8 hpi treated with TM have the MFI lower than the background signal in mock-infected cells, therefore are considered non-infected (Figure 18A). Also, by doing the same statistical analysis described for Figure 17F using only data of SG positive cells (regardless of cells being infected or not), it is possible to observe that there is no unmasking of dsRNA at 8hpi, with or without TM treatment, while the unmasking frequency remains similar for 16 hpi (Figure 18B).

To investigate if cells with SG are the ones in which dsRNA is more available in the cytoplasm or, in other words, if cells with SG are the ones with the highest percentage of unmasking, the dsRNA MFI of individual cells with SG (red dots) was plotted together with the dsRNA MFI of cells without SG (black dots). In the case of samples collected at 8hpi and permeabilized with TRI or SLO, cells with SG have dsRNA MFI values close to the mean of the entire population (Figure 18C). On the other hand, SG-positive cells at 16 hpi are among those with the highest dsRNA signal (Figure 18C). However, when confronting the MFI data of individual cells with the presence or absence of SG, not all cells with the highest levels of unmasking lead to SG formation. It could be related to some viral inhibitory mechanism(s) to prevent PKR activation directly, or even because SG may occur in an oscillating fashion, which creates windows of opportunity for viral polyprotein synthesis as suggested by Ruggieri and colleagues (Ruggieri et al., 2012). This event remains to be further elucidated to understand which viral strategy might interfere with this physiological cascade of events.

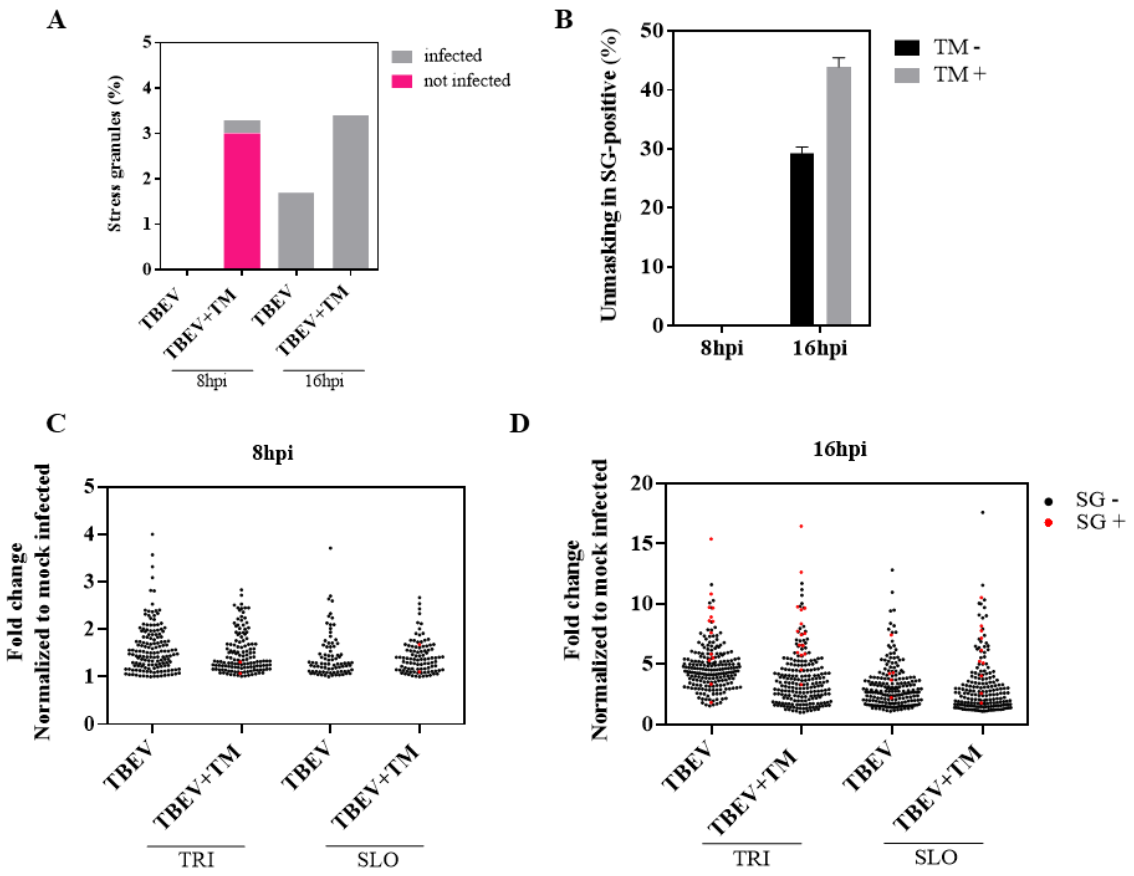

Figure 18. SG-positive cells are not necessarily the ones with the highest dsRNA MFI at 16hpi. TBEV-infected cells were either permeabilized with triton x-100 or SLO; immunofluorescence was performed to detect dsRNA J2 and eIF3 signals. A) Quantification of the number of infected and non-infected SG-positive cells at 8 and 16 hpi. B) Amount of dsRNA intermediates released in the cytoplasm of SG-positive cells in SLO-permeabilized cells in comparison to TRI-permeabilized. Quantification of the dsRNA MFI in individual SG-positive and SG- negative cells using ImageJ software is shown for C) 8 and D) 16 hpi.

3.5.The SG formed are functional and lead to translation stalling

The most fully characterized pathway for SG formation involves phosphorylation of the translation initiation factor eIF2α, leading to the accumulation of stalled translation preinitiation complexes. However, SG can also be induced by alternative mechanisms independent of eIF2α phosphorylation via inactivation of the translation factors eIF4A or eIF4G (Dang et al., 2006; Mokas et al., 2009). Generally, those structures are a response that

prevents abnormal protein generation by transient stalling translation in times of cellular stress.

Puromycin is an antibiotic, an analog of the 3' end aminoacyl t-RNA that associates with growing polypeptides chains leading to premature termination of translation (NATHANS, 1964). In order to investigate if the SG formed upon TBEV infection are functional for protein translation stallment, a puromycilation assay was performed. U2OS cells were mock-infected or infected with TBEV at an MOI of 1. At 24hpi, cells were then treated with puromycin (10 µg/mL) for 5 min, washed with PBS, fixed, permeabilized, and processed for IF. Cells were stained with the SG marker anti-eIF4B and with an anti-puromycin antibody.

In cells infected and not treated with puromycin, there is no detection of puromycin signal. In mock-infected and infected cells treated with puromycin, intense cytoplasmic puromycin staining was detected. In contrast, very low or inexistent levels of puromycin were detected in infected cells with SG. This indicates that the presence of SG in cells infected with TBEV greatly reduces cell translation and that the SG are fully functional (Figure 19).

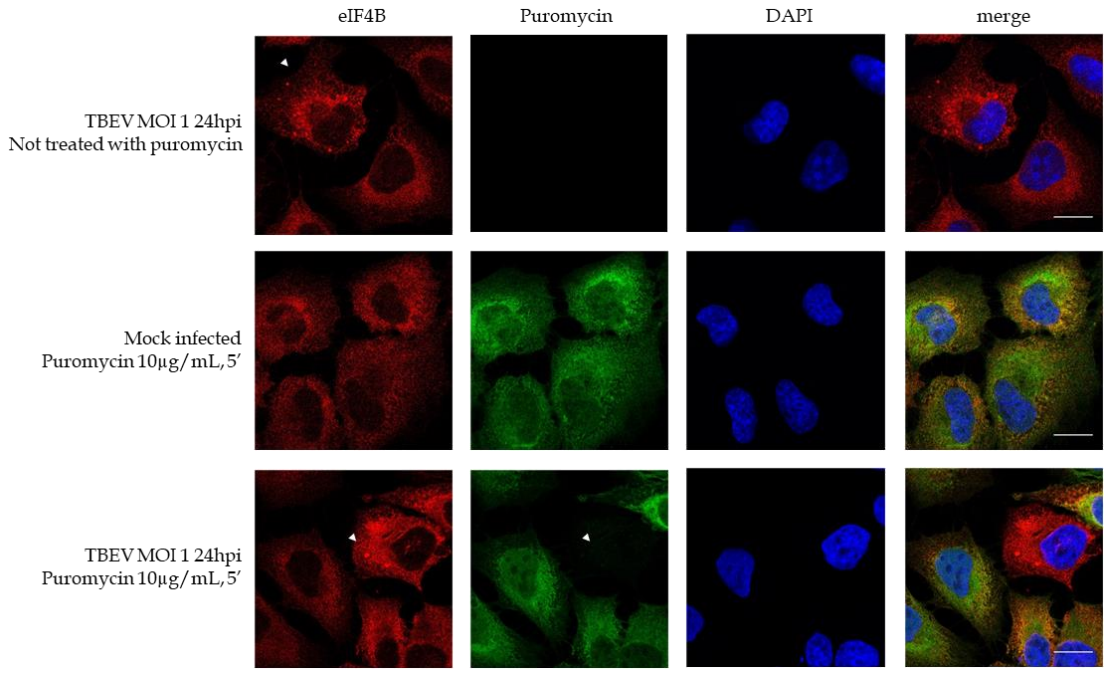

Figure 19. The SG formed after TBEV infection can stall protein translation. U2OS cells were either mock-infected or infected with TBEV at an MOI of 1. SG were detected with α-eIF4B and newly synthetized proteins were detected with α-puromycin antibody. The white arrows indicates cells with SG. Scale bars represent 20 µm.

3.6. NS4B and NS5 proteins inhibit significant and specifically PIC-induced stress granules

Flaviviruses such as ZIKV, DENV, WNV and JEV have been reported to block SG biogenesis (Emara & Brinton, 2007a; Hou, 2017; Katoh et al., 2013) suggesting that its modulation may be of clinical relevance. Based on the data described above, the signaling step(s) targeted by TBEV to disrupt SG formation is likely upstream of eIF2α phosphorylation, when activation of PKR occurs. It was plausible to reason that viral components were responsible for interfering with the SG response, and that ectopic expression of viral proteins would induce the response like it happens during infection. To investigate this, all 7 TBEV non-structural proteins, that have been individually cloned in a high expression plasmid and flanked by FLAG tag (Overby et al., 2010), were screened to identify candidates proteins that may be involved in SG formation modulation. The screen for candidates was only performed in non-structural, because it is mostly among them the viral effectors that modulate cellular responses.

Initially, protein extracts from U2OS cells Lipofectamine-transfected with the non-structural proteins and controls were resolved in an SDS-Page gel and transferred to a nitrocellulose membrane to confirm the expression of the proteins. The western blot analysis shown in Figure 20A demonstrates that the proteins were well expressed, with β-Actin as the loading control. Similarly, the expression was also confirmed by IF analysis where FLAG is visualized in green and eIF4B in red (Figure 20B).

Once confirmed that a good protein expression level was achieved, cells were then submitted to PKR stimulation 16 hours after protein transfection. As shown in Figure 20C, the quantification of the IF results indicates that EGFP does not interfere with the formation of SG as the percentage of cells with SG is comparable to that found in cells mock-transfected and treated with PIC the. In contrast, all viral proteins seem to have some level of inhibition of PIC-induced SG, between 40 and 90% inhibition. It is not yet clear why all viral proteins have some level of inhibition. The most significant decrease in the number of cells with SG upon PIC transfection is observed in the presence of NS4B and NS5 proteins compared to cells stimulated and transfected with EGFP or mock transfected (Figure 20C) suggesting a direct role of these proteins in counteracting SG. For example, Figure 20D shows a representative confocal image of U2OS cells overexpressing NS4B and transfected with PIC. It is possible to observe that the cells positive for FLAG signal (green), cells expressing

NS4B, do not form PIC-induced SG. The same experimental approach was performed using different SG inducers: ARS (Figure 20E) and Tg (Figure 20F) transfected with NS4B and NS5. The effect observed indicates that NS4B and NS5 interference on SG formation is specific to those induced by PKR since the proteins do not significantly reduce the number of ARS or Tg-induced SG.

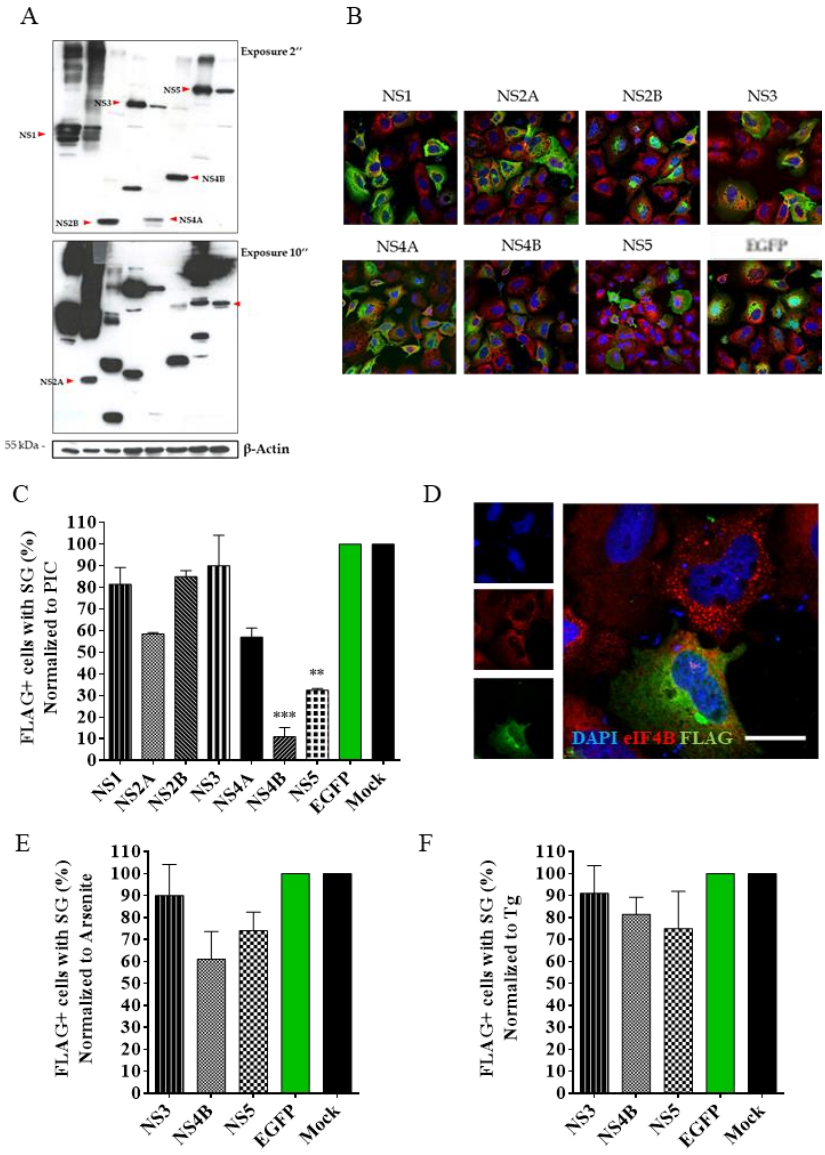

Figure 20. NS4 and NS5 proteins significantly inhibit PIC-induced SG. U2OS cells were transfected with individual non-structural TBEV proteins. Transfection efficiency was confirmed with A) WB and B) IF. C) Cells were transfected with NS proteins and controls. D) Representative image of cells transfected with NS4B and treated with PIC. Cells were further stimulated with E) arsenite and F) thapsigargin as control experiments. For statistical purposes, 200±10 cells were counted. Scale bars represent 20 µm. Values were normalized to the average found in EGFP. The statistical analysis performed was pANOVA < 0.001 comparing EGFP group with all the others.

In order to understand if the expression of these proteins can interfere with the activation of PKR, HEK 293T cells were transfected with NS4B and NS5, previously identified as capable of interfering with the formation of PKR-induced SG; NS3 as a viral protein that does not interfere significantly with SG formation as a negative control; NS5A of Hepatitis C Virus (HCV), that has been described to interact with the dsRNA binding site of PKR and prevent its activation (Gale et al., 1998); and Tat of HIV as an unrelated negative control. All proteins are FLAG-tagged. Then, cells were stimulated with 500 ng of PIC and collected for western blot analysis to study the activation of PKR at the protein level.

The results of the immunoblot analysis are shown in Figure 21. It is important to observe that PKR does not become phosphorylated only by transfecting the proteins. Instead, it is activated upon exposure to the dsRNA mimic, as seen in the lane with the protein extract of cells that had been mock-transfected and stimulated with PIC, as well as in NS3 sample, compared to that of cells mock-transfected and not PIC-stimulated. As expected, NS5A interferes with PKR activation as described elsewhere, while Tat does not. On the other hand, NS4B greatly impacts PKR phosphorylation and so does NS5 but with a lesser extent. Moreover, the effect on PKR phosphorylation impacts the downstream cascade as shown on the blot of p-eIF2α.

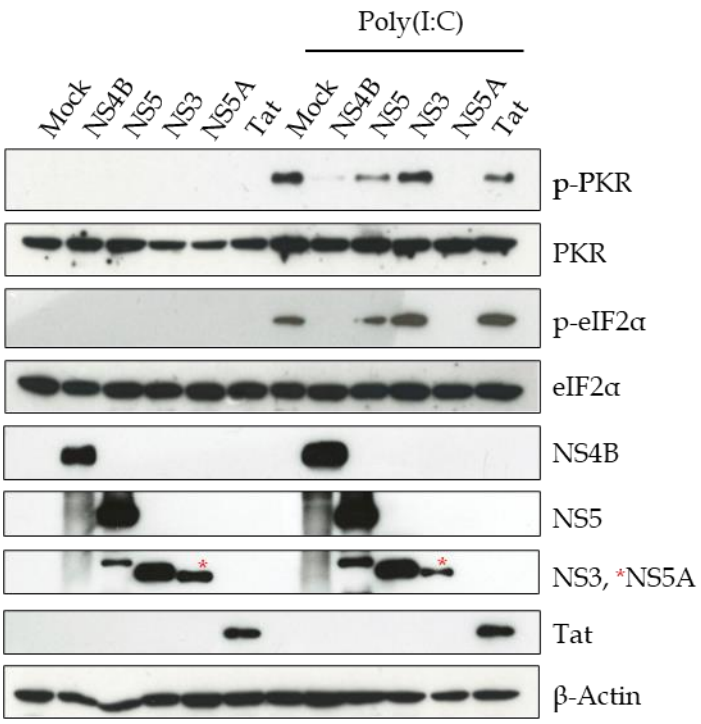

Figure 21. NS4B and NS5 proteins interfere with PKR activation by PIC. U2OS cells were transfected with 500 ng of non-structural proteins, and further transfected with 500 ng of PIC. A) Western blot analysis of total and phosphorylated PKR, and eIF2α, FLAG-tagged proteins (NS4B: 27 kDa, NS5: 103 kDa, NS3: 70 kDa, NS5A: 68 kDa, Tat: 14 kDa) and β-Actin as loading control.

3.7. SG response can be rescued by overexpressing PKR

The next step adopted was to study if the overexpression of the PKR protein could rescue the phenotype of SG formation after PIC transfection, probably by counteracting the effect of NS4B and NS5 proteins on PKR suppression.

First, PKR was isolated by PCR from cDNA samples obtained from RNA extracted from U2OS cells, using specific primers containing the desired restriction sites. Then the insert and the pWPI vector carrying a puromycin resistance cassette were double-digested with the restriction enzymes, followed by dephosphorylation of the vector, ligation, and finally transformation into XL10-gold chemo competent cells (Figure 22A). The colonies obtained were screened by ApaI digestion (Figure 22B) and PCR (Figure 17C), and two of the ten colonies screened were positive for efficient ligation. Colony 5 (C5) was selected for containing the desired construct, confirmed by Sanger sequencing. These bacteria were

further grown and the plasmid pWPI_PURO-PKR was extracted using a MidiPrep kit (Figure 22A).

Lentiviruses carrying pWPI_PURO-PKR were produced as explained in materials and methods, and used to transduce U2OS cells to stably express PKR protein (U2OS_PKR). After selection with puromycin, PKR overexpression was assessed by western blot analysis (Figure 22D) and compared to the expression level of PKR in U2OS *wild type* (U2OS_WT).

U2OS_PKR and U2OS_WT cells were plated on 12-well plates with coverslips and transfected with NS4B and NS5 proteins first, then with PIC using Lipofectamine LTX. Confocal images were acquired staining eIF4B as marker of SG and FLAG, and the phenotype was quantified with ImageJ. The percentages of FLAG-positive cells with SG were normalized to the average value found in mock-transfected cells stimulated with PIC. The results displayed in Figure 22E strongly indicate that PIC-induced SG formation is rescued in the presence of both NS4B and NS5 in U2OS_PKR cells showing around 70 % of cells with SG respectively, as opposed to the result obtained transfecting U2OS_WT cells where NS4B shows 10 % of cells with SG and NS5 25 % (Figure 20C).

Next, aiming at demonstrating a rescue of the SG response in the context of a complex system, U2OS_PKR cells were infected with TBEV at an MOI of 1. Surprisingly, the number of infected cells with SG went from the 5 % observed in U2OS_WT to only 10 % in cells overexpressing PKR (Figure 22F), suggesting that the level of PKR overexpression reached was not enough to saturate the cascade of events leading to SG inhibition during the course of an actual infection, or the approach chosen is not ideal and more factors should be considered. Altogether, these results demonstrate that upon PIC simulation, U2OS_PKR display a higher percentage of cells with SG in the presence of NS4B or NS5. However, this phenotype is not observed when the cells are infected and this result needs to be further investigated.

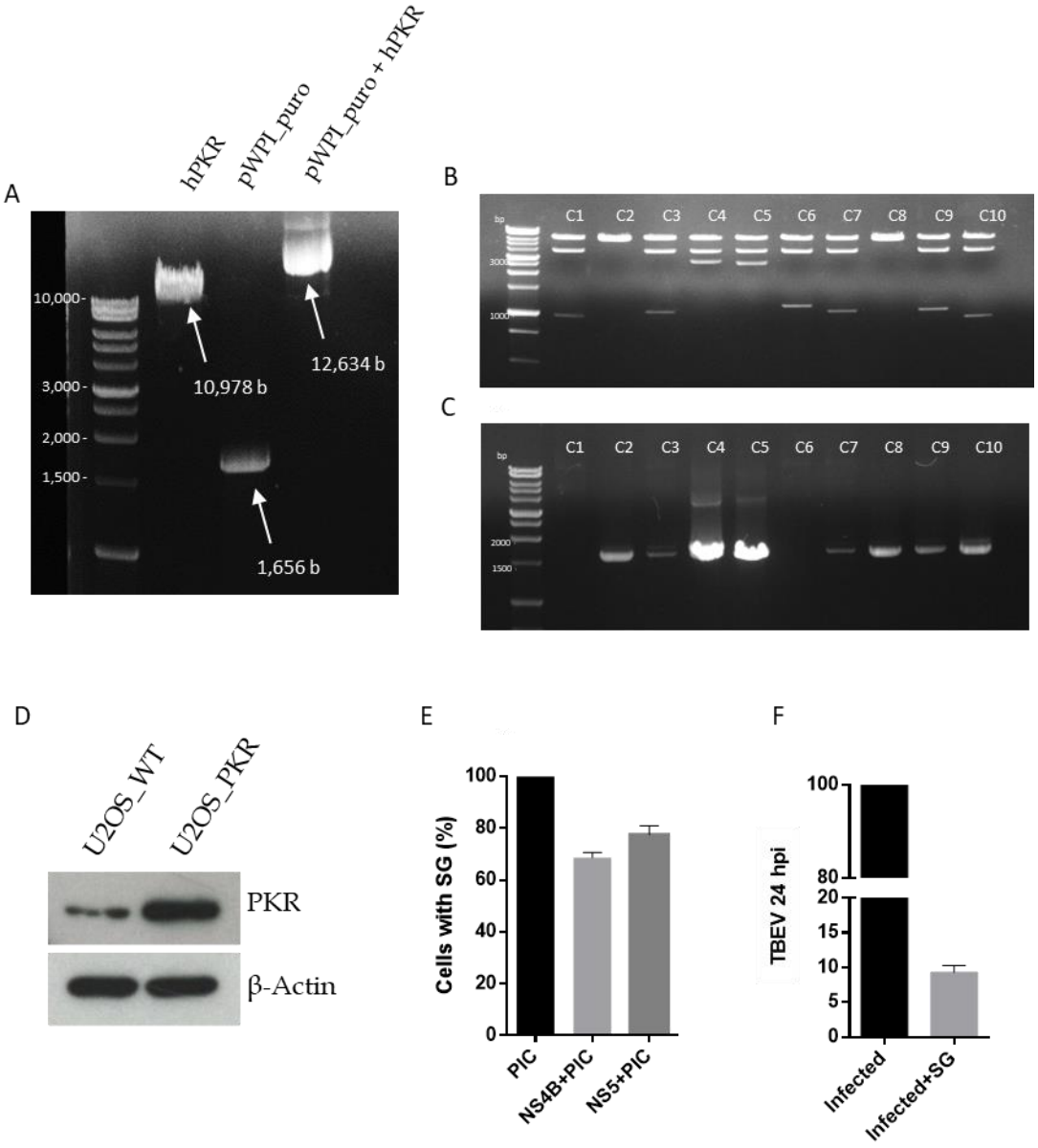

Figure 22. SG formation is rescued in cells overexpressing PKR and transfected with NS4B. PKR protein was cloned to produce stably overexpressing U2OS cells. A) Agarose gel showing insert, vector, and ligation product. Bacteria colonies were screened after transformation by B) ApaI digestion and C) PCR. D) WB shows PKR protein levels in the U2OS_PKR cells compared to WT. E) Percentage of cells presenting SG transfected with NS4B or NS5 protein and treated with PIC. F) Percentage of U2OS_PKR cell infected with TBEV at an MOI OF 1 for 24h presenting SG.

3.8. IFNβ expression is impaired in the absence of SG assembly

IFN induction is the first step through which a host cell mounts a rapid antiviral response and "signals" to neighboring cells that a pathogen has been detected (Kumar et al., 2021). Not surprisingly, antagonizing IFN expression is of advantage to many viruses, particularly during the early stages of infection. As mentioned before, SG formation starts in parallel with detection of IFNβ mRNA at 16 hpi. In order to explore the possible link between SG and induction of IFNβ, the next set of experiments sought to investigate the effects of SG formation deficiency in the innate response and viral replication.

The G3BP1 enzyme mediates stress granules assembly, and its absence prevents SG formation (Matsuki et al., 2013). Therefore, a cell line knocked-out for both G3BP1 and its isoform G3BP2 (U2OS_ΔΔG3BP; kindly provided by Dr. Nicolas Locker), U2OS_shPKR cell line, and U2OS_WT as control were used to perform qRT-PCR analysis of TBEV RNA and IFNβ expression in infected cells treated with TM.

The results displayed in Figure 23 shows that TBEV can replicate 1log more in U2OS_ΔΔG3BP cells compared to U2OS_WT throughout the course of infection. Although, the greatest impact is in the IFNβ where the mRNA is detected 100 times less abundant then in control. Furthermore, UPR activation does not seem to induce an earlier antiviral response at 16 hpi, and an increase of IFNβ mRNA levels can only be detected at 24 hpi. These observations suggest that the knock-out of G3BP plays an important pro-viral role. When looking at U2OS_PKR cells, TBEV seems to replicate less efficiently than in WT cells, in general 1log less. Although a bit more abundant, there is also a longer delay in IFNβ mRNA detection and a similar kinetic pattern compared to U2OS_ΔΔG3BP.

Taken together, the current data suggest that, compared to U2OS_WT cells, there is a marked decrease in IFNβ expression in the cell lines deficient for SG formation (Figure 23, bottom line). It could indicate that SG are critical for the antiviral response supporting the hypothesis that TBEV developed strategies to inhibit their formation for its own benefit.

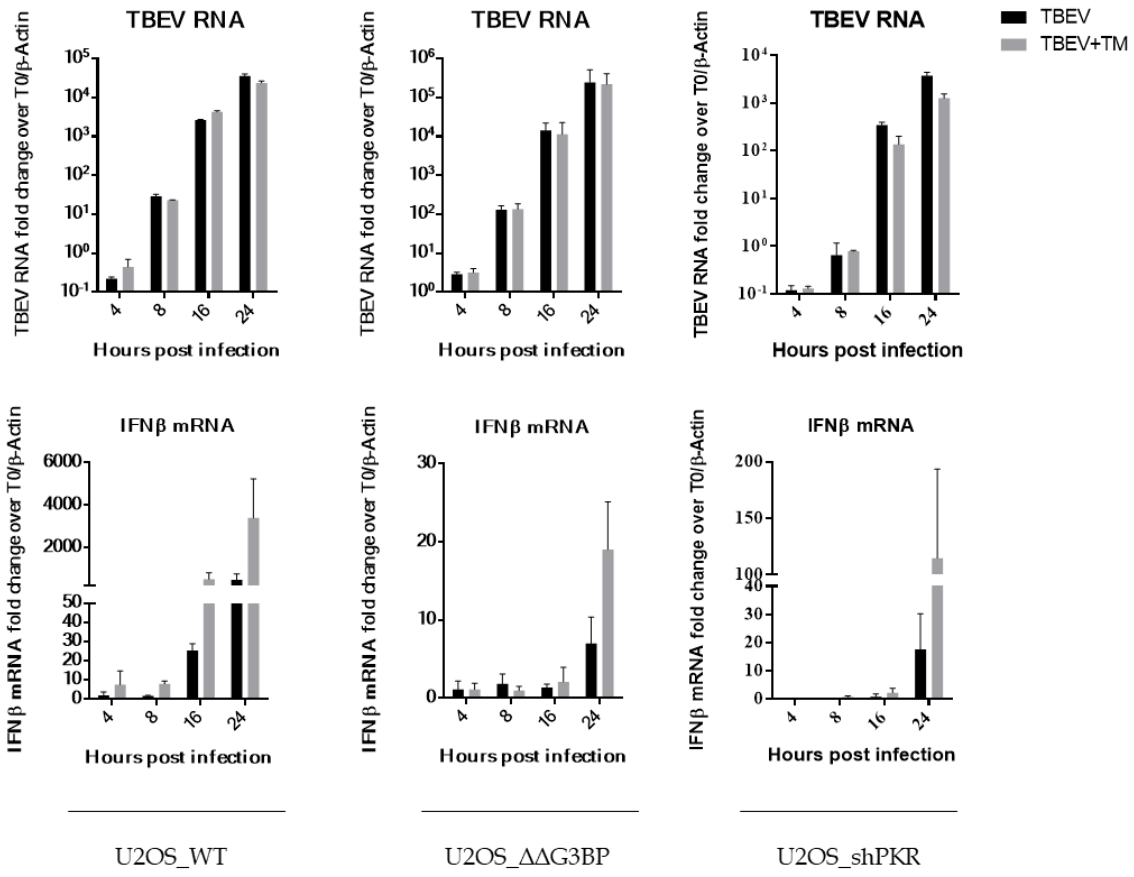

Figure 23. SG formation modulates IFNβ response. U2OS wild type, with G3BP knocked-out or with PKR knocked-down were infected, treated with tunicamycin, and, after indicated hours after infection, collected for qPCR analysis. The top panels show viral RNA levels and lower ones IFNβ mRNA.

4. DISCUSSION

Flaviviruses are the most prevalent arthropod-borne viruses worldwide and comprise over 70 different members (Daep et al., 2014; Gupta et al., 2014). The struggle to control infections is owed mainly to the rapidly evolving nature of viruses, especially RNA viruses, that continuously evade host cell responses. Therefore, the interplay between viruses and innate immunity becomes more addressed each day and studying it is fundamental to find sustained control, vaccines, and therapies.

It was previously demonstrated in our lab that both IFNβ response and SG formation are delayed during TBEV replication. RNAseq identified the UPR as one of the earliest cellular responses activated after infection, and its pre-activation leads to an even earlier and stronger general antiviral state, IFNβ expression, and stress granules formation. This project aimed at understanding if these events are connected and at characterizing the viral evasion of regulation mechanisms. UPR therapeutical modulation would, along with other factors, increase the incidence of SG and, therefore, lead to a stronger antiviral state and a better outcome of the disease.

Although the entire population is infected, I found that only a low percentage of cells form SG. The fully functional stress granules depend on PKR activation by viral dsRNA released from replication vesicles. I could also demonstrate that the NS4B and NS5 proteins can remarkably impair the formation of poly(I:C)-induced SG, and there is a rescue when PKR is overexpressed. Furthermore, cells deficient in the SG response seem to have lower IFNβ activity.

4.1. TBEV restricts the assembly of cellular stress granules

In response to environmental stress, eIF2α is phosphorylated, mRNA is stalled, and RNA-binding proteins are recruited, which accumulate in the cytoplasm to form stress granules. In TBEV infected cells, there is the formation of SG containing G3BP, eIF3, and eIF4B. In a study performed in our lab, we demonstrated that the SG component TIA-1 is an antiviral protein that is trafficked to sites of viral replication to bind TBEV RNA and impair viral translation, and its depletion leads to increased viral replication (Albornoz et al., 2014). However, the actual number of cells that presented this response was not known. Therefore, prompted by this question, I examined the phenotype quantitatively. To address this point, I infected cells with TBEV and treated them with tunicamycin to pre-activate the unfolded protein response. Immunofluorescence analysis at 24 hours post-infection indicated that the number of G3BP and eIF3-containing SG formed in infected cells was quite low, around 5 % (Figure 12B). As expected, I saw an increase in cells infected and treated with TM;

however, it was still meager, around 15 %. A hypothesis to explain that observation was the possibility that the cell line selected for this study was not competent for SG formation, which would induce an artifact and be interpreted as virus-related activity. However, this is not the case since I showed a strong induction of SG by treating the U2OS cells with different sterile stimuli (Figure 14B). These observations argue for a TBEV-induced mechanism to inhibit SG formation in infected cells.

The current subject is not a very explored field of study yet, but it is already established that, for example, along with TBEV (Albornoz et al., 2014), HCV (Garaigorta et al., 2012), and ZIKV (Bonenfant et al., 2019) can induce SG formation in infected cells. While Hou and colleagues showed that ZIKV induces eIF2α phosphorylation (Hou et al., 2017), several earlier studies reported different findings. In these studies, infection of mammalian cells with DENV, WNV, JEV, and ZIKV did not significantly upregulate p-eIF2α levels (Ambrose & Mackenzie, 2011; Elbahesh et al., 2011b; Roth et al., 2017; Tu et al., 2012). In the report by Roth and colleagues, DENV and ZIKV were shown to impair eIF2α phosphorylation induced by exogenous stress through an undefined mechanism (Roth et al., 2017). The discrepancy between some studies may be due to the use of different cell lines (i.e., Huh-7 vs. A549 cells) or virus strains (i.e., ZIKV MR766 strain and PL-Cal strain).

As mentioned before, TBEV infection barely induces the formation of SG in U2OS cells. In this work, I demonstrated that this phenotype is also observed in other cell types, such as neuroblastoma cells and primary skin fibroblasts (Figure 13C). These pioneering observations demonstrate that the findings obtained during this study are not cell type-dependent but rather a general consequence of viral evasion mechanisms from cellular responses. The usage of neural cells is especially relevant considering that TBEV tropism for the central nervous system is critical for pathogenesis, although not much is known about the mechanisms that make human brain cells more susceptible to TBEV infection (Blom et al., 2018; Fares et al., 2020).

4.2. TBEV-induced stress granules depend on the PKR kinase

During genome replication, flaviviruses produce dsRNA that the cytosolic pattern recognition receptors can detect. Although it is still not fully clear how these viral RNA sensors gain access to viral replication complexes, PRR are crucial for initiating antiviral responses during flavivirus infection. My next series of experiments sought to identify the specific ISR kinase responsible for the SG formation observed in TBEV-infected cells, based on two candidate kinases studied in previous studies performed by our group.

Our lab previously determined the kinetics of PERK, PKR, and eIF2α activation during TBEV infection. PERK and eIF2α are phosphorylated early, at 8 hpi. However, while eIF2α sustains and increases the phosphorylation over time, PERK activation peaks at 14 hpi and is downregulated till it is no longer detectable at 24 hpi. PKR phosphorylation, on the other hand, starts at 16 hpi and increases at 24 hpi (Carletti, 2015). Kinetically consistent with PKR activation at 16 hpi, the formation of TBEV-induced SG (Figure 12D) and expression of IFNβ mRNA (Miorin et al., 2012) also happen. This data set led us to hypothesize that SG have an antiviral role as described before for other viruses; therefore, TBEV developed strategies to suppress SG formation.

To define which ISR kinase is responsible for the induction of SG upon TBEV infection, I produced cell lines expressing short hairpin sequences that silence the expression of PERK and PKR proteins using the Lentivirus approach. I determined that TBEV-induced SG are PKR-dependent by showing no SG assembly when this kinase is knocked-down, while the percentage of cells containing SG in PERK knocked-down cells is the same as the control (Figure 15D). In fact, I also demonstrated in Figure 9B that TBEV significantly decreases the number of cells with PIC-induced SG, while TBEV inhibition of SG induced by ARS and Tg is not significant. It indicates that TBEV mechanism to inhibit SG is upstream of eIF2α phosphorylation, specifically targeting PKR activity somehow.

PKR initiates a cascade of events resulting in phosphorylation of eIF2α and stress granule formation. These events are associated with stalled translation initiation complexes, which diminish the capacity of host cells to support viral replication. To illustrate the importance of PKR antiviral activity: both vesicular stomatitis virus and influenza virus replicate with higher titers in $PKR^{-/-}$ mice than wild-type mice (Balachandran et al., 2000). Similarly, $PKR^{-/-}$ mice succumb to infection at a higher frequency when infected with Bunyamwera virus than wild-type mice (Streitenfeld et al., 2003). Another report shows that PKR-deficient mice suffer aggravated pathology and increased lethality following WNV infection (Samuel et al., 2006). Recently, Zheng and colleagues discovered that the nucleocapsid (N) protein of SARS-CoV-2 impairs SG formation by blocking PKR phosphorylation (Zheng et al., 2021).

Moreover, PKR can be activated by detecting dsRNA. It has been shown, however that Flavivirus can shield their replication intermediates from PRR detection. Replication vesicles ensure minimal or no exposure of viral nucleic acids to the host immune system by shielding them from cellular PRRs and nucleases (J. Mackenzie, 2005; J. M. Mackenzie et al., 1999; Miorin et al., 2012, 2013; Overby et al., 2010). These invaginations of the ER

membrane retain an open connection to the surrounding cytoplasm via a pore that could be involved in importing host factors and nucleotides required for RNA replication and exporting newly synthesized viral genomes (Miorin et al., 2013; Welsch et al., 2009). When UPR is activated with tunicamycin treatment, there is an earlier and higher percentage of infected cells with SG (Figure 7C) and IFNβ mRNA levels (Figure 18). One interesting hypothesis is that UPR activation by TM treatment leads to instability of replication vesicles with a not yet clear mechanism, which in turn releases dsRNA earlier than in *wild-type* infection.

By performing selective permeabilization of the plasma membrane, I could identify that dsRNA is released from the replication vesicles at 16 hpi, in a process that we called unmasking (Figure 17F). That pathogen-associated molecular pattern is the substrate to activate the PKR kinase, which in turn phosphorylates eIF2α to form SG. Interestingly, the SG observed at 8 hpi upon tunicamycin treatment are present in cells that, due to the experiment premise, were considered non-infected - it is possible that those cells were infected, but with too low dsRNA signal. Moreover, the method selected for analysis might have had biases in some steps, for example manual selection of the area to study.

Viral infections trigger host cells' inflammatory response that releases cytokines and interferons into the extracellular space. These molecules can then increase the ability of yet not infected cells to fight the virus. Several PRRs have been identified in detecting flavivirus-specific PAMPs, recognizing viral genome and replication intermediates to start the intrinsic cascade of events that culminates in the IFN response. (Suthar et al., 2013). Three types of RNA sensors recognize distinct non-self RNA structures of flaviviruses: the Toll-like receptor (TLR) family (TLR3 and TLR7), the RIG-I-like receptor (RLR) family (RIG-I and MDA5), and PKR (Diamond & Gale, 2012; Ye et al., 2013). PKR is both a cytosolic PRR that detects viral dsRNA, and an ISG capable of controlling viral replication by blocking the translation of the viral genome (Diamond & Gale, 2012). It is highly possible that the same process that allows PKR to be activated and start the antiviral response that aims to restore homeostasis by pausing host translation through SG also activate RIG-I. This hypothesis could alternatively explain why stress granules and IFNβ seem to be kinetically linked during TBEV infection.

4.3. TBEV non-structural proteins can inhibit stress granules

It is important to mention again that SG are formed in only 5 % of TBEV-infected cells at a late time point. It is essential to consider that TBEV has a strong mechanism to inhibit SG.

Very few cells have the SG phenotype, which was enough to start characterizations. However, they might be a glimpse detected through a window of opportunity offered by the technique used to analyze SG. The fixation of cells would only reveal the scenario of that exact moment in which the cells suffered the PFA crosslinking and considering the oscillatory nature of SG (Iadevaia et al., 2022; Ruggieri et al., 2012), it is interesting to wonder whether those cells only showed that antiviral response due to eg. a specific phase of cell cycle that renders the cells more responsive. Therefore, it is highly reasonable to assume that TBEV has a mechanism to counteract the PKR-dependent formation of SG, such as in the case of HCV and JEV that recruit NS5A and NS2A respectively to bind PKR and prevent its dimerization (Gale et al., 1998; Tu et al., 2012).

The non-structural proteins of Flaviviruses are not integrated into the virion but instead, they participate in viral replication, virion assembly, modulation of cellular pathways, and evasion of immune responses (Klema et al., 2015; Roosendaal et al., 2006; Yon et al., 2005; Zou, Lee, et al., 2015). NS3 and NS5 are both large multifunctional proteins and the only two viral proteins with enzymatic activities. With NS2B as a cofactor, NS3 serves as a serine protease that cleaves specific junctions within the viral polypeptide to produce mature structural and non-structural proteins (Chambers et al., 1990). NS5 is the largest viral protein and is comprised of two enzymatic domains: the RNA-dependent RNA polymerase (RdRP) and the methyltransferase (MTase) domain. While the RdRP domain is required for viral RNA synthesis, the MTase domain enables 5′-RNA capping of nascent viral genomes (Ray et al., 2006; Sabine et al., 1999).

NS1 is a glycoprotein that exists in multiple oligomeric forms. In the ER, it is produced as a soluble monomer that dimerizes and becomes associated with the luminal face of the ER to assist in replication complex formation (Scaturro et al., 2015; Westaway et al., 1997; Winkler et al., 1989). In mammalian cells, NS1 can also be secreted as hexamers (Mora-Cárdenas et al., 2020). Exactly how NS1 facilitates viral RNA synthesis is unclear, but it may act as a scaffold that anchors the replication machinery to the ER from the luminal side by interacting with other non-structural proteins that are inserted at the ER membrane (Scaturro et al., 2015; Youn et al., 2012).

The remaining four non-structural proteins, NS2A, NS2B, NS4A, and NS4B, are relatively small membrane proteins with no described enzymatic functions. Although little is known about their precise modes of action, all of them are required for efficient viral replication. NS2A is important for viral genome synthesis and packaging (Kümmerer & Rice, 2002; Xie et al., 2015). NS2B, as mentioned before, is a cofactor for the viral protease NS3; disruption

of the NS2B-NS3 interaction destroys the proteolytic activity of NS3 (Jan et al., 1995; Yusof et al., 2000). NS4A and NS4B induce membrane rearrangements that are crucial for the creation of replication vesicles (Miller et al., 2007; Roosendaal et al., 2006), but their modes of action remain unknown. Finally, mutagenesis studies of DENV and WNV propose NS4B involvement in cell culture adaptation and pathogenicity in animal models (Zmurko et al., 2015), suggesting a more direct role of this protein in viral replication. Dalrymple and colleagues also described that NS4B of both DENV and WNV inhibits activation of IRF3 and thereby reduces the expression of IFNβ (Dalrymple et al., 2015).

To identify protein candidates that could be responsible for inhibiting SG observed during TBEV infection, I screened all non-structural proteins by ectopic expression of single proteins. The structural proteins were excluded from this analysis because we believed that the non-structural would play a major role in this context. In fact, Arakawa and colleagues described this year a rescue on SG formation in JEV sub-genomic replicon cells treated with a drug that inhibits the valosin-containing protein (VCP). In those cells, genome replication and viral protein translation happen without the structural proteins. The group suggested that structural proteins are not involved in JEV-mediated SG inhibition and that SG are strongly formed in infected cells absent of VCP function (Arakawa et al., 2022).

Plasmids containing the single TBEV non-structural proteins (NS1, NS2A, NS2B, NS3, NS4A, NS4B, and NS5) flanked by a FLAG tag (Overby et al., 2010) were transfected into U2OS cells to study whether one or more could be responsible for the inhibition of SG during infection. After protein transfection, cells were stimulated with PIC to initiate the formation of PKR-dependent SG. PKR activation with the dsRNA analog leads to 70% of cells with SG (data not shown). If one or more proteins were to interfere directly with the response, a reduction in this percentage should be expected. As opposed to the control, I observed that, while all viral proteins have some level of inhibition, NS4B and NS5 proteins significantly reduced the percentage of cells with SG (Figure 20C). This observation strongly indicates that those two proteins may play a role in the SG response inhibition. Further western blot analysis showed that NS4B and NS5 proteins could decrease the levels of PKR phosphorylation, with a more evident effect in the case of NS4B (Figure 21).

Once viral dsRNA binds to one of the two double-stranded RNA binding motifs (DRBM) of PKR, the kinase dimerizes and phosphorylates (Cesaro et al., 2021; Mayo et al., 2019). In the literature, the term widely used is auto-phosphorylation since it refers to monomers of the same protein. But I prefer to call it trans-activation because, although monomers of the same protein, they are still two separate entities (Figure 8). The NS4B, and NS5 proteins

could interfere with one of the steps of PKR activation, such as the NS5A protein of HCV that binds to the DRBM and prevents PKR phosphorylation (Gale et al., 1998).

Focusing more in NS4B, it is reasonable to hypothesize that an efficient mechanism dictates the PKR activation state in the abundant presence of this viral protein, considering the strong inhibition of PIC-induced PKR phosphorylation when NS4B is overexpressed (Figure 21). It is known that NS4B has transmembrane domains anchoring it to the replication vesicle and that RV stability is directly dependent on NS4B proper function (D. L. Lin et al., 2019; Zmurko et al., 2015). One explanation could be that at late stages of TBEV infection, the RV are saturated with replication intermediates and proteins, and the pore connecting it to the cytoplasm enlarges, letting dsRNA escape which activates PKR. A similar process would happen with UPR activation, ultimately causing the vesicles to be unstable at earlier time points due to ER stress. In that way, NS4B would then directly bind to PKR, to prevent the monomers from changing conformation or impair dimerization, and eventually avoid PKR transactivation. This scenario is illustrated in Figure 24.

Aiming at neutralizing the effect of the viral proteins on SG formation, a cell line stably expressing PKR was developed. (Figure 22D). After transfecting the cells with NS4B and NS5, I observed that the kinase overexpression rescues the phenotype of SG formation upon PIC transfection, arguing for saturation of those viral proteins' activity by PKR overexpression. Interestingly, when the cells were infected with TBEV, the percentage of cells with SG only doubled compared to U2OS_WT. It could be that the technique used did not induce a level sufficiently high to buffer the effect observed in sterile conditions or the viral mechanism to inhibit the SG formation is much more complicated and require other steps beyond NS4B/NS5 activity to occur efficiently. Another possibility is that the target of the viral proteins is not directly PKR, but another factor required for PKR activation (eg. viral proteins may compete with PKR for dsRNA binding, or they might lead to dsRNA degradation). These observations need to be further investigated.

4.4.Cells deficient in the formation of mature SG have low IFNβ levels

So far, it was demonstrated in this work that TBEV forms PKR-dependent SG at late time points, and that the NS4B and NS5 proteins interfere with different extents to this response. The initial hypothesis was that SG formed upon TBEV infection serve as a platform for the IFNβ response, considering previous observation that IFNβ and SG happen kinetically together.

In a pioneer work, Onomoto and colleagues suggested that viral-induced SG may act as a platform for viral RNA sensing and activation of IFN response. They called the compartments antiviral SG. First, they demonstrated that the NS1 protein of IAV inhibits eIF2α phosphorylation by blocking PKR activation. By infecting cells with a NS1-deficient virus (IAV ΔNS1), they showed that not only the PRRs MDA5, RIG-I, and PKR localize to the IAV ΔNS1-induced SG, but surprisingly also viral RNA. Moreover, they also described that inhibition of SG formation during IAV ΔNS1 infection by silencing G3BP1 reduces the expression of IFNβ (Onomoto et al., 2012). The same group elegantly described further on, using the Newcastle disease virus (NDV) as a model, that the cells with SG are the first ones to start the IFNβ production (Oh et al., 2016). Their findings unraveled a new function of SG as platforms for interaction between viral RNA and host antiviral proteins to initiate the cascade of events of the intrinsic innate response.

To investigate if SG could play a role in the IFNβ response, qRT-PCR analysis was performed in TBEV-infected cells that are deficient on SG formation. The cell lines used were U2OS_shPKR produced in this study and unable to form the PKR-dependent SG, and U2OS_ΔΔG3BP. It has been previously shown that knock-down of G3BP1 leads to the formation of smaller SG, suggesting that stalled mRNA is not sufficiently protected or degraded faster (Aulas et al., 2015). SG have been proposed to be composed of a stable core and a variable shell where proteins and RNAs are dynamically exchanged with the cytoplasm (Jain et al., 2016). It was recently proposed that the UBAP2L protein is essential to SG core, and it acts upstream of G3BP1. UBAP2L-positive SG are formed upon cellular exposure to diverse stresses but it does not inhibit translation, even in U2OS_ΔΔG3BP cells (Cirillo et al., 2020). These models propose G3BP1 as an essential component of SG, along with others such as TIA-1, Caprin1, and TIAR, and its knock-out prevents SG formation (data not shown).

Results showed that without SG formation, cells infected with TBEV have a much lower expression of IFNβ mRNA than WT cells (Figure 23). PKR is both a cytosolic PRR and an ISG capable of controlling viral replication by blocking the translation of viral genome (Diamond and Gale Jr., 2012). It has been proposed that PKR can facilitate activation of IRF3 by interacting with it, but precisely if and how this happens is unclear (Pham et al., 2016). While activation of this kinase induces production of IFNs against WNV infection (Diamond and Gale Jr., 2012), studies of DENV suggest that it is dispensable for IFN-mediated inhibition of viral replication (Diamond and Harris, 2001). Hence, the observations in the case of TBEV remain to be furth elucidated. However, looking at G3BP knocked-out

cells, there is not only a great impairment in IFNβ levels but also an increase in TBEV RNA. It clearly argues for an antiviral feature of TBEV-induced SG.

Iadevaia and colleagues described this year formation of paracrine granules (PG) in bystander cells during Feline Calicivirus (FCV) infection. They are SG-like structures and, although not canonical and different in composition, they are independent of eIF2α and induce translation shut-off. The group demonstrated that PG assembly happens in cells treated with a virus-free supernatant and can impair viral replication. Finally, they propose that as a paracrine stress signal sent from infected cells (Iadevaia et al., 2022). Initially, the same group had already identified that the NS6 protein of FCV can prevent SG formation by cleaving G3BP1 (Humoud et al., 2016), and in fact, PG were shown to be independent of G3BP1 (Iadevaia et al., 2022). In contrast, a virus from the same family, the Murine Norovirus (MNV), does not impair G3BP1 integrity and induces formation of SG-like foci with a different composition from canonical stress granules (Brocard et al., 2020). It was further shown for MNV that G3BP1 has a critical role in the life cycle, being described as a pro-viral protein (Hosmillo et al., 2019). Those are essential contributions to the field and must be considered in different models to investigate if this newly discovered cellular structures may aid not yet infected cells to boost their antiviral response.

Despite being a relatively young field, interesting viral strategies have already been reported for the modulation of SG formation during infection. Given the implication of SG in cell survival, a better understanding of how virus modulates SG formation may help develop therapies to control infections.

5. PERSPECTIVES AND CONCLUSION

5.1.Future directions

This study demonstrates that the TBEV-induced SG are PKR dependent, and that NS4B and NS5 proteins are able to impair phosphorylation of PKR upon poly(I:C) transfection. In this context, a detailed study of protein-protein interactions during TBEV infection could give us more insights into the different strategies adopted to escape the viral stress responses for a successful replication. The first protein to be further studied would be NS4B that, as shown in Figure 16, strongly inhibits PKR phosphorylation. A flexible loop located between transmembrane domain (TMD) 3 and 4, called the cytoplasmic loop, is the only part of the NS4B protein exposed to the host cytoplasm and is speculated to be essential for mediating NS4B interactions with other proteins (Zmurko et al., 2015). It would be interesting to understand if there is physical interaction between the cytoplasmatic loop of NS4B and PKR. Therefore, immunoprecipitation studies and mutations on the TBEV NS4B plasmid could deepen this aspect. In the future, manipulating the reverse genetics system, established by the group of Daniel Ruzek (Haviernik et al., 2021) and kindly shared with us, could further support the findings and better characterize the mechanism for SG inhibition. A model for the hypothesis raised by this work is presented in Figure 24.

TBEV infection can cause an acute disease with neurological symptoms with significant and usually long-term severity (Donoso Mantke et al., 2008; ECDC, 2022a). Currently, there are no approved drug agents against TBEV. In the Region where ICGEB is situated, the treatment protocol for individuals with recent tick bites is based only on observation and amelioration of the symptoms as they come. It would also be interesting to study pharmacological NS4B inhibitors against TBEV infection while a host-directed therapy is unavailable. For example, it would be fascinating to test on TBEV the JNJ-A07 drug aiming to disrupt the possible interaction of NS4B with PKR, which was reported remarkably efficient against DENV, and binds with high affinity to DENV NS4B cytoplasmatic loop with very low cytotoxicity and high barrier for viral resistance (Kaptein et al., 2021). Also the BDAA drug described for YFV which showed that by inhibiting NS4B activity impairs viral replication and increases RIG-I mediated innate immunity (Z. Gao et al., 2022). In this way, the current work would strongly impact the local public health and help reduce the number of severe cases by proposing an early treatment protocol.

The manuscript for this work is in preparation, and further data acquisition on NS4B and NS5-mediated SG inhibition is still ongoing. The results presented are the latest complete data at the time of writing this thesis.

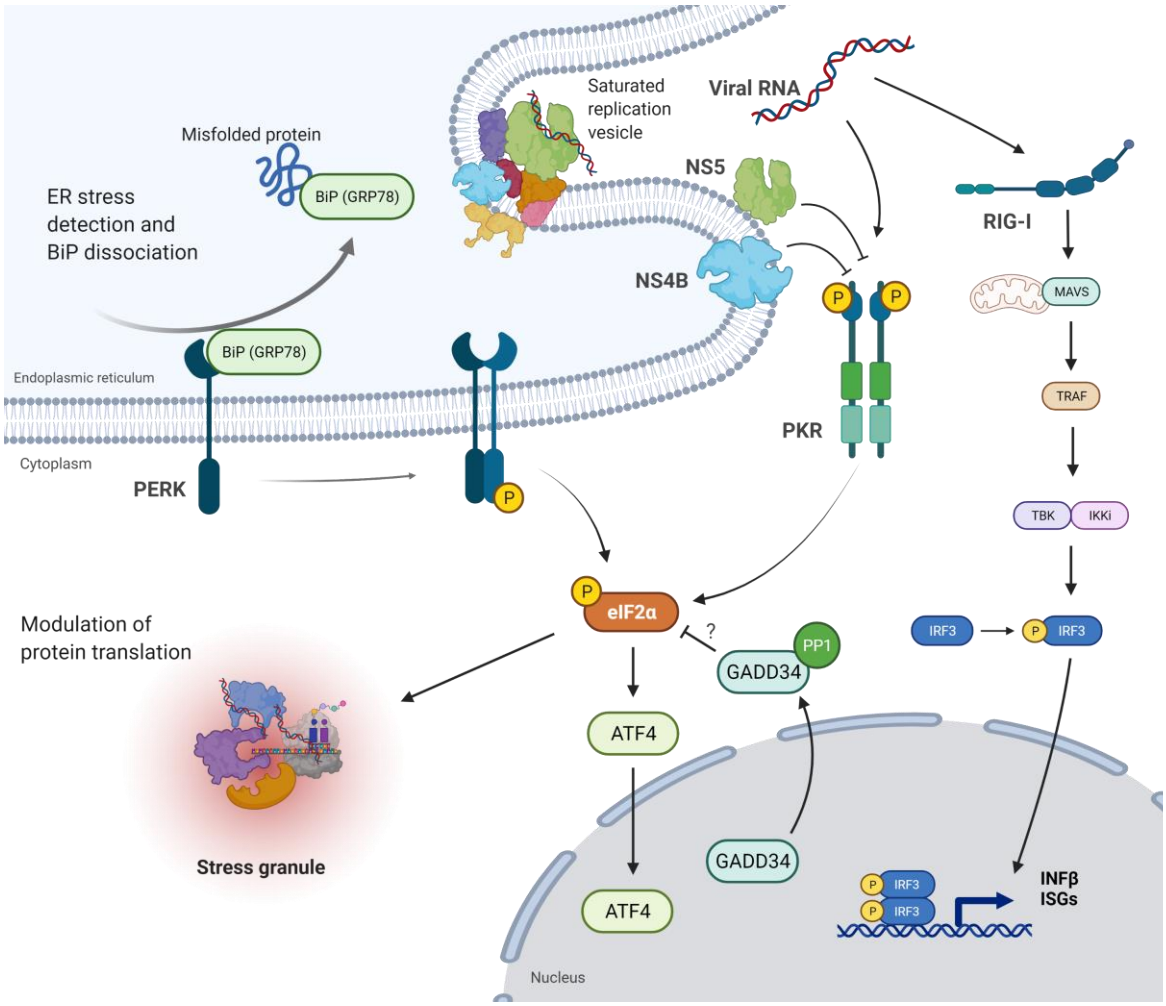

Figure 24. Pathways activated during TBEV infection. Based on the results of this study, a model is here proposed. At early time points, the replication vesicles stably support TBEV viral RNA replication by protecting dsRNA from pattern recognition receptors. Around 16 hours post infection, as the vesicles start to saturate the ER lumen with viral proteins and RNA, the pore connecting the vesicle to the cytoplasm enlarges leading to contemporaneous activation of RIG-I and PKR, and subsequent chain of events downstream of both sensors. Similar outcome can be achieved by chemically pre-activating the unfolded protein response. To escape the modulation of protein synthesis and carry on with production of new virions, NS4B and NS5 proteins inhibits PKR activation and ultimately stress granules formation. Created with BioRender.com.

5.2.Concluding remarks

As obligate intracellular parasites, viruses have evolved diverse strategies to exploit host cell machinery to create favorable environments for replication. Virtually all RNA viruses, including Flaviviruses, encode multi-functional proteins to achieve this goal. From the small

capsid protein to the comparatively large polymerase, Flavivirus' proteins have been shown to interact with a growing list of host factors likely as means to facilitate viral replication and evade antiviral systems. Characterizing these host-virus interactions provides insights into virus biology and advances our knowledge of the cellular processes involved. Furthermore, as demonstrated in this thesis, interactions between TBEV components and antiviral pathways revealed novel insights in SG formation during the viral life cycle. In turn, these findings underline the importance of PRR, and the cellular stress response in controlling viral infections. Further elucidating the interactions between Flaviviruses and the host cell signaling pathways warrants promise for developing new host-directed therapeutic strategies.

PART II

6. INTRODUCTION

There have been several outbreaks of viruses from the Coronavirus (CoV) family in the past. An example is the Severe Acute Respiratory Syndrome (SARS)-CoV that emerged in 2002 in the Guangdong province in China. The virus spread to five continents, infected more than 8,000 people, and caused 774 deaths (Drosten et al., 2003; Ksiazek et al., 2003). In 2012, a new coronavirus named Middle East Respiratory Syndrome (MERS) emerged in the Arabian Peninsula and until this date the virus remains a public health concern in that area. MERS spread to 27 countries infecting over 3,000 individuals and claiming 858 lives (WHO, 2021; Zahid Naeem, 2013).

In December of 2019, the world heard for the first time about the newly emerged Severe Acute Respiratory Syndrome 2 (SARS-CoV-2). It was initially identified in Wuhan, China, and after failed attempts to control it, the virus rapidly spread across the globe raising humongous attention. The World Health Organization (WHO) declared a pandemic on 11 March 2020 (WHO, 2020). To date, the pandemic caused almost 400 million cases and more than 5.7 million deaths (WHO, 2022).

The SARS CoV-2 infectious disease, the Coronavirus disease 2019 (COVID-19), resembles that of SARS-CoV and MERS. It is characterized by enormous inflammatory responses resulting in damage to the respiratory system (Lu et al., 2020; Tan et al., 2021). The consequence to the body is therefore not only due to the viral infection itself, but also the host's immune response. There is great difference between individuals, and characteristics such as age, comorbidities and history of lung disease must be considered; some may experience minor symptoms resembling a common cold, while others can develop the aggressive form of the disease that is often fatal (Tay et al., 2020).

6.1. SARS-CoV-2 entry

Coronaviruses are enveloped viruses with a positive sense, single-stranded RNA genome, ranging from 26 to 32 kb in length, and belong to the *Coronaviridae* family. These viruses present a protein called Spike (S) on the surface, and its crown-like structure inspires the name (crown = *corona* in latin). The S protein has two subunits, S1 and S2. The S1 subunit contains a receptor-binding domain (RBD) that recognizes and binds to the host receptor angiotensin-converting enzyme 2 (ACE2), while the S2 subunit mediates viral cell membrane fusion. The SARS-CoV-2 virion has about 120 nm in diameter with large projections of heavily glycosylated trimeric Spike proteins. Other surface proteins are the membrane (M) and envelope (E) proteins, while, inside the envelope, the nucleocapsid (N) protein wraps the viral RNA (Trougakos et al., 2021; V'kovski et al., 2021) (Figure 25).

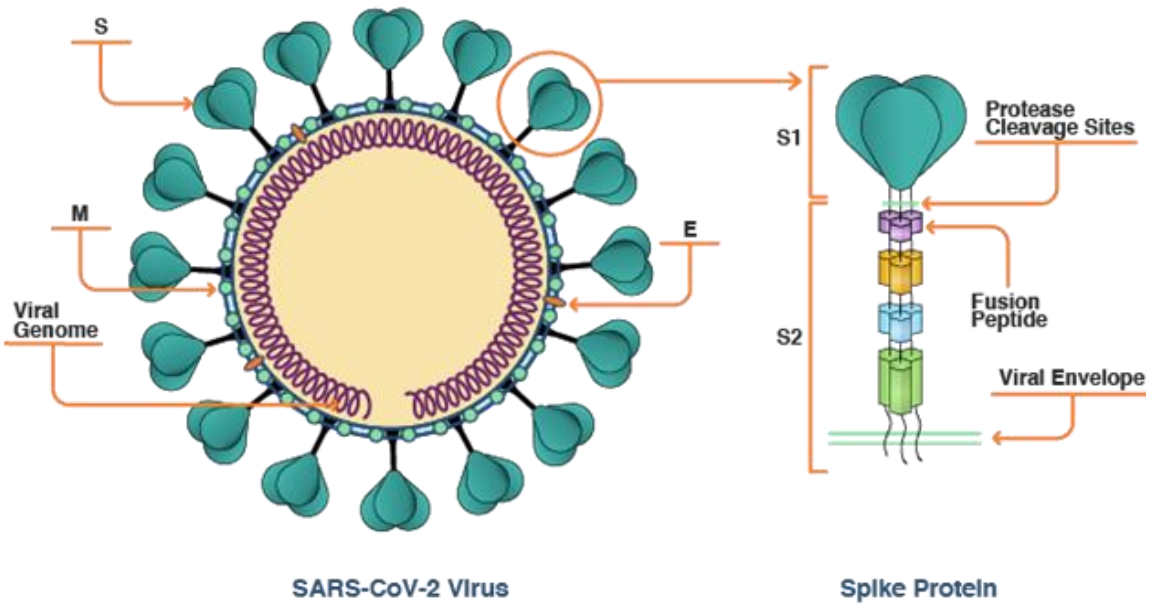

Figure 25. SARS-CoV-2 structure. Adapted from (Granet, 2021)

ACE2 is present in human epithelial cells in the lungs and in the small intestine, but mRNA has also been identified in other organs like the heart, arteries and kidney (Gembardt et al., 2005; Hamming et al., 2004). ACE2 is a membrane-bound protein whose main function is to lower blood pressure by mediating the hydrolysis of angiotensin II into angiotensin (1-7), which works as a vasodilator (Burrell et al., 2004; Chamsi-Pasha et al., 2014).

SARS-CoV-2 has two different potential pathways for entry (Figure 26). In both entry methods, Spike binds to ACE2 via RBD in the S1 region with high affinity (Shang et al., 2020; South et al., 2020). The pathway adopted usually depends on whether human proteases are present to prime the S protein into the two subunits. Several human proteases can cleave the S protein, including transmembrane serine proteinase 2 (TMPRSS2), furin, elastase and trypsin. TMPRSS2 is abundantly expressed in human lungs cells, and it is thought to play an important role in the virus entry into cells from the respiratory system. If the proteases happen to be near the Spike-ACE2 binding interface, they will cleave the S protein to expose the S2 region and the fusion peptides. These fusion peptides are more hydrophobic, or lipid-like, amino acids, and it merges into the cell membrane to induce viral membrane−cell membrane fusion and subsequent entry of the viral genome into the cell (Hoffmann et al., 2020; Mollica et al., 2020; Shang et al., 2020; V'kovski et al., 2021) (Figure 26).

When the virus enters via an endosome, the S1 region binds to the ACE2 receptor translocating the ACE2-virus complex to an endosome. Then, an endosomal acid protease,

called cathepsin L, activates the S protein by cleaving the protein into S1 and S2 (Belouzard et al., 2009). The S2 protein fuses the membrane of the virus with the membrane of the endosome leading to the release of the virus into the cytoplasm (Belouzard et al., 2009; Ou et al., 2020) (Figure 26).

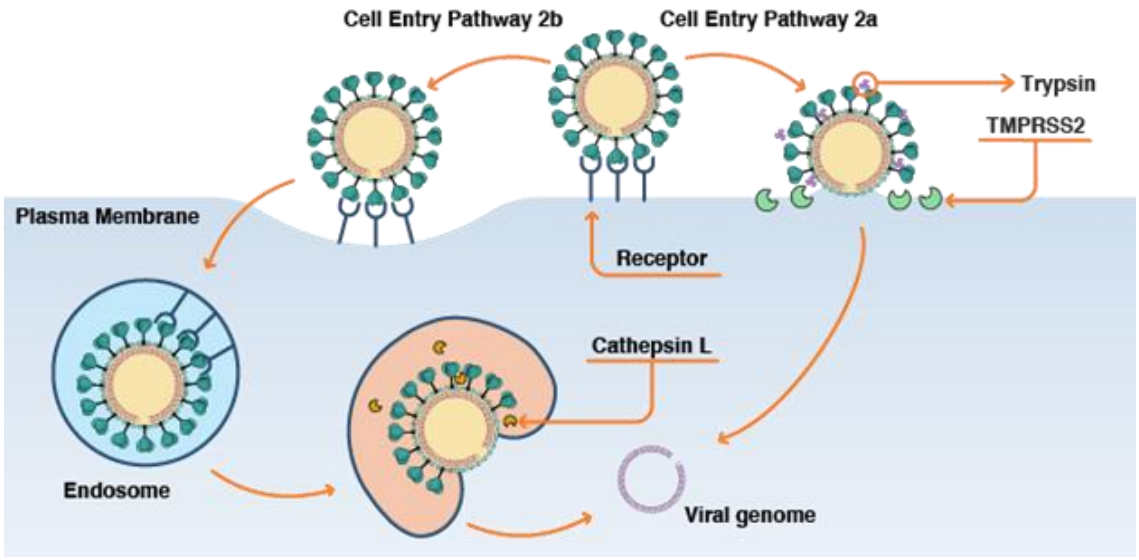

Figure 26. Virus entry. Adapted from (Granet, 2021)

6.2. SARS-CoV-2 replication

Once the viral RNA is released into the host cell it hijacks the replication of the cell to form new virus particles that can infect other cells. This happens in four steps: the translation of viral replication machinery, replication of the genome, translation of viral structural proteins and finally, the virion assembly. When the viral RNA is released into the host cell, the viral genome is first unveiled in the cytoplasm (V'kovski et al., 2021). ORF1a and ORF1ab are translated to produce pp1a and pp1ab viral replicase polyproteins. The polyproteins are cleaved by the Papain like protease (PIpro-) and 3C-like protease (3CLPRO) which are encoded by ORF1a-b. This results in 16 non-structural proteins; NSP1-11 are encoded in ORF1a and NSP12-16 are encoded in ORF1b. These replicase-transcriptase proteins, together with other viral proteins and, possibly, cellular proteins, assemble into the RNA transcription complex, with its main player being the RNA-dependent RNA polymerase (RdRp) (Malone et al., 2022; Ricardo-Lax et al., 2021). This complex drives the production of negative sense RNA through both replication and transcription. Negative sense RNA intermediates are generated to serve as the templates for the synthesis of positive sense

genomic RNA (gRNA) and subgenomic RNA (sgRNA). The RdRp uses the (+) strand gRNA as a template, which will become the genome of the new virus particle. sgRNAs produced through the transcription are translated into structural proteins. Spike, envelope and membrane proteins enter the ER and the nucleocapsid protein is combined with the (+) strand genomic RNA to become a nucleoprotein complex. In the endoplasmic Golgi apparatus complex, the proteins merge into a complete virus particle, and are excreted from primary cells to extracellular regions through the Golgi apparatus via exocytosis. The mature virions can infect new target cells which results in the production of more virus particles (Malone et al., 2022; Ricardo-Lax et al., 2021; Shang et al., 2020; Trougakos et al., 2021; V'kovski et al., 2021)

6.3. COronaVIrus Disease 2019

All things considered, the main question regarding the pathogenesis of SARS-CoV-2 still remains: what is the underlying mechanism that defines whether an individual gets a dysfunctional or healthy immune response to this virus. Even though no conclusive results have been published to answer previous query, some researches have made suggestions for the underlying reasons. The most likely mechanism seems to be the individual differences in the immune response. Other reports suggests a link between the age of the individual and the severity of the infection, which seems to become more severe the older a person is (Rothan & Byrareddy, 2020).

Compared to younger patients, older ones are more likely to suffer severe symptoms, to suffer hospitalization, and to die (Romero Starke et al., 2020). An analysis estimated there is chance of death in confirmed COVID-19 cases at more than 13 % in the group of patients 80 years or older, compared to around 0.15 % for patients in their 30s, and basically zero percent for patients under 20 in China (Y. Zhang et al., 2021). A study of early cases in the USA performed by the Centers for Disease Control and Prevention (CDC) had similar observations (CDC, 2022). It may be explained by the fact that older immune systems tend to be less efficient at clearing viral infections. Liu et al. suggest that the loss of T cells during the SARS-CoV-2 infection may result in aggravated inflammatory responses (J. Liu et al., 2020). Severe COVID-19 is driven not only by viral damage to cells but also by a "storm" of inflammatory cytokines that harms the organs. It is possible that there are age-related changes in the immune system that make the middle-aged and older individuals more vulnerable to this storm than younger ones, even if they are possess good health with no comorbidities (J. Liu et al., 2020; Tan et al., 2021).

Patients who develop severe or fatal COVID-19 usually present at least a major underlying health condition, such as chronic obstructive pulmonary disorder, asthma, diabetes, obesity, kidney disease or cardiovascular disease (Fathi et al., 2021; Zhou et al., 2020). In some cases, the explanations for these links are obvious. For example, diabetes and obesity are associated with a lower resistance to viral infections. It was previously suggested that obesity, especially in men, is associated with treatment requiring mechanical ventilation (Goyal et al., 2020). Asthma and chronic obstructive pulmonary disorder involve lung function impairment, and higher susceptibility to inflammation in the lungs (Zhou et al., 2020).

A study shows that common treatments for high blood pressure and diabetes may worsen COVID-19 risk, since some of the drugs used for treatments can increase the levels of ACE2 (Snyder & Johnson, 2020). Moreover, an unusually weakened immune system, for example due to organ transplants or cancer treatments, that require patients to use immune-suppressing therapy, is another factor that may significantly increase the incidence of severe COVID-19 (Mollica et al., 2020; South et al., 2020; Zhou et al., 2020).

As a single-stranded RNA virus, SARS-CoV-2 has the ability to mutate promptly. Over time, as it spreads around the world finding resistance to infect organisms, it will keep developing genetically distinct strains to adapt. Some of these variants may spread more quickly or cause more severe disease. However, to date there are no evidence that the SARS-CoV-2 circulating variants causes very clinically different diseases from each other or that their genetic differences explain the range of symptom severity some patients may experience (ECDC, 2022c; Gómez et al., 2021).

6.4.Anti SARS-CoV-2 therapy

As of February 2022, five COVID-19 vaccines are authorised in the Europe: Comirnaty (BNT162b2) by BioNTech and Pfizer, Spikevax (mRNA-1273) by Moderna, Vaxzevria (AZD1222) by AstraZeneca, COVID-19 Vaccine Janssen (Ad26.COV 2.5), and Nuvaxovid (NVX-CoV2373) by Novavax (ECDC, 2022b).

While vaccines prevent a virus from infecting an organism by providing immunity, antivirals work to treat the body from an ongoing infection by slowing it down and ultimately stopping it. SARS-CoV-2 vaccines are rightly being celebrated, but antiviral drugs could - and would - have a crucial, life-saving role (Dolgin, 2021; Pardi & Weissman, 2020). Several therapeutical products have been studied to investigate their safety and efficacy as potential agents for COVID-19 prophylaxis or treatment. These include antivirals, interferons and monoclonal antibodies (Hwang et al., 2022; Mei & Tan, 2021; Xiao et al., 2020).

In a communication on 14 December 2021, Pfizer presented data of a Phase 2/3 trial of the oral antiviral PaxlovidTM, a combination of nirmatrelvir, an investigational viral protease inhibitor that blocks the replication of SARS-CoV-2, with ritonavir (Pfizer, 2021). The results of this randomised study with 2,246 adults showed an 89% reduction in risk of COVID-19-related hospitalisation and death rates in patients who were at high risk of progressing to severe disease, compared to placebo-treated patients. Adverse events were mostly mild (Mahase, 2021).

Although scientists and companies are making concerted efforts, most governments are not treating this issue with the same urgency as they have to vaccines. Investigating approaches for a therapy may help the world go through the current pandemic, and to not be as poorly prepared for the next one (Dolgin, 2021).

7.MATERIALS AND METHODS

7.1. Materials

7.1.1. Cells

Mammalian

- U2OS: Human osteosarcoma;
    - U2OS_ACE2: produced in this work; U2OS transduced with a lentivirus carrying ACE2
- Vero E6: African green monkey kidney;
    - Vero E6_ACE2: produced in this work; Vero E6 transduced with a lentivirus carrying ACE2
- HEK 293T: Human embryonic kidney, mut SV40 large T antigen.
    - HEK293T_ACE2: produced in this work; HEK293T transduced with a lentivirus carrying ACE2
- Huh7: Humana hepatocarcinoma
    - Huh7_ACE2: produced in this work; Huh7 transduced with a lentivirus carrying ACE2

Bacteria

- XL10-Gold Ultracompetent Cells (Stratagene - cat.num. 200315). Genotype: Tetr Δ(mcrA)183 Δ(mcrCB-hsdSMR-mrr)173 endA1 supE44 thi-1recA1 gyrA96 relA1 lac Hte [F′ proAB lacIqZΔM15 Tn10 (Tetr) Amy (Kanr)].

7.1.2. Media

Mammalian

• DMEM complete medium: Dulbecco's Modified Eagle Medium (Gibco - cat.num. 31885-023) supplemented with 10% fetal bovine serum (FBS) (Euroclone - cat.num. ECS0180L). For selection of stable cell lines, Puromycin Dihydrochloride (Invitrogen – A1113803) was added at a concentration of 1 μg/mL.

• Cryo medium: for long-term storage cells were frozen at -80 °C in 90% FBS, 10% DMSO.

Bacteria

Luria-Bertani (LB) Medium: 10 g bacto-trypton, 5 g bacto-yeast extract, 10 g NaCl per 1 liter medium. Ampicillin was added at a concentration of 100 μg/ml. For hardening 1.5 % agar-agar was added to the liquid medium.

7.1.3. Drugs

- Miglustat (NB-DNJ) was purchased from Sigma-Aldrich, St Louis, MO, USA (cat. num. B8299) and dissolvedin DMSO to obtain a stock solution, while Celgosivir was dissolved in distilled water.
- The oxysterol 27OHC complexed with 2-hydroxypropyl-β-cyclodextrin (2HP-βCD:27OHC) was kindly provided by Panoxyvir Ltd (Turin, Italy).

7.1.4. Antibodies

Primary antibodies

Target	Species	Source	Catalog number	Dilution
eIF3η	Goat	Santa Cruz	sc-16377	IF 1:100
mSIP-CR3022	Mouse	Produced *in house*		IF 1:200
ACE2	Rabbit	Abcam	ab15348	WB 1:500
β-Actin/HRP	Mouse	Sigma	A3854	WB 1:50000

Table 4. Primary antibodies used in this study

Secondary antibodies

Donkey, anti-mouse IgG, Alexa Fluor 488; 1:500 for IF (Molecular Probes cat.num. A21202)
Donkey anti-mouse IgG, Alexa Fluor 594; 1:500 for IF (Molecular Probes cat.num. A21203)
Goat polyclonal, anti-rabbit immunoglobulins/HRP; 1:10000 for WB (DakoCytomation cat.num. P0448)

7.1.5. Vectors

Plasmid	Relevant characteristics	Source	Catalog number
psPAX2	Packaging Vector	Addgene	12260
pMDG.2	Encodes VSV-G Envelope protein	Addgene	12259
pWPI_PURO	Lentivector with empty backbone and puromycin resistance gene	Addgene	12254

ACE2	Encodes the human ACE2 receptor	Addgene	1786
pWPI_PURO-ACE2	Lentivector expressing human PKR	Produced in this study	

Table 5. Plasmids used in this study

7.1.6. Primers

Name	Sequence 5' to 3'
ACE2 cloning Fw	TTGGCGCGCCATGTCAAGCTCTTCCTGG
ACE2 cloning Rv	AGATACGCGTCTAAAAGGAGGTCTGAACATC

Table 6. Primers used in this study. The restriction sites are indicated in sublined text.

7.2.Methods

7.2.1. Mammalian cell culture

Adherent mammalian cells were cultivated with DMEM supplemented with 10% FBS. Monolayers of cells were grown at 37 °C, 5 % CO_2 in DMEM complete medium. When needed, cells were passaged with 0.05 % trypsin + 0.02 % EDTA and seeded at the appropriate dilution. Passaging and experiments were performed with monolayer around 75 % confluent. Cell culture was done in aseptic conditions, cells were routinely screened for Mycoplasma contamination and new cell stocks were revived at regular intervals.

7.2.2. Plasmid construction

The PCR amplification reactions were performed using the specific cloning primers described in Table 6 and the PFU DNA Polymerase (Promega, cat.num. M774A) according to manufacture's instructions, under the following thermal cycling conditions: 94 °C 5min, - 94 °C 1min, 60 °C 30sec, 72 °C 3min for 35 cycles -, and 72 °C 5min. The PCR product was purified using the NucleoSpin Gel and PCR clean-up kit (Macherey-Nagel cat.num. 740609.250). Further, the pWPI_PURO cloning plasmid and the insert were double digested with AscI and MluI restriction enzymes. After purification, the digested PCR product was ligated overnight at 16°C with gentle agitation using T4 DNA Ligase enzyme (New England Biolabs - cat.num. M0202S) into the linearized pWPI-PURO vector a 1:5 molar ratio.
At every step, the size and integrity of both linearized vector and PCR product were analyzed by separating the DNA in 1 % Agarose gel for 45 minutes at 90V. Gel preparation: UltraPure™ Agarose powder (Invitrogen cat.num. 16500-500) melted in 0.5X TBE buffer

and mixed with 250 ng/mL of Ethidium Bromide. Agarose gels were visualized using the UVIdoc HD2 gel documentation system (UVITEC Cambridge).

7.2.3. Plasmid transformation

XL10-Gold chemo-competent cells were used for transformation of all plasmids in this study. Cells were incubated with the plasmids on ice for 30 min. They were then heat-shocked at 42°C for 45 seconds, moved immediately to ice for 2 minutes followed by addition of LB medium without antibiotics. Cells were then incubated at 37°C for 1 hour with agitation, then were plated onto LB agar with the required antibiotic. They were grown overnight at 37 °C. On the next day, colonies were picked and pre-inoculated into 5 ml of LB medium containing the required antibiotic.

7.2.4. Plasmid DNA extraction

After approximately 16 hours cell growth, plasmid DNA was extracted using NucleoSpin Plasmid (Macherey-Nagel cat.num.1801/003) for minipreps or NucleoBond Xtra Midi (Macherey-Nagel cat. num. 1803/009) for midipreps. Extracted DNA was authenticated by restriction endonuclease digestion and sequencing. Restriction endonucleases and their specific buffers were purchased from New England Biolabs (NEB).

7.2.5. Production of infectious Lentiviral particles

Lentiviral (LV) particles were produced in HEK293T cells using calcium phosphate transfection method. The following mix was prepared:

- 5 µg expression plasmid,
- 3.75 µg psPAX2 packaging plasmid
- 1.25 µg pMD2.G envelope plasmid
- 50 µL of sterile 2.5 M $CaCl_2$ was added to each tube.
- Sterile H_2O to 500 µL final volume

This mixture was incubated for 5 min at room temperature and then added dropwise to 500 µL sterile 2X HBS by gently vortexing and incubated at room temperature for 20 min. The transfection mixture was then added dropwise to the cells and incubated for ~16h. In sequence, the media was changed to remove the transfection reagents and replaced with fresh complete media. Cells were then incubated at 37 °C, 5% CO_2 for 24 h. The following day,

media containing the lentiviral particles were collected and centrifuged at 2250 rpm for 10 min at 4 °C to pellet any HEK-293T cells that were accidentally collected during harvesting. The supernatant was filtered with 0.45 µm sterile filters. The filtered lentiviral stocks were aliquoted and stored at -80 °C.

7.2.6. Transduction of target cells with clarified *Lentiviruses*

To produce stable cell lines with silenced target proteins, $3x10^5$ U2OS cells were prepared in 1 mL together with 1 mL of LV suspension + 6 mL of complete medium. The mixture was plated in 10 cm dishes and incubated at 37 °C. One day after, medium was replaced with fresh complete medium to remove excess of reagents, and on the next day, complete medium containing 1 µg/mL of puromycin was added to start selection. A control plate of not transduced cells was also subjected to puromycin treatment as an indicator of the selection status. Silencing efficiency was evaluated by WB analyses.

7.2.7. SARS-CoV2 infection of cells

Working stocks of SARS-CoV2 ICGEB-FVG_5 isolated in Trieste, Italy, were routinely propagated and titrated on Vero E6 cells. Plaque assay was performed by incubating dilutions of SARS-CoV-2 on Vero E6 monolayers at 37 °C for 1 h, which were then washed with phosphate buffered saline (PBS) and overlaid with DMEM 2% FBS containing 1.5% carboxymethylcellulose (CMC, Sigma-Aldrich cat.num. C5678) for 3 days. The cells were then fixed with 3.7% paraformaldehyde (PFA, Sigma-Aldrich, cat.num. P6148) and stained with crystal violet 1%. A cytotoxicity assay was performed with Alamar Blue (Invitrogen, cat.num. DAL1100) according to the manufacturer's instructions.

7.2.8. Indirect immunofluorescence assay

Cells were seeded onto 15x15mm glass coverslips in 12-well plates, or onto 12mm round coverslips in 24-well plates. After desired treatment, cells were washed once with PBS and fixed in 3.7 % PFA in PHEM buffer solution for 20 minutes at room temperature. Thereafter, cells were washed three times with PBS followed by and incubation of 5 minutes with 100 mM Glycine in PBS in order to saturate excesses of PFA and to stop the fixation reaction. Cells were permeabilized for 5 minutes with 0.1 % Triton X-100 in PBS and washed three times, 5 min each. Before incubation with antibodies, a blocking step was performed at 37°C for 30 minutes with 1 % BSA and 0.1 % Tween in PBS. Antibodies were

diluted to the desired concentration in blocking solution to prevent unspecific binding. The coverslips were inverted onto 50 µL drops of primary antibody and incubated overnight at 4 °C in a humidified container. After incubation, coverslips were positioned back into plate wells and rinsed three times with PBS + 0.1 % Tween 20 and incubated with secondary antibodies for 1 hour at 37°C. coverslips were finally washed three times with washing solution and mounted on slides using 5 µL of Fluoro-Gel II mounting medium with DAPI.

7.2.9. Next generation fluorescence *in situ* hybridization chain reaction

The solutions and custom-made probes to perform the *in situ* hybridization chain reaction (HCR) of mRNA transcripts were acquired from Molecular Instruments (Los Angeles, California). Cells were fixed with 3.7 % PFA, the reaction was quenched with glycine in 1X PBS for 5 min. Fixed cells were permeabilized with 0.1 % Triton X-100 in 1X PBS for 10 min at room temperature. Following, the online available manufacture's protocol called "mammalian cells on a slide" was followed.

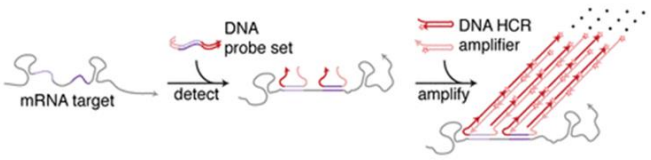

Figure 27. Fluorescent hybridization chain reaction. Adapted from (Choi et al., 2014)

7.2.10. Imaging of fixed cells

Fluorescent images of fixed cells were captured with the Carl Zeiss LSM880 laser scanning confocal microscope. The pinhole of the microscope was adjusted to get an optical slice of less than 1.0 µm for any wavelength acquired. The fluorophore AlexaFluor 488 was excited with 488 nm line of the Argon Laser, while the fluorophore AlexaFluor 594 was excited with the HeNe Laser 543 nm. Their emissions were collected using the appropriate filters. For statistical purposes, 200±10 cells were counted for each condition.

Cells with the desired phenotype were counted using the ImageJ software, and its Cell Counter plug-in. The results are presented in percentage. In case the case of analysing the mean fluorescence intensity (MFI) of a specific channel, the cellular area was selected manually and the average of the fluorescence intensity values was obtained and used to perform statistical analysis.

8. RESULTS AND DISCUSSION

Considering the last worldwide developments regarding SARS-CoV-2 outbreak, the Molecular Virology Lab assumed a pivotal role in ICGEB's response against the pandemic. Our team was lucky enough to have one outstanding leadership inside the laboratory. We took advantage of being one of few places to have a BSL3 facility in the country, and we promptly isolated and sequenced the virus to contribute to the efforts to track mutations (Licastro et al., 2020). Once with an established viral stock, we could collaborate with multiple projects inside and out of the Centre, help public and private companies to install disinfection protocols, and extensively support the local health services with assays, reagents, sequencing, and consulting.

Although it was a stressful and challenging period for everyone (and it still is), we managed to work as a multifunctional team by involving the individuals in tasks according to their expertise to work efficiently and fast in every project. For that reason, I exclusively dedicated my time and efforts to work related to CoV-2 emergency for 9 months, being responsible for the immunofluorescence assays. I was involved in several multidisciplinary projects, and I briefly describe a few of them here.

8.1.Fluorescence *in situ* hybridization of the nucleocapsid RNA

Fluorescence in situ hybridization (FISH) is the most commonly used imaging technique for nucleic-acids in fixed samples. FISH employs the fluorophore-labeled sequence-specific oligonucleotides to reveal DNA or RNA upon complementary hybridization. The concept of imaging nucleic acid via hybridization was first reported in 1969 by Pardue and colleagues. They used the radioactive DNA probe that specifically binds a target DNA via hybridization. This method allowed the visualization of the cellular location of the specific DNA fractions by autoradiography (Pardue & Gall, 1969). The method to fluorescently label nucleic acid was first described in 1982 when a group mapped genes in Drosophila chromosomes by using biotin-labelled probes, an anti-biotin antibody raised in rabbit and a fluorescein-labelled anti-rabbit secondary antibody (Langer-Safer et al., 1982). Since then, FISH has been applied to identify specific nucleic acid sequences as well as reveal the sites for RNA processing, transportation, and localization. In 1998, Femino and colleagues made the breakthrough in single-molecule FISH (smFISH) by designing multiple oligonucleotides that bind along a target RNA to label five fluorophores per molecule (Femino et al., 1998).

A more recent technique called hybridization chain reaction (HCR)-FISH uses a primary set of probes to bind the target RNA in a sequence-specific manner (Figure 27). A pair of fluorophore-labeled nucleotides that form metastable hairpins are then added. The hairpins

bind the readout sequence and start the chain reaction. The signal is amplified by forming a long polymer labeled with multiple fluorophores (Choi et al., 2010, 2014; Dirks & Pierce, 2004).

We purchase from Molecular Instruments the kit to perform HCR-FISH targeting the N gene of SARS-CoV-2 to have specific detection of infected cells. First, Vero E6 cells were infected at an MOI of 0.1 and collected at 24 hpi by fixation with 3.7 % PFA. After following the HCR-FISH protocol described in the methods session using a pair of hairpins labeled with Alexa Fluor 488, images were acquired at the confocal microscope showing that the technique works very specifically (Figure 28). This approach was widely used in multiple projects. It helped observing, for example, that primary cells collected from the respiratory tract of deceased infected patients show different profile of infection.

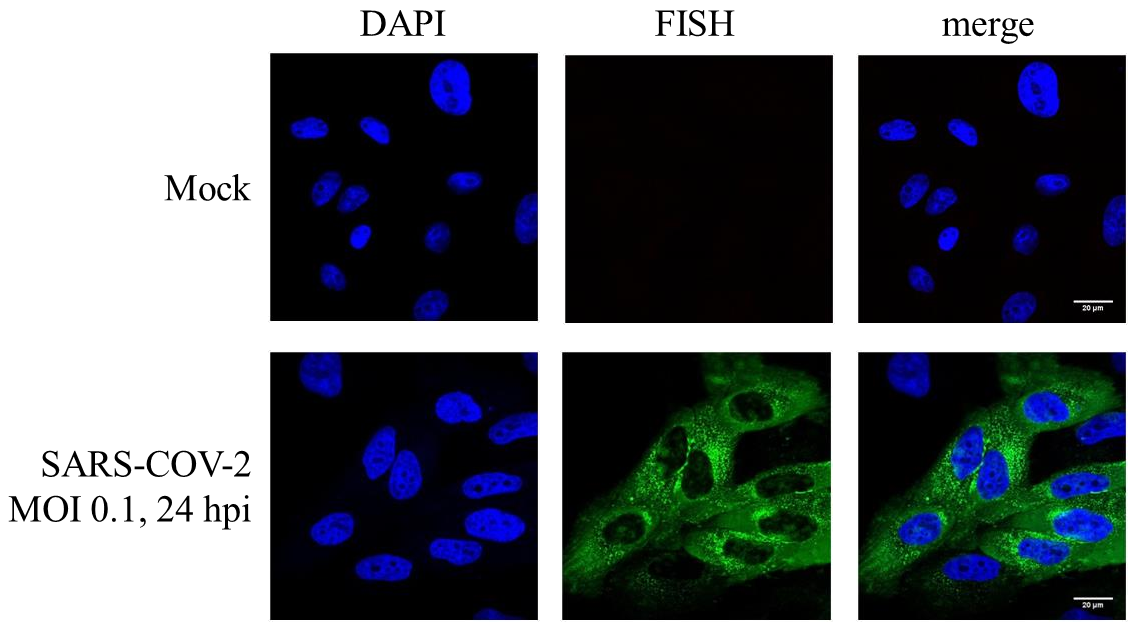

Figure 28. HCR-FISH of the N protein mRNA. Vero E6 cells well infected or mock-infected at an MOI of 0.1 with SARS-CoV-2 for 24 hpi. Cells were then subjected to the HCR-FISH protocol using specific probes for nucleocapsid mRNA. Nuclei were stained with DAPI and are seen in blue, and FISH is seen in green.

8.2. Characterizing the mSIP-CR3022 mouse monoclonal antibody in IF

Our group generated *in house* a recombinant monoclonal reactive with the receptor-binding domain of the S protein based on a mouse small immune protein (SIP) scaffold (mSIP-CR3022) (Rajasekharan et al., 2021). We produced our own antibody since the availability

of reagents and delivery services in the beginning of the pandemic was scarce. Briefly, the DNA fragment encoding for the heavy and light chains of human monoclonal antibodies, clone CR3022 (Meulen et al., 2006; Tian et al., 2020), was synthetized as single-chain variable fragment (scFV) and cloned into a mouse IgG2b expression vector as described previously (Petris et al., 2014). The plasmid was transfected in CHO cells and further purified by the Biotechnology Development Unit (BDU) in ICGEB.

Once the purified molecule was available, I proceeded with immunofluorescence analysis to evaluate if the antibody could bind the target in fixed cells with specificity. Vero E6 cells were plated onto 15mm glass coverslips and infected at an MOI of 0.1 with SARS-CoV-2 for 24 hours. A few concentrations were tested (data not shown) until reaching the optimum of 1:200 dilution (2.75 ng/mL) As shown in Figure 29, non-infected Huh7 cells do not show unspecific signal, in the same way the secondary antibody does not have background signal. Cells infected, treated with the mSIP-CR3022 anti-Spike antibody, and developed with an anti-mouse fluorescent secondary antibody shows what seems to be specific signal to Spike protein.

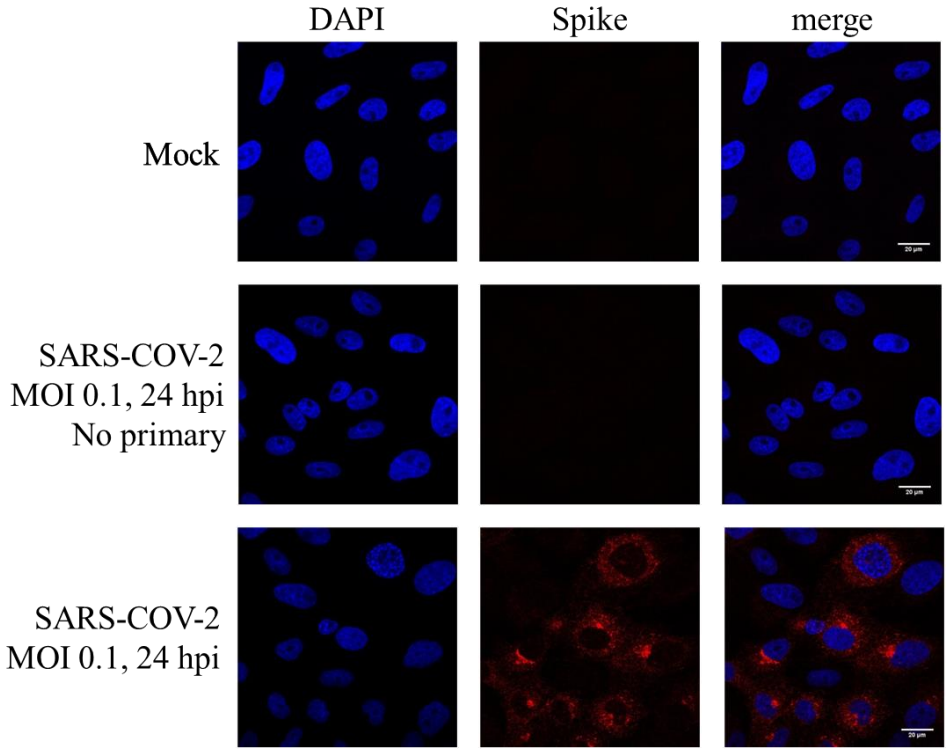

Figure 29. The mSIP-CR3022 anti-Spike antibody can be used in immunofluorescence. Vero E6 cells were infected with SARS-CoV-2 at an MOI of 0.1. Twenty-four hours post-infection, cells were fixed, permeabilized, and immunostained for IF analysis with α-Spike (mSIP-CR3022) (red). Nuclei were stained with DAPI and are seen in blue.

To further confirm the specificity of the signal, immunofluorescence was combined with HCR-FISH. To achieve this, fixed cells were first submitted to the FISH protocol. After development of the signal with the pair of hairpins, cells were then blocked with 1 % BSA and stained with CR3022 antibody. It is possible to observe that both signals colocalize well which demonstrate that the affinity of the produced antibody to the Spike protein is specific (Figure 30).

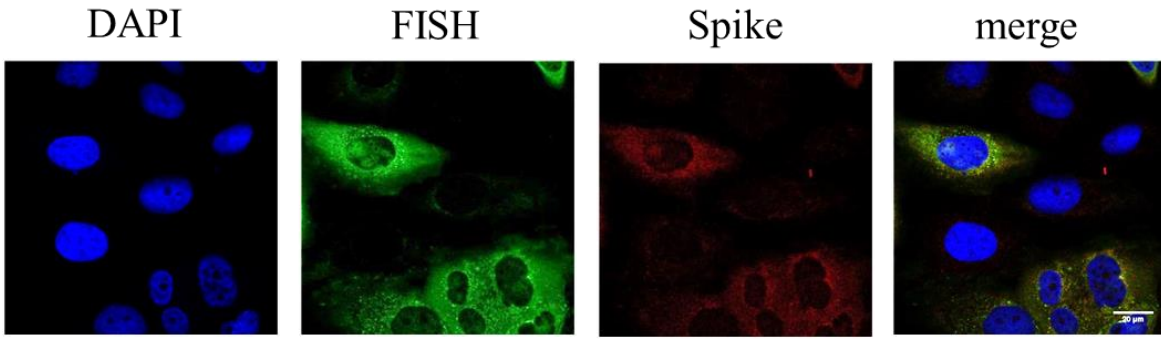

Figure 30. The mSIP-CR3022 anti-Spike antibody works specifically. Vero E6 cells well infected at an MOI of 0.1 with SARS-CoV-2 for 24 hpi. Cells were subjected to the HCR-FISH protocol using specific probes for nucleocapsid mRNA (green), and then immunostained for IF analysis with α-Spike (red). Nuclei were stained with DAPI and are seen in blue.

8.3. Creating cell lines that support SARS-CoV-2 infection

To establish an infectious SARS-CoV-2 model in mammalian cells, several cell lines available in the Lab were tested, including U2OS (osteosarcoma), HEK293T (human embryonic kidney cells), Vero E6 (African green monkey kidney), and Huh7 (hepatocellular carcinoma). The cell lines did not support SARS-CoV-2 infection, except for from Vero E6 and Huh7, that have in fact been previously reported to be infectable with SARS-CoV (Cinatl et al., 2003; Gillim-Ross et al., 2004; Mossel et al., 2005).

SARS-CoV-2 has higher for the ACE2 receptor than SARS-CoV, and it has been proposed that it could lead in viral replication in diverse organs during the COVID-19 infection (Glowacka et al., 2010; Wan et al., 2020). In line with this, it was previously observed that overexpression of ACE2 enhanced disease severity in a mouse model (X.-H. Yang et al., 2007), and made cell lines support SARS-CoV infection (Mossel et al., 2005). To establish

cell lines that are permissive to SARS-CoV2 infection, I overexpressed the ACE2 receptor using Lentivirus approach.

First, ACE2 was amplified by PCR using specific primers containing the desired restriction sites. Then the insert and the pWPI vector carrying a puromycin resistance cassette were double-digested with the restriction enzymes, followed by dephosphorylation of the vector, ligation, and finally transformation into XL10-gold chemo competent cells (Figure 31A). The colonies obtained were screened by PCR (Figure 31B) and ApaI digestion (Figure 31C), and several of the ten colonies screened were positive for efficient ligation. Colony 7 (C7) was selected for containing the desired construct, confirmed by Sanger sequencing. These bacteria were further grown and the plasmid pWPI_PURO-ACE2 was extracted using a MidiPrep kit.

Lentiviruses carrying pWPI_PURO-ACE2 were produced as explained in materials and methods, and used to transduce U2OS, HEK293T, Huh7 and Vero E6 cells to stably express the ACE2 protein. After selection with puromycin, ACE2 overexpression was assessed by western blot analysis (Figure 31D). Interestingly, the HEK293T cell line seems to produce two isoforms of the protein. Vero E6 were quite resistant to puromycin selection, and after a screening, the concentration of 5 µg/mL of puromycin was used to selected transduced cells for 3 days (Figure 31D).

The cell lines were created with the following aims:

- U2OS: Is the main cell line used in the Lab for molecular biology studies, and we hence have several tools to study infection in these cells. They were transduced aiming to be a tool for further studies in different projects. Representative images are shown in Figure 32.

- HEK293: We developed in the Lab Lentivirus particles pseudotyped with SARS-CoV-2 Spike glycoprotein by following the standard Lentivirus production protocol. We use a plasmid encoding the Spike protein instead of envelope protein of vesicular stomatitis virus (VSV), to be used for neutralization assays in BSL2 environment. The creation of HEK293_ACE2 cells greatly increased the efficiency of pseudoviruses transduction.

- Huh7: As mentioned before, we know that these cells can support SARS-CoV-2 infection, however only in 40 % of cells initially infected at an MOI of 0.1 and collected at 48 hpi (no significant changes were seen by changing the MOI) (data not shown). Hence, to increase the permissibility of these cells, they were transduced with ACE2. This tool made it possible to perform high content screening (HCS) assays that need excellent phenotype of infection to study and discover antivirals in a high throughput manner, using the automated HCS facility in ICGEB.

- Vero E6: Similarly, we also know that this cell line can be infected with SARS-CoV-2. The aim in transducing with ACE2 was to increase the sensibility of these cells to prepare virus stock with higher titres, and to isolate virus from human sample more efficiently.

- Apart from those that are routinely used in Lab to date, we also collaborated with different groups by sharing the reagent hereby produced. For example, Hoxb8 are hematopoietic cells from mouse that can be differentiated into myeloid cells such as macrophages and dendritic cells. They were transduced to study the immune response of innate immune cells during SARS-CoV-2 infection; among other projects.

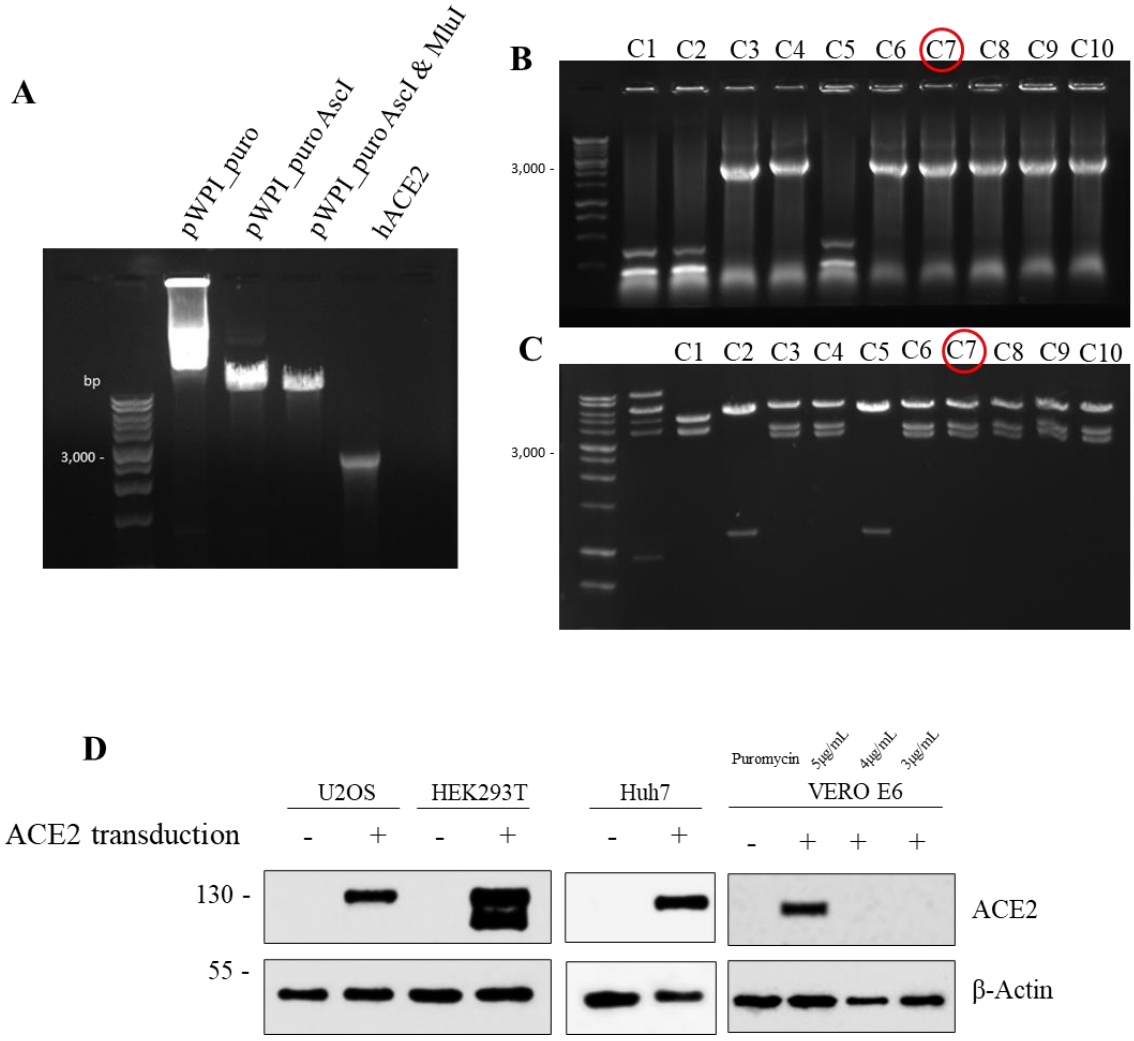

Figure 31. Exogenous expression of ACE2. A) Agarose gel showing insert, vector, and digested vector. After ligation and transformation, bacteria colonies were screened by B) PCR and C) ApaI digestion. D) U2OS, HEK293T, Huh7 and Vero cells were transduced with Lentivirus to express ACE2. All cell lines were selected with 1 µg/mL, except for Vero E6 that was selected with 5 µg/mL.

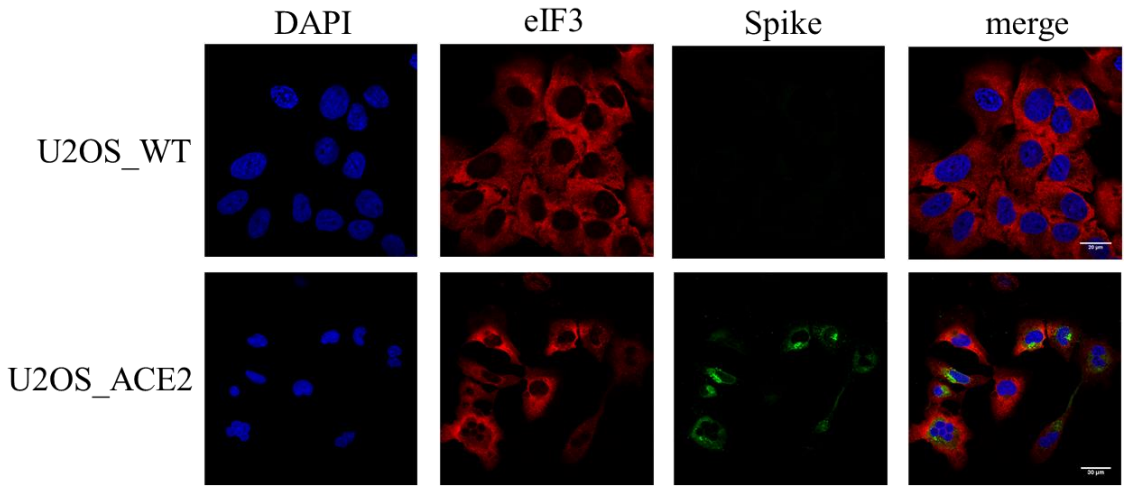

Figure 32. U2OS_ACE2 cells can support SARS-CoV-2 infection. U2OS WT or U2OS_ACE2 cells were infected with SARS-CoV-2 at an MOI of 0.1. Forty-eight hours post-infection, cells were fixed, permeabilized, and immunostained for IF analysis with α-eIF3 (red) and α-Spike (green). Nuclei were stained with DAPI and are seen in blue.

8.4.Repurposing of Miglustat to treat SARS-CoV-2

The iminosugar N-butyl-1-deoxynojirimycin (Miglustat, Zavesca) inhibits -glucosidases I and II, that are involved in the early stages of glycoprotein oligosaccharide processing in the ER (Elbein, 1991). Most enveloped viruses need glycosylation for surface protein folding and secretion, modulation of the oligosaccharides to induce a reduction in infectivity. The use of iminosugars to targeting the misfold viral glycoprotein as a therapeutic approach has thus far been applied to several viral infections including immune deficiency virus type 1 (HIV-1), hepatitis B and C viruses, Dengue and other flaviviruses, and Ebola virus (J. Chang et al., 2013; Dwek et al., 2002; Fischl et al., 1994; Tierney et al., 1995; Wu et al., 2002). An additional property of some iminosugars is the glucosyltransferase inhibition activity which made Miglustat a well characterized drug for the therapy of rare genetic lysosome storage diseases, such as Gaucher and Niemann-Pick type C (Platt et al., 2018).

Repurposing clinically available drugs to treat the COVID-19 is a relevant approach, as very few treatment options are available. I demonstrated the efficiency of the SARS-CoV-2 infection of Huh7 cells in the presence of Miglustat. As shown in Figure 33A, and quantified in Figure 33B, Miglustat made the number of Huh7 infected cells remain at similar level observed 24 hpi, while the mock treated cells had an increase in the infected cells at 48 hpi

as expected from an expansion of the infection in the cell culture. I also noted that the mean fluorescence intensity of the Spike signal decreased significantly in treated cells (Figure 34).

The drug seems to act at the post-entry level and leads to a decrease of viral proteins production and secretion of infectious viruses. The mechanism lies in the inhibitory activity toward glucosidases that are involved in the early stages of protein N-linked oligosaccharide processing in the ER, leading to a marked decrease of the viral Spike protein. These results point to a relevant role of this approach for the treatment of COVID-19.

The complete work has been published in a peer-reviewed journal and a copy can be found as an Appendix of this thesis.

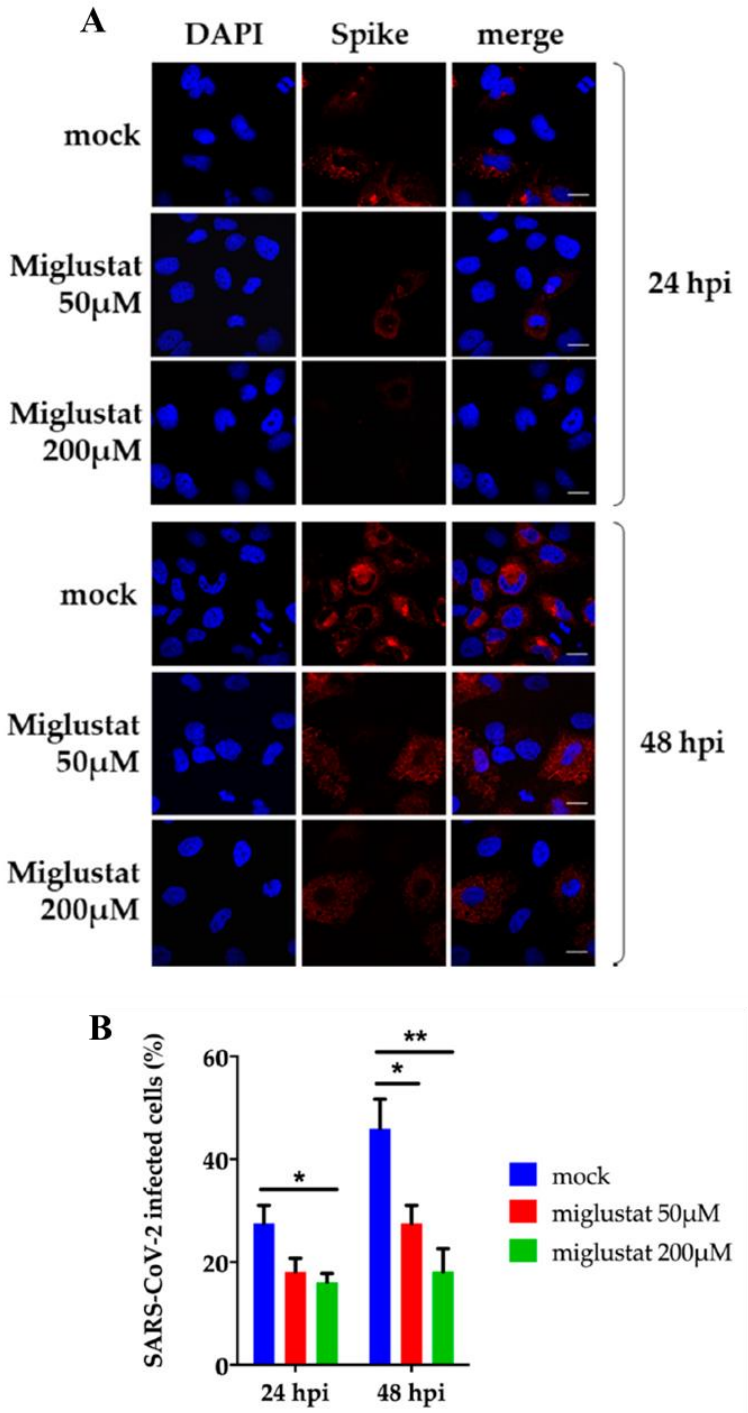

Figure 33. Anti-SARS-CoV-2 activity of Miglustat. Huh7 cells were infected with SARS-CoV-2 at an MOI of 0.1 and incubated with Miglustat as indicated. A) Cells were fixed and stained with mSIP-3022 antibody against Spike (red) to acquire confocal images. The nuclei were stained by DAPI. The bar corresponds to 20 µm. B) Quantification of SARS-CoV-2 infected cells. 200 cells per condition were plotted. p-values are indicated by ** $p < 0.01$ highly significant; * $p < 0.05$ significant, measured with a paired two-tailed t-test

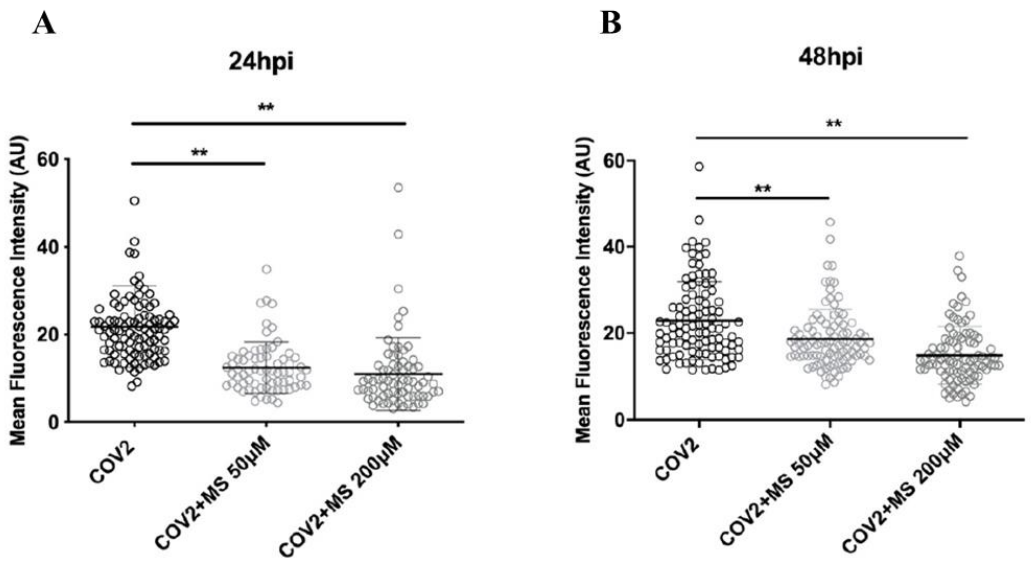

Figure 34. Effect of Miglustat (MS) on the mean fluorescence intensity of Spike staining in Huh7 cells. Huh7 cells were infected with SARS-CoV-2 at an MOI of 0.1 and incubated with Miglustat. Cells were then fixed and stained with mSIP-3022 antibody against Spike (red) to acquire confocal images at 24 hours (A) or 48 hours (B). Mean fluorescence intensity of the Spike signal was quantified by ImageJ. Results from 200 cells per condition were plotted in arbitrary units.

8.5. The cholesterol metabolite 27-hydroxycholesterol inhibits SARS-CoV-2

Specific side-chain cholesterol oxidation products of the oxysterols family have been shown to inhibit a large variety of both enveloped and non-enveloped human viral pathogens. The 27-hydroxycholesterol (27OHC) molecule is present in our body as a physiological product of the oxidative metabolism of cholesterol (Cagno et al., 2017; Civra et al., 2014, 2018, 2020). Colleagues in Milan monitored the levels of 27OHC in the blood of individuals who were positive for SARS-CoV-2, with asymptomatic, moderate, or severe COVID-19. Interestingly, it was observed a dramatic drop in the molecule levels in the blood of patients with COVID-19, reaching a 50 % inhibition in the severe cases (Marcello et al., 2020).

The relevance of the previous observations was further investigated by testing the compound activity *in vitro*. To improve its solubility and stability, 27OHC was complexed with 2-hydroxypropyl-β-cyclodextrin (2HP-βCD), a carrier commonly used in drug formulations. Therefore, the complex (2HP-βCD:27OHC) and the carrier alone were tested in parallel to rule out any contribution of the carrier to the antiviral activity. Huh7 cells were seeded on coverslips and infected with SARS-CoV-2 at an MOI of 0.1. After 1 h, inoculum was

removed and fresh DMEM +2% FBS containing 2HP-βCD:27OHC or 2HP-βCD was added to the cells. After 48 h incubation, cells were fixed with 3.7 % PFA, and the standard immunofluorescence protocol was followed to stain spike protein using the mSIP-CR3022 recombinant antibody at a 1:200 dilution.

As shown in Figure 35A, and quantified in Figure 35B, 2HP-βCD:27OHC significantly ($pANOVA < 0.001$) reduced the number of infected cells at 48 hpi both at 3 μM and 20 μM. In contrast, 2HP-βCD failed to show any anti-COV2 activity, demonstrating no significant difference from the untreated control in the number of infected cells.

The exogenous administration of 27-hydroxycholesterol may represent in the near future a valid antiviral strategy in the worsening of diseases caused by present and emerging coronaviruses. The high biocompatibility of the molecule, due to its physiological origin makes 27OHC a candidate to reach clinical trials in humans as soon as possible to propose it as an antiviral strategy complementary to vaccines in dealing with current but also future pandemics.

The complete work has been published in a peer-reviewed journal and a copy can be found as an Appendix of this thesis.

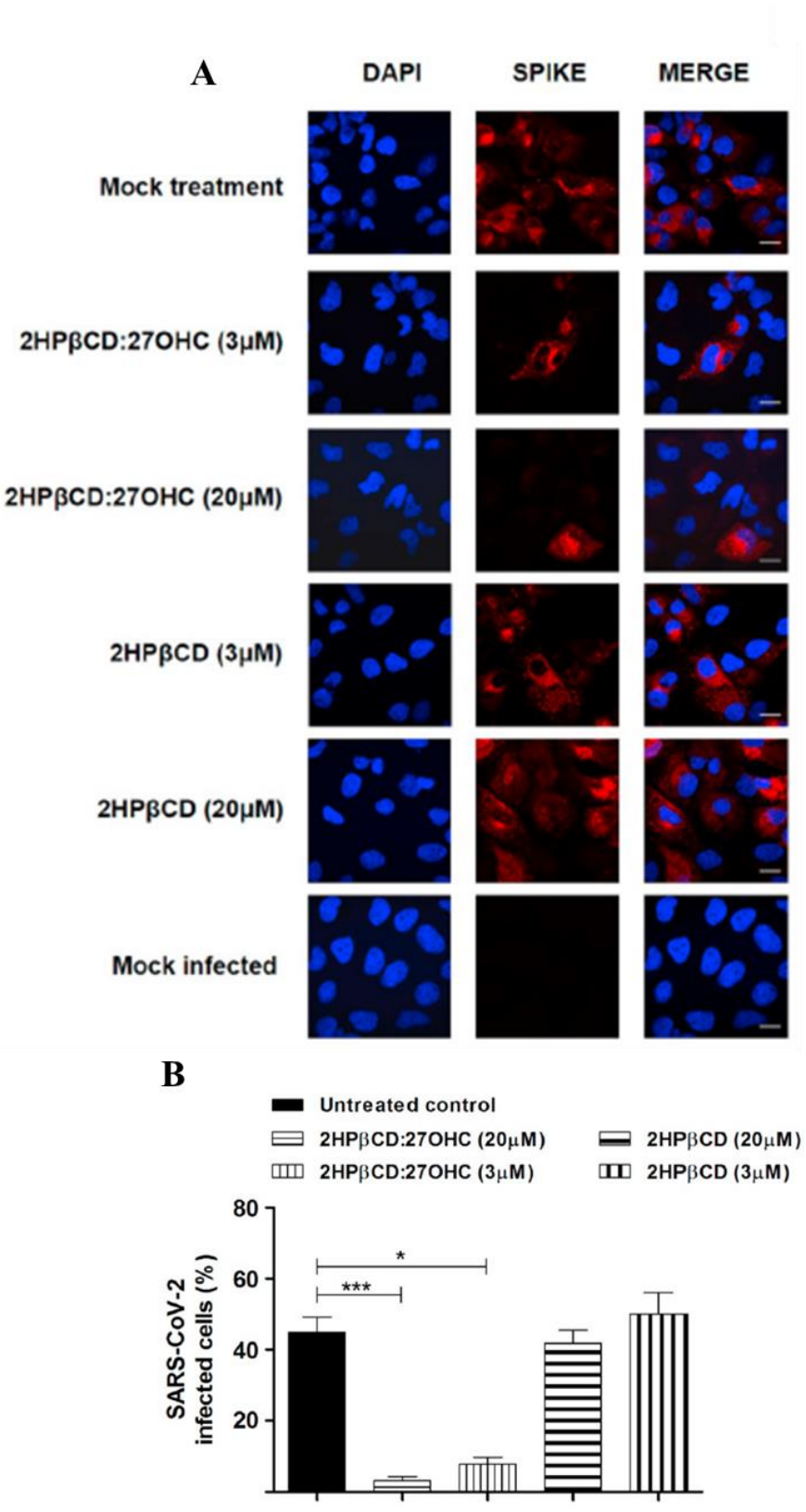

Figure 35. Anti-SARS-CoV-2 activity of 27OHC. Huh-7 cells were infected with SARS-CoV-2 in the presence of 2HP-βCD:27OHC, then fixed at 48 hpi and stained with DAPI and specific antibodies (A). Panel B shows the quantification of SARS-CoV-2 positive cells.

9. CONCLUDING REMARKS

During the period that I worked with SARS-CoV-2, I supported projects and established tools and reagents for the Lab that are still in use to date. Those were challenging times but also an excellent opportunity to learn new techniques, lead collaborations, exercise adaptability, and grow professionally and personally.

Until this moment, seven hundred and sixteen days have passed since the spread of COVID-19 led the WHO to declare a state of a pandemic. It should not come as a shock that some doctoral students had or are having a hard time trying to complete their degrees during the SARS-CoV-2 pandemic. These experiences range from feeling abandoned to finding ways to manage the disruptions to their thesis progress - I affirm that based on testimonials I received from other fellows. Not only was I able to carry with my work in the Lab but I also dedicated my time being the elected PhD representative of the Program in ICGEB (2019 - 2021). PhD students reported feeling engulfed by the quarantine and overall restrictions during the worst period of the pandemic. We tried to stablish online group activities, we offered support to each other (paying special attention to those who lived alone) and we shared approaches that helped keep the work going in the distance.

In my personal case, the outbreak and its restrictions eventually prevented me from having the networking opportunities that come in participating in on-site conferences. The crisis also raised uncertainty about the significance of my work. Suddenly, my project was no longer in the main topic of the Lab, and for a moment, all the world could speak about was CoV-2. At times, I could not receive timely feedback from advisors or discuss my research progress with peers. However, there were also many mental health challenges towards completing the work. I experienced lack of focus, motivation, and energy for no apparent reasons, and sometimes I struggled to deal with those feelings to push the work forward. But the most considerable toll of living during a pandemic for me was being a foreigner miles away from home. I feel psychologically affected by the pandemic for not being able to see or access my family, my support system. Taken together, all of this can be overwhelming, causing feelings of powerlessness and anxiety.

I write this atypical thesis conclusion during these atypical times hoping to immortalize the perceptions of a PhD candidate during the SARS-CoV-2 pandemic. I wish that the lessons the world learned remain to help us tailor measures and approaches in future pandemics.

10. REFERENCES

Abdiyeva, K., Turebekov, N., Yegemberdiyeva, R., Dmitrovskiy, A., Yeraliyeva, L., Shapiyeva, Z., Nurmakhanov, T., Sansyzbayev, Y., Froeschl, G., Hoelscher, M., Zinner, J., Essbauer, S., & Frey, S. (2020). Vectors, molecular epidemiology and phylogeny of TBEV in Kazakhstan and central Asia. *Parasites & Vectors*, *13*(1), 504. https://doi.org/10.1186/s13071-020-04362-1

Advani, V. M., & Ivanov, P. (2020). Stress granule subtypes: an emerging link to neurodegeneration. *Cellular and Molecular Life Sciences*, *77*(23), 4827–4845. https://doi.org/10.1007/s00018-020-03565-0

Aguirre, S., Maestre, A. M., Pagni, S., Patel, J. R., Savage, T., Gutman, D., Maringer, K., Bernal-Rubio, D., Shabman, R. S., Simon, V., Rodriguez-Madoz, J. R., Mulder, L. C. F., Barber, G. N., & Fernandez-Sesma, A. (2012). DENV Inhibits Type I IFN Production in Infected Cells by Cleaving Human STING. *PLoS Pathogens*, *8*(10), e1002934. https://doi.org/10.1371/journal.ppat.1002934

Akey, D. L., Brown, W. C., Dutta, S., Konwerski, J., Jose, J., Jurkiw, T. J., DelProposto, J., Ogata, C. M., Skiniotis, G., Kuhn, R. J., & Smith, J. L. (2014). Flavivirus NS1 structures reveal surfaces for associations with membranes and the immune system. *Science (New York, N.Y.)*, *343*(6173), 881–885. https://doi.org/10.1126/science.1247749

Albornoz, A., Carletti, T., Corazza, G., & Marcello, A. (2014). The Stress Granule Component TIA-1 Binds Tick-Borne Encephalitis Virus RNA and Is Recruited to Perinuclear Sites of Viral Replication To Inhibit Viral Translation. *Journal of Virology*, *88*(12), 6611–6622. https://doi.org/10.1128/JVI.03736-13

Ambrose, R. L., & Mackenzie, J. M. (2011). West Nile virus differentially modulates the unfolded protein response to facilitate replication and immune evasion. *Journal of Virology*, *85*(6), 2723–2732. https://doi.org/10.1128/JVI.02050-10

Ambrose, R. L., & Mackenzie, J. M. (2013). ATF6 Signaling Is Required for Efficient West Nile Virus Replication by Promoting Cell Survival and Inhibition of Innate Immune Responses. *Journal of Virology*, *87*(4), 2206–2214. https://doi.org/10.1128/JVI.02097-12

Amen, T., & Kaganovich, D. (2021). Stress granules inhibit fatty acid oxidation by modulating mitochondrial permeability. *Cell Reports*, *35*(11), 109237. https://doi.org/10.1016/j.celrep.2021.109237

Amicizia, D., Domnich, A., Panatto, D., Lai, P. L., Cristina, M. L., Avio, U., & Gasparini, R. (2013). Epidemiology of tick-borne encephalitis (TBE) in Europe and its prevention by available vaccines. *Human Vaccines & Immunotherapeutics*, *9*(5), 1163–1171. https://doi.org/10.4161/hv.23802

Amorim, R., Temzi, A., Griffin, B. D., & Mouland, A. J. (2017). Zika virus inhibits eIF2α-dependent stress granule assembly. *PLoS Neglected Tropical Diseases*, *11*(7), 1–20. https://doi.org/10.1371/journal.pntd.0005775

Anchisi, S., Guerra, J., & Garcin, D. (2015). RIG-I ATPase Activity and Discrimination of Self-RNA versus Non-Self-RNA. *MBio*, *6*(2). https://doi.org/10.1128/mBio.02349-14

Anderson, P., & Kedersha, N. (2006). RNA granules. *Journal of Cell Biology*, *172*(6), 803–808. https://doi.org/10.1083/jcb.200512082

Andersson, C. R., Vene, S., Insulander, M., Lindquist, L., Lundkvist, Å., & Günther, G. (2010). Vaccine failures after active immunisation against tick-borne encephalitis. *Vaccine*, *28*(16), 2827–2831. https://doi.org/10.1016/j.vaccine.2010.02.001

Apte-Sengupta, S., Sirohi, D., & Kuhn, R. J. (2014). Coupling of replication and assembly in flaviviruses. *Current Opinion in Virology*, *9*, 134–142. https://doi.org/10.1016/j.coviro.2014.09.020

Arakawa, M., Tabata, K., Ishida, K., Kobayashi, M., Arai, A., Ishikawa, T., Suzuki, R., Takeuchi, H., Tripathi, L. P., Mizuguchi, K., & Morita, E. (2022). Flavivirus recruits the valosin-containing protein (VCP)/NPL4 complex to induce stress granule disassembly for efficient viral genome replication. *The Journal of Biological Chemistry*, 101597. https://doi.org/10.1016/j.jbc.2022.101597

Ashour, J., Laurent-Rolle, M., Shi, P.-Y., & García-Sastre, A. (2009). NS5 of Dengue Virus Mediates STAT2 Binding and Degradation. *Journal of Virology*, *83*(11), 5408–5418. https://doi.org/10.1128/JVI.02188-08

Aulas, A., Caron, G., Gkogkas, C. G., Mohamed, N.-V., Destroismaisons, L., Sonenberg, N., Leclerc, N., Parker, J. A., & vande Velde, C. (2015). G3BP1 promotes stress-induced RNA granule interactions to preserve polyadenylated mRNA. *The Journal of Cell Biology*, *209*(1), 73–84. https://doi.org/10.1083/jcb.201408092

Aulas, A., Fay, M. M., Lyons, S. M., Achorn, C. A., Kedersha, N., Anderson, P., & Ivanov, P. (2017). Stress-specific differences in assembly and composition of stress granules and related foci. *Journal of Cell Science*, *130*(5), 927–937. https://doi.org/10.1242/jcs.199240

Aulas, A., Lyons, S. M., Fay, M. M., Anderson, P., & Ivanov, P. (2018). Nitric oxide triggers the assembly of "type II" stress granules linked to decreased cell viability. *Cell Death & Disease*, *9*(11), 1129. https://doi.org/10.1038/s41419-018-1173-x

Avirutnan, P., Zhang, L., Punyadee, N., Manuyakorn, A., Puttikhunt, C., Kasinrerk, W., Malasit, P., Atkinson, J. P., & Diamond, M. S. (2007). Secreted NS1 of Dengue Virus Attaches to the Surface of Cells via Interactions with Heparan Sulfate and Chondroitin Sulfate E. *PLoS Pathogens*, *3*(11), e183. https://doi.org/10.1371/journal.ppat.0030183

Azim, M., & Surani, H. (1979). Glycoprotein synthesis and inhibition of glycosylation by tunicamycin in preimplantation mouse embryos: Compaction and trophoblast adhesion. *Cell*, *18*(1), 217–227. https://doi.org/10.1016/0092-8674(79)90370-2

Balachandran, S., Roberts, P. C., Brown, L. E., Truong, H., Pattnaik, A. K., Archer, D. R., & Barber, G. N. (2000). Essential role for the dsRNA-dependent protein kinase PKR in innate immunity to viral infection. *Immunity*, *13*(1), 129–141. https://doi.org/10.1016/s1074-7613(00)00014-5

Barrows, N. J., Campos, R. K., Liao, K.-C., Prasanth, K. R., Soto-Acosta, R., Yeh, S.-C., Schott-Lerner, G., Pompon, J., Sessions, O. M., Bradrick, S. S., & Garcia-Blanco, M. A. (2018). Biochemistry and Molecular Biology of Flaviviruses. *Chemical Reviews*, *118*(8), 4448–4482. https://doi.org/10.1021/acs.chemrev.7b00719

Basu, M., Courtney, S. C., & Brinton, M. A. (2017). Arsenite-induced stress granule formation is inhibited by elevated levels of reduced glutathione in West Nile virus-infected cells. *PLoS Pathogens*, *13*(2), e1006240. https://doi.org/10.1371/journal.ppat.1006240

Bayer, A., Lennemann, N. J., Ouyang, Y., Bramley, J. C., Morosky, S., Marques, E. T. D. A., Cherry, S., Sadovsky, Y., & Coyne, C. B. (2016). Type III Interferons Produced by Human Placental Trophoblasts Confer Protection against Zika Virus Infection. *Cell Host & Microbe*, *19*(5), 705–712. https://doi.org/10.1016/j.chom.2016.03.008

Beatty, P. R., Puerta-Guardo, H., Killingbeck, S. S., Glasner, D. R., Hopkins, K., & Harris, E. (2015). Dengue virus NS1 triggers endothelial permeability and vascular leak that is prevented by NS1 vaccination. *Science Translational Medicine*, *7*(304). https://doi.org/10.1126/scitranslmed.aaa3787

Belouzard, S., Chu, V. C., & Whittaker, G. R. (2009). Activation of the SARS coronavirus spike protein via sequential proteolytic cleavage at two distinct sites. *Proceedings of the National Academy of Sciences*, *106*(14), 5871–5876. https://doi.org/10.1073/pnas.0809524106

Best, S. M., Morris, K. L., Shannon, J. G., Robertson, S. J., Mitzel, D. N., Park, G. S., Boer, E., Wolfinbarger, J. B., & Bloom, M. E. (2005). Inhibition of Interferon-Stimulated JAK-STAT Signaling by a Tick-Borne Flavivirus and Identification of NS5 as an Interferon Antagonist. *Journal of Virology*, *79*(20), 12828–12839. https://doi.org/10.1128/JVI.79.20.12828-12839.2005

Bidet, K., Dadlani, D., & Garcia-Blanco, M. A. (2014). G3BP1, G3BP2 and CAPRIN1 are required for translation of interferon stimulated mRNAs and are targeted by a dengue virus non-coding RNA. *PLoS Pathogens*, *10*(7), e1004242. https://doi.org/10.1371/journal.ppat.1004242

Billoir, R, de C., Tolou, P, de M., Gould, & X, de L. (2000). Phylogeny of the genus flavivirus using complete coding sequences of arthropod-borne viruses and viruses with no known vector. *The Journal of General Virology*, *81 Pt 9*, 2339. https://doi.org/10.1099/0022-1317-81-9-2339

Blom, K., Cuapio, A., Sandberg, J. T., Varnaite, R., Michaëlsson, J., Björkström, N. K., Sandberg, J. K., Klingström, J., Lindquist, L., Gredmark Russ, S., & Ljunggren, H.-G. (2018). Cell-Mediated Immune Responses and Immunopathogenesis of Human Tick-Borne Encephalitis Virus-Infection. *Frontiers in Immunology*, *9*. https://doi.org/10.3389/fimmu.2018.02174

Bogovic, P., & Strle, F. (2015). Tick-borne encephalitis: A review of epidemiology, clinical characteristics, and management. *World Journal of Clinical Cases*, *3*(5), 430–441. https://doi.org/10.12998/wjcc.v3.i5.430

Bollati, M., Alvarez, K., Assenberg, R., Baronti, C., Canard, B., Cook, S., Coutard, B., Decroly, E., de Lamballerie, X., Gould, E. A., Grard, G., Grimes, J. M., Hilgenfeld, R., Jansson, A. M., Malet, H., Mancini, E. J., Mastrangelo, E., Mattevi, A., Milani, M., … Bolognesi, M. (2010). Structure and functionality in flavivirus NS-proteins: perspectives for drug design. *Antiviral Research*, *87*(2), 125–148. https://doi.org/10.1016/j.antiviral.2009.11.009

Bonenfant, G., Williams, N., Netzband, R., Schwarz, M. C., Evans, M. J., & Pager, C. T. (2019). Zika Virus Subverts Stress Granules To Promote and Restrict Viral Gene Expression. *Journal of Virology*, *93*(12). https://doi.org/10.1128/jvi.00520-19

Borden, E. C., Sen, G. C., Uze, G., Silverman, R. H., Ransohoff, R. M., Foster, G. R., & Stark, G. R. (2007). Interferons at age 50: past, current and future impact on biomedicine. *Nature Reviews Drug Discovery*, *6*(12), 975–990. https://doi.org/10.1038/nrd2422

Braakman, I., & Bulleid, N. J. (2011). Protein Folding and Modification in the Mammalian Endoplasmic Reticulum. *Annual Review of Biochemistry*, *80*(1), 71–99. https://doi.org/10.1146/annurev-biochem-062209-093836

Brady, O. J., Osgood-Zimmerman, A., Kassebaum, N. J., Ray, S. E., de Araújo, V. E. M., da Nóbrega, A. A., Frutuoso, L. C. V, Lecca, R. C. R., Stevens, A., de Oliveira, B., de Lima Jr., J. M., Bogoch, I. I., Mayaud, P., Jaenisch, T., Mokdad, A. H., Murray, C. J. L., Hay, S. I., Reiner Jr., R. C., & Marinho, F. (2019). The association between Zika virus infection and microcephaly in Brazil 2015–2017: An observational analysis of over 4 million births. *PLOS Medicine*, *16*(3), 1–21. https://doi.org/10.1371/journal.pmed.1002755

Brangwynne, C. P., Eckmann, C. R., Courson, D. S., Rybarska, A., Hoege, C., Gharakhani, J., Jülicher, F., & Hyman, A. A. (2009). Germline P Granules Are Liquid Droplets That Localize by Controlled Dissolution/Condensation. *Science*, *324*(5935), 1729–1732. https://doi.org/10.1126/science.1172046

Brett D. Lindenbach Heinz-J, & C. Rice. (2007). Flaviviridae: The Viruses and Their Replication. *Semantic Scholar*.

Brocard, M., Iadevaia, V., Klein, P., Hall, B., Lewis, G., Lu, J., Burke, J., Willcocks, M. M., Parker, R., Goodfellow, I. G., Ruggieri, A., & Locker, N. (2020). Norovirus infection results in eIF2α independent host translation shut-off and remodels the G3BP1 interactome evading stress granule formation. *PLOS Pathogens*, *16*(1), e1008250. https://doi.org/10.1371/journal.ppat.1008250

Buchan, J. R., Kolaitis, R.-M., Taylor, J. P., & Parker, R. (2013). Eukaryotic Stress Granules Are Cleared by Autophagy and Cdc48/VCP Function. *Cell*, *153*(7), 1461–1474. https://doi.org/10.1016/j.cell.2013.05.037

Buchan, J. R., & Parker, R. (2009). Eukaryotic Stress Granules: The Ins and Outs of Translation. *Molecular Cell*, *36*(6), 932–941. https://doi.org/10.1016/j.molcel.2009.11.020

Buchan, J. R., Yoon, J.-H., & Parker, R. (2011). Stress-specific composition, assembly and kinetics of stress granules in *Saccharomyces cerevisiae*. *Journal of Cell Science*, *124*(2), 228–239. https://doi.org/10.1242/jcs.078444

Burke, J. M., Lester, E. T., Tauber, D., & Parker, R. (2020). RNase L promotes the formation of unique ribonucleoprotein granules distinct from stress granules. *Journal of Biological Chemistry*, *295*(6), 1426–1438. https://doi.org/10.1074/jbc.RA119.011638

Burrell, L. M., Johnston, C. I., Tikellis, C., & Cooper, M. E. (2004). ACE2, a new regulator of the renin-angiotensin system. *Trends in Endocrinology and Metabolism: TEM*, *15*(4), 166–169. https://doi.org/10.1016/j.tem.2004.03.001

Cagno, V., Civra, A., Rossin, D., Calfapietra, S., Caccia, C., Leoni, V., Dorma, N., Biasi, F., Poli, G., & Lembo, D. (2017). Inhibition of herpes simplex-1 virus replication by 25-hydroxycholesterol and 27-hydroxycholesterol. *Redox Biology*, *12*, 522–527. https://doi.org/10.1016/j.redox.2017.03.016

Carletti, T. (2015). *The Unfolded Protein Response is required early during TBEV infection to trigger the Interferon Response*.

Carletti, T., Zakaria, M. K., Faoro, V., Reale, L., Kazungu, Y., Licastro, D., & Marcello, A. (2019). Viral priming of cell intrinsic innate antiviral signaling by the unfolded protein response. *Nature Communications*, *10*(1). https://doi.org/10.1038/s41467-019-11663-2

CDC. (2022, January 31). *Risk for COVID-19 Infection, Hospitalization, and Death By Age Group*. Https://Www.Cdc.Gov/Coronavirus/2019-Ncov/Covid-Data/Investigations-Discovery/Hospitalization-Death-by-Age.Html.

Cesaro, T., Hayashi, Y., Borghese, F., Vertommen, D., Wavreil, F., & Michiels, T. (2021). PKR activity modulation by phosphomimetic mutations of serine residues located three aminoacids upstream of double-stranded RNA binding motifs. *Scientific Reports*, *11*(1), 9188. https://doi.org/10.1038/s41598-021-88610-z

Cesaro, T., & Michiels, T. (2021). Inhibition of PKR by Viruses. *Frontiers in Microbiology*, *12*. https://doi.org/10.3389/fmicb.2021.757238

Chambers, T. J., Weir, R. C., Grakoui, A., McCourt, D. W., Bazan, J. F., Fletterick, R. J., & Rice, C. M. (1990). Evidence that the N-terminal domain of nonstructural protein NS3 from yellow fever virus is a serine protease responsible for site-specific cleavages in the viral polyprotein. *Proceedings of the National Academy of Sciences of the United States of America*, *87*(22), 8898–8902. https://doi.org/10.1073/pnas.87.22.8898

Chamsi-Pasha, M. A. R., Shao, Z., & Tang, W. H. W. (2014). Angiotensin-Converting Enzyme 2 as a Therapeutic Target for Heart Failure. *Current Heart Failure Reports*, *11*(1), 58–63. https://doi.org/10.1007/s11897-013-0178-0

Chang, J., Warren, T. K., Zhao, X., Gill, T., Guo, F., Wang, L., Comunale, M. A., Du, Y., Alonzi, D. S., Yu, W., Ye, H., Liu, F., Guo, J.-T., Mehta, A., Cuconati, A., Butters, T. D., Bavari, S., Xu, X., & Block, T. M. (2013). Small molecule inhibitors of ER α-glucosidases are active against multiple hemorrhagic fever viruses. *Antiviral Research*, *98*(3), 432–440. https://doi.org/10.1016/j.antiviral.2013.03.023

Chang, Y. S., Liao, C. L., Tsao, C. H., Chen, M. C., Liu, C. I., Chen, L. K., & Lin, Y. L. (1999). Membrane permeabilization by small hydrophobic nonstructural proteins of Japanese encephalitis virus. *Journal of Virology*, *73*(8), 6257–6264. https://doi.org/10.1128/JVI.73.8.6257-6264.1999

Chefalo, P. J., Oh, J., Rafie-Kolpin, M., Kan, B., & Chen, J. J. (1998). Heme-regulated eIF-2alpha kinase purifies as a hemoprotein. *European Journal of Biochemistry*, *258*(2), 820–830. https://doi.org/10.1046/j.1432-1327.1998.2580820.x

Chen, H.-L., Her, S.-Y., Huang, K.-C., Cheng, H.-T., Wu, C.-W., Wu, S.-C., & Cheng, J.-W. (2010). Identification of a heparin binding peptide from the Japanese encephalitis virus envelope protein. *Biopolymers*, *94*(3), 331–338. https://doi.org/10.1002/bip.21371

Chen, Y., Maguire, T., Hileman, R. E., Fromm, J. R., Esko, J. D., Linhardt, R. J., & Marks, R. M. (1997). Dengue virus infectivity depends on envelope protein binding to target cell heparan sulfate. *Nature Medicine*, *3*(8), 866–871. https://doi.org/10.1038/nm0897-866

Chiu, W.-W., Kinney, R. M., & Dreher, T. W. (2005). Control of Translation by the 5′- and 3′-Terminal Regions of the Dengue Virus Genome. *Journal of Virology*, *79*(13), 8303–8315. https://doi.org/10.1128/JVI.79.13.8303-8315.2005

Choi, H. M. T., Beck, V. A., & Pierce, N. A. (2014). Next-generation in situ hybridization chain reaction: higher gain, lower cost, greater durability. *ACS Nano*, *8*(5), 4284–4294. https://doi.org/10.1021/nn405717p

Choi, H. M. T., Chang, J. Y., Trinh, L. A., Padilla, J. E., Fraser, S. E., & Pierce, N. A. (2010). Programmable in situ amplification for multiplexed imaging of mRNA expression. *Nature Biotechnology*, *28*(11), 1208–1212. https://doi.org/10.1038/nbt.1692

Chu, J. J. H., & Ng, M. L. (2004). Infectious Entry of West Nile Virus Occurs through a Clathrin-Mediated Endocytic Pathway. *Journal of Virology*, *78*(19), 10543–10555. https://doi.org/10.1128/JVI.78.19.10543-10555.2004

Cinatl, J., Morgenstern, B., Bauer, G., Chandra, P., Rabenau, H., & Doerr, H. W. (2003). Treatment of SARS with human interferons. *Lancet (London, England)*, *362*(9380), 293–294. https://doi.org/10.1016/s0140-6736(03)13973-6

Cirillo, L., Cieren, A., Barbieri, S., Khong, A., Schwager, F., Parker, R., & Gotta, M. (2020). UBAP2L Forms Distinct Cores that Act in Nucleating Stress Granules Upstream of G3BP1. *Current Biology*, *30*(4), 698-707.e6. https://doi.org/10.1016/j.cub.2019.12.020

Civra, A., Cagno, V., Donalisio, M., Biasi, F., Leonarduzzi, G., Poli, G., & Lembo, D. (2014). Inhibition of pathogenic non-enveloped viruses by 25-hydroxycholesterol and 27-hydroxycholesterol. *Scientific Reports*, *4*, 7487. https://doi.org/10.1038/srep07487

Civra, A., Colzani, M., Cagno, V., Francese, R., Leoni, V., Aldini, G., Lembo, D., & Poli, G. (2020). Modulation of cell proteome by 25-hydroxycholesterol and 27-hydroxycholesterol: A link between cholesterol metabolism and antiviral defense. *Free Radical Biology and Medicine*, *149*, 30–36. https://doi.org/https://doi.org/10.1016/j.freeradbiomed.2019.08.031

Civra, A., Francese, R., Gamba, P., Testa, G., Cagno, V., Poli, G., & Lembo, D. (2018). 25-Hydroxycholesterol and 27-hydroxycholesterol inhibit human rotavirus infection by sequestering viral particles into late endosomes. *Redox Biology*, *19*, 318–330. https://doi.org/10.1016/j.redox.2018.09.003

Connor, J. H., Weiser, D. C., Li, S., Hallenbeck, J. M., & Shenolikar, S. (2001). Growth Arrest and DNA Damage-Inducible Protein GADD34 Assembles a Novel Signaling Complex Containing Protein Phosphatase 1 and Inhibitor 1. *Molecular and Cellular Biology*, *21*(20), 6841–6850. https://doi.org/10.1128/MCB.21.20.6841-6850.2001

Costa-Mattioli, M., & Walter, P. (2020). The integrated stress response: From mechanism to disease. *Science*, *368*(6489). https://doi.org/10.1126/science.aat5314

Courtney, S. C., Scherbik, S. V, Stockman, B. M., & Brinton, M. A. (2012). West nile virus infections suppress early viral RNA synthesis and avoid inducing the cell stress granule response. *Journal of Virology*, *86*(7), 3647–3657. https://doi.org/10.1128/JVI.06549-11

Cugola, F. R., Fernandes, I. R., Russo, F. B., Freitas, B. C., Dias, J. L. M., Guimarães, K. P., Benazzato, C., Almeida, N., Pignatari, G. C., Romero, S., Polonio, C. M., Cunha, I., Freitas, C. L., Brandão, W. N., Rossato, C., Andrade, D. G., Faria, D. de P., Garcez, A. T., Buchpigel, C. A., … Beltrão-Braga, P. C. B. (2016). The Brazilian Zika virus strain causes birth defects in experimental models. *Nature*, *534*(7606), 267–271. https://doi.org/10.1038/nature18296

Dabo, S., & Meurs, E. (2012). dsRNA-Dependent Protein Kinase PKR and its Role in Stress, Signaling and HCV Infection. *Viruses*, *4*(11), 2598–2635. https://doi.org/10.3390/v4112598

Daep, C. A., Muñoz-Jordán, J. L., & Eugenin, E. A. (2014). Flaviviruses, an expanding threat in public health: focus on dengue, West Nile, and Japanese encephalitis virus. *Journal of Neurovirology*, *20*(6), 539–560. https://doi.org/10.1007/s13365-014-0285-z

Dai, X., Shang, G., Lu, S., Yang, J., & Xu, J. (2018). A new subtype of eastern tick-borne encephalitis virus discovered in Qinghai-Tibet Plateau, China. *Emerging Microbes & Infections*, *7*(1), 1–9. https://doi.org/10.1038/s41426-018-0081-6

Dalrymple, N. A., Cimica, V., & Mackow, E. R. (2015). Dengue Virus NS Proteins Inhibit RIG-I/MAVS Signaling by Blocking TBK1/IRF3 Phosphorylation: Dengue Virus Serotype 1 NS4A Is a Unique Interferon-Regulating Virulence Determinant. *MBio*, *6*(3), e00553-15. https://doi.org/10.1128/mBio.00553-15

Dang, Y., Kedersha, N., Low, W.-K., Romo, D., Gorospe, M., Kaufman, R., Anderson, P., & Liu, J. O. (2006). Eukaryotic initiation factor 2alpha-independent pathway of stress granule induction by the natural product pateamine A. *The Journal of Biological Chemistry*, *281*(43), 32870–32878. https://doi.org/10.1074/jbc.M606149200

Dauber, B., Schneider, J., & Wolff, T. (2006). Double-Stranded RNA Binding of Influenza B Virus Nonstructural NS1 Protein Inhibits Protein Kinase R but Is Not Essential To Antagonize Production of Alpha/Beta Interferon. *Journal of Virology*, *80*(23), 11667–11677. https://doi.org/10.1128/JVI.01142-06

Demicheli, V., Debalini, M. G., & Rivetti, A. (2009). Vaccines for preventing tick-borne encephalitis. *Cochrane Database of Systematic Reviews*. https://doi.org/10.1002/14651858.CD000977.pub2

Demina, T. V., Dzhioev, Yu. P., Verkhozina, M. M., Kozlova, I. V., Tkachev, S. E., Plyusnin, A., Doroshchenko, E. K., Lisak, O. V., & Zlobin, V. I. (2010). Genotyping and characterization of the geographical distribution of tick-borne encephalitis virus variants with a set of molecular probes. *Journal of Medical Virology*, *82*(6), 965–976. https://doi.org/10.1002/jmv.21765

den Boon, J. A., & Ahlquist, P. (2010). Organelle-Like Membrane Compartmentalization of Positive-Strand RNA Virus Replication Factories. *Annual Review of Microbiology*, *64*(1), 241–256. https://doi.org/10.1146/annurev.micro.112408.134012

Diamond, M. S., & Gale, M. J. (2012). Cell-intrinsic innate immune control of West Nile virus infection. *Trends in Immunology*, *33*(10), 522–530. https://doi.org/10.1016/j.it.2012.05.008

Diamond, M. S., & Harris, E. (2001). Interferon Inhibits Dengue Virus Infection by Preventing Translation of Viral RNA through a PKR-Independent Mechanism. *Virology*, *289*(2), 297–311. https://doi.org/10.1006/viro.2001.1114

Dirks, R. M., & Pierce, N. A. (2004). Triggered amplification by hybridization chain reaction. *Proceedings of the National Academy of Sciences*, *101*(43), 15275–15278. https://doi.org/10.1073/pnas.0407024101

Dobler, G. (2010). Zoonotic tick-borne flaviviruses. *Veterinary Microbiology*, *140*(3–4), 221–228. https://doi.org/10.1016/j.vetmic.2009.08.024

Dolgin, E. (2021). The race for antiviral drugs to beat COVID — and the next pandemic. *Nature*, *592*(7854), 340–343. https://doi.org/10.1038/d41586-021-00958-4

Donnelly, N., Gorman, A. M., Gupta, S., & Samali, A. (2013). The eIF2α kinases: their structures and functions. *Cellular and Molecular Life Sciences*, *70*(19), 3493–3511. https://doi.org/10.1007/s00018-012-1252-6

Donoso Mantke, O., Schädler, R., & Niedrig, M. (2008). A survey on cases of tick-borne encephalitis in European countries. *Euro Surveillance : Bulletin Europeen Sur Les Maladies Transmissibles = European Communicable Disease Bulletin*, *13*(17).

Drosten, C., Günther, S., Preiser, W., van der Werf, S., Brodt, H.-R., Becker, S., Rabenau, H., Panning, M., Kolesnikova, L., Fouchier, R. A. M., Berger, A., Burguière, A.-M., Cinatl, J., Eickmann, M., Escriou, N., Grywna, K., Kramme, S., Manuguerra, J.-C., Müller, S., … Doerr, H. W. (2003). Identification of a novel coronavirus in patients with severe acute respiratory syndrome. *The New England Journal of Medicine*, *348*(20), 1967–1976. https://doi.org/10.1056/NEJMoa030747

Duan, X., Lu, X., Li, J., & Liu, Y. (2008). Novel binding between pre-membrane protein and vacuolar ATPase is required for efficient dengue virus secretion. *Biochemical and Biophysical Research Communications*, *373*(2), 319–324. https://doi.org/10.1016/j.bbrc.2008.06.041

Dwek, R. A., Butters, T. D., Platt, F. M., & Zitzmann, N. (2002). Targeting glycosylation as a therapeutic approach. *Nature Reviews. Drug Discovery*, *1*(1), 65–75. https://doi.org/10.1038/nrd708

ECDC. (2021, March 21). *Tick-borne encephalitis - Annual Epidemiological Report for 2019*. Https://Www.Ecdc.Europa.Eu/En/Publications-Data/Tick-Borne-Encephalitis-Annual-Epidemiological-Report-2019.

ECDC. (2022a). *Factsheet about tick-borne encephalitis (TBE)*. https://www.ecdc.europa.eu/en/tick-borne-encephalitis/facts/factsheet

ECDC. (2022b, January 21). *Vaccines*. Https://Www.Ecdc.Europa.Eu/En/Covid-19/Latest-Evidence/Vaccines.

ECDC. (2022c, February 3). *SARS-CoV-2 variants of concern as of 03 February 2022*. Https://Www.Ecdc.Europa.Eu/En/Covid-19/Variants-Concern.

Eiermann, N., Haneke, K., Sun, Z., Stoecklin, G., & Ruggieri, A. (2020). Dance with the Devil: Stress Granules and Signaling in Antiviral Responses. *Viruses*, *12*(9). https://doi.org/10.3390/v12090984

Elbahesh, H., Scherbik, S. V, & Brinton, M. A. (2011a). West Nile virus infection does not induce PKR activation in rodent cells. *Virology*, *421*(1), 51–60. https://doi.org/10.1016/j.virol.2011.08.008

Elbahesh, H., Scherbik, S. v, & Brinton, M. A. (2011b). West Nile virus infection does not induce PKR activation in rodent cells. *Virology*, *421*(1), 51–60. https://doi.org/10.1016/j.virol.2011.08.008

Elbein, A. D. (1991). Glycosidase inhibitors: inhibitors of N-linked oligosaccharide processing. *FASEB Journal : Official Publication of the Federation of American Societies for Experimental Biology*, *5*(15), 3055–3063. https://doi.org/10.1096/fasebj.5.15.1743438

Ellgaard, L., & Helenius, A. (2003). Quality control in the endoplasmic reticulum. *Nature Reviews Molecular Cell Biology*, *4*(3), 181–191. https://doi.org/10.1038/nrm1052

Emara, M. M., & Brinton, M. A. (2007). Interaction of TIA-1/TIAR with West Nile and dengue virus products in infected cells interferes with stress granule formation and processing body assembly. *Proceedings of the National Academy of Sciences*, *104*(21), 9041–9046. https://doi.org/10.1073/pnas.0703348104

Evans, J. D., Crown, R. A., Sohn, J. A., & Seeger, C. (2011). West Nile Virus Infection Induces Depletion of IFNAR1 Protein Levels. *Viral Immunology*, *24*(4), 253–263. https://doi.org/10.1089/vim.2010.0126

Fares, M., Cochet-Bernoin, M., Gonzalez, G., Montero-Menei, C. N., Blanchet, O., Benchoua, A., Boissart, C., Lecollinet, S., Richardson, J., Haddad, N., & Coulpier, M. (2020). Pathological modeling of TBEV infection reveals differential innate immune responses in human neurons and astrocytes that correlate with their susceptibility to infection. *Journal of Neuroinflammation*, *17*(1), 76. https://doi.org/10.1186/s12974-020-01756-x

Fathi, M., Vakili, K., Sayehmiri, F., Mohamadkhani, A., Hajiesmaeili, M., Rezaei-Tavirani, M., & Eilami, O. (2021). The prognostic value of comorbidity for the severity of COVID-19: A systematic review and meta-analysis study. *PLOS ONE*, *16*(2), e0246190. https://doi.org/10.1371/journal.pone.0246190

Femino, A. M., Fay, F. S., Fogarty, K., & Singer, R. H. (1998). Visualization of single RNA transcripts in situ. *Science (New York, N.Y.)*, *280*(5363), 585–590. https://doi.org/10.1126/science.280.5363.585

Fischl, M. A., Resnick, L., Coombs, R., Kremer, A. B., Pottage, J. C. J., Fass, R. J., Fife, K. H., Powderly, W. G., Collier, A. C., & Aspinall, R. L. (1994). The safety and efficacy of combination N-butyl-deoxynojirimycin (SC-48334) and zidovudine in patients with HIV-1 infection and 200-500 CD4 cells/mm3. *Journal of Acquired Immune Deficiency Syndromes*, *7*(2), 139–147.

Gale, M. J., Blakely, C. M., Kwieciszewski, B., Tan, S. L., Dossett, M., Tang, N. M., Korth, M. J., Polyak, S. J., Gretch, D. R., & Katze, M. G. (1998). Control of PKR protein kinase by hepatitis C virus nonstructural 5A protein: molecular mechanisms of kinase regulation. *Molecular and Cellular Biology*, *18*(9), 5208–5218. https://doi.org/10.1128/MCB.18.9.5208

Gale, M. J., Korth, M. J., Tang, N. M., Tan, S.-L., Hopkins, D. A., Dever, T. E., Polyak, S. J., Gretch, D. R., & Katze, M. G. (1997). Evidence That Hepatitis C Virus Resistance to Interferon Is Mediated through Repression of the PKR Protein Kinase by the Nonstructural 5A Protein. *Virology*, *230*(2), 217–227. https://doi.org/10.1006/viro.1997.8493

Gao, B., Gong, X., Fang, S., Weng, W., Wang, H., Chu, H., Sun, Y., Meng, C., Tan, L., Song, C., Qiu, X., Liu, W., Forlenza, M., Ding, C., & Liao, Y. (2021). Inhibition of anti-viral stress granule formation by coronavirus endoribonuclease nsp15 ensures efficient virus replication. *PLOS Pathogens*, *17*(2), e1008690. https://doi.org/10.1371/journal.ppat.1008690

Gao, Z., Zhang, X., Zhang, L., Wu, S., Ma, J., Wang, F., Zhou, Y., Dai, X., Bullitt, E., Du, Y., Guo, J.-T., & Chang, J. (2022). A yellow fever virus NS4B inhibitor not only suppresses viral replication, but also enhances the virus activation of RIG-I-like receptor-mediated innate immune response. *PLOS Pathogens*, *18*(1), 1–26. https://doi.org/10.1371/journal.ppat.1010271

Garaigorta, U., & Chisari, F. V. (2009). Hepatitis C virus blocks interferon effector function by inducing protein kinase R phosphorylation. *Cell Host & Microbe*, *6*(6), 513–522. https://doi.org/10.1016/j.chom.2009.11.004

Garaigorta, U., Heim, M. H., Boyd, B., Wieland, S., & Chisari, F. v. (2012). Hepatitis C virus (HCV) induces formation of stress granules whose proteins regulate HCV RNA replication and virus assembly and egress. *Journal of Virology*, *86*(20), 11043–11056. https://doi.org/10.1128/JVI.07101-11

García Cordero, J., León Juárez, M., González-Y-Merchand, J. A., Cedillo Barrón, L., & Gutiérrez Castañeda, B. (2014). Caveolin-1 in Lipid Rafts Interacts with Dengue Virus NS3 during Polyprotein Processing and Replication in HMEC-1 Cells. *PLoS ONE*, *9*(3), e90704. https://doi.org/10.1371/journal.pone.0090704

García, M. A., Meurs, E. F., & Esteban, M. (2007). The dsRNA protein kinase PKR: virus and cell control. *Biochimie*, *89*(6–7), 799–811. https://doi.org/10.1016/j.biochi.2007.03.001

Gelpi, E., Preusser, M., Garzuly, F., Holzmann, H., Heinz, F. X., & Budka, H. (2005). Visualization of Central European Tick-Borne Encephalitis Infection in Fatal Human Cases. *Journal of Neuropathology & Experimental Neurology*, *64*(6), 506–512. https://doi.org/10.1093/jnen/64.6.506

Gelpi, E., Preusser, M., Laggner, U., Garzuly, F., Holzmann, H., Heinz, F., & Budka, H. (2006). Inflammatory response in human tick-borne encephalitis: analysis of postmortem brain tissue. *Journal of NeuroVirology*, *12*(4), 322–327. https://doi.org/10.1080/13550280600848746

Gembardt, F., Sterner-Kock, A., Imboden, H., Spalteholz, M., Reibitz, F., Schultheiss, H.-P., Siems, W.-E., & Walther, T. (2005). Organ-specific distribution of ACE2 mRNA and correlating peptidase activity in rodents. *Peptides*, *26*(7), 1270–1277. https://doi.org/https://doi.org/10.1016/j.peptides.2005.01.009

Germi, R., Crance, J.-M., Garin, D., Guimet, J., Lortat-Jacob, H., Ruigrok, R. W. H., Zarski, J.-P., & Drouet, E. (2002). Heparan Sulfate-Mediated Binding of Infectious Dengue Virus Type 2 and Yellow Fever Virus. *Virology*, *292*(1), 162–168. https://doi.org/10.1006/viro.2001.1232

Gilks, N., Kedersha, N., Ayodele, M., Shen, L., Stoecklin, G., Dember, L. M., & Anderson, P. (2004). Stress Granule Assembly Is Mediated by Prion-like Aggregation of TIA-1. *Molecular Biology of the Cell*, *15*(12), 5383–5398. https://doi.org/10.1091/mbc.e04-08-0715

Gillim-Ross, L., Taylor, J., Scholl, D. R., Ridenour, J., Masters, P. S., & Wentworth, D. E. (2004). Discovery of novel human and animal cells infected by the severe acute respiratory syndrome coronavirus by replication-specific multiplex reverse transcription-PCR. *Journal of Clinical Microbiology*, *42*(7), 3196–3206. https://doi.org/10.1128/JCM.42.7.3196-3206.2004

Glowacka, I., Bertram, S., Herzog, P., Pfefferle, S., Steffen, I., Muench, M. O., Simmons, G., Hofmann, H., Kuri, T., Weber, F., Eichler, J., Drosten, C., & Pöhlmann, S. (2010). Differential downregulation of ACE2 by the spike proteins of severe acute respiratory syndrome coronavirus and human coronavirus NL63. *Journal of Virology*, *84*(2), 1198–1205. https://doi.org/10.1128/JVI.01248-09

Gómez, C. E., Perdiguero, B., & Esteban, M. (2021). Emerging SARS-CoV-2 Variants and Impact in Global Vaccination Programs against SARS-CoV-2/COVID-19. *Vaccines*, *9*(3), 243. https://doi.org/10.3390/vaccines9030243

Gopal, N. N., Huey-Nan, W., & K., K. (2022). Mutation of Putative N-Glycosylation Sites on Dengue Virus NS4B Decreases RNA Replication. *Journal of Virology*, *89*(13), 6746–6760. https://doi.org/10.1128/JVI.00423-15

Gopala Reddy, S. B., Chin, W.-X., & Shivananju, N. S. (2018). Dengue virus NS2 and NS4: Minor proteins, mammoth roles. *Biochemical Pharmacology*, *154*, 54–63. https://doi.org/10.1016/j.bcp.2018.04.008

Gould, E. A., & Solomon, T. (2008). Pathogenic flaviviruses. *Lancet (London, England)*, *371*(9611), 500–509. https://doi.org/10.1016/S0140-6736(08)60238-X

Goyal, P., Choi, J. J., Pinheiro, L. C., Schenck, E. J., Chen, R., Jabri, A., Satlin, M. J., Campion, T. R., Nahid, M., Ringel, J. B., Hoffman, K. L., Alshak, M. N., Li, H. A., Wehmeyer, G. T., Rajan, M., Reshetnyak, E., Hupert, N., Horn, E. M., Martinez, F. J., … Safford, M. M. (2020). Clinical Characteristics of Covid-19 in New York City. *New England Journal of Medicine*, *382*(24), 2372–2374. https://doi.org/10.1056/NEJMc2010419

Grabowski, J. M., Perera, R., Roumani, A. M., Hedrick, V. E., Inerowicz, H. D., Hill, C. A., & Kuhn, R. J. (2016). Changes in the Proteome of Langat-Infected Ixodes scapularis ISE6 Cells: Metabolic Pathways Associated with Flavivirus Infection. *PLoS Neglected Tropical Diseases*, *10*(2), e0004180. https://doi.org/10.1371/journal.pntd.0004180

Granet, R. (2021). *The enemy within: How SARS-CoV-2 uses our own proteins to infect our cells*. CAS. https://www.cas.org/resource/blog/covid-19-spike-protein

Gritsun, T. S., & Gould, E. A. (2006a). *Origin and Evolution of 3'Utr of Flaviviruses: Long Direct Repeats as A Basis for the Formation of Secondary Structures and Their Significance for Virus Transmission* (pp. 203–248). https://doi.org/10.1016/S0065-3527(06)69005-2

Gritsun, T. S., & Gould, E. A. (2006b). The 3′ untranslated region of tick-borne flaviviruses originated by the duplication of long repeat sequences within the open reading frame. *Virology*, *354*(1), 217–223. https://doi.org/10.1016/j.virol.2006.03.052

Gritsun, T. S., & Gould, E. A. (2007). Origin and evolution of flavivirus 5′UTRs and panhandles: Trans-terminal duplications? *Virology*, *366*(1), 8–15. https://doi.org/10.1016/j.virol.2007.04.011

Groskreutz, D. J., Babor, E. C., Monick, M. M., Varga, S. M., & Hunninghake, G. W. (2010). Respiratory Syncytial Virus Limits α Subunit of Eukaryotic Translation Initiation Factor 2 (eIF2α) Phosphorylation to Maintain Translation and Viral Replication. *Journal of Biological Chemistry*, *285*(31), 24023–24031. https://doi.org/10.1074/jbc.M109.077321

Guillén-Boixet, J., Kopach, A., Holehouse, A. S., Wittmann, S., Jahnel, M., Schlüßler, R., Kim, K., Trussina, I. R. E. A., Wang, J., Mateju, D., Poser, I., Maharana, S., Ruer-Gruß, M., Richter, D., Zhang, X., Chang, Y.-T., Guck, J., Honigmann, A., Mahamid, J., … Franzmann, T. M. (2020). RNA-Induced Conformational Switching and Clustering of G3BP Drive Stress Granule Assembly by Condensation. *Cell*, *181*(2), 346-361.e17. https://doi.org/10.1016/j.cell.2020.03.049

Guo, J.-T., Hayashi, J., & Seeger, C. (2005). West Nile Virus Inhibits the Signal Transduction Pathway of Alpha Interferon. *Journal of Virology*, *79*(3), 1343–1350. https://doi.org/10.1128/JVI.79.3.1343-1350.2005

Gupta, S. K., Singh, S., Nischal, A., Pant, K. K., & Seth, P. K. (2014). Molecular-based identification and phylogeny of genomic and proteomic sequences of mosquito-borne flavivirus. *Genes & Genomics*, *36*(1), 31–43. https://doi.org/10.1007/s13258-013-0137-x

Gwon, Y., Maxwell, B. A., Kolaitis, R.-M., Zhang, P., Kim, H. J., & Taylor, J. P. (2021). Ubiquitination of G3BP1 mediates stress granule disassembly in a context-specific manner. *Science*, *372*(6549). https://doi.org/10.1126/science.abf6548

Hakulinen, J. K., Hering, J., Brändén, G., Chen, H., Snijder, A., Ek, M., & Johansson, P. (2017). MraY–antibiotic complex reveals details of tunicamycin mode of action. *Nature Chemical Biology*, *13*(3), 265–267. https://doi.org/10.1038/nchembio.2270

Hamming, I., Timens, W., Bulthuis, M., Lely, A., Navis, G., & van Goor, H. (2004). Tissue distribution of ACE2 protein, the functional receptor for SARS coronavirus. A first step in understanding SARS pathogenesis. *The Journal of Pathology*, *203*(2), 631–637. https://doi.org/10.1002/path.1570

Han, A. P., Yu, C., Lu, L., Fujiwara, Y., Browne, C., Chin, G., Fleming, M., Leboulch, P., Orkin, S. H., & Chen, J. J. (2001). Heme-regulated eIF2alpha kinase (HRI) is required for translational regulation and survival of erythroid precursors in iron deficiency. *The EMBO Journal*, *20*(23), 6909–6918. https://doi.org/10.1093/emboj/20.23.6909

Han, T. W., Kato, M., Xie, S., Wu, L. C., Mirzaei, H., Pei, J., Chen, M., Xie, Y., Allen, J., Xiao, G., & McKnight, S. L. (2012). Cell-free Formation of RNA Granules: Bound RNAs Identify Features and Components of Cellular Assemblies. *Cell*, *149*(4), 768–779. https://doi.org/10.1016/j.cell.2012.04.016

Hansson, K. E., Rosdahl, A., Insulander, M., Vene, S., Lindquist, L., Gredmark-Russ, S., & Askling, H. H. (2020). Tick-borne Encephalitis Vaccine Failures: A 10-year Retrospective Study Supporting the Rationale for Adding an Extra Priming Dose in Individuals Starting at Age 50 Years. *Clinical Infectious Diseases*, *70*(2), 245–251. https://doi.org/10.1093/cid/ciz176

Harding, H. P., Zhang, Y., Zeng, H., Novoa, I., Lu, P. D., Calfon, M., Sadri, N., Yun, C., Popko, B., Paules, R., Stojdl, D. F., Bell, J. C., Hettmann, T., Leiden, J. M., & Ron, D. (2003). An integrated stress response regulates amino acid metabolism and resistance to oxidative stress. *Molecular Cell*, *11*(3), 619–633. https://doi.org/10.1016/s1097-2765(03)00105-9

Haviernik, J., Eyer, L., Yoshii, K., Kobayashi, S., Cerny, J., Nougairède, A., Driouich, J.-S., Volf, J., Palus, M., de Lamballerie, X., Gould, E. A., & Ruzek, D. (2021). Development and characterization of recombinant tick-borne encephalitis virus expressing mCherry reporter protein: A new tool for high-throughput screening of antiviral compounds, and neutralizing antibody assays. *Antiviral Research*, *185*, 104968. https://doi.org/10.1016/j.antiviral.2020.104968

He, Z., Zhu, X., Wen, W., Yuan, J., Hu, Y., Chen, J., An, S., Dong, X., Lin, C., Yu, J., Wu, J., Yang, Y., Cai, J., Li, J., & Li, M. (2016). Dengue Virus Subverts Host Innate Immunity by Targeting Adaptor Protein MAVS. *Journal of Virology*, *90*(16), 7219–7230. https://doi.org/10.1128/JVI.00221-16

Heinz, F. X., Holzmann, H., Essl, A., & Kundi, M. (2007). Field effectiveness of vaccination against tick-borne encephalitis. *Vaccine*, *25*(43), 7559–7567. https://doi.org/10.1016/j.vaccine.2007.08.024

Heinz, F. X., Mandl, C. W., Holzmann, H., Kunz, C., Harris, B. A., Rey, F., & Harrison, S. C. (1991). The flavivirus envelope protein E: isolation of a soluble form from tick-borne encephalitis virus and its crystallization. *Journal of Virology*, *65*(10), 5579–5583. https://doi.org/10.1128/JVI.65.10.5579-5583.1991

Heinz, F. X., Stiasny, K., Holzmann, H., Grgic-Vitek, M., Kriz, B., Essl, A., & Kundi, M. (2013). Vaccination and Tick-borne Encephalitis, Central Europe. *Emerging Infectious Diseases*, *19*(1), 69–76. https://doi.org/10.3201/eid1901.120458

Hetz, C. (2012). The unfolded protein response: controlling cell fate decisions under ER stress and beyond. *Nature Reviews Molecular Cell Biology*, *13*(2), 89–102. https://doi.org/10.1038/nrm3270

Hetz, C., Zhang, K., & Kaufman, R. J. (2020). Mechanisms, regulation and functions of the unfolded protein response. *Nature Reviews Molecular Cell Biology*, *21*(8), 421–438. https://doi.org/10.1038/s41580-020-0250-z

Hoffmann, M., Kleine-Weber, H., Schroeder, S., Krüger, N., Herrler, T., Erichsen, S., Schiergens, T. S., Herrler, G., Wu, N.-H., Nitsche, A., Müller, M. A., Drosten, C., & Pöhlmann, S. (2020). SARS-CoV-2 Cell Entry Depends on ACE2 and TMPRSS2 and Is Blocked by a Clinically Proven Protease Inhibitor. *Cell*, *181*(2), 271-280.e8. https://doi.org/10.1016/j.cell.2020.02.052

Hofmann, S., Kedersha, N., Anderson, P., & Ivanov, P. (2021). Molecular mechanisms of stress granule assembly and disassembly. *Biochimica et Biophysica Acta (BBA) - Molecular Cell Research*, *1868*(1), 118876. https://doi.org/10.1016/j.bbamcr.2020.118876

Holden, K. L., & Harris, E. (2004). Enhancement of dengue virus translation: role of the 3′ untranslated region and the terminal 3′ stem-loop domain. *Virology*, *329*(1), 119–133. https://doi.org/10.1016/j.virol.2004.08.004

Hosmillo, M., Lu, J., McAllaster, M. R., Eaglesham, J. B., Wang, X., Emmott, E., Domingues, P., Chaudhry, Y., Fitzmaurice, T. J., Tung, M. K., Panas, M. D., McInerney, G., Locker, N., Wilen, C. B., & Goodfellow, I. G. (2019). Noroviruses subvert the core stress granule component G3BP1 to promote viral VPg-dependent translation. *ELife*, *8*. https://doi.org/10.7554/eLife.46681

Hou, S., Kumar, A., Xu, Z., Airo, A. M., & Stryapunina, I. (2017). Zika Virus Hijacks Stress Granule Proteins and Modulates the Host Stress Response. *Journal of Virology*, *91*(16), 1–21.

Hou, S., Kumar, A., Xu, Z., Airo, A. M., Stryapunina, I., Wong, C. P., Branton, W., Tchesnokov, E., Götte, M., Power, C., & Hobman, T. C. (2017). Zika Virus Hijacks Stress Granule Proteins and Modulates the Host Stress Response. *Journal of Virology*, *91*(16). https://doi.org/10.1128/JVI.00474-17

Humoud, M. N., Doyle, N., Royall, E., Willcocks, M. M., Sorgeloos, F., van Kuppeveld, F., Roberts, L. O., Goodfellow, I. G., Langereis, M. A., & Locker, N. (2016). Feline Calicivirus Infection Disrupts Assembly of Cytoplasmic Stress Granules and Induces G3BP1 Cleavage. *Journal of Virology*, *90*(14), 6489–6501. https://doi.org/10.1128/JVI.00647-16

Hwang, Y.-C., Lu, R.-M., Su, S.-C., Chiang, P.-Y., Ko, S.-H., Ke, F.-Y., Liang, K.-H., Hsieh, T.-Y., & Wu, H.-C. (2022). Monoclonal antibodies for COVID-19 therapy and SARS-CoV-2 detection. *Journal of Biomedical Science*, *29*(1), 1. https://doi.org/10.1186/s12929-021-00784-w

Iadevaia, V., Burke, J. M., Eke, L., Moller-Levet, C., Parker, R., & Locker, N. (2022). Novel stress granules-like structures are induced via a paracrine mechanism during viral infection. *Journal of Cell Science*. https://doi.org/10.1242/jcs.259194

ICTV. (2011). *ICTV 9th Report - Positive Sense RNA Viruses*. Https://Talk.Ictvonline.Org/Ictv-Reports/Ictv_9th_report/Positive-Sense-Rna-Viruses-2011/w/Posrna_viruses/258/Flaviviridae-Figures.

Ivanov, P., Kedersha, N., & Anderson, P. (2019). Stress Granules and Processing Bodies in Translational Control. *Cold Spring Harbor Perspectives in Biology*, *11*(5), a032813. https://doi.org/10.1101/cshperspect.a032813

Jain, S., Wheeler, J. R., Walters, R. W., Agrawal, A., Barsic, A., & Parker, R. (2016). ATPase-Modulated Stress Granules Contain a Diverse Proteome and Substructure. *Cell*, *164*(3), 487–498. https://doi.org/10.1016/j.cell.2015.12.038

Jan, L. R., Yang, C. S., Trent, D. W., Falgout, B., & Lai, C. J. (1995). Processing of Japanese encephalitis virus non-structural proteins: NS2B-NS3 complex and heterologous proteases. *The Journal of General Virology*, *76 (Pt 3)*, 573–580. https://doi.org/10.1099/0022-1317-76-3-573

Johnston, B. P., & McCormick, C. (2019). Herpesviruses and the Unfolded Protein Response. *Viruses*, *12*(1), 17. https://doi.org/10.3390/v12010017

Jousse, C., Oyadomari, S., Novoa, I., Lu, P., Zhang, Y., Harding, H. P., & Ron, D. (2003). Inhibition of a constitutive translation initiation factor 2α phosphatase, CReP, promotes survival of stressed cells. *Journal of Cell Biology*, *163*(4), 767–775. https://doi.org/10.1083/jcb.200308075

Kaptein, S. J. F., Goethals, O., Kiemel, D., Marchand, A., Kesteleyn, B., Bonfanti, J.-F., Bardiot, D., Stoops, B., Jonckers, T. H. M., Dallmeier, K., Geluykens, P., Thys, K., Crabbe, M., Chatel-Chaix, L., Münster, M., Querat, G., Touret, F., de Lamballerie, X., Raboisson, P., … Neyts, J. (2021). A pan-serotype dengue virus inhibitor targeting the NS3–NS4B interaction. *Nature*, *598*(7881), 504–509. https://doi.org/10.1038/s41586-021-03990-6

Kastan, J. P., Dobrikova, E. Y., Bryant, J. D., & Gromeier, M. (2020). CReP mediates selective translation initiation at the endoplasmic reticulum. *Science Advances*, *6*(23). https://doi.org/10.1126/sciadv.aba0745

Kato, H., Takahasi, K., & Fujita, T. (2011). RIG-I-like receptors: cytoplasmic sensors for non-self RNA. *Immunological Reviews*, *243*(1), 91–98. https://doi.org/10.1111/j.1600-065X.2011.01052.x

Kato, M., Han, T. W., Xie, S., Shi, K., Du, X., Wu, L. C., Mirzaei, H., Goldsmith, E. J., Longgood, J., Pei, J., Grishin, N. V., Frantz, D. E., Schneider, J. W., Chen, S., Li, L., Sawaya, M. R., Eisenberg, D., Tycko, R., & McKnight, S. L. (2012). Cell-free Formation of RNA Granules: Low Complexity Sequence Domains Form Dynamic Fibers within Hydrogels. *Cell*, *149*(4), 753–767. https://doi.org/10.1016/j.cell.2012.04.017

Katoh, H., Okamoto, T., Fukuhara, T., Kambara, H., Morita, E., Mori, Y., Kamitani, W., & Matsuura, Y. (2013). Japanese encephalitis virus core protein inhibits stress granule formation through an interaction with Caprin-1 and facilitates viral propagation. *Journal of Virology*, *87*(1), 489–502. https://doi.org/10.1128/JVI.02186-12

Kaufman, R. J. (1999). Double-stranded RNA-activated protein kinase mediates virus-induced apoptosis: A new role for an old actor. *Proceedings of the National Academy of Sciences*, *96*(21), 11693–11695. https://doi.org/10.1073/pnas.96.21.11693

Kaufusi, P. H., Kelley, J. F., Yanagihara, R., & Nerurkar, V. R. (2014). Induction of endoplasmic reticulum-derived replication-competent membrane structures by West Nile virus non-structural protein 4B. *PloS One*, *9*(1), e84040. https://doi.org/10.1371/journal.pone.0084040

Kedersha, N., Cho, M. R., Li, W., Yacono, P. W., Chen, S., Gilks, N., Golan, D. E., & Anderson, P. (2000). Dynamic Shuttling of Tia-1 Accompanies the Recruitment of mRNA to Mammalian Stress Granules. *Journal of Cell Biology*, *151*(6), 1257–1268. https://doi.org/10.1083/jcb.151.6.1257

Kedersha, N., Panas, M. D., Achorn, C. A., Lyons, S., Tisdale, S., Hickman, T., Thomas, M., Lieberman, J., McInerney, G. M., Ivanov, P., & Anderson, P. (2016). G3BP–Caprin1–USP10 complexes mediate stress granule condensation and associate with 40S subunits. *Journal of Cell Biology*, *212*(7). https://doi.org/10.1083/jcb.201508028

Khromykh, A. A., Varnavski, A. N., Sedlak, P. L., & Westaway, E. G. (2001). Coupling between Replication and Packaging of Flavivirus RNA: Evidence Derived from the Use of DNA-Based Full-Length cDNA Clones of Kunjin Virus. *Journal of Virology*, *75*(10), 4633–4640. https://doi.org/10.1128/JVI.75.10.4633-4640.2001

Klema, V. J., Padmanabhan, R., & Choi, K. H. (2015). Flaviviral Replication Complex: Coordination between RNA Synthesis and 5'-RNA Capping. *Viruses*, *7*(8), 4640–4656. https://doi.org/10.3390/v7082837

Kojima, E., Takeuchi, A., Haneda, M., Yagi, F., Hasegawa, T., Yamaki, K.-I., Takeda, K., Akira, S., Shimokata, K., & Isobe, K.-I. (2003). The function of GADD34 is a recovery from a shutoff of protein synthesis induced by ER stress—elucidation by GADD34-deficient mice. *The FASEB Journal*, *17*(11), 1–18. https://doi.org/10.1096/fj.02-1184fje

Konior, R., Brzostek, J., Poellabauer, E. M., Jiang, Q., Harper, L., & Erber, W. (2017). Seropersistence of TBE virus antibodies 10 years after first booster vaccination and response to a second booster vaccination with FSME-IMMUN 0.5 mL in adults. *Vaccine*, *35*(28), 3607–3613. https://doi.org/10.1016/j.vaccine.2017.03.059

Kozlovskaya, L. I., Osolodkin, D. I., Shevtsova, A. S., Romanova, L. Iu., Rogova, Y. V., Dzhivanian, T. I., Lyapustin, V. N., Pivanova, G. P., Gmyl, A. P., Palyulin, V. A., & Karganova, G. G. (2010). GAG-binding variants of tick-borne encephalitis virus. *Virology*, *398*(2), 262–272. https://doi.org/10.1016/j.virol.2009.12.012

Kroschewski, H., Allison, S. L., Heinz, F. X., & Mandl, C. W. (2003). Role of heparan sulfate for attachment and entry of tick-borne encephalitis virus. *Virology*, *308*(1), 92–100. https://doi.org/10.1016/S0042-6822(02)00097-1

Ksiazek, T. G., Erdman, D., Goldsmith, C. S., Zaki, S. R., Peret, T., Emery, S., Tong, S., Urbani, C., Comer, J. A., Lim, W., Rollin, P. E., Dowell, S. F., Ling, A.-E., Humphrey, C. D., Shieh,

W.-J., Guarner, J., Paddock, C. D., Rota, P., Fields, B., … Anderson, L. J. (2003). A Novel Coronavirus Associated with Severe Acute Respiratory Syndrome. *New England Journal of Medicine*, *348*(20), 1953–1966. https://doi.org/10.1056/NEJMoa030781

Kumar, A., Taghi Khani, A., & Swaminathan, S. (2021). Type I interferons: One stone to concurrently kill two birds, viral infections and cancers. *Current Research in Virological Science*, *2*, 100014. https://doi.org/https://doi.org/10.1016/j.crviro.2021.100014

Kümmerer, B. M., & Rice, C. M. (2002). Mutations in the yellow fever virus nonstructural protein NS2A selectively block production of infectious particles. *Journal of Virology*, *76*(10), 4773–4784. https://doi.org/10.1128/jvi.76.10.4773-4784.2002

Kuno, G., Chang, G. J., Tsuchiya, K. R., Karabatsos, N., & Cropp, C. B. (1998). Phylogeny of the genus Flavivirus. *Journal of Virology*, *72*(1), 73–83.

Kunz, C. (2003). TBE vaccination and the Austrian experience. *Vaccine*, *21*, S50–S55. https://doi.org/10.1016/S0264-410X(02)00813-7

Labuda, M., Austyn, J. M., Zuffova, E., Kozuch, O., Fuchsberger, N., Lysy, J., & Nutall, P. A. (1996). Importance of Localized Skin Infection in Tick-Borne Encephalitis Virus Transmission. *Virology*, *219*(2), 357–366. https://doi.org/10.1006/viro.1996.0261

Langereis, M. A., Feng, Q., & van Kuppeveld, F. J. (2013). MDA5 Localizes to Stress Granules, but This Localization Is Not Required for the Induction of Type I Interferon. *Journal of Virology*, *87*(11), 6314–6325. https://doi.org/10.1128/JVI.03213-12

Langer-Safer, P. R., Levine, M., & Ward, D. C. (1982). Immunological method for mapping genes on Drosophila polytene chromosomes. *Proceedings of the National Academy of Sciences of the United States of America*, *79*(14), 4381–4385. https://doi.org/10.1073/pnas.79.14.4381

Lee, A. J., & Ashkar, A. A. (2018). The Dual Nature of Type I and Type II Interferons. *Frontiers in Immunology*, *9*. https://doi.org/10.3389/fimmu.2018.02061

Lee, E., & Lobigs, M. (2008). E Protein Domain III Determinants of Yellow Fever Virus 17D Vaccine Strain Enhance Binding to Glycosaminoglycans, Impede Virus Spread, and Attenuate Virulence. *Journal of Virology*, *82*(12), 6024–6033. https://doi.org/10.1128/JVI.02509-07

Li, K., Phoo, W. W., & Luo, D. (2014). Functional interplay among the flavivirus NS3 protease, helicase, and cofactors. *Virologica Sinica*, *29*(2), 74–85. https://doi.org/10.1007/s12250-014-3438-6

Li, X.-D., Deng, C.-L., Ye, H.-Q., Zhang, H.-L., Zhang, Q.-Y., Chen, D.-D., Zhang, P.-T., Shi, P.-Y., Yuan, Z.-M., & Zhang, B. (2016). Transmembrane Domains of NS2B Contribute to both Viral RNA Replication and Particle Formation in Japanese Encephalitis Virus. *Journal of Virology*, *90*(12), 5735–5749. https://doi.org/10.1128/JVI.00340-16

Licastro, D., Rajasekharan, S., Dal Monego, S., Segat, L., D'Agaro, P., & Marcello, A. (2020). Isolation and Full-Length Genome Characterization of SARS-CoV-2 from COVID-19 Cases in Northern Italy. In *Journal of virology* (Vol. 94, Issue 11). https://doi.org/10.1128/JVI.00543-20

Ličková, M., Fumačová Havlíková, S., Sláviková, M., & Klempa, B. (2021). Alimentary Infections by Tick-Borne Encephalitis Virus. *Viruses*, *14*(1), 56. https://doi.org/10.3390/v14010056

Lin, D. L., Inoue, T., Chen, Y.-J., Chang, A., Tsai, B., & Tai, A. W. (2019). The ER Membrane Protein Complex Promotes Biogenesis of Dengue and Zika Virus Non-structural Multi-pass Transmembrane Proteins to Support Infection. *Cell Reports*, *27*(6), 1666-1674.e4. https://doi.org/10.1016/j.celrep.2019.04.051

Lin, R.-J., Chang, B.-L., Yu, H.-P., Liao, C.-L., & Lin, Y.-L. (2006). Blocking of Interferon-Induced Jak-Stat Signaling by Japanese Encephalitis Virus NS5 through a Protein Tyrosine Phosphatase-Mediated Mechanism. *Journal of Virology*, *80*(12), 5908–5918. https://doi.org/10.1128/JVI.02714-05

Lindenbach, B. D., & Rice, C. M. (1999). Genetic interaction of flavivirus nonstructural proteins NS1 and NS4A as a determinant of replicase function. *Journal of Virology*, *73*(6), 4611–4621. https://doi.org/10.1128/JVI.73.6.4611-4621.1999

Lindenbach, B. D., & Rice, C. M. (2003). *Molecular biology of flaviviruses* (pp. 23–61). https://doi.org/10.1016/S0065-3527(03)59002-9

Lindquist, M. E., Lifland, A. W., Utley, T. J., Santangelo, P. J., & Crowe, J. E. (2010). Respiratory Syncytial Virus Induces Host RNA Stress Granules To Facilitate Viral Replication. *Journal of Virology*, *84*(23), 12274–12284. https://doi.org/10.1128/JVI.00260-10

Liu, J., Li, S., Liu, J., Liang, B., Wang, X., Wang, H., Li, W., Tong, Q., Yi, J., Zhao, L., Xiong, L., Guo, C., Tian, J., Luo, J., Yao, J., Pang, R., Shen, H., Peng, C., Liu, T., … Zheng, X. (2020). Longitudinal characteristics of lymphocyte responses and cytokine profiles in the peripheral blood of SARS-CoV-2 infected patients. *EBioMedicine*, *55*, 102763. https://doi.org/10.1016/j.ebiom.2020.102763

Liu, W. J., Chen, H. B., Wang, X. J., Huang, H., & Khromykh, A. A. (2004). Analysis of Adaptive Mutations in Kunjin Virus Replicon RNA Reveals a Novel Role for the Flavivirus Nonstructural Protein NS2A in Inhibition of Beta Interferon Promoter-Driven Transcription. *Journal of Virology*, *78*(22), 12225–12235. https://doi.org/10.1128/JVI.78.22.12225-12235.2004

Liu, Z.-W., Zhu, H.-T., Chen, K.-L., Dong, X., Wei, J., Qiu, C., & Xue, J.-H. (2013). Protein kinase RNA-like endoplasmic reticulum kinase (PERK) signaling pathway plays a major role in reactive oxygen species (ROS)-mediated endoplasmic reticulum stress-induced apoptosis in diabetic cardiomyopathy. *Cardiovascular Diabetology*, *12*, 158. https://doi.org/10.1186/1475-2840-12-158

Lotrič-Furlan, S., Bogovič, P., Avšič-Županc, T., Jelovšek, M., Lusa, L., & Strle, F. (2017). Tick-borne encephalitis in patients vaccinated against this disease. *Journal of Internal Medicine*, *282*(2), 142–155. https://doi.org/10.1111/joim.12625

Lu, R., Zhao, X., Li, J., Niu, P., Yang, B., Wu, H., Wang, W., Song, H., Huang, B., Zhu, N., Bi, Y., Ma, X., Zhan, F., Wang, L., Hu, T., Zhou, H., Hu, Z., Zhou, W., Zhao, L., … Tan, W. (2020). Genomic characterisation and epidemiology of 2019 novel coronavirus: implications for virus origins and receptor binding. *The Lancet*, *395*(10224), 565–574. https://doi.org/10.1016/S0140-6736(20)30251-8

Mackenzie, J. (2005). Wrapping things up about virus RNA replication. *Traffic (Copenhagen, Denmark)*, *6*(11), 967–977. https://doi.org/10.1111/j.1600-0854.2005.00339.x

Mackenzie, J. M., Jones, M. K., & Westaway, E. G. (1999). Markers for trans-Golgi membranes and the intermediate compartment localize to induced membranes with distinct replication functions in flavivirus-infected cells. *Journal of Virology*, *73*(11), 9555–9567. https://doi.org/10.1128/JVI.73.11.9555-9567.1999

Mackenzie, J. M., & Westaway, E. G. (2001). Assembly and maturation of the flavivirus Kunjin virus appear to occur in the rough endoplasmic reticulum and along the secretory pathway, respectively. *Journal of Virology*, *75*(22), 10787–10799. https://doi.org/10.1128/JVI.75.22.10787-10799.2001

Mackenzie, J. S., Gubler, D. J., & Petersen, L. R. (2004). Emerging flaviviruses: the spread and resurgence of Japanese encephalitis, West Nile and dengue viruses. *Nature Medicine*, *10*(12), S98–S109. https://doi.org/10.1038/nm1144

Mahase, E. (2021). Covid-19: Pfizer's paxlovid is 89% effective in patients at risk of serious illness, company reports. *BMJ*, n2713. https://doi.org/10.1136/bmj.n2713

Malone, B., Urakova, N., Snijder, E. J., & Campbell, E. A. (2022). Structures and functions of coronavirus replication–transcription complexes and their relevance for SARS-CoV-2 drug design. *Nature Reviews Molecular Cell Biology*, *23*(1), 21–39. https://doi.org/10.1038/s41580-021-00432-z

Mandl, C. W., Holzmann, H., Meixner, T., Rauscher, S., Stadler, P. F., Allison, S. L., & Heinz, F. X. (1998). Spontaneous and engineered deletions in the 3' noncoding region of tick-borne encephalitis virus: construction of highly attenuated mutants of a flavivirus. *Journal of Virology*, *72*(3), 2132–2140. https://doi.org/10.1128/JVI.72.3.2132-2140.1998

Mandl, C. W., Kroschewski, H., Allison, S. L., Kofler, R., Holzmann, H., Meixner, T., & Heinz, F. X. (2001). Adaptation of Tick-Borne Encephalitis Virus to BHK-21 Cells Results in the Formation of Multiple Heparan Sulfate Binding Sites in the Envelope Protein and Attenuation In Vivo. *Journal of Virology*, *75*(12), 5627–5637. https://doi.org/10.1128/JVI.75.12.5627-5637.2001

Manivannan, P., Siddiqui, M. A., & Malathi, K. (2020). RNase L Amplifies Interferon Signaling by Inducing Protein Kinase R-Mediated Antiviral Stress Granules. *Journal of Virology*, *94*(13). https://doi.org/10.1128/JVI.00205-20

Manokaran, G., Finol, E., Wang, C., Gunaratne, J., Bahl, J., Ong, E. Z., Tan, H. C., Sessions, O. M., Ward, A. M., Gubler, D. J., Harris, E., Garcia-Blanco, M. A., & Ooi, E. E. (2015). Dengue subgenomic RNA binds TRIM25 to inhibit interferon expression for epidemiological fitness. *Science*, *350*(6257), 217–221. https://doi.org/10.1126/science.aab3369

Mansfield, J. P., Shellam, G. R., Mackenzie, J. S., Urosevic, N., & van Maanen, M. (1997). Molecular characterization of virus-specific RNA produced in the brains of flavivirus-susceptible and -resistant mice after challenge with Murray Valley encephalitis virus. *Journal of General Virology*, *78*(1), 23–29. https://doi.org/10.1099/0022-1317-78-1-23

Mansfield, K. L., Johnson, N., Phipps, L. P., Stephenson, J. R., Fooks, A. R., & Solomon, T. (2009). Tick-borne encephalitis virus – a review of an emerging zoonosis. *Journal of General Virology*, *90*(8), 1781–1794. https://doi.org/10.1099/vir.0.011437-0

Marcello, A., Civra, A., Milan Bonotto, R., Nascimento Alves, L., Rajasekharan, S., Giacobone, C., Caccia, C., Cavalli, R., Adami, M., Brambilla, P., Lembo, D., Poli, G., & Leoni, V.

(2020). The cholesterol metabolite 27-hydroxycholesterol inhibits SARS-CoV-2 and is markedly decreased in COVID-19 patients. *Redox Biology*, *36*, 101682. https://doi.org/10.1016/j.redox.2020.101682

Markoff, L. (2003). *5′- and 3′-noncoding regions in flavivirus RNA* (pp. 177–228). https://doi.org/10.1016/S0065-3527(03)59006-6

Matsuki, H., Takahashi, M., Higuchi, M., Makokha, G. N., Oie, M., & Fujii, M. (2013). Both G3BP1 and G3BP2 contribute to stress granule formation. *Genes to Cells : Devoted to Molecular & Cellular Mechanisms*, *18*(2), 135–146. https://doi.org/10.1111/gtc.12023

Maximova, O. A., & Pletnev, A. G. (2018). Flaviviruses and the Central Nervous System: Revisiting Neuropathological Concepts. *Annual Review of Virology*, *5*(1), 255–272. https://doi.org/10.1146/annurev-virology-092917-043439

Maxwell, B. A., Gwon, Y., Mishra, A., Peng, J., Nakamura, H., Zhang, K., Kim, H. J., & Taylor, J. P. (2021). Ubiquitination is essential for recovery of cellular activities after heat shock. *Science*, *372*(6549). https://doi.org/10.1126/science.abc3593

Mayo, C. B., Erlandsen, H., Mouser, D. J., Feinstein, A. G., Robinson, V. L., May, E. R., & Cole, J. L. (2019). Structural Basis of Protein Kinase R Autophosphorylation [Research-article]. *Biochemistry*, *58*(27), 2967–2977. https://doi.org/10.1021/acs.biochem.9b00161

Mei, M., & Tan, X. (2021). Current Strategies of Antiviral Drug Discovery for COVID-19. *Frontiers in Molecular Biosciences*, *8*. https://doi.org/10.3389/fmolb.2021.671263

Mikulasova, A., Gillespie, L. K., Ambrose, R. L., Aktepe, T. E., Trenerry, A. M., Liebscher, S., & Mackenzie, J. M. (2021). A Putative Lipid-Associating Motif in the West Nile Virus NS4A Protein Is Required for Efficient Virus Replication. *Frontiers in Cell and Developmental Biology*, *9*. https://doi.org/10.3389/fcell.2021.655606

Miller, S., Kastner, S., Krijnse-Locker, J., Bühler, S., & Bartenschlager, R. (2007). The Non-structural Protein 4A of Dengue Virus Is an Integral Membrane Protein Inducing Membrane Alterations in a 2K-regulated Manner*. *Journal of Biological Chemistry*, *282*(12), 8873–8882. https://doi.org/https://doi.org/10.1074/jbc.M609919200

Miller, S., Sparacio, S., & Bartenschlager, R. (2006). Subcellular localization and membrane topology of the Dengue virus type 2 Non-structural protein 4B. *The Journal of Biological Chemistry*, *281*(13), 8854–8863. https://doi.org/10.1074/jbc.M512697200

Miorin, L., Albornoz, A., Baba, M. M., D'Agaro, P., & Marcello, A. (2012). Formation of membrane-defined compartments by tick-borne encephalitis virus contributes to the early delay in interferon signaling. *Virus Research*, *163*(2), 660–666. https://doi.org/10.1016/j.virusres.2011.11.020

Miorin, L., Romero-Brey, I., Maiuri, P., Hoppe, S., Krijnse-Locker, J., Bartenschlager, R., & Marcello, A. (2013). Three-dimensional architecture of tick-borne encephalitis virus replication sites and trafficking of the replicated RNA. *Journal of Virology*, *87*(11), 6469–6481. https://doi.org/10.1128/JVI.03456-12

Mokas, S., Mills, J. R., Garreau, C., Fournier, M.-J., Robert, F., Arya, P., Kaufman, R. J., Pelletier, J., & Mazroui, R. (2009). Uncoupling stress granule assembly and translation initiation inhibition. *Molecular Biology of the Cell*, *20*(11), 2673–2683. https://doi.org/10.1091/mbc.e08-10-1061

Mollica, V., Rizzo, A., & Massari, F. (2020). The pivotal role of TMPRSS2 in coronavirus disease 2019 and prostate cancer. *Future Oncology*, *16*(27), 2029–2033. https://doi.org/10.2217/fon-2020-0571

Mora-Cárdenas, E., Aloise, C., Faoro, V., Knap Gašper, N., Korva, M., Caracciolo, I., D'Agaro, P., Avšič-Županc, T., & Marcello, A. (2020). Comparative specificity and sensitivity of NS1-based serological assays for the detection of flavivirus immune response. *PLOS Neglected Tropical Diseases*, *14*(1), e0008039. https://doi.org/10.1371/journal.pntd.0008039

Morrison, J., Laurent-Rolle, M., Maestre, A. M., Rajsbaum, R., Pisanelli, G., Simon, V., Mulder, L. C. F., Fernandez-Sesma, A., & García-Sastre, A. (2013). Dengue Virus Co-opts UBR4 to Degrade STAT2 and Antagonize Type I Interferon Signaling. *PLoS Pathogens*, *9*(3), e1003265. https://doi.org/10.1371/journal.ppat.1003265

Mossel, E. C., Huang, C., Narayanan, K., Makino, S., Tesh, R. B., & Peters, C. J. (2005). Exogenous ACE2 expression allows refractory cell lines to support severe acute respiratory syndrome coronavirus replication. *Journal of Virology*, *79*(6), 3846–3850. https://doi.org/10.1128/JVI.79.6.3846-3850.2005

Muñoz-Jordán, J. L., Laurent-Rolle, M., Ashour, J., Martínez-Sobrido, L., Ashok, M., Lipkin, W. I., & García-Sastre, A. (2005). Inhibition of Alpha/Beta Interferon Signaling by the NS4B Protein of Flaviviruses. *Journal of Virology*, *79*(13), 8004–8013. https://doi.org/10.1128/JVI.79.13.8004-8013.2005

Muñoz-Jordán, J. L., Sánchez-Burgos, G. G., Laurent-Rolle, M., & García-Sastre, A. (2003). Inhibition of interferon signaling by dengue virus. *Proceedings of the National Academy of Sciences*, *100*(24), 14333–14338. https://doi.org/10.1073/pnas.2335168100

Munoz-Jordan, J. L., Sanchez-Burgos, G. G., Laurent-Rolle, M., & Garcia-Sastre, A. (2003). Inhibition of interferon signaling by dengue virus. *Proceedings of the National Academy of Sciences*, *100*(24), 14333–14338. https://doi.org/10.1073/pnas.2335168100

Murray, C. L., Jones, C. T., & Rice, C. M. (2008). Architects of assembly: roles of Flaviviridae non-structural proteins in virion morphogenesis. *Nature Reviews. Microbiology*, *6*(9), 699–708. https://doi.org/10.1038/nrmicro1928

NATHANS, D. (1964). PUROMYCIN INHIBITION OF PROTEIN SYNTHESIS: INCORPORATION OF PUROMYCIN INTO PEPTIDE CHAINS. *Proceedings of the National Academy of Sciences of the United States of America*, *51*(4), 585–592. https://doi.org/10.1073/pnas.51.4.585

Nawa, M., Takasaki, T., Yamada, K.-I., Kurane, I., & Akatsuka, T. (2003). Interference in Japanese encephalitis virus infection of Vero cells by a cationic amphiphilic drug, chlorpromazine. *Journal of General Virology*, *84*(7), 1737–1741. https://doi.org/10.1099/vir.0.18883-0

Neyts, J., Leyssen, P., & De Clercq, E. (1999). Infections with flaviviridae. *Verhandelingen - Koninklijke Academie Voor Geneeskunde van Belgie*, *61*(6), 661–669.

Ng, M. L., & Lau, L. C. L. (1988). Possible involvement of receptors in the entry of Kunjin virus into Vero cells. *Archives of Virology*, *100*(3–4), 199–211. https://doi.org/10.1007/BF01487683

Novoa, I., Zeng, H., Harding, H. P., & Ron, D. (2001). Feedback Inhibition of the Unfolded Protein Response by GADD34-Mediated Dephosphorylation of eIF2α. *Journal of Cell Biology*, *153*(5), 1011–1022. https://doi.org/10.1083/jcb.153.5.1011

Nowinski, S. M., Solmonson, A., Rusin, S. F., Maschek, J. A., Bensard, C. L., Fogarty, S., Jeong, M.-Y., Lettlova, S., Berg, J. A., Morgan, J. T., Ouyang, Y., Naylor, B. C., Paulo, J. A., Funai, K., Cox, J. E., Gygi, S. P., Winge, D. R., DeBerardinis, R. J., & Rutter, J. (2020). Mitochondrial fatty acid synthesis coordinates oxidative metabolism in mammalian mitochondria. *ELife*, *9*. https://doi.org/10.7554/eLife.58041

Oh, S. W., Onomoto, K., Wakimoto, M., Onoguchi, K., Ishidate, F., Fujiwara, T., Yoneyama, M., Kato, H., & Fujita, T. (2016). Leader-Containing Uncapped Viral Transcript Activates RIG-I in Antiviral Stress Granules. *PLoS Pathogens*, *12*(2), 1–22. https://doi.org/10.1371/journal.ppat.1005444

Onomoto, K., Jogi, M., Yoo, J. S., Narita, R., Morimoto, S., Takemura, A., Sambhara, S., Kawaguchi, A., Osari, S., Nagata, K., Matsumiya, T., Namiki, H., Yoneyama, M., & Fujita, T. (2012). Critical role of an antiviral stress granule containing RIG-I and PKR in viral detection and innate immunity. *PLoS ONE*, *7*(8). https://doi.org/10.1371/journal.pone.0043031

Onomoto, K., Yoneyama, M., Fung, G., Kato, H., & Fujita, T. (2014). Antiviral innate immunity and stress granule responses. *Trends in Immunology*, *35*(9), 420–428. https://doi.org/10.1016/j.it.2014.07.006

Ou, X., Liu, Y., Lei, X., Li, P., Mi, D., Ren, L., Guo, L., Guo, R., Chen, T., Hu, J., Xiang, Z., Mu, Z., Chen, X., Chen, J., Hu, K., Jin, Q., Wang, J., & Qian, Z. (2020). Characterization of spike glycoprotein of SARS-CoV-2 on virus entry and its immune cross-reactivity with SARS-CoV. *Nature Communications*, *11*(1), 1620. https://doi.org/10.1038/s41467-020-15562-9

Overby, A. K., Popov, V. L., Niedrig, M., & Weber, F. (2010). Tick-Borne Encephalitis Virus Delays Interferon Induction and Hides Its Double-Stranded RNA in Intracellular Membrane Vesicles. *Journal of Virology*, *84*(17), 8470–8483. https://doi.org/10.1128/JVI.00176-10

Pakos-Zebrucka, K., Koryga, I., Mnich, K., Ljujic, M., Samali, A., & Gorman, A. M. (2016). The integrated stress response. *EMBO Reports*, *17*(10), 1374–1395. https://doi.org/10.15252/embr.201642195

Panas, M. D., Ivanov, P., & Anderson, P. (2016). Mechanistic insights into mammalian stress granule dynamics. *Journal of Cell Biology*, *215*(3), 313–323. https://doi.org/10.1083/jcb.201609081

Pardi, N., & Weissman, D. (2020). Development of vaccines and antivirals for combating viral pandemics. *Nature Biomedical Engineering*, *4*(12), 1128–1133. https://doi.org/10.1038/s41551-020-00658-w

Pardue, M. L., & Gall, J. G. (1969). Molecular hybridization of radioactive DNA to the DNA of cytological preparations. *Proceedings of the National Academy of Sciences of the United States of America*, *64*(2), 600–604. https://doi.org/10.1073/pnas.64.2.600

Paul, D., & Bartenschlager, R. (2015). Flaviviridae Replication Organelles: Oh, What a Tangled Web We Weave. *Annual Review of Virology*, *2*(1), 289–310. https://doi.org/10.1146/annurev-virology-100114-055007

Peña, J., & Harris, E. (2011). Dengue Virus Modulates the Unfolded Protein Response in a Time-dependent Manner. *Journal of Biological Chemistry*, *286*(16), 14226–14236. https://doi.org/10.1074/jbc.M111.222703

Petris, G., Bestagno, M., Arnoldi, F., & Burrone, O. R. (2014). New Tags for Recombinant Protein Detection and O-Glycosylation Reporters. *PLOS ONE*, *9*(5), 1–9. https://doi.org/10.1371/journal.pone.0096700

Pfizer. (2021). *Pfizer Announces Additional Phase 2/3 Study Results Confirming Robust Efficacy of Novel COVID-19 Oral Antiviral Treatment Candidate in Reducing Risk of Hospitalization or Death*. https://www.pfizer.com/news/press-release/press-release-detail/pfizer-announces-additional-phase-23-study-results

Pham, A. M., Santa Maria, F. G., Lahiri, T., Friedman, E., Marié, I. J., & Levy, D. E. (2016). PKR Transduces MDA5-Dependent Signals for Type I IFN Induction. *PLOS Pathogens*, *12*(3), e1005489. https://doi.org/10.1371/journal.ppat.1005489

Pijlman, G. P., Funk, A., Kondratieva, N., Leung, J., Torres, S., van der Aa, L., Liu, W. J., Palmenberg, A. C., Shi, P.-Y., Hall, R. A., & Khromykh, A. A. (2008). A Highly Structured, Nuclease-Resistant, Noncoding RNA Produced by Flaviviruses Is Required for Pathogenicity. *Cell Host & Microbe*, *4*(6), 579–591. https://doi.org/10.1016/j.chom.2008.10.007

Platt, F. M., d'Azzo, A., Davidson, B. L., Neufeld, E. F., & Tifft, C. J. (2018). Lysosomal storage diseases. *Nature Reviews. Disease Primers*, *4*(1), 27. https://doi.org/10.1038/s41572-018-0025-4

Protter, D. S. W., & Parker, R. (2016). Principles and Properties of Stress Granules. *Trends in Cell Biology*, *26*(9), 668–679. https://doi.org/10.1016/j.tcb.2016.05.004

Pulkkinen, L. I. A., Butcher, S. J., & Anastasina, M. (2018). Tick-Borne Encephalitis Virus: A Structural View. *Viruses*, *10*(7). https://doi.org/10.3390/v10070350

Rabouw, H. H., Langereis, M. A., Knaap, R. C. M., Dalebout, T. J., Canton, J., Sola, I., Enjuanes, L., Bredenbeek, P. J., Kikkert, M., de Groot, R. J., & van Kuppeveld, F. J. M. (2016). Middle East Respiratory Coronavirus Accessory Protein 4a Inhibits PKR-Mediated Antiviral Stress Responses. *PLOS Pathogens*, *12*(10), e1005982. https://doi.org/10.1371/journal.ppat.1005982

Rafie-Kolpin, M., Chefalo, P. J., Hussain, Z., Hahn, J., Uma, S., Matts, R. L., & Chen, J. J. (2000). Two heme-binding domains of heme-regulated eukaryotic initiation factor-2alpha kinase. N terminus and kinase insertion. *The Journal of Biological Chemistry*, *275*(7), 5171–5178. https://doi.org/10.1074/jbc.275.7.5171

Rajah, M. M., Monel, B., & Schwartz, O. (2020). The entanglement between flaviviruses and ER-shaping proteins. *PLOS Pathogens*, *16*(4), e1008389. https://doi.org/10.1371/journal.ppat.1008389

Rajasekharan, S., Milan Bonotto, R., Nascimento Alves, L., Kazungu, Y., Poggianella, M., Martinez-Orellana, P., Skoko, N., Polez, S., & Marcello, A. (2021). Inhibitors of Protein Glycosylation Are Active against the Coronavirus Severe Acute Respiratory Syndrome Coronavirus SARS-CoV-2. *Viruses*, *13*(5). https://doi.org/10.3390/v13050808

Randolph, S. E. (2008). Tick-borne encephalitis incidence in Central and Eastern Europe: consequences of political transition. *Microbes and Infection*, *10*(3), 209–216. https://doi.org/10.1016/j.micinf.2007.12.005

Randolph, S. E., Miklisová, D., Lysy, J., Rogers, D. J., & Labuda, M. (1999). Incidence from coincidence: patterns of tick infestations on rodents facilitate transmission of tick-borne encephalitis virus. *Parasitology*, *118*(2), 177–186. https://doi.org/10.1017/S0031182098003643

Rao, R. v, & Bredesen, D. E. (2004). Misfolded proteins, endoplasmic reticulum stress and neurodegeneration. *Current Opinion in Cell Biology*, *16*(6), 653–662. https://doi.org/10.1016/j.ceb.2004.09.012

Ray, D., Shah, A., Tilgner, M., Guo, Y., Zhao, Y., Dong, H., Deas, T. S., Zhou, Y., Li, H., & Shi, P.-Y. (2006). West Nile Virus 5′-Cap Structure Is Formed by Sequential Guanine N-7 and Ribose 2′-O Methylations by Nonstructural Protein 5. *Journal of Virology*, *80*(17), 8362–8370. https://doi.org/10.1128/JVI.00814-06

Reineke, L. C., Cheema, S. A., Dubrulle, J., & Neilson, J. R. (2018). Chronic starvation induces non-canonical pro-death stress granules. *Journal of Cell Science*. https://doi.org/10.1242/jcs.220244

Reineke, L. C., & Neilson, J. R. (2019). Differences between acute and chronic stress granules, and how these differences may impact function in human disease. *Biochemical Pharmacology*, *162*, 123–131. https://doi.org/10.1016/j.bcp.2018.10.009

Rezza, G., Farchi, F., Pezzotti, P., Ruscio, M., lo Presti, A., Ciccozzi, M., Mondardini, V., Paternoster, C., Bassetti, M., Merelli, M., Scotton, P. G., Luzzati, R., Simeoni, J., Mian, P., Mel, R., Carraro, V., Zanin, A., Ferretto, R., & Francavilla, E. (2015). Tick-borne encephalitis in north-east Italy: a 14-year retrospective study, January 2000 to December 2013. *Eurosurveillance*, *20*(40). https://doi.org/10.2807/1560-7917.ES.2015.20.40.30034

Ricardo-Lax, I., Luna, J. M., Thao, T. T. N., le Pen, J., Yu, Y., Hoffmann, H.-H., Schneider, W. M., Razooky, B. S., Fernandez-Martinez, J., Schmidt, F., Weisblum, Y., Trüeb, B. S., Berenguer Veiga, I., Schmied, K., Ebert, N., Michailidis, E., Peace, A., Sánchez-Rivera, F. J., Lowe, S. W., … Rice, C. M. (2021). Replication and single-cycle delivery of SARS-CoV-2 replicons. *Science*, *374*(6571), 1099–1106. https://doi.org/10.1126/science.abj8430

Riccò, M., Gualerzi, G., Ranzieri, S., Ferraro, P., & Bragazzi, N. L. (2020). Knowledge, Attitudes, Practices (KAP) of Italian Occupational Physicians towards Tick Borne Encephalitis. *Tropical Medicine and Infectious Disease*, *5*(3), 117. https://doi.org/10.3390/tropicalmed5030117

Riggs, C. L., Kedersha, N., Ivanov, P., & Anderson, P. (2020). Mammalian stress granules and P bodies at a glance. *Journal of Cell Science*, *133*(16). https://doi.org/10.1242/jcs.242487

Roby, J. A., Funk, A., & Khromykh, A. A. (2012). Flavivirus replication and assembly. In P.-Y. Shi (Ed.), *Molecular virology and control of flaviviruses* (pp. 21–49).

Rodriguez-Madoz, J. R., Belicha-Villanueva, A., Bernal-Rubio, D., Ashour, J., Ayllon, J., & Fernandez-Sesma, A. (2010). Inhibition of the Type I Interferon Response in Human Dendritic Cells by Dengue Virus Infection Requires a Catalytically Active NS2B3 Complex. *Journal of Virology*, *84*(19), 9760–9774. https://doi.org/10.1128/JVI.01051-10

Romero Starke, K., Petereit-Haack, G., Schubert, M., Kämpf, D., Schliebner, A., Hegewald, J., & Seidler, A. (2020). The Age-Related Risk of Severe Outcomes Due to COVID-19 Infection: A Rapid Review, Meta-Analysis, and Meta-Regression. *International Journal of*

Environmental Research and Public Health, *17*(16), 5974. https://doi.org/10.3390/ijerph17165974

Ron, D. (2002). Translational control in the endoplasmic reticulum stress response. *The Journal of Clinical Investigation*, *110*(10), 1383–1388. https://doi.org/10.1172/JCI16784

Roosendaal, J., Westaway, E. G., Khromykh, A., & Mackenzie, J. M. (2006). Regulated cleavages at the West Nile virus NS4A-2K-NS4B junctions play a major role in rearranging cytoplasmic membranes and Golgi trafficking of the NS4A protein. *Journal of Virology*, *80*(9), 4623–4632. https://doi.org/10.1128/JVI.80.9.4623-4632.2006

Roth, H., Magg, V., Uch, F., Mutz, P., Klein, P., Haneke, K., Lohmann, V., Bartenschlager, R., Fackler, O. T., Locker, N., Stoecklin, G., & Ruggieri, A. (2017). Flavivirus Infection Uncouples Translation Suppression from Cellular Stress Responses. *MBio*, *8*(1). https://doi.org/10.1128/mBio.02150-16

Roth, H., Magg, V., Uch, F., Mutz, P., Klein, P., Haneke, K., Lohmann, V., Bartenschlager, R., Fackler, O. T., Locker, N., Stoecklin, G., Ruggieri, A., & Buchmeier, M. J. (2017). Flavivirus Infection Uncouples Translation Suppression from Cellular Stress Responses. *MBio*, *8*(1), e02150-16. https://doi.org/10.1128/mBio.02150-16

Rothan, H. A., & Byrareddy, S. N. (2020). The epidemiology and pathogenesis of coronavirus disease (COVID-19) outbreak. *Journal of Autoimmunity*, *109*, 102433. https://doi.org/10.1016/j.jaut.2020.102433

Rozpedek, W., Markiewicz, L., Diehl, J. A., Pytel, D., & Majsterek, I. (2015). Unfolded Protein Response and PERK Kinase as a New Therapeutic Target in the Pathogenesis of Alzheimer's Disease. *Current Medicinal Chemistry*, *22*(27), 3169–3184. https://doi.org/10.2174/0929867322666150818104254

Ruggieri, A., Dazert, E., Metz, P., Hofmann, S., Bergeest, J. P., Mazur, J., Bankhead, P., Hiet, M. S., Kallis, S., Alvisi, G., Samuel, C. E., Lohmann, V., Kaderali, L., Rohr, K., Frese, M., Stoecklin, G., & Bartenschlager, R. (2012). Dynamic Oscillation of Translation and Stress Granule Formation Mark the Cellular Response to Virus Infection. *Cell Host and Microbe*, *12*(1), 71–85. https://doi.org/10.1016/j.chom.2012.05.013

Runge, S., Sparrer, K. M. J., Lässig, C., Hembach, K., Baum, A., García-Sastre, A., Söding, J., Conzelmann, K.-K., & Hopfner, K.-P. (2014). In Vivo Ligands of MDA5 and RIG-I in Measles Virus-Infected Cells. *PLoS Pathogens*, *10*(4), e1004081. https://doi.org/10.1371/journal.ppat.1004081

Sabine, S., Heinz-Jürgen, T., & Behrens, S.-E. (1999). The RNA-dependent RNA polymerases of different members of the family Flaviviridae exhibit similar properties in vitro. *Journal of General Virology*, *80*(10), 2583–2590. https://doi.org/https://doi.org/10.1099/0022-1317-80-10-2583

Sadler, A. J., & Williams, B. R. G. (2008). Interferon-inducible antiviral effectors. *Nature Reviews Immunology*, *8*(7), 559–568. https://doi.org/10.1038/nri2314

Saha, B., Jyothi Prasanna, S., Chandrasekar, B., & Nandi, D. (2010). Gene modulation and immunoregulatory roles of Interferonγ. *Cytokine*, *50*(1), 1–14. https://doi.org/10.1016/j.cyto.2009.11.021

Saiz, J.-C., Vázquez-Calvo, Á., Blázquez, A. B., Merino-Ramos, T., Escribano-Romero, E., & Martín-Acebes, M. A. (2016). Zika Virus: the Latest Newcomer. *Frontiers in Microbiology*, *7*, 496. https://doi.org/10.3389/fmicb.2016.00496

Samuel, M. A., Whitby, K., Keller, B. C., Marri, A., Barchet, W., Williams, B. R. G., Silverman, R. H., Gale, M. J., & Diamond, M. S. (2006). PKR and RNase L contribute to protection against lethal West Nile Virus infection by controlling early viral spread in the periphery and replication in neurons. *Journal of Virology*, *80*(14), 7009–7019. https://doi.org/10.1128/JVI.00489-06

Sanders, D. W., Kedersha, N., Lee, D. S. W., Strom, A. R., Drake, V., Riback, J. A., Bracha, D., Eeftens, J. M., Iwanicki, A., Wang, A., Wei, M.-T., Whitney, G., Lyons, S. M., Anderson, P., Jacobs, W. M., Ivanov, P., & Brangwynne, C. P. (2020). Competing Protein-RNA Interaction Networks Control Multiphase Intracellular Organization. *Cell*, *181*(2), 306-324.e28. https://doi.org/10.1016/j.cell.2020.03.050

Scaturro, P., Cortese, M., Chatel-Chaix, L., Fischl, W., & Bartenschlager, R. (2015). Dengue Virus Non-structural Protein 1 Modulates Infectious Particle Production via Interaction with the Structural Proteins. *PLoS Pathogens*, *11*(11), e1005277. https://doi.org/10.1371/journal.ppat.1005277

Schuberth-Wagner, C., Ludwig, J., Bruder, A. K., Herzner, A.-M., Zillinger, T., Goldeck, M., Schmidt, T., Schmid-Burgk, J. L., Kerber, R., Wolter, S., Stümpel, J.-P., Roth, A., Bartok, E., Drosten, C., Coch, C., Hornung, V., Barchet, W., Kümmerer, B. M., Hartmann, G., & Schlee, M. (2015). A Conserved Histidine in the RNA Sensor RIG-I Controls Immune Tolerance to N1-2′O-Methylated Self RNA. *Immunity*, *43*(1), 41–51. https://doi.org/10.1016/j.immuni.2015.06.015

Shang, J., Wan, Y., Luo, C., Ye, G., Geng, Q., Auerbach, A., & Li, F. (2020). Cell entry mechanisms of SARS-CoV-2. *Proceedings of the National Academy of Sciences*, *117*(21), 11727–11734. https://doi.org/10.1073/pnas.2003138117

Sharma, N. R., Majerciak, V., Kruhlak, M. J., & Zheng, Z.-M. (2017). KSHV inhibits stress granule formation by viral ORF57 blocking PKR activation. *PLOS Pathogens*, *13*(10), e1006677. https://doi.org/10.1371/journal.ppat.1006677

Silverman, R. H. (2007). A scientific journey through the 2-5A/RNase L system. *Cytokine & Growth Factor Reviews*, *18*(5–6), 381–388. https://doi.org/10.1016/j.cytogfr.2007.06.012

Smit, J., Moesker, B., Rodenhuis-Zybert, I., & Wilschut, J. (2011). Flavivirus Cell Entry and Membrane Fusion. *Viruses*, *3*(2), 160–171. https://doi.org/10.3390/v3020160

Snyder, E. M., & Johnson, B. D. (2020). ACE2 and COVID-19: using antihypertensive medications and pharmacogenetic considerations. *Pharmacogenomics*, *21*(10), 695–703. https://doi.org/10.2217/pgs-2020-0048

Solomon, S., Xu, Y., Wang, B., David, M. D., Schubert, P., Kennedy, D., & Schrader, J. W. (2007). Distinct Structural Features of Caprin-1 Mediate Its Interaction with G3BP-1 and Its Induction of Phosphorylation of Eukaryotic Translation InitiationFactor 2α, Entry to Cytoplasmic Stress Granules, and Selective Interaction with a Subset of mRNAs. *Molecular and Cellular Biology*, *27*(6), 2324–2342. https://doi.org/10.1128/MCB.02300-06

Sommereyns, C., Paul, S., Staeheli, P., & Michiels, T. (2008). IFN-Lambda (IFN-λ) Is Expressed in a Tissue-Dependent Fashion and Primarily Acts on Epithelial Cells In Vivo. *PLoS Pathogens*, *4*(3), e1000017. https://doi.org/10.1371/journal.ppat.1000017

South, A. M., Diz, D. I., & Chappell, M. C. (2020). COVID-19, ACE2, and the cardiovascular consequences. *American Journal of Physiology-Heart and Circulatory Physiology*, *318*(5), H1084–H1090. https://doi.org/10.1152/ajpheart.00217.2020

Stern, O., Hung, Y.-F., Valdau, O., Yaffe, Y., Harris, E., Hoffmann, S., Willbold, D., & Sklan, E. H. (2013). An N-terminal amphipathic helix in dengue virus nonstructural protein 4A mediates oligomerization and is essential for replication. *Journal of Virology*, *87*(7), 4080–4085. https://doi.org/10.1128/JVI.01900-12

Streitenfeld, H., Boyd, A., Fazakerley, J. K., Bridgen, A., Elliott, R. M., & Weber, F. (2003). Activation of PKR by Bunyamwera virus is independent of the viral interferon antagonist NSs. *Journal of Virology*, *77*(9), 5507–5511. https://doi.org/10.1128/jvi.77.9.5507-5511.2003

Šumilo, D., Asokliene, L., Avsic-Zupanc, T., Bormane, A., Vasilenko, V., Lucenko, I., Golovljova, I., & Randolph, S. E. (2008). Behavioural responses to perceived risk of tick-borne encephalitis: Vaccination and avoidance in the Baltics and Slovenia. *Vaccine*, *26*(21), 2580–2588. https://doi.org/10.1016/j.vaccine.2008.03.029

Süss, J. (2011). Tick-borne encephalitis 2010: Epidemiology, risk areas, and virus strains in Europe and Asia—An overview. *Ticks and Tick-Borne Diseases*, *2*(1), 2–15. https://doi.org/10.1016/j.ttbdis.2010.10.007

Suthar, M. S., Aguirre, S., & Fernandez-Sesma, A. (2013). Innate immune sensing of flaviviruses. *PLoS Pathogens*, *9*(9), e1003541. https://doi.org/10.1371/journal.ppat.1003541

Szretter, K. J., Daniels, B. P., Cho, H., Gainey, M. D., Yokoyama, W. M., Gale, M., Virgin, H. W., Klein, R. S., Sen, G. C., & Diamond, M. S. (2012). 2′-O Methylation of the Viral mRNA Cap by West Nile Virus Evades Ifit1-Dependent and -Independent Mechanisms of Host Restriction In Vivo. *PLoS Pathogens*, *8*(5), e1002698. https://doi.org/10.1371/journal.ppat.1002698

Tan, L. Y., Komarasamy, T. V., & RMT Balasubramaniam, V. (2021). Hyperinflammatory Immune Response and COVID-19: A Double Edged Sword. *Frontiers in Immunology*, *12*. https://doi.org/10.3389/fimmu.2021.742941

Tay, M. Z., Poh, C. M., Rénia, L., MacAry, P. A., & Ng, L. F. P. (2020). The trinity of COVID-19: immunity, inflammation and intervention. *Nature Reviews Immunology*, *20*(6), 363–374. https://doi.org/10.1038/s41577-020-0311-8

ter Meulen, J., van den Brink, E. N., Poon, L. L. M., Marissen, W. E., Leung, C. S. W., Cox, F., Cheung, C. Y., Bakker, A. Q., Bogaards, J. A., van Deventer, E., Preiser, W., Doerr, H. W., Chow, V. T., de Kruif, J., Peiris, J. S. M., & Goudsmit, J. (2006). Human monoclonal antibody combination against SARS coronavirus: synergy and coverage of escape mutants. *PLoS Medicine*, *3*(7), e237. https://doi.org/10.1371/journal.pmed.0030237

Thangamani, S., Hermance, M. E., Santos, R. I., Slovak, M., Heinze, D., Widen, S. G., & Kazimirova, M. (2017). Transcriptional Immunoprofiling at the Tick-Virus-Host Interface during Early Stages of Tick-Borne Encephalitis Virus Transmission. *Frontiers in Cellular and Infection Microbiology*, *7*. https://doi.org/10.3389/fcimb.2017.00494

Thomas, M. G., Tosar, L. J. M., Desbats, M. A., Leishman, C. C., & Boccaccio, G. L. (2009). Mammalian Staufen 1 is recruited to stress granules and impairs their assembly. *Journal of Cell Science*, *122*(4), 563–573. https://doi.org/10.1242/jcs.038208

Tian, X., Li, C., Huang, A., Xia, S., Lu, S., Shi, Z., Lu, L., Jiang, S., Yang, Z., Wu, Y., & Ying, T. (2020). Potent binding of 2019 novel coronavirus spike protein by a SARS coronavirus-specific human monoclonal antibody. In *Emerging microbes & infections* (Vol. 9, Issue 1, pp. 382–385). https://doi.org/10.1080/22221751.2020.1729069

Tierney, M., Pottage, J., Kessler, H., Fischl, M., Richman, D., Merigan, T., Powderly, W., Smith, S., Karim, A., & Sherman, J. (1995). The tolerability and pharmacokinetics of N-butyl-deoxynojirimycin in patients with advanced HIV disease (ACTG 100). The AIDS Clinical Trials Group (ACTG) of the National Institute of Allergy and Infectious Diseases. *Journal of Acquired Immune Deficiency Syndromes and Human Retrovirology : Official Publication of the International Retrovirology Association*, *10*(5), 549–553.

Tkachev, S. E., Chicherina, G. S., Golovljova, I., Belokopytova, P. S., Tikunov, A. Yu., Zadora, O. v., Glupov, V. v., & Tikunova, N. v. (2017). New genetic lineage within the Siberian subtype of tick-borne encephalitis virus found in Western Siberia, Russia. *Infection, Genetics and Evolution*, *56*, 36–43. https://doi.org/10.1016/j.meegid.2017.10.020

Tourrière, H., Chebli, K., Zekri, L., Courselaud, B., Blanchard, J. M., Bertrand, E., & Tazi, J. (2003). The RasGAP-associated endoribonuclease G3BP assembles stress granules. *The Journal of Cell Biology*, *160*(6), 823–831. https://doi.org/10.1083/jcb.200212128

Trougakos, I. P., Stamatelopoulos, K., Terpos, E., Tsitsilonis, O. E., Aivalioti, E., Paraskevis, D., Kastritis, E., Pavlakis, G. N., & Dimopoulos, M. A. (2021). Insights to SARS-CoV-2 life cycle, pathophysiology, and rationalized treatments that target COVID-19 clinical complications. *Journal of Biomedical Science*, *28*(1), 9. https://doi.org/10.1186/s12929-020-00703-5

Tsai, N.-P., Ho, P.-C., & Wei, L.-N. (2008). Regulation of stress granule dynamics by Grb7 and FAK signalling pathway. *The EMBO Journal*, *27*(5), 715–726. https://doi.org/10.1038/emboj.2008.19

Tsai, W.-C., Gayatri, S., Reineke, L. C., Sbardella, G., Bedford, M. T., & Lloyd, R. E. (2016). Arginine Demethylation of G3BP1 Promotes Stress Granule Assembly. *Journal of Biological Chemistry*, *291*(43), 22671–22685. https://doi.org/10.1074/jbc.M116.739573

Tu, Y.-C., Yu, C.-Y., Liang, J.-J., Lin, E., Liao, C.-L., & Lin, Y.-L. (2012). Blocking double-stranded RNA-activated protein kinase PKR by Japanese encephalitis virus nonstructural protein 2A. *Journal of Virology*, *86*(19), 10347–10358. https://doi.org/10.1128/JVI.00525-12

Umareddy, I., Pluquet, O., Wang, Q. Y., Vasudevan, S. G., Chevet, E., & Gu, F. (2007). Dengue virus serotype infection specifies the activation of the unfolded protein response. *Virology Journal*, *4*, 91. https://doi.org/10.1186/1743-422X-4-91

van der Schaar, H. M., Rust, M. J., Chen, C., van der Ende-Metselaar, H., Wilschut, J., Zhuang, X., & Smit, J. M. (2008). Dissecting the Cell Entry Pathway of Dengue Virus by Single-Particle Tracking in Living Cells. *PLoS Pathogens*, *4*(12), e1000244. https://doi.org/10.1371/journal.ppat.1000244

V'kovski, P., Kratzel, A., Steiner, S., Stalder, H., & Thiel, V. (2021). Coronavirus biology and replication: implications for SARS-CoV-2. *Nature Reviews. Microbiology*, *19*(3), 155–170. https://doi.org/10.1038/s41579-020-00468-6

Walev, I., Bhakdi, S. C., Hofmann, F., Djonder, N., Valeva, A., Aktories, K., & Bhakdi, S. (2001). Delivery of proteins into living cells by reversible membrane permeabilization with streptolysin-O. *Proceedings of the National Academy of Sciences*, *98*(6), 3185–3190. https://doi.org/10.1073/pnas.051429498

Wallner, G., Mandl, C. W., Kunz, C., & Heinz, F. X. (1995). The Flavivirus 3′-Noncoding Region: Extensive Size Heterogeneity Independent of Evolutionary Relationships among Strains of Tick-Borne Encephalitis Virus. *Virology*, *213*(1), 169–178. https://doi.org/10.1006/viro.1995.1557

Wan, Y., Shang, J., Graham, R., Baric, R. S., & Li, F. (2020). Receptor Recognition by the Novel Coronavirus from Wuhan: an Analysis Based on Decade-Long Structural Studies of SARS Coronavirus. *Journal of Virology*, *94*(7). https://doi.org/10.1128/JVI.00127-20

Wang, B., Maxwell, B. A., Joo, J. H., Gwon, Y., Messing, J., Mishra, A., Shaw, T. I., Ward, A. L., Quan, H., Sakurada, S. M., Pruett-Miller, S. M., Bertorini, T., Vogel, P., Kim, H. J., Peng, J., Taylor, J. P., & Kundu, M. (2019). ULK1 and ULK2 Regulate Stress Granule Disassembly Through Phosphorylation and Activation of VCP/p97. *Molecular Cell*, *74*(4), 742-757.e8. https://doi.org/10.1016/j.molcel.2019.03.027

Wang, X., Liao, Y., Yap, P. L., Png, K. J., Tam, J. P., & Liu, D. X. (2009). Inhibition of Protein Kinase R Activation and Upregulation of GADD34 Expression Play a Synergistic Role in Facilitating Coronavirus Replication by Maintaining De Novo Protein Synthesis in Virus-Infected Cells. *Journal of Virology*, *83*(23), 12462–12472. https://doi.org/10.1128/JVI.01546-09

Ward, A. M., Bidet, K., Yinglin, A., Ler, S. G., Hogue, K., Blackstock, W., Gunaratne, J., & Garcia-Blanco, M. A. (2011). Quantitative mass spectrometry of DENV-2 RNA-interacting proteins reveals that the DEAD-box RNA helicase DDX6 binds the DB1 and DB2 3' UTR structures. *RNA Biology*, *8*(6), 1173–1186. https://doi.org/10.4161/rna.8.6.17836

Warrener, P., Tamura, J. K., & Collett, M. S. (1993). RNA-stimulated NTPase activity associated with yellow fever virus NS3 protein expressed in bacteria. *Journal of Virology*, *67*(2), 989–996. https://doi.org/10.1128/jvi.67.2.989-996.1993

Weber, S. C., & Brangwynne, C. P. (2012). Getting RNA and Protein in Phase. *Cell*, *149*(6), 1188–1191. https://doi.org/10.1016/j.cell.2012.05.022

Wek, R. C., Jiang, H.-Y., & Anthony, T. G. (2006). Coping with stress: eIF2 kinases and translational control. *Biochemical Society Transactions*, *34*(Pt 1), 7–11. https://doi.org/10.1042/BST20060007

Welsch, S., Miller, S., Romero-Brey, I., Merz, A., Bleck, C. K. E., Walther, P., Fuller, S. D., Antony, C., Krijnse-Locker, J., & Bartenschlager, R. (2009). Composition and three-dimensional architecture of the dengue virus replication and assembly sites. *Cell Host & Microbe*, *5*(4), 365–375. https://doi.org/10.1016/j.chom.2009.03.007

Wengler, G., Wengler, G., & Gross, H. J. (1978). Studies on virus-specific nucleic acids synthesized in vertebrate and mosquito cells infected with flaviviruses. *Virology*, *89*(2), 423–437. https://doi.org/10.1016/0042-6822(78)90185-x

Werme, K., Wigerius, M., & Johansson, M. (2008). Tick-borne encephalitis virus NS5 associates with membrane protein scribble and impairs interferon-stimulated JAK-STAT signalling. *Cellular Microbiology*, *10*(3), 696–712. https://doi.org/10.1111/j.1462-5822.2007.01076.x

Westaway, E. G., Mackenzie, J. M., Kenney, M. T., Jones, M. K., & Khromykh, A. A. (1997). Ultrastructure of Kunjin virus-infected cells: colocalization of NS1 and NS3 with double-stranded RNA, and of NS2B with NS3, in virus-induced membrane structures. *Journal of Virology*, *71*(9), 6650–6661. https://doi.org/10.1128/JVI.71.9.6650-6661.1997

White, J. P., & Lloyd, R. E. (2012). Regulation of stress granules in virus systems. *Trends in Microbiology*, *20*(4), 175–183. https://doi.org/10.1016/j.tim.2012.02.001

WHO. (2015). Vaccines and vaccination against yellow fever: WHO Position Paper, June 2013—Recommendations. *Vaccine*, *33*(1), 76–77. https://doi.org/10.1016/j.vaccine.2014.05.040

WHO. (2020). *WHO Director-General's opening remarks at the media briefing on COVID-19 - 11 March 2020*. Https://Www.Who.Int/Director-General/Speeches/Detail/Who-Director-General-s-Opening-Remarks-at-the-Media-Briefing-on-Covid-19---11-March-2020.

WHO. (2021). *Middle East respiratory syndrome coronavirus (MERS-CoV) – Saudi Arabia*. Https://Www.Who.Int/Emergencies/Disease-Outbreak-News/Item/2021-DON333.

WHO. (2022, February 9). *Coronavirus disease (COVID-19) pandemic*. Https://Www.Who.Int/Emergencies/Diseases/Novel-Coronavirus-2019.

Williams, B. R. G. (1999). PKR; a sentinel kinase for cellular stress. *Oncogene*, *18*(45), 6112–6120. https://doi.org/10.1038/sj.onc.1203127

Wilson, J. R., de Sessions, P. F., Leon, M. A., & Scholle, F. (2008). West Nile Virus Nonstructural Protein 1 Inhibits TLR3 Signal Transduction. *Journal of Virology*, *82*(17), 8262–8271. https://doi.org/10.1128/JVI.00226-08

Winkler, G., Maxwell, S. E., Ruemmler, C., & Stollar, V. (1989). Newly synthesized dengue-2 virus nonstructural protein NS1 is a soluble protein but becomes partially hydrophobic and membrane-associated after dimerization. *Virology*, *171*(1), 302–305. https://doi.org/10.1016/0042-6822(89)90544-8

Wolozin, B., & Ivanov, P. (2019). Stress granules and neurodegeneration. *Nature Reviews Neuroscience*, *20*(11), 649–666. https://doi.org/10.1038/s41583-019-0222-5

Wu, S.-F., Lee, C.-J., Liao, C.-L., Dwek, R. A., Zitzmann, N., & Lin, Y.-L. (2002). Antiviral effects of an iminosugar derivative on flavivirus infections. *Journal of Virology*, *76*(8), 3596–3604. https://doi.org/10.1128/jvi.76.8.3596-3604.2002

Xiao, X., Wang, C., Chang, D., Wang, Y., Dong, X., Jiao, T., Zhao, Z., Ren, L., dela Cruz, C. S., Sharma, L., Lei, X., & Wang, J. (2020). Identification of Potent and Safe Antiviral Therapeutic Candidates Against SARS-CoV-2. *Frontiers in Immunology*, *11*. https://doi.org/10.3389/fimmu.2020.586572

Xie, X., Zou, J., Puttikhunt, C., Yuan, Z., & Shi, P.-Y. (2015). Two distinct sets of NS2A molecules are responsible for dengue virus RNA synthesis and virion assembly. *Journal of Virology*, *89*(2), 1298–1313. https://doi.org/10.1128/JVI.02882-14

Yang, P., Mathieu, C., Kolaitis, R.-M., Zhang, P., Messing, J., Yurtsever, U., Yang, Z., Wu, J., Li, Y., Pan, Q., Yu, J., Martin, E. W., Mittag, T., Kim, H. J., & Taylor, J. P. (2020). G3BP1 Is a Tunable Switch that Triggers Phase Separation to Assemble Stress Granules. *Cell*, *181*(2), 325-345.e28. https://doi.org/10.1016/j.cell.2020.03.046

Yang, X.-H., Deng, W., Tong, Z., Liu, Y.-X., Zhang, L.-F., Zhu, H., Gao, H., Huang, L., Liu, Y.-L., Ma, C.-M., Xu, Y.-F., Ding, M.-X., Deng, H.-K., & Qin, C. (2007). Mice transgenic for human angiotensin-converting enzyme 2 provide a model for SARS coronavirus infection. *Comparative Medicine*, *57*(5), 450–459.

Yau, W.-L., Nguyen-Dinh, V., Larsson, E., Lindqvist, R., Överby, A. K., & Lundmark, R. (2019). Model System for the Formation of Tick-Borne Encephalitis Virus Replication Compartments without Viral RNA Replication. *Journal of Virology*, *93*(18). https://doi.org/10.1128/JVI.00292-19

Ye, J., Zhu, B., Fu, Z. F., Chen, H., & Cao, S. (2013). Immune evasion strategies of flaviviruses. *Vaccine*, *31*(3), 461–471. https://doi.org/10.1016/j.vaccine.2012.11.015

Yon, C., Teramoto, T., Mueller, N., Phelan, J., Ganesh, V. K., Murthy, K. H. M., & Padmanabhan, R. (2005). Modulation of the nucleoside triphosphatase/RNA helicase and 5'-RNA triphosphatase activities of Dengue virus type 2 nonstructural protein 3 (NS3) by interaction with NS5, the RNA-dependent RNA polymerase. *The Journal of Biological Chemistry*, *280*(29), 27412–27419. https://doi.org/10.1074/jbc.M501393200

Yoo, J., Mashalidis, E. H., Kuk, A. C. Y., Yamamoto, K., Kaeser, B., Ichikawa, S., & Lee, S.-Y. (2018). GlcNAc-1-P-transferase–tunicamycin complex structure reveals basis for inhibition of N-glycosylation. *Nature Structural & Molecular Biology*, *25*(3), 217–224. https://doi.org/10.1038/s41594-018-0031-y

Youn, S., Li, T., McCune, B. T., Edeling, M. A., Fremont, D. H., Cristea, I. M., & Diamond, M. S. (2012). Evidence for a Genetic and Physical Interaction between Nonstructural Proteins NS1 and NS4B That Modulates Replication of West Nile Virus. *Journal of Virology*, *86*(13), 7360–7371. https://doi.org/10.1128/JVI.00157-12

Yu, C.-Y., Chang, T.-H., Liang, J.-J., Chiang, R.-L., Lee, Y.-L., Liao, C.-L., & Lin, Y.-L. (2012). Dengue Virus Targets the Adaptor Protein MITA to Subvert Host Innate Immunity. *PLoS Pathogens*, *8*(6), e1002780. https://doi.org/10.1371/journal.ppat.1002780

Yu, I.-M., Zhang, W., Holdaway, H. A., Li, L., Kostyuchenko, V. A., Chipman, P. R., Kuhn, R. J., Rossmann, M. G., & Chen, J. (2008). Structure of the Immature Dengue Virus at Low pH Primes Proteolytic Maturation. *Science*, *319*(5871), 1834–1837. https://doi.org/10.1126/science.1153264

Yusof, R., Clum, S., Wetzel, M., Murthy, H. M., & Padmanabhan, R. (2000). Purified NS2B/NS3 serine protease of dengue virus type 2 exhibits cofactor NS2B dependence for cleavage of substrates with dibasic amino acids in vitro. *The Journal of Biological Chemistry*, *275*(14), 9963–9969. https://doi.org/10.1074/jbc.275.14.9963

Zahid Naeem. (2013). Middle East Respiratory Syndrome (MERS) - An update. *International Journal of Health Sciences*, *7*(3), V–VI. https://doi.org/10.12816/0006053

Zeidler, J. D., Fernandes-Siqueira, L. O., Carvalho, A. S., Cararo-Lopes, E., Dias, M. H., Ketzer, L. A., Galina, A., & da Poian, A. T. (2017). Short-term starvation is a strategy to unravel the cellular capacity of oxidizing specific exogenous/endogenous substrates in mitochondria. *Journal of Biological Chemistry*, *292*(34), 14176–14187. https://doi.org/10.1074/jbc.M117.786582

Zhang, P., McGrath, B. C., Reinert, J., Olsen, D. S., Lei, L., Gill, S., Wek, S. A., Vattem, K. M., Wek, R. C., Kimball, S. R., Jefferson, L. S., & Cavener, D. R. (2002). The GCN2 eIF2alpha kinase is required for adaptation to amino acid deprivation in mice. *Molecular and Cellular Biology*, *22*(19), 6681–6688. https://doi.org/10.1128/mcb.22.19.6681-6688.2002

Zhang, Y., Luo, W., Li, Q., Wang, X., Chen, J., Song, Q., Tu, H., Ren, R., Li, C., Li, D., Zhao, J., McGoogan, J. M., Shan, D., Li, B., Zhang, J., Dong, Y., Jin, Y., Mao, S., Qian, M., … Feng, Z. (2021). Risk Factors for Death Among the First 80 543 Coronavirus Disease 2019 (COVID-19) Cases in China: Relationships Between Age, Underlying Disease, Case Severity, and Region. *Clinical Infectious Diseases*. https://doi.org/10.1093/cid/ciab493

Zhao, J., Sun, L., Zhao, Y., Feng, D., Cheng, J., & Zhang, G. (2021). Coronavirus Endoribonuclease Ensures Efficient Viral Replication and Prevents Protein Kinase R Activation. *Journal of Virology*, *95*(7). https://doi.org/10.1128/JVI.02103-20

Zheng, Z.-Q., Wang, S.-Y., Xu, Z.-S., Fu, Y.-Z., & Wang, Y.-Y. (2021). SARS-CoV-2 nucleocapsid protein impairs stress granule formation to promote viral replication. *Cell Discovery*, *7*(1), 38. https://doi.org/10.1038/s41421-021-00275-0

Zhou, Y., Yang, Q., Chi, J., Dong, B., Lv, W., Shen, L., & Wang, Y. (2020). Comorbidities and the risk of severe or fatal outcomes associated with coronavirus disease 2019: A systematic review and meta-analysis. *International Journal of Infectious Diseases*, *99*, 47–56. https://doi.org/10.1016/j.ijid.2020.07.029

Zhu, G., & Lee, A. S. (2015). Role of the unfolded protein response, GRP78 and GRP94 in organ homeostasis. *Journal of Cellular Physiology*, *230*(7), 1413–1420. https://doi.org/10.1002/jcp.24923

Zmurko, J., Neyts, J., & Dallmeier, K. (2015). Flaviviral NS4b, chameleon and jack-in-the-box roles in viral replication and pathogenesis, and a molecular target for antiviral intervention. *Reviews in Medical Virology*, *25*(4), 205–223. https://doi.org/10.1002/rmv.1835

Zou, J., Lee, L. T., Wang, Q. Y., Xie, X., Lu, S., Yau, Y. H., Yuan, Z., Shochat, S. G., Kang, C., Lescar, J., Shi, P.-Y., & Dermody, T. S. (2015). Mapping the Interactions between the NS4B and NS3 Proteins of Dengue Virus. *Journal of Virology*, *89*(7), 3471–3483. https://doi.org/10.1128/JVI.03454-14

Zou, J., Xie, X., Wang, Q.-Y., Dong, H., Lee, M. Y., Kang, C., Yuan, Z., & Shi, P.-Y. (2015). Characterization of dengue virus NS4A and NS4B protein interaction. *Journal of Virology*, *89*(7), 3455–3470. https://doi.org/10.1128/JVI.03453-14

Züst, R., Cervantes-Barragan, L., Habjan, M., Maier, R., Neuman, B. W., Ziebuhr, J., Szretter, K. J., Baker, S. C., Barchet, W., Diamond, M. S., Siddell, S. G., Ludewig, B., & Thiel, V. (2011). Ribose 2′-O-methylation provides a molecular signature for the distinction of self and

non-self mRNA dependent on the RNA sensor Mda5. *Nature Immunology*, *12*(2), 137–143. https://doi.org/10.1038/ni.1979

11. APPENDIX

Redox Biology 36 (2020) 101682

Contents lists available at ScienceDirect

Redox Biology

journal homepage: www.elsevier.com/locate/redox

Research Paper

The cholesterol metabolite 27-hydroxycholesterol inhibits SARS-CoV-2 and is markedly decreased in COVID-19 patients

Alessandro Marcello [a,1], Andrea Civra [b,1], Rafaela Milan Bonotto [a], Lais Nascimento Alves [a], Sreejith Rajasekharan [a], Chiara Giacobone [c], Claudio Caccia [d], Roberta Cavalli [e], Marco Adami [f], Paolo Brambilla [c], David Lembo [b,**], Giuseppe Poli [g,*,2], Valerio Leoni [c]

[a] Laboratory of Molecular Virology, International Centre for Genetic Engineering and Biotechnology (ICGEB), Trieste, 34149, Italy
[b] Laboratory of Molecular Virology and Antiviral Research, Department of Clinical and Biological Sciences, University of Turin, San Luigi Hospital, Orbassano, Turin, 10043, Italy
[c] Laboratory of Clinical Chemistry, Hospitals of Desio and Monza, ASST-Monza and Department of Medicine and Surgery, University of Milano-Bicocca, Monza, 20900, Italy
[d] Unit of Medical Genetics and Neurogenetics, Fondazione IRCCS Istituto Neurologico Carlo Besta, Milan, 20133, Italy
[e] Department of Drug Science and Technology, University of Turin, Turin, Italy
[f] Department of Pharmacological and Biomolecular Sciences, University of Milan, 20133, Italy
[g] Unit of General Pathology and Physiopathology, Department of Clinical and Biological Sciences, University of Turin, San Luigi Hospital, Orbassano, Turin, 10043, Italy

ARTICLE INFO

Keywords:
Coronavirus
SARS-CoV-2
COVID-19
HCoV-OC43
Cholesterol
Oxysterols
27-Hydroxycholesterol

ABSTRACT

There is an urgent need to identify antivirals against the coronavirus SARS-CoV-2 in the current COVID-19 pandemic and to contain future similar emergencies early on. Specific side-chain cholesterol oxidation products of the oxysterols family have been shown to inhibit a large variety of both enveloped and non-enveloped human viral pathogens. Here we report on the in vitro inhibitory activity of the redox active oxysterol 27-hydroxycholesterol against SARS-CoV-2 and against one of the common cold agents HCoV-OC43 human coronavirus without significant cytotoxicity. Interestingly, physiological serum levels of 27-hydroxycholesterol in SARS-CoV-2 positive subjects were significantly decreased compared to the matched control group, reaching a marked 50% reduction in severe COVID-19 cases. Moreover, no correlation at all was observed between 24-hydroxycholesterol and 25-hydroxycholesterol serum levels and the severity of the disease. Opposite to that of 27-hydroxycholesterol was the behaviour of two recognized markers of redox imbalance, i.e. 7-ketocholesterol and 7β-hydroxycholesterol, whose serum levels were significantly increased especially in severe COVID-19. The exogenous administration of 27-hydroxycholesterol may represent in the near future a valid antiviral strategy in the worsening of diseases caused by present and emerging coronaviruses.

1. Introduction

The present COVID-19 pandemic caused by the coronavirus SARS-CoV-2 is yet another example of the dramatic impact of emerging viral infections on human morbidity and mortality worldwide. Currently, no specific drug for the new coronavirus is available and repurposing is the only strategy in place [1]. Clearly, there is an urgent need for drugs active against a wider number of viruses to contain future emergencies early on. Host directed therapy aims at targeting essential host factors for viral replication and triggering immune antiviral pathways [2]. Advantages of this approach include not only the possibility of targeting multiple viruses, but also an increased threshold to the emergence of resistance.

Selective cholesterol oxidation products, of the oxysterol family, which are ligands of Liver X Receptors (LXRs), have a well-recognized immunomodulatory role [3,4]. Oxysterols such as 25-hydroxycholesterol (25OHC) have shown to markedly inhibit the replication of a large variety of both enveloped and non-enveloped human viral

* Corresponding author.
** Corresponding author.
E-mail addresses: david.lembo@unito.it (D. Lembo), giuseppe.poli@unito.it (G. Poli).
[1] Equally contributing to the work.
[2] Lead contact.

https://doi.org/10.1016/j.redox.2020.101682
Received 20 July 2020; Received in revised form 1 August 2020; Accepted 6 August 2020
Available online 10 August 2020

pathogens [5–7]. However, another oxysterol of enzymatic origin, namely 27-hydroxycholesterol (27OHC), is gaining increasing consideration as a protective molecule not only against the respiratory virus Rhinovirus, but also against a wide range of other viral infections [8–11]. There is clear evidence that exogenously added 27OHC accumulates in plasma membrane lipid rafts, likely affecting viral entry but also modulating cell signaling stemming from such microdomains [12,13].

Both 25OHC and 27OHC are side-chain oxysterols physiologically present in human peripheral blood, cerebrospinal fluid [14,15], colostrum and milk [16]. 27OHC is constitutively the most abundant oxysterol in these biological fluids and present in various tissues and organs, being synthesized by the ubiquitous mitochondrial enzyme 27-cholesterol hydroxylase (Cyp27A1) [15].

Due to the emerging role of 27OHC as a broad-spectrum antiviral, we deemed relevant to investigate whether it could inhibit SARS-CoV-2 and other coronaviruses. Here we report on the in vitro antiviral activity of 27OHC against SARS-CoV-2 and the human coronavirus HCoV-OC-43. Moreover, we analyzed the serum levels of 27OHC in 123 healthy individuals, in 27 pauci-or a-symptomatic SARS-CoV-2 positive subjects (PACP) and in 117 COVID-19 patients and found quite a marked decrease of the oxysterol in COVID-19 patients that correlates with the severity of the disease. Another notable finding was the increase of serum 7-ketocholesterol and 7 β-hydroxycholesterol, two reliable markers of tissue oxidative imbalance, in moderate and severe COVID-19 patients.

2. Methods

2.1. Reagents

The oxysterol 27OHC complexed with 2-hydroxypropyl-β-cyclodextrin (2HP-βCD:27OHC) was kindly provided by Panoxyvir Ltd (Turin, Italy). The *anti*-RSV monoclonal antibody Ab35958 was purchased from Abcam (Cambridge, United Kingdom). The secondary antibody peroxidase-conjugated AffiniPure F (ab')2 Fragment Goat Anti-Mouse IgG (H+L) was purchased from Jackson ImmunoResearch Laboratories Inc. (West Grove, PA, USA). The recombinant antibody mSIP-3022 against SARS-CoV-2 Spike was previously described [17].

2.2. Cell lines and viruses

Vero E6 cells (African green monkey kidney cells) (ATCC®-1586) and human hepatocarcinoma Huh7 cells kindly provided by Ralf Bartenschlager (University of Heidelberg, Germany) were cultured in DMEM (Gibco) supplemented with 10% fetal bovine serum (Gibco). Human lung fibroblast MRC-5 (ATCC® CCL-171) and human epithelial cells Hep-2 (ATCC® CCL-23) were propagated in Dulbecco's Modified Eagle Medium (DMEM; Sigma, St. Louis, MO, USA) supplemented with 1% (v/v) penicillin/streptomycin solution (Euroclone, Milan, Italy) and heat inactivated, 10% (v/v) fetal bovine serum (Sigma).

SARS-CoV-2 isolate ICGEB_FVG_S5 was obtained at ICGEB as previously described [18]. Plaque assay was performed by incubating dilutions of SARS-CoV-2 on Vero E6 monolayers at 37 °C for 1 h. These were then washed with phosphate buffered saline (PBS) and overlaid with DMEM 2% FBS containing 1.5% carboxymethylcellulose for 3 days. Cells were then fixed with 3.7% paraformaldehyde (PFA) and stained with crystal violet 1%.

Human coronavirus strain OC43 (HCoV–O43) (ATCC® VR-1558) was purchased from ATCC (American Type Culture Collection, Rockville, MD, USA) and propagated in MRC-5 cells, at 33 °C, in a humidified 5% CO2 incubator. When the full cytopathic effect (CPE) developed, cells and supernatants were harvested, pooled, frozen, and thawed three times, then clarified and aliquoted. The virus was stored at −70 °C. CoV titers were determined by the standard plaque method. Briefly, MRC-5 cells were seeded 2 days before infection in 96-well plates, reaching 60%–70% confluence at the time of infection. The viral suspension was serially diluted in DMEM supplemented with 2% fetal bovine serum and inoculated; the infected wells were incubated at 33 °C for 1 h, allowing viruses to attach and enter the cells. After this time, cells were washed with medium, and overlaid with a 1:1 combination of 1.6% SeaPlaque Agarose (BioWhittaker Molecular Applications) and 2 × DMEM medium (Gibco BRL) as described elsewhere [8]. The plates were incubated at 33 °C for 3 days. After incubation, the plates were fixed and stained as described elsewhere [8], and the number of plaques formed was counted; viral titers were expressed in terms of plaque forming units per ml (PFU/ml). Respiratory syncytial virus (RSV) strain A2 (ATCC VR-1540) was propagated in Hep-2 and titrated by the indirect immunoperoxidase staining procedure as described elsewhere [19]. Viral titers were expressed as focus-forming unit (FFU) per ml. Viruses were stored at −80 °C.

2.3. COVID-19 patients and control individuals

We consecutively included in this study 144 adults with SARS-CoV-2 infection confirmed through real-time reverse-transcriptase–polymerase-chain-reaction (RT-PCR) assays of nasal and pharyngeal swabs, in accordance with WHO guidance [20–22]. RT-PCR was performed at San Gerardo Hospital, Monza, and subsequently at the Italian National Institute of Health, Rome, Italy.

Of them, 117 were COVID-19 patients hospitalized from March 2020 at Desio Hospital, ASST-Monza, Italy: 36 had moderate disease presentation (F:M = 13:23, age 65.5 ± 13.5 years, median = 67.12, IQR = 58.6–77.3, min-max range = 32.59–87.48) and 81 had severe disease presentation (F:M = 15:66, age = 69.73 ± 12.99, median = 72.38, IQR = 61.01–79.98, min-max = 33.68–92.27). All were sampled within 10 days from diagnosis (average: 2 days). Subjects were classified as severe if they presented one or more of the following symptoms: respiratory rate (RR) ≥ 30 breaths/min, finger oxygen saturation (SpO2) ≤ 93% at rest, and arterial partial pressure of oxygen (PaO2)/fraction of inspired oxygen (FIO2) ≤ 300 ratio [23,24]. The remaining 27 recruited subjects were SARS-CoV-2 positive patients with mild or minimal symptoms (PACP) not requiring hospitalization (age = 53.48 ± 6.43, median = 54.99, IQR = 47.75–59.15, min-max = 40.56–61.21). Controls were 123 apparently healthy individuals (F:M = 58:65, age = 68.22 ± 9.17, median = 65.46, IQR = 60.1–75.83, min-max = 57–89.99) collected at Desio Hospital before the pandemic outbreak.

2.4. Data collection

Basic information such as age, gender, comorbidities, clinical and laboratory data, chest radiograph (when performed), and outcome (survival or non-survival) was obtained from the electronic medical records of each patient and stored by a password-protected database.

2.5. Antiviral assays

The antiviral activity was determined by the plaque reduction assay. For SARS-CoV-2 experiments, Vero E6 cells were seeded in a 48 well plate, at 6×10^4 cells/well density and incubated at 37 °C overnight. For HCoV-OC43 and RSV, MRC-5 or Hep-2 cells, respectively were first seeded (at 2×10^4 cells/well) in 96 well plates and incubated at 37 °C overnight. The medium was removed from the plates and infection was performed respectively with 10–20 viral PFU per well of SARS-CoV-2 at 37 °C for 1 h, ca. 30 PFU of a stock of HCoV-OC43 at 33 °C for 1 h or ca. 30 PFU of RSV at 37 °C for 3 h, allowing the viruses to attach and enter the cells. After incubation, cells were washed with medium, and overlaid with medium containing 1% carboxymethylcellulose (CMC) with DMEM + 2% FBS, and compound dilutions for SARS-CoV-2 experiments, or with a 1:1 combination of 1.6% SeaPlaque Agarose and 2 × DMEM supplemented with different concentrations of compounds. After 72 h of incubation (33 °C, 5% CO2 for HCoV-OC43 or 37 °C, 5% CO2 for SARS-

CoV-2 and RSV), the medium with oxysterols was removed, and the plates were fixed with 3.7% paraformaldehyde (PFA) or 7.5% formaldehyde (Fluka) and stained with crystal violet (Sigma, St. Louis, Mo.). The number of plaques formed was counted. The plaque reduction assays were conducted in 2× replicate in two independent experiments. Blockade of viral infectivity was expressed as mean % ± standard error of the mean (SEM). Where possible, half-maximal antiviral effective concentration (EC_{50}) values were calculated by regression analysis using the dose-response curves generated from the experimental data using GraphPad PRISM 7 (GraphPad Software, San Diego, CA, USA). EC_{50} values were compared using the sum-of-squares F test.

2.6. Virus inactivation assay

Approximately 10^5 PFU of HCoV-OC43 were incubated with a concentration of 2HP-βCD:27OHC corresponding to EC_{90} in the antiviral assay. The HCoV-OC43/2HP-βCD:27OHC mixture was incubated for 1 h at 33 °C. A control experiment by treating the viral suspension with the blank formulation (2HP-βCD) was also performed. After the incubation, both treated and untreated viruses were titrated to the non-inhibitory concentration of 2HP-βCD:27OHC and the residual viral infectivity was determined by plaque counting. Statistical analysis was performed using One-Way Analysis of Variance (ANOVA), followed by Bonferroni post-hoc test. Significance was reported for p-value <0.05.

2.7. In vitro cytotoxicity assay

The cytotoxicity assay was conducted with Alamar Blue (Invitrogen) as recommended by the manufacturer's protocol. Vero E6 cells were seeded at 1×10^4 cells per well in a 96 well plate, and incubated at 37 °C overnight. Then 50 μL of compounds at the indicated concentrations were added to 150 μL of medium (final 200 μL). Plates were incubated at 37 °C for 3 days and then the colorimetric reagent was added (20 μL for 4 h). Measurements from compound-treated or vehicle-treated cells were normalized against those from untreated cells. The half maximum cytotoxic concentration (CC50) was calculated using GraphPad Prism Version 7. Cytotoxicity assay fluorescence readings were normalized for vehicle and percent plotted against dilutions expressed as antilog.

2.8. Cell viability assay

MRC-5 or Hep-2 cells were seeded at a density of 5×10^3/well in 96-well plates and treated the next day with 27OHC, 2HP-βCD:27OHC, or blank formulation at concentrations ranging from 0.07 to 150 μM to generate dose-response curves. Control samples (100% of viability) were prepared by treating cells with culture medium. After 72 h of incubation, cell viability was determined using a Cell Titer 96 Proliferation Assay Kit (Promega, Madison, WI, USA) and following the manufacturer's instructions. Absorbance was measured using a Microplate Reader (Model 680, Bio-Rad Laboratories, Hercules, CA, USA) at 490 nm. Viability of oxysterol-treated cells is expressed as a percentage relative to cells incubated with culture medium supplemented with equal volumes of ethanol.

2.9. Immunofluorescence

For SARS-CoV-2 analysis Huh7 cells were seeded on coverslips and infected with SARS-CoV-2 the following day at a multiplicity of infection (m.o.i.) of 0.1 PFU/cell. After 1 h, inoculum was removed and fresh DMEM +2% FBS containing 2HP-βCD:27OHC or 2HP-βCD was added to the cells. After 48 h incubation, cells were fixed with 3.7% PFA, treated with 100 mM glycine and 0.1% Triton X-100, with intermediate washes with PBS. A blocking step was performed at 37 °C for 30 min with 1% bovine serum albumin (BSA) and 0.1% Tween in PBS (blocking solution). The coverslips were then probed with the mSIP-3022 anti-Spike recombinant antibody diluted 1/200 with blocking solution and incubated overnight at 4 °C in humidified container. The reaction was completed by incubating fixed cells with polyclonal anti-mouse antibody conjugated with Alexa Fluor 594 (Molecular Probes, Oregon, USA) diluted 1/500 for 1 h at 37 °C. Coverslips were finally washed and mounted on glass slides using Fluoro-Gel II mounting medium with DAPI (Electron Microscopy Sciences, Pennsylvania, USA) and analyzed with a Zeiss LSM880 confocal microscope. For statistical purposes, 200 ± 10 cells were counted for each condition.

2.10. Clinical laboratory measurements

All clinical laboratory measurements were performed in the course of hospitalization. Count blood cells was performed on whole blood with K3-EDTA vacuum tubes and obtained by Sysmex XN-9000 platform (Sysmex, Germany). Blood chemistries were performed on serum vacuum tubes using COBAS 8000 platform (Roche Diagnostics, Germany).

2.11. Sterols and oxysterols quantification by isotope dilution GC-MS

To a screw-capped vial sealed with a Teflon septum, 0.25 mL of plasma were added together with 500 ng of D7-lathosterol, 50 ng of D6-lanosterol, 50 ng of D7-24S-hydroxycholesterol, 50 ng of D6-25-hydroxycholesterol, 50 ng of D6-27-hydroxycholesterol, 50 ng of D7-7-ketocholesterol, 50 ng of D7-7β-hydroxycholesterol (Avanti Polar Lipids), as internal standards, 50 μl of butylated hydroxytoluene (5 g/L) and 50 μl of K3-EDTA (10 g/L) to prevent auto-oxidation. Each vial was flushed with argon for 10 min to remove air. Alkaline hydrolysis was allowed to proceed at room temperature with magnetic stirring for 60 min in the presence of ethanolic 2 M potassium hydroxide solution. After hydrolysis, the sterols were extracted twice with 5 ml hexane. The organic solvents were evaporated under a gentle stream of argon and converted into trimethylsilyl ethers with BSTFA.

Gas chromatography mass spectrometry (GC-MS) analysis was performed on a GC equipped with an Elite column (30 m × 0.32 mmid × 0.25 mm film; PerkinElmer, USA) and injection was performed in splitless mode and using helium (1 ml/min) as a carrier gas. The temperature program was as follows: initial temperature of 180 °C was held for 1 min, followed by a linear ramp of 20 °C/min to 270 °C, and then a linear ramp of 5 °C/min to 290 °C, which was held for 10 min. The mass spectrometer operated in the selected ion-monitoring mode. Peak integration was performed manually, and sterols were quantified from selected-ion monitoring analysis against internal standards using standard curves for the listed sterols. Additional qualifier (characteristic fragment ions) ions were used for structural identification.

Inter-assay CV ranged between 2.3% for lathosterol and 5.3% for 25-hydroxycholesterol. Recovery ranged from 97 up to 104% (5–7).

2.12. Statistical analyses

Continuous variables were expressed as mean ± SD, median, interquartile ranges (IQR), min-max range and compared with the ANOVA or Mann-Whitney *U* test when non parametric distributed.

2.13. Ethics

The study was approved by the Ethical Committee of the Istituto Nazionale Malattie Infettive Lazzaro Spallanzani, Roma and stemmed as a sub-project of the Observational cohort study on the natural history of hospitalized SARS-CoV-2 patients: the STORM trial of the University of Milano Bicocca, Milan, Italy.

3. Results

3.1. 2HP-βCD:27OHC is endowed with antiviral activity against two pathogenic CoVs

The activity of 27OHC against SARS-CoV-2 and HCoV-OC43, was assessed on Vero-E6 and MRC-5 cells, respectively. To improve its solubility and stability, 27OHC was complexed with 2-hydroxypropyl-β-cyclodextrin, a carrier commonly used in drug formulations. Therefore, the complex (2HP-βCD:27OHC) and the carrier alone (2HP-βCD) were tested in parallel to rule out any contribution of the carrier to the antiviral activity.

As shown in Fig. 1 and Table 1, 2HP-βCD:27OHC, but not 2HP-βCD, exerted antiviral activity in a dose-response manner against both SARS-CoV-2 and HCoV-OC43 to maxima of inhibition of 100%, with EC_{50} values falling in the low micromolar range and with a favourable selectivity index (SI). Conversely, 2HP-βCD:27OHC did not inhibit the infectivity of RSV, an enveloped RNA virus also causing respiratory diseases, thus demonstrating that the antiviral specificity of 27OHC is broad but yet selective.

Time-of-addition experiments were then performed to investigate the step of viral replicative cycle inhibited by 2HP-βCD:27OHC. Two different conditions were used: briefly, cells were treated for 24 h before viral inoculum (pre-treatment protocol) or 3 h after inoculum (post-infection treatment protocol). 2HP-βCD:27OHC showed antiviral activity against the two CoVs both when it was added before and after inoculation (Fig. 2 and Table 2). However, the results show that 2HP-βCD:27OHC has greater efficacy against SARS-CoV-2 when added after infection, while it is more effective against HCoV-OC43 when added before inoculation. Furthermore, we investigated the ability of 2HP-βCD:27OHC to impair infectivity by directly targeting viral particles incubating HCoV-OC43 with 2HP-βCD:27OHC at high effective concentrations (EC_{90}) and then determining the viral titer at dilutions at which the treatment was no longer active when added on cells. As reported in Fig. S1, 2HP-βCD:27OHC was not able to inactivate HCoV-OC43 particles.

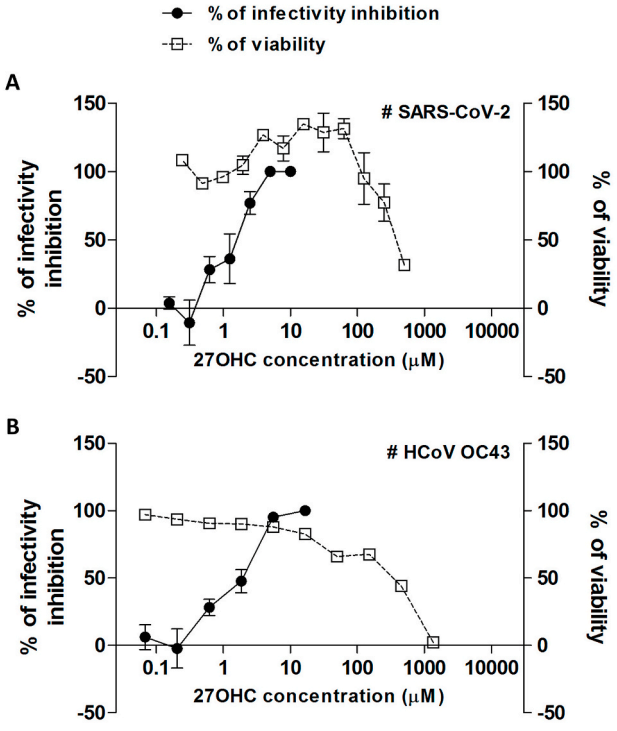

Fig. 1. Plaque reduction and cell viability assays. The antiviral activity of 2HP-βCD:27OHC was tested against SARS-CoV-2 (A) and HCoV OC43 (B), respectively on Vero-E6 cells and MRC-5 cells. Briefly, cells were infected for 1 h and treated for 72 h with increasing concentrations of 2HP-βCD:27OHC. Viral infections were detected as described in the Material and Methods section. Cell viability experiments were performed in the same conditions as for antiviral assays, in absence of viral inoculum. The percentage infectivity inhibition (black dots) and the percentage of cell viability (white squares) were calculated by comparing treated and untreated wells. Error bars represent the standard error of the mean (SEM) of 2 independent experiments.

The efficiency of SARS-CoV-2 and HCoV-OC43 infection was finally measured respectively in the human cell line Huh7 and MRC-5, in the presence of 2HP-βCD:27OHC. As shown in Fig. 3A and C, and quantified in Fig. 3B and D, 2HP-βCD:27OHC significantly ($p_{ANOVA} < 0.001$) reduced the number of infected cells 48 h post infection both at 3 μM and 20 μM. By contrast, 2HP-βCD failed to show any *anti*-CoV activity, showing no significant difference from the untreated control, in terms of number of infected cells.

3.2. Clinical laboratory parameters in moderate and severe COVID-19 patients

The in vitro evidence of effective inhibition of SARS-CoV-2 by the formulation 27OHC+2HP-βCD prompted us to carry on an observational cohort study in COVID-19 patients with the aim to monitor 27OHC serum content in the different stages of the disease. As detailed in the Methods section, the groups studied here were: 1) control, 2) pauci-asymptomatic SASR-CoV-2 positive individuals (PACP), 3) moderate COVID-19, 4) severe COVID-19. No age differences were observed between controls and COVID-19 patients, while the subjects of the pauci-asymptomatic group were significantly younger than all the other groups ($P < 0.001$ for all).

With regard to the standard laboratory parameters measured only in the hospitalized patients (see Table 3), HB and HCT, already below the normal values, were significantly lower in severe COVID-19 compared to moderate COVID-19 ($P = 0.04$ for both). Also serum creatinine was increased both in moderate and severe patients, being significantly higher in the severe COVID-19 group as compared to the moderate COVID-19 one ($P = 0.03$). Alanine Aminotransferase (ALT) and Lactate Dehydrogenase (LDH) were moderately above the normal range, while Creatine Kinase (CK) was much higher respect to the normal values, in all cases without significant difference between the two groups of patients. C Reactive Protein (CRP), resulted to be markedly elevated in COVID-19 with a tendency to increase in the severe cases, and Procalcitonin (PCT), a marker of sepsis, showed a net average increase in the severe COVID-19 group, that however did not reach statistical significance.

3.3. Sterols quantification in the serum from SARS-CoV-2 infected and control individuals

The main objective of this observational cohort study was indeed the evaluation of the trend of serum 27OHC concentration in hospitalized moderate and severe COVID-19 patients as well as in PACP versus a control group, but a prior overall look at cholesterol metabolism was deemed essential. Of note, serum concentration of cholesterol and precursor sterols lanosterol, desmosterol (Bloch pathway of cholesterol synthesis) and lathosterol (Kandutsch-Russell pathway of cholesterol synthesis) were all significantly reduced in both moderate and severe COVID-19 patients in comparison to controls ($P < 0.001$) (Fig. 4 and Table S1).

The PACP group showed a cholesterol metabolism picture quite similar to that of the control group, with just a modest but significant reduction in cholesterol and lanosterol serum levels (Fig. 4).

Table 1
Antiviral activity of 2HP-βCD:27OHC.

ID	Virus	EC50[a] (μM) – 95% C.I.[b]	EC90[c] (μM) – 95% C.I.	CC50[d] (μM) – 95% C.I.	SI[e]
2HP-βCD:27OHC	SARS-CoV-2	1.4 (1.1–1.9)	4.0 (2.1–7.6)	364.5 (258.2–572.8)	260.4
	CoV-OC43	1.6 (1.1–2.3)	6.6 (3.0–14.4)	188.5 (123.2–288.5)	117.8
	RSV	n.a.	n.a.	>1350	n.a.
2HP-βCD	SARS-CoV-2	n.a.	n.a.	170.1 (136.8–211.7)	n.a.
	CoV-OC43	n.a	n.a.	>1350	n.a.
	RSV	n.a.	n.a.	>1350	n.a.

n.a. not assessable.
27OHC: 27-hydroxycholesterol.
[a] EC_{50} half-maximal effective concentration.
[b] CI confidence interval.
[c] EC_{90}90% effective concentration.
[d] CC_{50} half maximal cytotoxic concentration.
[e] SI selectivity index.

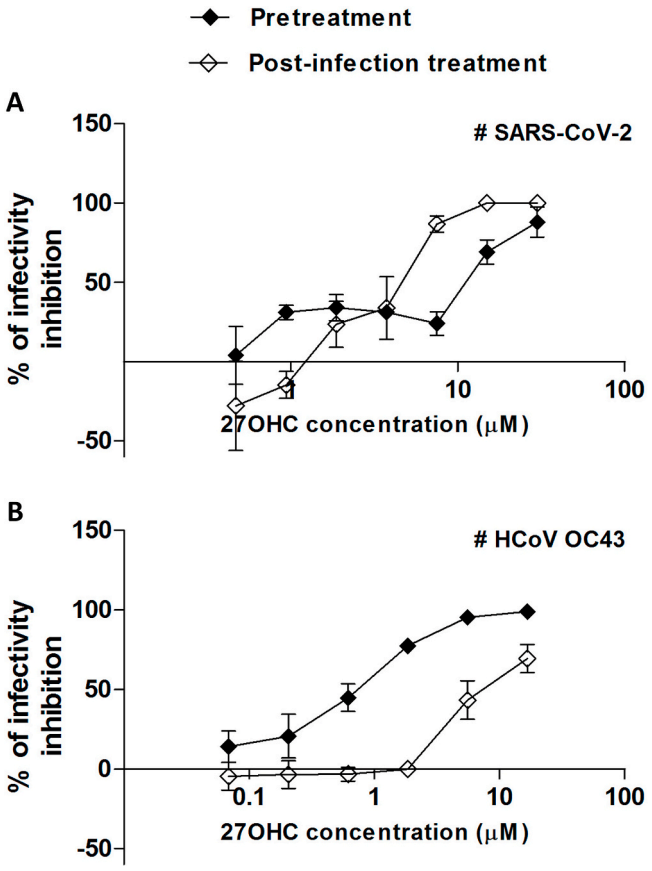

Fig. 2. Time-of-addition experiments. The step of SARS-CoV-2 (A) and HCoV OC43 (B) replicative cycle inhibited by 2HP-βCD:27OHC was investigated. Time-of-addition experiments were performed by treating cells before or after viral inoculum (named respectively "pretreatment" and "post-infection treatment" protocols). The percentage of infectivity inhibition was calculated by comparing the number of viral plaques in treated and untreated wells. Error bars represent the SEM of 2 independent experiments.

3.4. Oxysterols quantification in the serum from COVID-19 patients, PACP and control individuals

By far, the most interesting finding of the cohort study was the marked reduction of serum 27OHC in both moderate and severe COVID-19 patients compared to controls ($P < 0.001$ for both) (Fig. 5 and Table S1).

Actually, the serum 27OHC was already significantly reduced in the PACP group, the mean 27OHC decrease being of 17% in PACP group, 30% in the moderate and of 50% in the severe COVID-19 group (Fig. 5). The PACP group was in between controls and COVID groups (Fig. 5 and Table S1). With regard to the other side chain oxysterols physiologically present in human blood, namely 24OHC and 25OHC, only a slight but significant decrease was observed in all three groups of infected subjects, with the only exception of a modest but significant increase of 25OHC in the PACP group. No correlation at all was observed between 24OHC and 25OHC serum levels and the severity of the disease.

Opposite to that of side chain oxysterols was the behaviour in COVID-19 shown by the two B-ring non enzymatic oxysterols of major pathological meaning, namely 7βOHC and 7KC, actually recognized markers of oxidative stress [25,26]. Serum concentration of both oxysterols showed a significant while moderate increment in severe COVID-19 patients as respect to controls ($P < 0.001$ for both). Serum 7KC but not 7βOHC was significantly increased in the moderate COVID-19 patients as well ($P = 0.002$). In the SARS-CoV-2 positive but pauci- or a-symptomatic subjects, both markers of oxidative stress did not show any significant difference when compared to the control individuals (Fig. 6).

Table 2
Time-of-addition experiments with 2HP-βCD:27OHC.

Virus	Protocol	EC50[a] (μM) – 95% C.I.[b]	EC90[c] (μM) – 95% C.I.
CoV-OC43	pretreatment	0.7 (0.5–1.0)	4.6 (1.9–11.2)
	post-infection treatment	8.3 (5.7–12.1)	34.6 (13.8–86.7)
SARS-CoV-2	pretreatment	7.8 (4.4–13.8)	123.4 (24.2–628.9)
	post-infection treatment	4.3 (3.0–6.2)	9.2 (4.0–21.0)

n.a. not assessable.
[a] EC_{50} half-maximal effective concentration.
[b] CI confidence interval.
[c] EC_{90}90% effective concentration.

4. Discussion

The data reported in this study demonstrate that 27OHC blocks the replication in vitro of two human CoVs belonging to the β-coronavirus genus: SARS-CoV-2 and HCoV-OC43. These findings further confirm the broad spectrum of antiviral activity of 27OHC, which has been already demonstrated for herpes simplex virus, rhinovirus, rotavirus and papillomavirus [5]. Since all of these viruses are phylogenetically unrelated, with ample diversity in their replicative cycles and structures, it is unlikely that 27OHC targets specific functions such as viral enzymes or anti-receptors. Moreover, 27OHC does not directly inactivate the viral particle as shown also in previous studies [8] (Fig. S1). The ability to

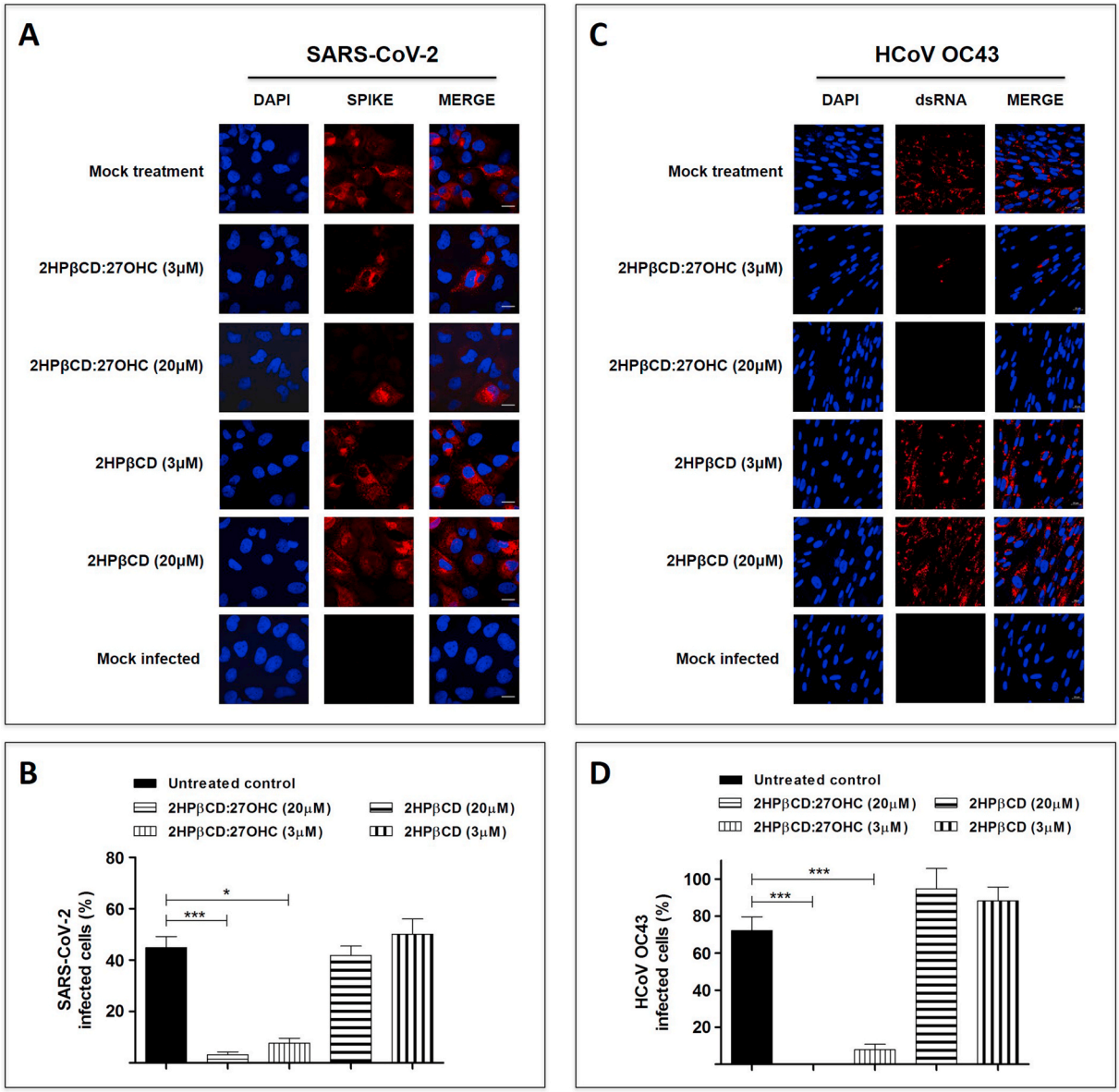

Fig. 3. Infectivity inhibition as assessed by immunofluorescence experiments. Huh-7 (A) and MRC-5(C) cells were infected with SARS-CoV-2 and HCoV OC43 in the presence of 2HP-βCD:27OHC, then fixed at 48 h post-infection and stained with DAPI and specific antibodies. Panels B and D show respectively the number of SARS-CoV-2 and HCoV OC43 positive cells. On the *y* axis, this value is expressed as % of the virus positive cells as compared to DAPI positive cells. Error bars represent the SEM of 2 independent experiments.

impair viral entry and/or replication when added up to 24 h before virus inoculum supports the idea that 27OHC modifies cell structures rather than targeting viral components. Indeed, the host-targeting antiviral mode of action has already been reported by Civra et al. [10], showing that 27OHC induces accumulation of cholesterol in the late endosomal compartment resulting in sequestering human rotavirus particles inside these vesicles, thereby preventing cytoplasmic viral replication. Since also CoVs entry into the host cells involves the endocytic pathway [27–29], the *anti*-CoVs activity of 27OHC appears due, at least in part, to the transient modification of the endosomal membrane composition and function exerted by the oxysterol.

This is especially true in case of 27OHC externally added to the cells, that is in a pharmaceutical mode, in other words as a drug product. Exogenously added 27OHC was proven to almost exclusively accumulate in lipid rafts, as opposed to oxysterols of not enzymatic origin that randomly localize in plasma membranes [12]. Thus, 27OHC is modifying structure and most likely function of these crucial membrane lipid-protein clusters, where by the way the ACE-2 receptor exploited by SARS-CoV-2 to enter the target cells is located [30], and it certainly induces a modification of multivesicular endosome biogenesis, that by lipid rafts is regulated [31]. Further, we very recently observed in HeLa cells a significant 27OHC-dependent down-regulation of cation independent isoform of mannose-6-phosphate receptor (MPRci) [11], a transporter located at late endosomes whose activity appears crucial for all viruses exploiting the endosomal way to enter and diffuse within cells [32–34]. All together, these facts and findings point to the inhibition of virus entry as the primary protective mechanism of 27OHC externally added to cells.

In this relation, very likely appears the involvement of redox reactions at the 27OHC concentration range proven to inhibit SARS-CoV-2 and CoV-OC43 replication, since similar oxysterol's amounts have been previously demonstrated to transiently increase the level of oxidant species in human promonocytic cells through the activation of NADPH oxidase and the modulation of mitochondrial membrane potential [35].

Table 3
Laboratory parameters of hospitalized COVID-19 patients.

Parameter (normal range values)	COVID-19 moderate, n = 36		COVID-19 severe, n = 81		Mann-Withney *U* test
	Mean ± SD	Median IQR Min-Max	Mean ± SD	Median IQR Min-Max	
RBC (4.5–6.5 x 10^9/L)	4.28 ± 0.65	4.39 3.80–4.76 2.67–5.67	4.03 ± 0.69	4.06 3.60–4.46 2.02–6.66	0.07
HB (13–18 mg/dL)	12.61 ± 2.14	13.15 11.05–14.05 7.80–16.70	12.06 ± 2.81	12.00 10.78–13.30 6.70–31.10	0.04
HTC (40–54%)	36.94 ± 6.27	36.50 33.35–41.90 20.80–50.90	34.45 ± 4.65	35.50 31.75–37.50 19.50–44.30	0.04
WBC (4–11 x 10^9/L)	12.35 ± 20.16	7.95 5.85–11.15 2.90–127.00	8.69 ± 4.26	7.70 5.53–11.40 3.50–22.40	0.48
PLT (140–450 x 10^9/L)	262.61 ± 117.17	235.50 171.50–350.00 18.00–525.00	253.51 ± 121.43	231.00 174.75–306.50 13.00–580.00	0.73
NEUT (1.2–6.93 x 10^9/L)	8.20 ± 6.71	5.70 3.85–10.54 1.29–30.62	6.91 ± 4.16	5.46 3.90–9.53 1.67–20.61	0.73
EOS (0–0.37 x 10^9/L)	0.04 ± 0.07	0.00 0.00–0.05 0.00–0.25	0.04 ± 0.09	0.00 0.00–0.04 0.00–0.60	0.86
BASO (0–0.1 x 109/L)	0.00 ± 0.03	0.00 0.00–0.00 0.00–0.13	0.02 ± 0.05	0.00 0.00–0.00 0.00–0.35	0.12
LYMP (0.85–3.23 x 10^9/L	0.89 ± 0.41	0.81 0.69–0.96 0.30–2.20	1.03 ± 0.77	0.82 0.57–1.20 0.17–4.80	0.86
MONO (0–0.67 x 10^9/L)	0.70 ± 0.54	0.48 0.34–0.91 0.08–2.52	0.47 ± 0.28	0.42 0.26–0.62 0.10–1.62	0.05
N/L	10.81 ± 11.18	8.10 5.12–10.99 1.34–47.56	10.94 ± 12.11	7.80 3.63–14.35 0.84–83.94	0.92
CREA (0.5–1.2 mg/dL)	1.45 ± 2.16	0.91 0.80–1.14 0.60–13.35	1.55 ± 1.52	1.14 0.85–1.52 0.35–8.11	0.03
ALT (9–59 U/L)	93.20 ± 141.99	52.00 32.00–99.00 16.00–780.00	74.05 ± 153.77	36.00 24.50–63.50 13.00–1206	0.10
CK (38–174 U/L)	763.73 ± 2438.05	115.00 61.50–180.00 14.00–9565.00	401.84 ± 788.81	156.00 68.00–302.00 9.00–4397	0.35
LDH (125–220 U/L)	369.48 ± 122.89	353.00 280.25–465.50 142.00–620.00	374.07 ± 143.08	347.50 289.50–411.50 171.00–1108	0.88
PCT (0–0.5 ng/mL)	0.44 ± 0.50	0.30 0.16–0.49 0.04–2.24	1.77 ± 5.60	0.27 0.10–0.63 0.03–38.39	0.79
CRP (0.0–5.0 mg/L)	108.48 ± 83.28	91.84 52.38–146.59 4.79–330.79	116.07 ± 87.46	97.60 44.94–162.31 4.22–377.10	0.69

Data are presented as Mean ± SD and as Median, interquartile range IQR, Min-Max.
Red Blood Cells, RBC; Haemoglobin, Hb; Haematocrit (Hct); White Blood Cells, WBC; Platelet Count, PLT; Neutrophil count, NEUT; Eosinophil count, EOS; Basophil count, BASO; Lymphocyte count, LYMP; Monocyte count, MONO; neutrophils/lymphocyte ratio, N/L; creatinine, CREA; alanine aminotranspherase ALT; creatinine-chinase, CK; lactic dehydrogenase, LDH; procalcitonin, PCT; C reactive protein, CRP.

How such a transient oxidative imbalance exerted by 27OHC contributes to its *anti*-SARS-CoV-2 and *anti*-CoV-OC43 activity is matter of ongoing studies, that are also considering this oxysterol ability to induce autophagy [36], a cellular degradation process in principle favouring the elimination of viral pathogens by delivering viral particles for lysosomal degradation and closely interacting with innate immunity [37]. Notably, the pro-autophagic effect of 27OHC observed in human promonocytic cells was abolished by cell pretratment with a selective NADPH oxidase inhibitor [36].

27OHC has also been shown to modulate the immune-response to infections by increasing the expression of dendritic cell markers and MHC classes I and II molecules [38,39] or by activating the TLR4/NF-κB signaling pathway [40], or to induce expression, synthesis and release of Heat Shock Protein 60 (HSP60) [41], a chaperone molecule of mitochondrial origin, recognized to play an important role in the intercellular immune network [42]. Finally, all immune cells express the oxysterols' receptors Liver X (LXRs) [43], but how their activity could be modulated by molecules like 27OHC still has to be elucidated.

The physiological nature of 27OHC and its potential role as first line constitutive effector of the antiviral defences of human body prompted us to analyse the 27OHC serum levels in COVID-19 patients at different stages of disease progression.

Standard laboratory findings achieved in hospitalized patients were consistent with previous reports on COVID-19 [44–47]. Of particular interest were the low or very low serum cholesterol levels observed in moderate and severe COVID-19 patients, respectively (Fig. 4 and Table S1), indicating a severe impairment of cholesterol metabolism. Serum cholesterol has just been shown to be significantly decreased in

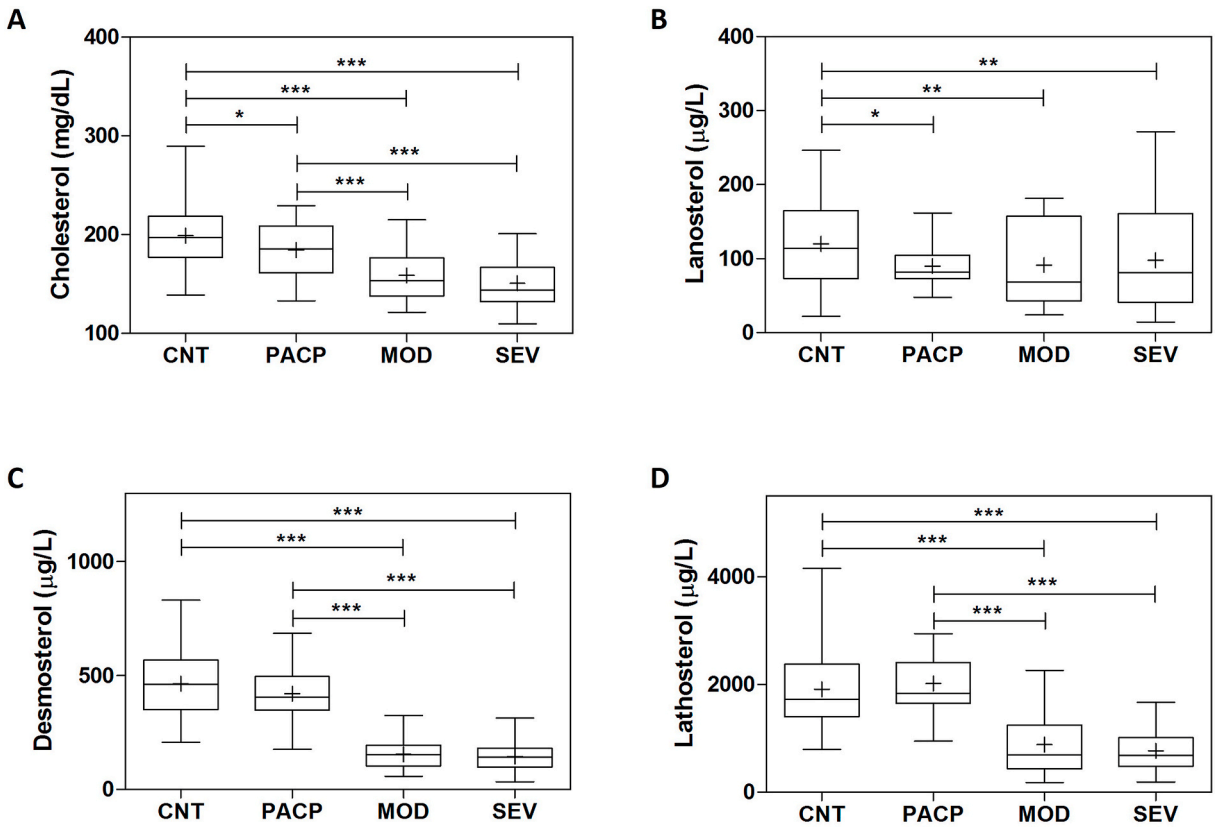

Fig. 4. Serum content of cholesterol and main precursor sterols in SARS-CoV-2 infected subjects. CNT (n = 123): controls; PACP (n = 27): pauci-/a-symptomatic; MOD (n = 36): moderate-COVID-19 patients; SEV (n = 81): severe COVID-19 patients. Mann-Withney *U* test, *P < 0.05; **P < 0.01; ***P < 0.001 (also see Supplementary Table 1).

COVID-19 patients in direct relation with the severity of the disease, with data highly consistent with those obtained in this study [48], while the reduction of the main sterol precursors of cholesterol in COVID-19 has not been reported in the literature yet. A big impairment of cholesterol metabolism, at least in severe COVID-19 patients, was actually expected since a net reduction of cholesterol biosynthesis was described as associated with massive acute phase reaction [49]. Certainly remarkable is the fact that, despite such a profound derangement of cholesterol metabolism in COVID-19, of the three cholesterol oxidation products of enzymatic origin physiologically present in human blood, i.e. 24OHC, 25OHC and 27OHC, only 27OHC showed a pronounced decrease whose intensity tightly correlated to the disease progression (Fig. 5).

The drop in 27OHC serum concentration appeared to be a specific event, since 24OHC was slightly reduced only in moderate (P = 0.036) and severe (P = 0.029) COVID-19 cases, while 25OHC exhibited a small but significant decline only in severe patients (P = 0.018) and it was even slightly increased in the PACP group (P = 0.033 compared to controls, P < 0.001 compared to severe COVID-19 patients), possibly as a consequence of a transiently beneficial INFγ-mediated induction of cholesterol-25-hydroxylase (Fig. 5) [6,50].

Still with regard to the quantification of oxysterols in SARS-CoV-2 infected subjects, a consistent while moderate increase of serum 7-keto-cholesterol and 7β-cholesterol, recognized in vivo markers of oxidative stress, was observed in COVID-19 patients but not in pauci- and a-symptomatic individuals. Actually, an expected finding, because of the serious inflammatory state afflicting those patients, but, to our knowledge, a not yet reported observation.

It is not easy, at present, to identify the reason for the detected selective drop in the 27OHC serum level during SARS-CoV-2 infection in the course of COVID-19. The most plausible hypothesis is that a progressive "mitochondrial stress" would occur at systemic level in those pathological conditions, and that such an impairment would affect the activity of the ubiquitous mitochondrial 27-cholesterol hydroxylase (Cyp27A1) [51], which is the enzyme that converts cholesterol to 27OHC.

Whatever is the actual cause of the progressive reduction of 27OHC in the course of COVID-19, this observational clinical study definitely suggests the opportunity of counteracting such an event, in order to reinforce or reintegrate the antiviral defence system with the administration of suitably formulated 27OHC endowed with antiviral activity.

Notably, the inhibitory activity also shown against CoV-OC43, which is responsible for 10–20% of the cases of common cold together with CoV-229E [52], further highlights the broad antiviral effect of 27OHC, thus opening interesting perspectives on its consideration in future strategies against emerging coronaviruses.

5. Conclusions

In conclusion, this report demonstrates the antiviral activity of 27OHC against SARS-Cov-2 and one related β-coronavirus and shows the dramatic decrease of physiological levels of 27OHC in severe COVID-19. Although the latter observation deserves further investigation, the identification of 27OHC as a novel physiological antiviral with a broad spectrum against β-coronaviruses may be of great importance for the treatment of SARS-CoV-2 infections and possible future epidemics.

Declaration of interests

Andrea Civra, David Lembo, Giuseppe Poli are the founders of Panoxyvir Ltd., a start-up developing the use of specific oxysterols as broad antiviral agents. Panoxyvir Ltd., together with ICGEB, the affiliation of

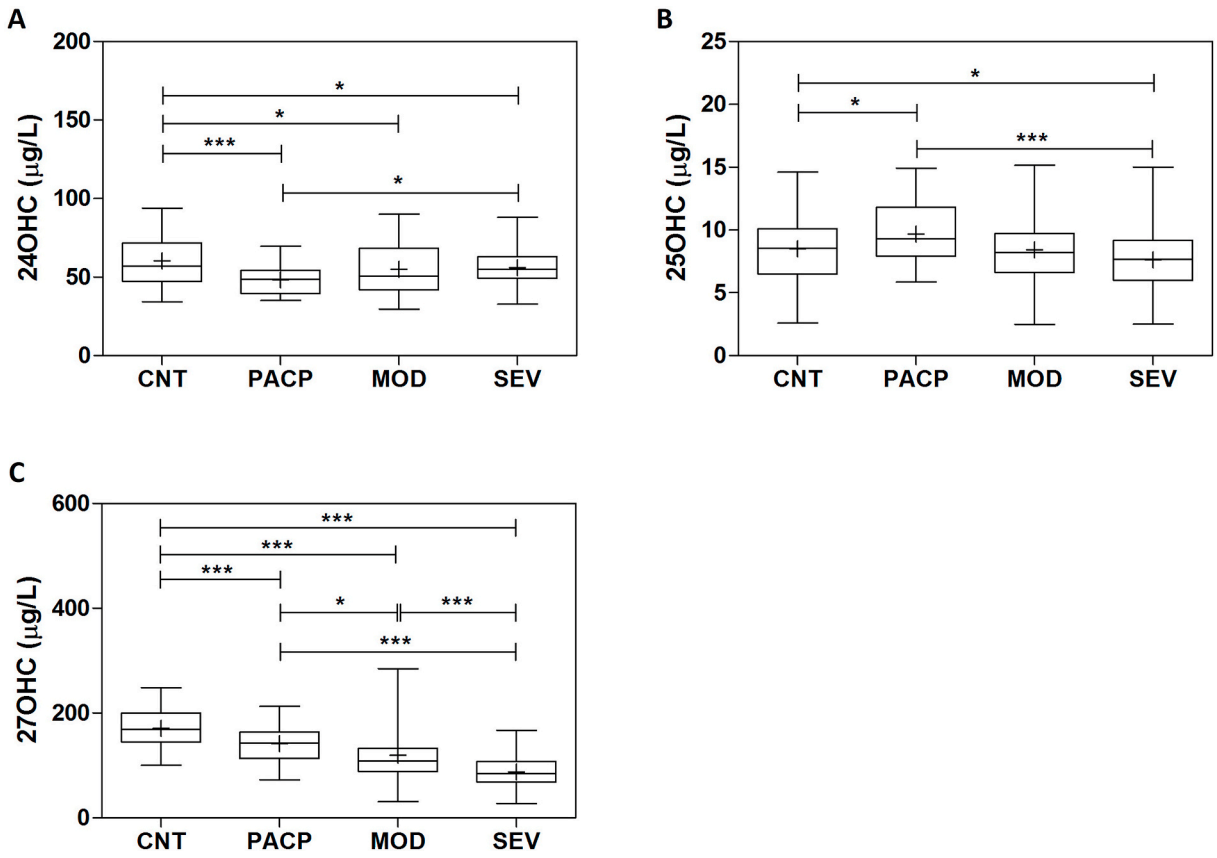

Fig. 5. Serum concentration of side-chain oxysterols 24OHC, 25OHC, 27OHC in SARS-CoV-2 infected subjects. CNT (n = 123): controls; PACP (n = 27): pauci-/a-symptomatic; MOD (n = 36): moderate-COVID-19 patients; SEV (n = 81): severe COVID-19 patients. Mann-Withney *U* test, *P < 0.05; **P < 0.01; ***P < 0.001 (also see Supplementary Table 1).

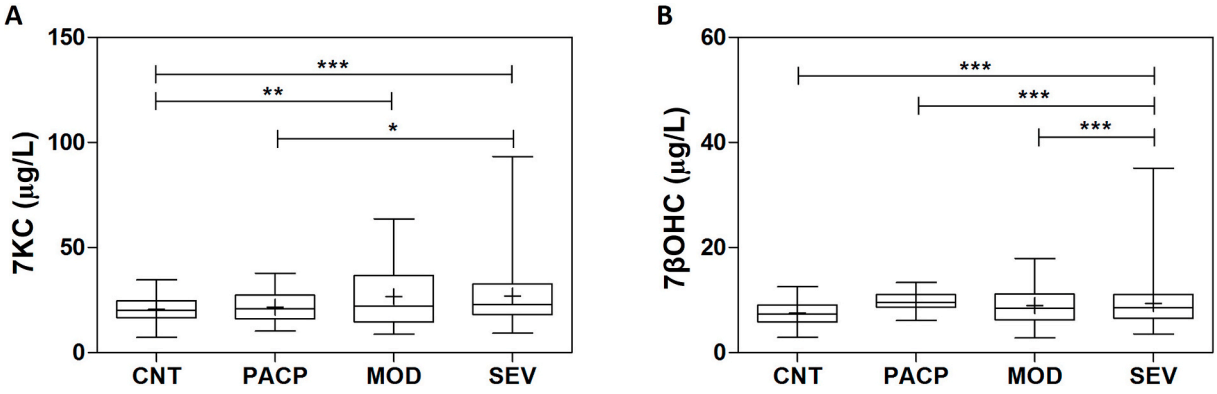

Fig. 6. Serum level of 7KC and 7βOHC in SARS-CoV-2 positive subjects. CNT (n = 123): controls; PACP (n = 27): pauci-/a-symptomatic; MOD (n = 36): moderate-COVID-19 patients; SEV (n = 81): severe COVID-19 patients. Mann-Withney *U* test, *P < 0.05; **P < 0.01; ***P < 0.001 (also see Supplementary Table 1).

the fourth inventor Alessandro Marcello, filed on April 2020 an application to patent the use of 27-hydroxycholesterol in the treatment and/or prevention of diseases caused by Coronaviruses (app n. 102020000008977). Panoxyvir did not provide any financial support to this study. All authors declare no other competing financial interests or conflicts of interest.

Author contributions

Conceptualization, D.L., G.P., and V.L.; Methodology, A.M., V.L., S. R., M.A., R.C.; Investigation, A.M., A.C., V.L., R.B., L.A.N., C.G., C.C., R. C.; Writing – Original Draft, G.P., V.L., D.L.; Writing – Review & Editing, A.M., D.L., V.L., A.C., and G.P.; Funding Acquisition, A.M., D.L.; Resources, P.B., C.G., M.A.; Supervision, A.M, D.L., V.L.; Project administration: D.L. and G.P.

Acknowledgements

The authors gratefully acknowledge Dr. Rosanna Falbo, Laboratory of Clinical Chemistry, Hospital of Desio, ASST-Monza, for linguistic revision of the manuscript. This work was supported by Beneficentia Stiftung, Vaduz, Liechtenstein and SNAM Foundation, San Donato Milanese, Milan, Italy (grants to A.M.), by the University of Turin, Italy (grant RILO19 and LEMB_RIC_COMP_20_01 to D.L.), by CRT

Foundation, Turin, Italy (grant CIVA_CRT_20_01 to A.C.).

Appendix A. Supplementary data

Supplementary data to this article can be found online at https://doi.org/10.1016/j.redox.2020.101682.

References

[1] J.M. Sanders, M.L. Monogue, T.Z. Jodlowski, J.B. Cutrell, Pharmacologic treatments for coronavirus disease 2019 (COVID-19): a review, J. Am. Med. Assoc. 323 (2020) 1824–1836, https://doi.org/10.1001/jama.2020.6019.

[2] M.K. Zakaria, T. Carletti, A. Marcello, Cellular targets for the treatment of Flavivirus infections, Front. Cell. Infect. Microbiol. 8 (2018) 398, https://doi.org/10.3389/fcimb.2018.00398.

[3] S.J. Bensinger, P. Tontonoz, Integration of metabolism and inflammation by lipid-activated nuclear receptors, Nature 454 (2008) 470–477, https://doi.org/10.1038/nature07202.

[4] S.J. Bensinger, M.N. Bradley, S.B. Joseph, N. Zelcer, E.M. Janssen, M.A. Hausner, R. Shih, J.S. Parks, P.A. Edwards, B.D. Jamieson, P. Tontonoz, LXR signaling couples sterol metabolism to proliferation in the acquired immune response, Cell 134 (2008) 97–111, https://doi.org/10.1016/j.cell.2008.04.052.

[5] D. Lembo, V. Cagno, A. Civra, G. Poli, Oxysterols: an emerging class of broad spectrum antiviral effectors, Mol. Aspect. Med. 49 (2016) 23–30.

[6] S.Y. Liu, R. Aliyari, K. Chikere, G. Li, M.D. Marsden, J.K. Smith, O. Pernet, H. Guo, R. Nusbaum, J.A. Zack, A.N. Freiberg, L. Su, B. Lee, G. Cheng, Interferon-inducible cholesterol-25-hydroxylase broadly inhibits viral entry by production of 25-hydroxycholesterol, Immunity 38 (2013) 92–105.

[7] C. Li, Y.-Q. Deng, S. Wang, F. Ma, R. Aliyari, X.-Y. Huang, N.-N. Zhang, M. Watanabe, H.-L. Dong, P. Liu, X.-F. Li, Q. Ye, M. Tian, S. Hong, J. Fan, H. Zhao, L. Li, N. Vishlaghi, J.E. Buth, C. Au, Y. Liu, N. Lu, P. Du, F.X.-F. Qin, B. Zhang, D. Gong, X. Dai, R. Sun, B.G. Novitch, Z. Xu, C.-F. Qin, G. Cheng, 25-Hydroxycholesterol protects host against Zika virus infection and its associated microcephaly in a mouse model, Immunity 46 (2017) 446–456, https://doi.org/10.1016/j.immuni.2017.02.012.

[8] A. Civra, V. Cagno, M. Donalisio, F. Biasi, G. Leonarduzzi, G. Poli, D. Lembo, Inhibition of pathogenic non-enveloped viruses by 25-hydroxycholesterol and 27-hydroxycholesterol, Sci. Rep. 4 (2014) 7487.

[9] V. Cagno, A. Civra, D. Rossin, S. Calfapietra, C. Caccia, V. Leoni, N. Dorma, F. Biasi, G. Poli, D. Lembo, Inhibition of herpes simplex-1 virus replication by 25-hydroxycholesteroland 27-hydroxycholesterol, Redox. Biol. 12 (2017) 522–527.

[10] A. Civra, R. Francese, P. Gamba, G. Testa, V. Cagno, G.G. Poli, D. Lembo, 25-Hydroxycholesterol and 27-hydroxycholesterol inhibit human rotavirus infection by sequestering viral particles into late endosomes, Redox. Biol. 19 (2018) 318–330, https://doi.org/10.1016/j.redox.2018.09.003.

[11] A. Civra, M. Colzani, V. Cagno, R. Francese, V. Leoni, G. Aldini, D. Lembo, G. Poli, Modulation of cell proteome by 25-hydroxycholesterol and 27-hydroxycholesterol: a link between cholesterol metabolism and antiviral defense, Free Radic. Biol. Med. 149 (2020) 30–36, https://doi.org/10.1016/j.freeradbiomed.2019.08.031.

[12] K. Ragot, J.J. Mackrill, A. Zarrouk, T. Nury, V. Aires, A. Jacquin, A. Athias, J. P. Pais de Barros, A. Véjux, J.M. Riedinger, D. Delmas, G. Lizard, Absence of correlation between oxysterol accumulation in lipid raft microdomains, calcium increase, and apoptosis induction on 158N murine oligodendrocytes, Biochem. Pharmacol. 86 (2013) 67–79, https://doi.org/10.1016/j.bcp.2013.02.028.

[13] S. Dambal, M. Alfaqih, S. Sanders, E. Maravilla, A. Ramirez-Torres, G.C. Galvan, M. Reis-Sobreiro, M. Rotinen, L.M. Driver, M.S. Behrove, T. Jovanovic Talisman, J. Soon, S. You, J. Turkson, J.-T. Chi, M.R. Freeman, E. Macias, S.J. Freedland, 27-Hydroxycholesterol impairs plasma membrane lipid raft signaling as evidenced by inhibition of IL6-JAK-STAT3 signaling in prostate cancer cells, Mol. Canc. Res. 18 (2020) 671–684, https://doi.org/10.1158/1541-7786.MCR-19-0974.

[14] V. Leoni, C. Caccia, Oxysterols as biomarkers in neurodegenerative diseases, Chem. Phys. Lipids 164 (2011) 515–524, https://doi.org/10.1016/j.chemphyslip.2011.04.002.

[15] I. Björkhem, V. Leoni, S. Meaney, Genetic connections between neurological disorders and cholesterol metabolism, J. Lipid Res. 51 (2010) 2489–2503, https://doi.org/10.1194/jlr.R006338.

[16] A. Civra, V. Leoni, C. Caccia, S. Sottemano, P. Tonetto, A. Coscia, C. Peila, G. E. Moro, P. Gaglioti, E. Bertino, G. Poli, D. Lembo, Antiviral oxysterols are present in human milk at diverse stages of lactation, J. Steroid Biochem. Mol. Biol. 193 (2019) 105424, https://doi.org/10.1016/j.jsbmb.2019.105424.

[17] S. Rajasekharan, R.M. Bonotto, Y. Kazungu, L.N. Alves, M. Poggianella, P. Martinez Orellana, N. Skoko, S. Polez, A. Marcello, Repurposing of Miglustat to Inhibit the Coronavirus Severe Acquired Respiratory Syndrome SARS-CoV-2. BioRxiv 2020 preprint. doi: 10.1101/2020.05.18.101691.

[18] D. Licastro, S. Rajasekharan, S. Dal Monego, L. Segat, P. D'Agaro, A. Marcello, Isolation and full-length genome characterization of SARS-CoV-2 from COVID-19 cases in northern Italy, J. Virol. 94 (2020), https://doi.org/10.1128/JVI.00543-20 e0054.3-20.

[19] V. Cagno, M. Donalisio, A. Civra, M. Volante, E. Veccelli, P. Oreste, M. Rusnati, D. Lembo, Highly sulfated K5 Escherichia Coli polysaccharide derivatives inhibit respiratory syncytial virus infectivity in cell lines and human tracheal-bronchial histocultures, Antimicrob. Agents Chemother. 58 (2014) 4782–4794, https://doi.org/10.1128/AAC.02594-14.

[20] Y. Deng, W. Liu, K. Liu, Y.Y. Fang, J. Shang, L. Zhou, K. Wang, F. Leng, S. Wei, L. Chen, H.G. Liu, Clinical characteristics of fatal and recovered cases of coronavirus disease 2019 in Wuhan, China: a retrospective study, Chin. Med. J. 133 (2020) 1261–1267, https://doi.org/10.1097/CM9.0000000000000824.

[21] Y. Gao, T. Li, M. Han, X. Li, D. Wu, Y.Y. Xu, Zhu, Y. Liu, X. Wang, L. Wang, Diagnostic utility of clinical laboratory data determinations for patients with the severe COVID-19, J. Med. Virol. 92 (2020) 791–796, https://doi.org/10.1002/jmv.25770.

[22] S. Tian, N. Hu, J. Lou, K. Chen, X. Kang, Z. Xiang, H. Chen, D. Wang, N. Liu, D. Liu, G. Chen, Y. Zhang, D. Li, J. Li, H. Lian, S. Niu, L. Zhang, J. Zhang, Characteristics of COVID-19 infection in Beijing, J. Infect. 80 (2020) 401–406, https://doi.org/10.1016/j.jinf.2020.02.018.

[23] F. Zhou, T. Yu, R. Du, G. Fan, Y. Liu, Z. Liu, J. Xiang, Y. Wang, B. Song, X. Gu, L. Guan, Y. Wei, H. Li, X. Wu, J. Xu, S. Tu, Y. Zhang, H. Chen, B. Cao, Clinical course and risk factors for mortality of adult inpatients with COVID-19 in Wuhan, China: a retrospective cohort study, Lancet 395 (10229) (2020) 1054–1062, https://doi.org/10.1016/S0140-6736(20)30566-3.

[24] Z. Wu, J.M. McGoogan, Characteristics of and important lessons from the coronavirus disease 2019 (COVID-19) outbreak in China: summary of a report of 72 314 cases from the Chinese center for disease control and prevention, JAMA Feb 24 (2020), https://doi.org/10.1001/jama.2020.2648.

[25] M. Arca, S. Natoli, F. Micheletta, S. Riggi, E. Di Angelantonio, A. Montali, T. M. Antonini, R. Antonini, U. Diczfalusy, L. Iuliano, Increased plasma levels of oxysterols, in vivo markers of oxidative stress, in patients with familial combined hyperlipidemia: reduction during atorvastatin and fenofibrate therapy, Free Radic. Biol. Med. 42 (2007) 698–705, https://doi.org/10.1016/j.freeradbiomed.2006.12.013.

[26] C. Zerbinati, L. Iuliano, Cholesterol and related sterols autoxidation, Free Radic. Biol. Med. 111 (2017) 151–155, https://doi.org/10.1016/j.freeradbiomed.2017.04.013.

[27] Y. Inoue, N. Tanaka, Y. Tanaka, S. Inoue, K. Morita, M. Zhuang, T. Hattori, K. Sugamura, Clathrin-dependent entry of severe acute respiratory syndrome coronavirus into target cells expressing ACE2 with the cytoplasmic tail deleted, J. Virol. 81 (2007) 8722–8729, https://doi.org/10.1128/JVI.00253-07.

[28] H. Wang, P. Yang, K. Liu, F. Guo, Y. Zhang, G. Zhang, C. Jiang, SARS coronavirus entry into host cells through a novel clathrin- and caveolae-independent endocytic pathway, Cell Res. 18 (2008) 290–301, https://doi.org/10.1038/cr.2008.15.

[29] T. Tang, M. Bidon, J.A. Jaimes, G.R. Whittaker, S. Daniel, Coronavirus membrane fusion mechanism offers a potential target for antiviral development, Antivir. Res. 178 (2020) 104792, https://doi.org/10.1016/j.antiviral.2020.104792.

[30] Y. Lu, D.X. Liu, J.P. Tam, Lipid rafts are involved in SARS-CoV entry into Vero E6 cells, Biohcim. Biophys. Res. Communs. 369 (2008) 344–349, https://doi.org/10.1016/j.bbrc.2008.02.023.

[31] C. Bissig, J. Gruenberg, Lipid sorting and multivesicular endosome biogenesis, Cold Spring Harb. Perspect. Biol. 5 (2013) a016816, https://doi.org/10.1101/cshperspect.a016816.

[32] M. Gary-Bobo, P. Nirdé, A. Jeanjean, A. Morère, M. Garcia, Mannose 6-phosphate receptor targeting and its applications in human diseases, Curr. Med. Chem. 14 (2007) 2945–2953, https://doi.org/10.2174/092986707782794005.

[33] Y. Chen, K.M. Honeychurch, G. Yang, C.M. Byrd, C. Harver, D.E. Hruby, R. Jordan, Vaccinia virus p37 interacts with host proteins associated with LE-derived transport vesicle biogenesis, Virol. J. 6 (2009) 44, https://doi.org/10.1186/1743-422X-6-44.

[34] M.A. Díaz-Salinas, L.A. Casorla, T. López, S. López, C.F. Arias, Most rotavirus strains require the cation-independent mannose-6-phosphate receptor, sortilin-1, and cathepsins to enter cells, Virus Res. 245 (2018) 44–51, https://doi.org/10.1016/j.virusres.2017.12.002.

[35] B. Vurusaner, P. Gamba, G. Testa, S. Gargiulo, F. Biasi, C. Zerbinati, L. Iuliano, G. Leonarduzzi, H. Basaga, G. Poli, Survival signaling elicited by 27-hydroxycholesterol through the combined modulation of cellular redox state and ERK/Akt phosphorylation, Free Radic. Biol. Med. 77 (2014) 376–385, https://doi.org/10.1016/j.freeradbiomed.2014.07.026.

[36] B. Vurusaner, S. Gargiulo, G. Testa, P. Gamba, G. Leonarduzzi, G. Poli, H. Basaga, The role of autophagy in survival response induced by 27-hydroxycholesterol in human promonocytic cells, Redox. Biol. 17 (2018) 400–410, https://doi.org/10.1016/j.redox.2018.05.010.

[37] Y. Tian, M.-L. Wang, J. Zhao, Crosstalk between autophagy and type I interferon responses in innate antiviral immunity, Viruses 11 (2019) 132, https://doi.org/10.3390/v11020132.

[38] Y. Son, S.-M. Kim, S.-A. Lee, S.-K. Eo, K. Kim, Oxysterols induce transition of monocytic cells to phenotypically mature dendritic cell-like cells, Biochem. Biophys. Res. Commun. 438 (2013) 161–168, https://doi.org/10.1016/j.bbrc.2013.07.046.

[39] Y. Son, J. Choi, B. Kim, Y.C. Park, S.-K. Eo, H.R. Cho, S.S. Bae, C.D. Kim, K. Kim, Cyclosporin A inhibits differentiation and activation of monocytic cells induced by 27-hydroxycholesterol, Int. Immunopharm. 69 (2019) 358–367, https://doi.org/10.1016/j.intimp.2019.01.045.

[40] S. Gargiulo, P. Gamba, G. Testa, D. Rossin, B. Biasi, G. Poli, G. Leonarduzzi, Relation between TLR4/NF-κB signaling pathway activation by 27-hydroxycholesterol and 4-hydroxynonenal, and atherosclerotic plaque instability, Aging Cell 14 (2015) 569–581, https://doi.org/10.1111/acel.12322.

[41] B.-Y. Kim, Y. Son, J. Choi, S.-K. Eo, Y.C. Park, K. Kim, 27-Hydroxycholesterol upregulates the production of heat shock protein 60 of monocytic cells, J. Steroid Biochem. Mol. Biol. 172 (2017) 29–35, https://doi.org/10.1016/j.jsbmb.2017.04.015.

[42] F. Quintana, I.R. Cohen, Theop HSP60 immune system network, Trends Immunol. 32 (2011) 89–95, https://doi.org/10.1016/j.it.2010.11.001.
[43] Y. Kidani, S.J. Bensinger, LXR and PPAR as integrators of lipid homeostasis and immunity, Immunol. Rev. 249 (2012) 72–83, https://doi.org/10.1111/j.1600-065X.2012.01153.x.
[44] Y. Zhou, Z. Yang, Y. Guo, S. Geng, S. Gao, S. Ye, Y. Hu, Y.Y. Wang, A new predictor of disease severity in patients with COVID-19 in Wuhan, China, medRxiv (2020), https://doi.org/10.1101/2020.03.24.20042119, 2020.03.24.20042119.
[45] G. Lippi, M. Plebani, The critical role of laboratory medicine during coronavirus disease 2019 (COVID-19) and other viral outbreaks, Clin. Chem. Lab. Med. 58 (7) (2020) 1063–1069, https://doi.org/10.1515/cclm-2020-0240.
[46] N. Chen, M. Zhou, X. Dong, J. Qu, F. Gong, Y. Han, Y. Qiu, J. Wang, Y. Liu, Y. Wei, J. Xia, T. Yu, X. Zhang, L. Zhang, Epidemiological and clinical characteristics of 99 cases of 2019 novel coronavirus pneumonia in Wuhan, China: a descriptive study, Lancet 395 (10223) (2020) 507–513, https://doi.org/10.1016/S0140-6736(20)30211-7.
[47] G. Grasselli, A. Zangrillo, A. Zanella, M. Antonelli, L. Cabrini, A. Castelli, D. Cereda, A. Coluccello, G. Foti, R. Fumagalli, G. Iotti, N. Latronico, L. Lorini, S. Merler, G. Natalini, A. Piatti, M.V. Ranieri, A.M. Scandroglio, E. Storti, M. Cecconi, A. Pesenti, COVID-19 Lombardy ICU Network, Baseline characteristics and outcomes of 1591 patients infected with SARS-CoV-2 admitted to ICUs of the Lombardy Region, Italy. JAMA 323 (16) (2020) 1574–1581, https://doi.org/10.1001/jama.2020.5394.
[48] X. Wei, W. Zeng, J. Su, H. Wan, X. Yu, X. Cao, W. Tan, H. Wang, Hypolipidemia is associated with the severity of COVID-19, J. Clin. Lipidol. 14 (2020) 297–304, https://doi.org/10.1016/j.jacl.2020.04.008.
[49] Y.A. Carpentier, O. Scruel, Changes in the concentration and composition of plasma lipoproteins during the acute phase response, Curr. Opin. Clin. Nutr. Metab. Care 5 (2002) 153–158, https://doi.org/10.1097/00075197-200203000-00006.
[50] M. Blanc, W.Y. Hsieh, K.A. Robertson, K.A. Kropp, T. Forster, G. Shui, P. Lacaze, S. Watterson, S.J. Griffiths, N.J. Spann, A. Meljon, S. Talbot, K. Krishnan, D. F. Covey, M.R. Wenk, M. Craigon, Z. Ruzsics, J. Haas, A. Angulo, W.J. Griffiths, C. K. Glass, Y. Wang, P. Ghazal, The transcription factor STAT-1 couples macrophage synthesis of 25-hydroxycholesterol to the interferon antiviral response, Immunity 38 (2013) 106–118.
[51] I. Bjorkhem, Are side-chain oxidized oxysterols regulators also in vivo? J. Lipid Res. 50 (2009) 213–218, https://doi.org/10.1194/jlr.R800025-JLR200. Suppl.S.
[52] T. Heikinnen, A. Järvinen, The common cold, Lancet 361 (2003) 51–59, https://doi.org/10.1016/S0140-6736(03)12162-9.

viruses

MDPI

Article

Inhibitors of Protein Glycosylation Are Active against the Coronavirus Severe Acute Respiratory Syndrome Coronavirus SARS-CoV-2

Sreejith Rajasekharan [1,†,‡], Rafaela Milan Bonotto [1,†], Lais Nascimento Alves [1], Yvette Kazungu [1], Monica Poggianella [1], Pamela Martinez-Orellana [1], Natasa Skoko [2], Sulena Polez [2] and Alessandro Marcello [1,*]

1 Laboratory of Molecular Virology, International Centre for Genetic Engineering and Biotechnology (ICGEB) Padriciano, 99-34149 Trieste, Italy; sreejith.rajasekharan@icgeb.org or rajasekharan@leibniz-hpi.de (S.R.); Rafaela.Bonotto@icgeb.org (R.M.B.); Lais.Nascimento@icgeb.org (L.N.A.); kazungu@icgeb.org (Y.K.); poggiane@icgeb.org (M.P.); Pamela.Martinez@icgeb.org (P.M.-O.)

2 Biotechnology Development, International Centre for Genetic Engineering and Biotechnology (ICGEB) Padriciano, 99-34149 Trieste, Italy; skoko@icgeb.org (N.S.); polez@icgeb.org (S.P.)

* Correspondence: marcello@icgeb.org; Tel.: +39-040-375-7384

† These authors contributed equally to this work.

‡ Current address: Systems Arbovirology, Heinrich Pette Institute, Leibniz Intitute for Experimental virology, Martinistrasse 52, 20251 Hamburg, Germany.

check for updates

Citation: Rajasekharan, S.; Milan Bonotto, R.; Nascimento Alves, L.; Kazungu, Y.; Poggianella, M.; Martinez-Orellana, P.; Skoko, N.; Polez, S.; Marcello, A. Inhibitors of Protein Glycosylation are Active against the Coronavirus Severe Acute Respiratory Syndrome Coronavirus SARS-CoV-2. *Viruses* **2021**, *13*, 808. https://doi.org/10.3390/v13050808

Academic Editor: Christopher C. Broder

Received: 2 February 2021
Accepted: 27 April 2021
Published: 30 April 2021

Publisher's Note: MDPI stays neutral with regard to jurisdictional claims in published maps and institutional affiliations.

Abstract: Repurposing clinically available drugs to treat the new coronavirus disease 2019 (COVID-19) is an urgent need in the course of the Severe Acute Respiratory Syndrome coronavirus (SARS-CoV-2) pandemic, as very few treatment options are available. The iminosugar Miglustat is a well-characterized drug for the treatment of rare genetic lysosome storage diseases, such as Gaucher and Niemann-Pick type C, and has also been described to be active against a variety of enveloped viruses. The activity of Miglustat is here demonstrated in the micromolar range for SARS-CoV-2 in vitro. The drug acts at the post-entry level and leads to a marked decrease of viral proteins and release of infectious viruses. The mechanism resides in the inhibitory activity toward α-glucosidases that are involved in the early stages of glycoprotein N-linked oligosaccharide processing in the endoplasmic reticulum, leading to a marked decrease of the viral Spike protein. Indeed, the antiviral potential of protein glycosylation inhibitors against SARS-CoV-2 is further highlighted by the low-micromolar activity of the investigational drug Celgosivir. These data point to a relevant role of this approach for the treatment of COVID-19.

Keywords: COVID-19; SARS-CoV-2; coronavirus; inhibitor; antiviral; Miglustat; spike; Celgosivir

1. Introduction

The novel Severe Acute Respiratory Syndrome coronavirus (SARS-CoV-2), the etiologic agent of coronavirus disease 2019 (COVID-19), has now spread worldwide causing a global pandemic [1,2]. To date there have been more than 120 million confirmed cases and almost 3 million deaths worldwide spurring a global effort to tackle the disease [3]. SARS-CoV-2 belongs to the genus Betacoronavirus of the order/family/sub-family Nidovirales/Coronaviridae/Coronavirinae [4]. The virion is enveloped and contains a single RNA genome of positive polarity.

Morphologically, SARS-CoV-2 is about 120 nm in diameter with large projections of heavily glycosylated trimeric Spike (S) proteins. Other surface proteins include the membrane (M) and envelope (E) proteins, while, inside the envelope, the helical nucleocapsid (N) wraps the viral RNA.

The virus targets cells of the upper and lower respiratory tract epithelia through the viral Spike that binds to the angiotensin-converting enzyme 2 (ACE2) receptor, a process facilitated by the host type 2 transmembrane serine protease, TMPRSS2. Once inside the

cell, viral polyproteins are synthesized that encode for the replication machinery required to synthesize new RNA via the RNA-dependent RNA polymerase activity.

Replication is cytoplasmatic at the level of the endoplasmic reticulum (ER), which is heavily rearranged. Structural proteins are then synthesized leading to the completion of assembly and the release of viral particles [5,6]. Currently, specific antiviral treatment against SARS-CoV-2 is limited to the repurposed drug remdesivir, which received emergency use authorization for COVID-19 treatment; however, debate on its real efficacy remains open. Indeed, in addition to remdesivir, several antiviral drugs being proposed are from the repurposing of drugs developed for other viral infections.

Lopinavir, ritonavir, (hydroxy)chloroquine, umifenovir, and favipiravir are examples that are currently being evaluated; however, none have been conclusively shown to be effective [7]. A recent addition to the armamentarium of strategies to inhibit SARS-CoV-2 is represented by neutralizing monoclonal antibodies, although their narrow window of applicability and sensitivity to Spike immunological escape mutations makes them non-resolutive [8].

The iminosugar Miglustat (Zavesca; *N*-butyl-1-deoxynojirimycin, NB-DNJ) inhibits α-glucosidases I and II, which are involved in the early stages of glycoprotein N-linked oligosaccharide processing in the ER [9]. As most enveloped viruses require glycosylation for surface protein folding and secretion, modulation of the oligosaccharides to induce a reduction in infectivity is a strategy for the treatment of immune deficiency virus type 1 (HIV-1), culminating in phase I/II clinical trials [10,11].

The use of iminosugars to misfold viral glycoprotein as a therapeutic approach has thus far been applied to several other viral infections including: hepatitis B and C viruses, Dengue and other flaviviruses, and Ebola virus [12–14]. An additional property of certain iminosugars is the glucosyltransferase inhibition activity, which is the basis for the current therapy of rare genetic lysosome storage diseases, such as Gaucher and Niemann-Pick type C [15]. This activity of Miglustat could impact virus entry by modification of the plasma membrane.

Celgosivir is an investigational prodrug of the natural α-glucosidases I inhibitor castanospermine, which was initially developed, similarly to Miglustat, as an HIV-1 inhibitor up to Phase I–II clinical trials [16,17]. Phase II clinical trials have also been conducted in patients with hepatitis C virus infection and showed poor efficacy as monotherapy but were synergistic in combination with pegylated Interferon α-2b [18]. With the advent of highly effective direct acting antivirals for HCV, the use of interferon and associated drugs is not the primary recommended treatment option for HCV.

Finally, the Phase 1b CELADEN trial investigated the safety and efficacy of Celgosivir in patients with Dengue fever [19]. Although safe and well tolerated, Celgosivir did not significantly reduce the viral load or fever burden in Dengue patients. However, early intervention may be required as shown in animal studies [20]. Careful evaluation of the CELADEN trial suggested that new dosing regimens could achieve better responses in patients with secondary Dengue infection [21].

The wealth of data on the clinical use of Miglustat for the treatment of lysosomal storage disorders and the antiviral properties observed on enveloped viruses make Miglustat an ideal candidate of drug repurposing for COVID-19. In this work, Miglustat was shown to be active for the inhibition of SARS-CoV-2 in different cell types at concentrations compatible with those obtained for the treatment of Gaucher and Niemann-Pick type C in patients.

Time of addition studies indicated that the inhibitory activity was at the post-entry level and affected the release of infectious viruses. The proper folding and release of the Spike protein and progeny virus appeared to be affected. In addition, the glycosylation inhibitor Celgosivir, which has also been shown to be active against various viruses, has been tested for SARS-CoV-2 and showed potent activity. These data further highlight the opportunity of using inhibitors of this essential pathway for the treatment of COVID-19.

2. Materials and Methods

2.1. Cells, Virus and Antiviral Assay

Vero E6 cells (ATCC-1586) HEK 293T (ATCC CRL-3216), A549 (ATCC CCL-185), U2OS (ATCC HTB-96), human hepatocarcinoma Huh-7 cells kindly provided by Ralf Bartenschlager (University of Heidelberg, Heidelberg, Germany), lung adenocarcinoma Calu-3 (ATCC HTB-55), and Huh-7 cells engineered by lentivirus transduction to overexpress the human ACE2 (Huh7-hACE2) [22] were cultured in Dulbecco's modified Eagle's medium (DMEM, ThermoFisher, Paisley, UK) supplemented with 10% foetal bovine serum (FBS, ThermoFisher, Paisley, UK) and antibiotics. Cell cultures were maintained at 37 °C under 5% CO2. Cells were routinely tested for mycoplasma contamination.

Working stocks of SARS-CoV-2 ICGEB-FVG_5 isolated in Trieste, Italy, were routinely propagated and titrated on Vero E6 cells [23]. Plaque assay was performed by incubating dilutions of SARS-CoV-2 on Vero E6 monolayers at 37 °C for 1 h, which were then washed with phosphate buffered saline (PBS) and overlaid with DMEM 2% FBS containing 1.5% carboxymethylcellulose (CMC, Sigma-Aldrich, St Louis, USA) for 3 days. The cells were then fixed with 3.7% paraformaldehyde (PFA, Sigma-Aldrich, St Louis, MO, USA) and stained with crystal violet 1%. A cytotoxicity assay was performed with Alamar Blue (ThermoFisher, Eugene, OR, USA) according to the manufacturer's instructions.

2.2. Drugs and Proteins

Miglustat (NB-DNJ) and Celgosivir (MX-3253, MBI-3253) were purchased from Sigma-Aldrich, St Louis, MO, USA (B8299 and SML2314, respectively). Miglustat was dissolved in DMSO to obtain a stock solution, while Celgosivir was dissolved in distilled water.

The SARS-CoV-2 Spike protein receptor-binding domain (RBD) was expressed from pCAGGS using a construct generously provided by Florian Krammer (Mount Sinai, New York, NY, USA) [24]. The plasmid was transfected in 293T cells, and cell extracts and supernatants were harvested at 24 h post-transfection. Miglustat 200 μM was added after transfection and maintained in the medium until the end of the experiment.

Sequence coding for the full-length Spike protein was obtained from the isolate Wuhan-Hu-1 (NCBI Reference Sequence: NC_045512.2). The nucleotide sequence, fused to an immunoglobulin leader sequence (sec) at the N-terminus, with the codon optimized for expression in mammalian cells, was obtained as a synthetic DNA fragment from GenScript Biotech (Leiden, The Netherlands) and cloned as HindIII/ApaI into a pCDNA3 vector.

2.3. Plaque Reduction Assay

Vero E6 cells were seeded at 6×10^4 cells/well density in a 48-well plate and incubated at 37 °C overnight. The cells were infected with 30 viral PFU/well and incubated at 37 °C for 1 h. Following incubation, the virus was removed, and the wells washed with 1× PBS. The infected cells were maintained with 800 μL of overlay medium containing 1.5% CMC with DMEM + 2% heat-inactivated FBS, and Miglustat dilutions. The cells were then incubated at 37 °C for 3 days. Finally, the cells were fixed with 3.7% PFA and stained with crystal violet.

The plaques were counted, and the values were normalized to the vehicle (DMSO). The plaque reduction assays were conducted in double replicates for three independent experiments. The inhibition was calculated with the formula: (1-(average plaques Miglustat/average plaques Vehicle)) × 100 and plotted against dilutions as the antilog. For the cytotoxicity assay, the fluorescence readings were normalized for vehicle and percent plotted against the dilutions. The half maximal effective concentration (EC_{50}) and cytotoxic concentration (CC_{50}) were calculated using GraphPad Prism Version 7.

2.4. Immunofluorescence, Immunoblotting, and Flow-Cytometry

A recombinant monoclonal reactive with the receptor-binding domain of the S protein was generated based on a mouse small immune protein (SIP) scaffold (mSIP-3022) [25]. The DNA fragment encoding for the variable regions VL (NCBI accession code: DQ168570.1)

and VH (NCBI accession code: DQ168569.1) of human monoclonal antibodies, clone CR3022 [26,27], was synthetized as scFV by GenScript Biotech (Leiden, Netherlands) and cloned into ApaLI-BspEI sites upstream of the Hinge-CH2-CH3 domains of the mouse IgG2b expression vector as described previously [28].

The plasmid was transfected in ExpiCHO-S cells (Life-Technologies, Bleiswijr, The Netherlands) following the manufacturer's instructions. Eight days post transfection, the supernatant was loaded on the HiTrap protein G HP 1 mL column (GE Healthcare, Chicago, IL, USA) in binding buffer (20 mM sodium phosphate pH 7.0) and eluted with acetic acid 50 mM pH 2.7. The eluted antibody was immediately neutralized with 1 M Tris pH 8, and analysed by RP-HPLC and by SDS PAGE to maintain the dimeric structure. The production yield was 0.8 mg/mL. For immunofluorescence, the cells were fixed in 3.7% PFA, permeabilized with 0.1% Triton and processed with mSIP-3022 as per standard procedure [29].

Since mSIP-3022 did not react with the denatured S protein, a convalescent serum from a COVID-19 patient was used for immunoblotting at a 1:200 dilution. The images were acquired on a Zeiss LSM880 confocal microscope. For immunoblotting, whole-cell lysates were resolved by 12% SDS-PAGE and blotted onto nitrocellulose membranes. The membranes were blocked in 5% nonfat milk in Tris-buffered saline (TBS) plus 0.1% Tween 20 (TBST), followed by incubation with the human serum diluted 1:200 in the same solution for 1 h at room temperature.

After washing three times with TBST, secondary horseradish peroxidase (HRP)-conjugated antibodies were incubated for 1 h at room temperature. The blots were developed using a chemioluminescent HRP substrate (Millipore, Billerica, USA). An anti-his antibody (monoclonal #8722 Sigma) was used at 1/2000 dilution for immunoblotting. The anti-Spike RBD mouse monoclonal MAB105420 (R&D systems, Northest Minneapolis, MN, USA) was used at the concentration of 2 μg/mL for immunoblotting.

HEK 293T cells expressing the Spike protein on the cell surface were incubated for 40 min in 3% BSA in PBS buffer and then stained with the mSIP-3022 (1 μg/mL) or MAB105420 (1 μg/mL) antibodies in the same buffer. After washes and incubation with secondary goat anti mouse IgG antibody diluted 1/1000 (Alexa 488 Jackson Immunofloures-cence, Cambridge, UK), the cells were analysed with FacsCalibur and Cell-Quest software (Beckton Dickson, Sanjose, CA, USA).

2.5. Viral RNA Quantification

The 812bp SARS-CoV-2_multitarget (MTG) synthetic RNA sequence was synthesized and cloned into the pEX-A128 vector (Eurofins Genomics, Ebersberg, Germany). The primers and probes (FAM-BBQ/BHQ1) for rRT-qPCR are listed in Supplementary Table S1 and include also a specific set for the unique detection of the SARS-CoV-2_MTG as well as of the endogenous RNAse P.

The DNA of pEX-A128-SARS-CoV-2_MTG was linearized with EcoRI and purified by the NucleoSpin Gel and PCR Clean-up kit (Macherey-Nagel catalog no: REF 740609.50). Synthetic RNA was obtained by T7 in vitro transcription with MEGAscript T7 Kit n. AM1333 (ThermoFisher, Rockford, IL, USA) according to manufacturer's specifications. The RNA was then quantified by UV light absorbance using a nanodrop and loaded on a 6% Acrylamide/8 M Urea gel.

Synthetic and viral RNAs were reverse transcribed and amplified with the Luna Universal Probe One-Step Reaction Mix (New England BioLabs, Ipswich, MA, USA, catalogue no. E3006L). Uniform reaction conditions were set to a 10 min RT reaction at 55 °C, with denaturation at 95 °C for 3 min, 45 cycles of amplification with extension at 58 °C for 30 s, and denaturation at 95 °C for 15 s. Primers were used at the concentrations shown in Supplementary Table S1. The amplification reactions were performed on a BioRad Cfx96 Thermocycler.

More detailed information on the SARS-CoV-2_multitarget (MTG) synthetic RNA is available at https://www.icgeb.org/covid19-resources/ (accessed on 29 April 2021).

2.6. High Content Assay

The assay is described in detail elsewhere [30]; briefly, Huh 7-hACE2 cells were seeded overnight to adhere to a 96-well plate, treated with serial dilution of the compounds, and then infected with SARS-CoV-2 with appropriate controls (vehicle, not infected, infected and not treated, and infected and treated with the control inhibitor hydroxychloroquine). The plates were incubated for 20 h at 37 °C, and then fixed with 4% PFA, permeabilized with 0.1% of Triton-X for 15 min and incubated in blocking buffer (PBS containing 1% of BSA).

The antibody mSIP-3022 was diluted in blocking buffer and incubated for 2 h at 37 °C. The cells were washed twice in PBS and incubated with the secondary antibody AlexaFluor488-conjugated goat anti-mouse IgG (Cat No. A-11001, ThermoFisher, Rockford, IL, USA) plus DAPI for 1 h at 37 °C. Each plate was kept in PBS after washing. Digital images were acquired using the Operetta high content imaging system (Perkin Elmer, Walthem, MA, USA). The digital images were taken from nine different fields of each well. The total number of cells (nuclei) and the number of infected cells were analysed using the Columbus Image Data Storage and Analysis System (Perkin Elmer, Waltham, MA, USA).

2.7. Statistics

Typically, three independent experiments in triplicate repeats were conducted for each condition examined. The average values are shown with the standard deviation and *p*-values, measured with a paired two-tailed *t*-test. Only significant *p*-values are indicated by the asterisks above the graphs (** $p < 0.01$ highly significant; * $p < 0.05$ significant). Where asterisks are missing, the differences were calculated to be non-significant (n.s.).

3. Results

3.1. Anti-SARS-CoV-2 Activity of Miglustat in Vero E6 and Huh7 Cells

The antiviral properties of Miglustat were initially assessed by performing a plaque assay. SARS-CoV-2 strain ICGEB-FVG_5 was used to infect Vero E6 cells for 1 h. After removal of the inoculum and a wash in PBS, the cells were overlaid with medium containing 1.5% CMC and dilutions of the drug as indicated in Figure 1a. At 72 h post-infection, the cells were fixed and stained to reveal plaques, which were visually counted. In parallel, the cytotoxicity was assessed by the Alamar blue method at the indicated dilutions of drug. The effective concentration for 50% inhibition (EC_{50}) of Miglustat was 41 ± 22 μM with no apparent cytotoxicity up to 1000 μM (CC_{50} > 1000 μM). The plaque assay was performed in Vero E6 cells, which is standard for the growth of SARS-CoV-2. However, further analysis would be better performed in cells of human origin.

To establish an infectious model in human cells, a number of available cell lines were tested, including U2OS (osteosarcoma), A549 (adenocarcinoma of the human alveolar basal epithelial), HEK 293 (human embryonic kidney cells), and Huh7 (hepatocellular carcinoma). None of the cell lines tested supported SARS-CoV-2 infection except for the Huh7 hepatocellular carcinoma cell line. As shown in Supplementary Figure S1A, Huh7 supported SARS-CoV-2 infection, albeit delayed by 24 h and at a lower efficiency compared to Vero E6. Miglustat showed an EC_{50} of 13.45 ± 0.7 μM and a CC_{50} > 1000 μM in Huh7 as measured with the virus yield inhibition assay and by the Alamar blue method for cytotoxicity.

To stain infected cells, a protocol for immunofluorescence was established. To this end, a recombinant monoclonal based on an SIP mouse scaffold (mSIP-3022) was generated carrying the CDR regions of the antibody CR3022 reactive against the receptor binding domain (RBD) of the Spike protein of SARS-CoV-1, which showed high binding affinity also for SARS-CoV-2 Spike protein [27]. As shown in Supplementary Figure S1B, mSIP-3022 efficiently stains the Spike protein in the cytoplasm of infected Vero E6 and Huh7 cells 24 h post-infection.

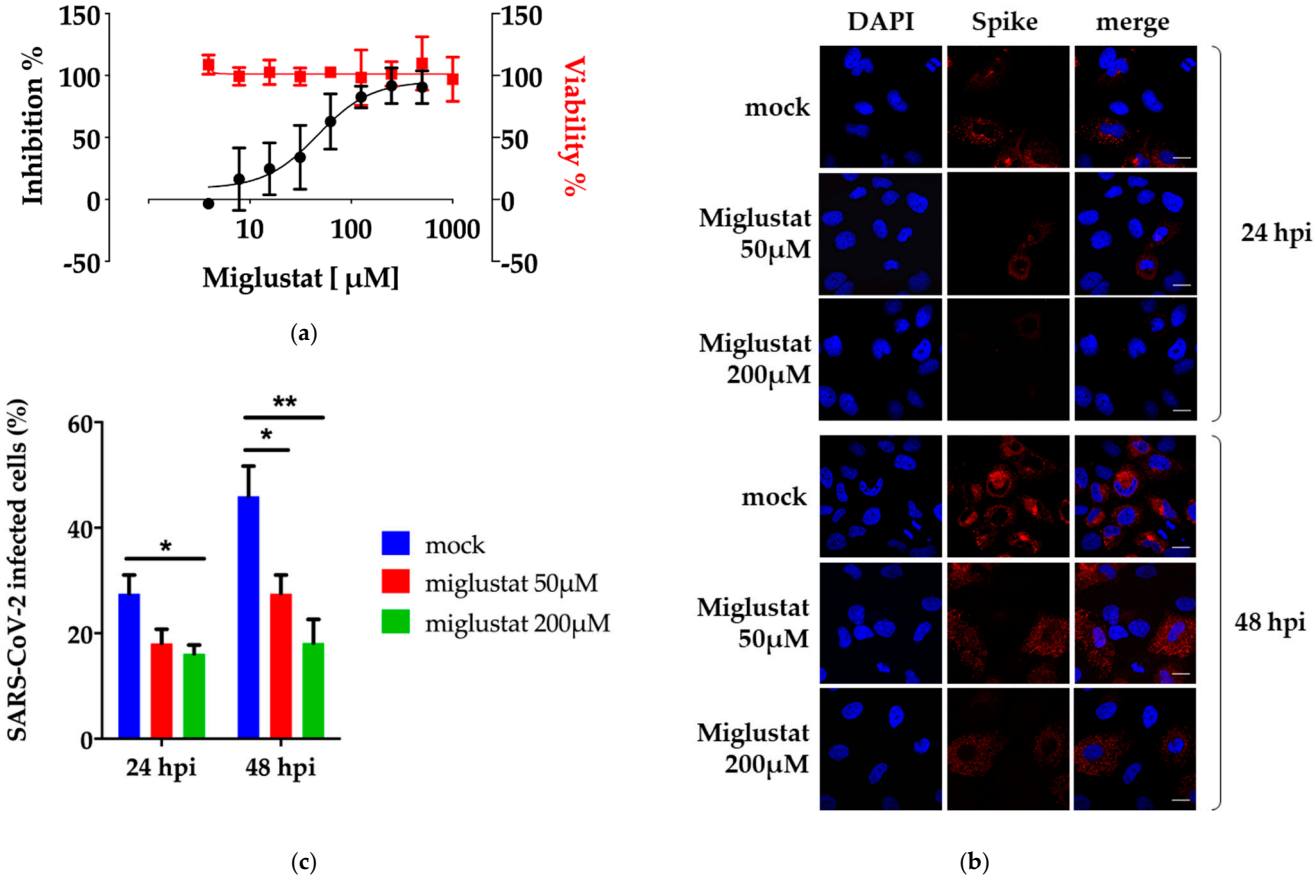

Figure 1. Anti-SARS-CoV-2 activity of Miglustat. (**a**) Antiviral plaque assay. Miglustat at the indicated concentrations was added to Vero E6 monolayers infected with SARS-CoV-2. Following incubation for three days, the cells were fixed and stained to count the viral plaques against vehicle control, which were plotted as the percent inhibitory activity (black dots). The cytotoxicity was measured by the Alamar blue method and data plotted as percent viability (red squares). (**b**) Immunofluorescence assay. Huh7 cells were infected with SARS-CoV-2 moi = 0.1 and incubated with Miglustat as indicated. The cells were then fixed and stained with mSIP-3022 antibody against Spike (red) to acquire confocal images. The nuclei were stained by DAPI. The bar corresponds to 20 μm. (**c**) Quantification of infected cells. SARS-CoV-2 infected cells were counted. The results from 200 cells per condition were plotted as the percent of infected cells. Each pair of mock/treatment conditions was analysed and only significant differences are marked by the asterisks, significant *p*-values are indicated by ** $p < 0.01$ highly significant; * $p < 0.05$ significant, measured with a paired two-tailed *t*-test.

Next, the efficiency of the SARS-CoV-2 infection of Huh7 cells was assessed in the presence of Miglustat. As shown in Figure 1b and quantified in Figure 1c, Miglustat maintained the number of Huh7 infected cells at the level observed 24 hpi, while the mock treated cells showed an increase of infected cells at 48 hpi as expected from an expansion of the infection in the cell culture. We also noted that the mean fluorescence intensity of the Spike signal decreased significantly in treated cells (Supplementary Figure S2).

Finally, we also measured the inhibitory activity of Miglustat in the human lung cell line Calu-3 to obtain a more physiological cellular model of infection. Miglustat had an EC_{50} of 80.5 ± 23 μM and a CC_{50} > 1000 μM in Calu-3 cells as measured with the virus yield inhibition assay and by the Alamar blue method, respectively.

These data confirm the inhibitory effect of Miglustat in cells of human origin and suggest that the activity of Miglustat is at the level of replication and/or secretion of new infectious virus and not at the binding and entry level.

3.2. Dissection of Miglustat Antiviral Activity by Time of Addition Experiments

To better characterize this hypothesis, a time-of-addition (TOA) experiment was performed. Different conditions were used: pre-treatment, co-treatment, and post-treatment.

Huh7 cells were pre-treated with 200 μM Miglustat for 3 h and then infected for 1 h in the absence of drug (moi = 0.1). Afterward, the virus was removed and the cells were cultured in drug-free medium until the end of the experiment. For co-treatment, the drug was added together with the virus during infection, and then the cells were maintained in drug-free medium.

For the post-entry experiment, the drug was added at 3 h post-infection and maintained until the end of the experiment. As shown in Figure 2a, addition of the drug did not affect the viral entry, and the drug was not virucidal when administered concomitant with infection. Replication (intracellular viral RNA) was slightly affected at 48 hpi and significantly at 72 hpi consistent with the idea that Miglustat was effective at the post-entry level. This was reflected by the reduction of intracellular nucleocapsid N protein observed at both time points (Figure 2b).

Interestingly, a strong reduction of infectious virus was observed in the post-entry conditions (Figure 2c,d) paralleled by a decrease of extracellular viral genomes (Figure 2e,f) and N protein (Figure 2g). To note, the quantification of viral genomes was obtained by a method developed for the purpose that takes advantage of a synthetic RNA carrying several of the targets for amplification currently in use (Supplementary Figure S3 and Table S1). This approach is freely available by accessing the ICGEB COVID-19 Resources pages (https://www.icgeb.org/covid19-resources/) (accessed on 29 April 2021).

As we measured only a minor effect of the drug on intracellular viral RNA together with a more pronounced inhibition on released viral genomes and on infectivity, we decided to explore the later stages of the viral lifecycle in greater detail.

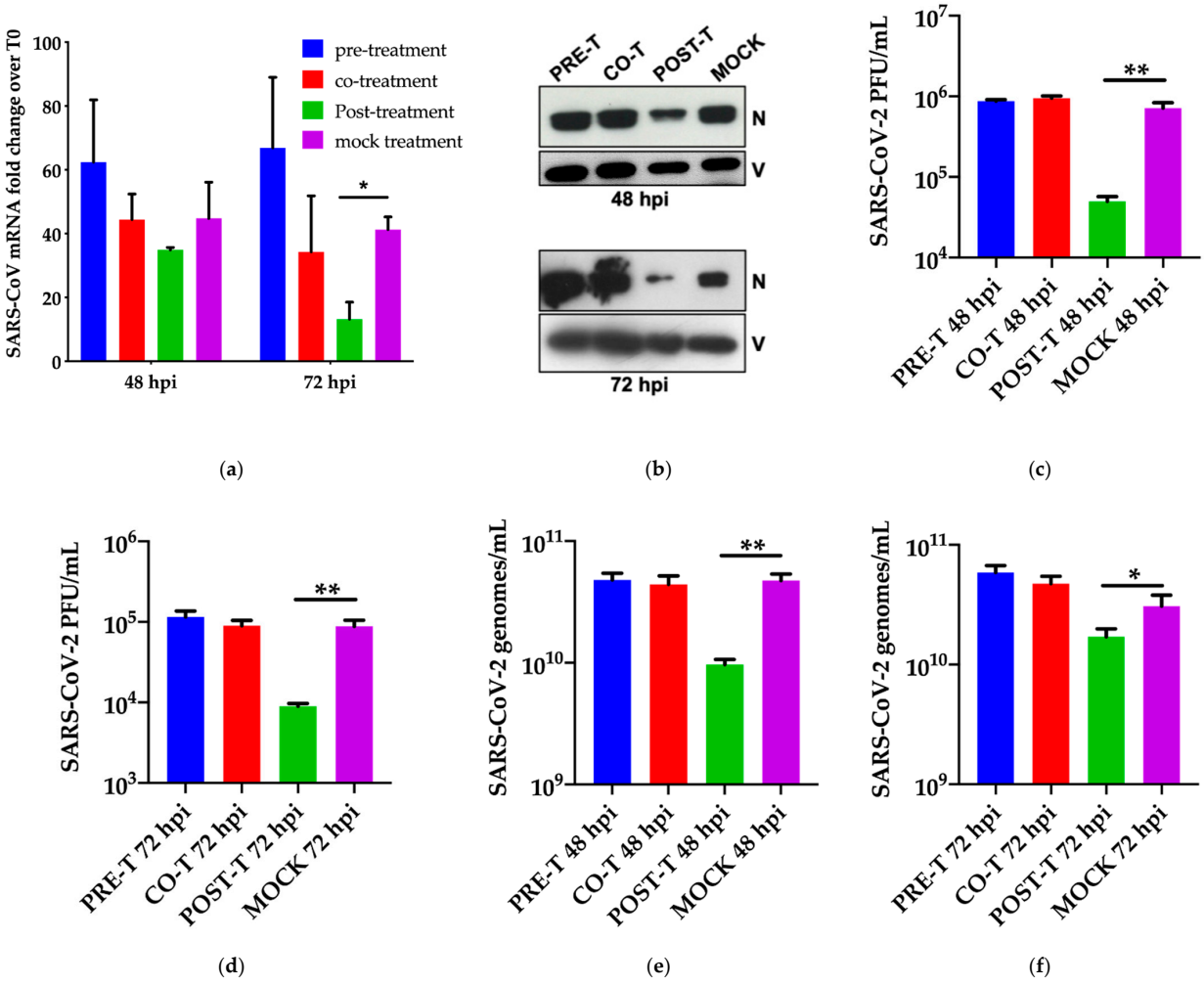

(**a**) (**b**) (**c**)

(**d**) (**e**) (**f**)

Figure 2. *Cont.*

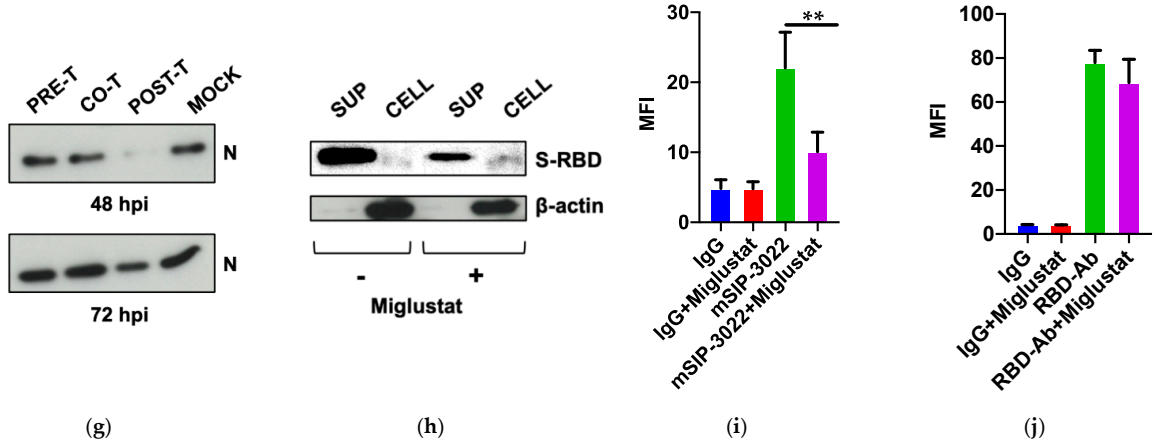

(**g**) (**h**) (**i**) (**j**)

Figure 2. Time of addition studies and the role of Spike. (**a**) Time-of-addition experiment: SARS-CoV-2 genomic RNA. Huh7 cells were infected at moi = 0.1 and incubated with Miglustat before infection (pre-treatment), during infection (co-treatment), and after infection (post-treatment) as described in the text. At the indicated time points, the total RNA was extracted from the infected cells and analysed by RT qPCR. The data are shown as fold-change normalized to their respective T0 values. (**b**) Time-of-addition experiment: SARS-CoV-2 proteins. Protein extracts from Huh7 cells treated as in (**a**) were immunoblotted with a COVID-19 convalescent human serum. The N protein is indicated with Vimentin as the loading control. (**c**,**d**) Time-of-addition experiment: SARS-CoV-2 infectious virus. The infectious virus produced in the experiment was measured as PFU/mL on Vero E6 cells as indicated. (**e**,**f**) Time-of-addition experiment: SARS-CoV-2 secreted genomes. The SARS-CoV-2 genomes in the supernatant of infected cells were quantified by RT qPCR as indicated. (**g**) Time-of-addition experiment: SARS-CoV-2 secreted virions. The virion protein N of secreted SARS-CoV-2 was detected with a convalescent human serum. The loading controls are shown in Figure 2b showing the cell extract results of infected cells. (**h**) Secretion of SARS-CoV-2 Spike RBD. The his-tagged Spike-RBD was expressed for 24 h in HEK-293T cells in the presence of Miglustat and protein detected by immunoblot for the his-tag both in supernatant and cell extracts with β-actin as the loading control. (**i**,**j**) Surface expression of SARS-CoV-2 Spike. Full-length SARS-CoV-2 Spike was expressed in HEK-293T cells for 24 h in the presence of Miglustat and its expression and correct folding on the cell surface was detected with the mSIP-3022 antibody (**i**) or with the anti RBD antibody MAB10540 (**j**). The control was incubated with the secondary antibody only (IgG). Significant *p*-values are indicated by ** $p < 0.01$ highly significant; * $p < 0.05$ significant, measured with a paired two-tailed *t*-test.

3.3. Effect of Miglustat on the Spike Protein

We expected Miglustat activity at the post-entry level to target the proper folding of glycoproteins. The Spike protein and its receptor-binding domain are heavily glycosylated and undergo folding and glycosylation through the ER before being secreted and exposed on the plasma membrane. Previous data on the Spike protein of SARS-CoV-1 indicated that both glycosylation and secretion were affected by Miglustat [31,32]. Therefore, we took advantage of an expression vector for SARS-CoV-2 Spike RBD to assess the effect of Miglustat treatment on protein release from transfected 293T cells. As shown in Figure 2h, the protein was highly abundant in the cell supernatant in normal conditions; however, upon treatment with 200 μM Miglustat, the amount of protein in the supernatant was reduced.

Conversely, RBD was more abundant in the intracellular extracts of treated cells, consistent with the accumulation of misfolded proteins in the ER (Supplementary Figure S4). These data point to the role of Miglustat as an inhibitor of the proper folding and/or release of functional Spike protein. To reinforce this observation, full-length Spike protein was transfected in 293T cells, and the fully folded protein expressed on the cell surface was detected by the conformation-dependent mSIP-3022 antibody (Figure 2i). The antibody CR3022 was not developed for this study as it was discovered against SARS-CoV in 2003 [26] and further characterized for SARS-CoV-2 [27].

In this work, we cloned the complementarity-determining region (CDR) in a mouse small immune protein (mSIP) scaffold and verified that it was able to detect Spike in immunofluorescence and flow-cytometry. CR3022 was recently described to bind to Spike

RBD of SARS-CoV-2 in a conformation-dependent mode through what is called protein "breathing", which requires the unmasking of a cryptic epitope bound by the antibody [33]. Indeed, when we repeated the experiment with a different SARS-CoV-2 Spike RBD antibody able to bind a linear epitope (MAB10540), we demonstrated that Spike was still present on the surface of cells expressing Spike and only marginally affected by Miglustat treatment (Figure 2j). These data are not conclusive on the role of Miglustat in Spike folding but are suggestive that the impact of the drug treatment could be both at the secretion and folding level.

3.4. Anti-SARS-CoV-2 Activity of Miglustat and Celgosivir

To highlight the role of inhibitors of glycosylases in the context of SARS-CoV-2 infection, both Miglustat and the Castanospermine pro-drug Celgosivir were tested in parallel in a high-throughput assay based on Huh7-hACE2 cells recently developed [30]. As shown in Figure 3a, Miglustat confirmed its antiviral potential with an EC_{50} of 19.9 ± 3.4 μM. Celgosivir was also inhibitory as hypothesized, with a remarkable EC_{50} of 1 ± 0.2 μM (Figure 3b). In both cases, the number of viable nuclei increased upon treatment, a result of the protection from infection and lack of cytotoxicity up to the highest concentrations tested (500 and 200 μM, respectively). CC_{50} was also measured by the Alamar blue assay with values exceeding 1000 μM for both drugs.

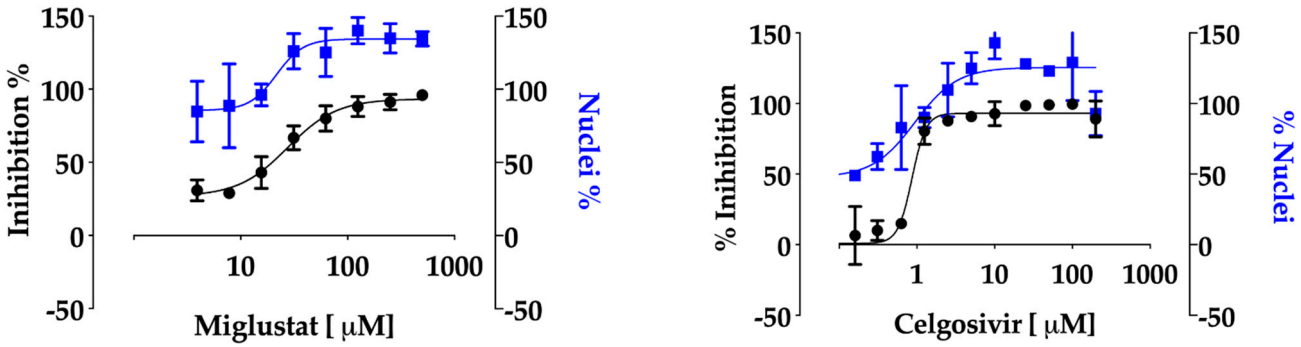

Figure 3. Anti-SARS-CoV-2 activity of Miglustat and Celgosivir. (**a**) Dose response of Miglustat in Huh-7hACE2 cells. Miglustat, at the indicated concentrations, was added to cell monolayers infected with SARS-CoV-2. Following incubation for 20 h, the cells were fixed and stained with the anti-Spike recombinant antibody mSIP-3022. Immunofluorescence images of infected cells (black) and the number of nuclei (blue) were collected and analysed by the Operetta high content imaging system using the Columbus Image Data Storage and Analysis software. (**b**) The dose response of Celgosivir in Huh7-hACE2 cells. Celgosivir, at the indicated concentrations, was added to cell monolayers infected with SARS-CoV-2 and processed as above.

4. Discussion

Host directed antiviral therapy is a strategy of inhibiting virus infection by targeting host factors that are essential for viral replication [34]. Currently, there is a pressing need for antiviral drugs in the context of SARS-CoV-2 infection. Miglustat is a drug that is in current clinical use for the treatment of certain genetic disorders and was shown to be active against a variety of viral infections making it a suitable candidate for drug repurposing toward SARS-CoV-2 [35]. In this work, the activity of Miglustat against SARS-CoV-2 has been demonstrated in vitro on Vero E6 cells with EC_{50} values ranging from 13 to 80 μM in different cell lines.

The standard dosage for lysosomal storage diseases, such as Gaucher or Niemann-Pick, is 100 mg/three times a day, with a maximum daily dose of 600 mg/day. A single dose of 100 mg Miglustat reached a peak in plasma concentration of around 3–5 μM within 4 h, while the half-life was approximately 8 h. When this dose was administered every 4 h/six times per day, the plasma concentration of Miglustat stabilized around

10 μM [36]. When 200 mg Miglustat was administered every 8 h/three times a day, the plasma concentration could be also higher than 10 μM in 24 h. However, increased dosage could lead to well-described adverse reactions that include tremors, diarrhoea, numbness, and thrombocytopenia. The concentration of Miglustat at the site of SARS-CoV-2 replication in the lungs is not known.

Miglustat has been shown to act through two different mechanisms: at the level of virus entry, by perturbing the plasma membrane, and at the level of folding and secretion of virion proteins by affecting the essential glycosylation steps in the ER. The first mechanism is not supported by the data since pre-treatment of cells with Miglustat three hours before infection did not inhibit SARS-CoV-2. However, the possibility remains open that Miglustat affects a receptor that has a slow turnover and is affected only marginally in three hours.

For example, hACE2, the human receptor of Spike, has been shown to be targeted by Miglustat, although the kinetics have not been investigated [37]. The correct folding and secretion of glycoproteins is a process that is tightly controlled in the ER by chaperons, such as Calnexin, that recognize specific glycosylation intermediates [38]. Miglustat interferes with this process resulting in the accumulation of misfolded proteins and a defect in secretion. Consistently, the Spike protein of SARS-CoV-1 was shown to bind Calnexin, and disruption of this function caused a decrease of virus infectivity [32].

The inhibition of glycosylation of viral proteins in the ER exerts a potent antiviral effect, which is further demonstrated by the activity of Celgosivir against SARS-CoV-2, with an EC50 of 1 ± 0.2 μM. Pharmacokinetics data from the CELANDEN clinical trial showed that Celgosivir was rapidly converted to Catastanospermine in vivo with a maximum peak concentration of 30.2 μM and a minimum concentration always above 2 μM throughout the dosing period [21].

After this work was posted as preprint in May 2020, two other reports explored the use of glucosidase inhibitors for the treatment of SARS-CoV-2. Nunez-Santos et al. tested and confirmed Miglustat and Castanospermine, the active component of the prodrug Celgosivir, as glycosylation inhibitors of SARS-CoV-2 Spike and the hACE2 receptor [37]. In their work, they failed to demonstrate a functional effect on syncytia formation or on the interaction of Spike with hACE2. However, their approach was mostly based on transfected Spike and did not consider infection assays.

ACE2 glycosylation inhibitors have been already shown to be functional in inhibiting other human coronaviruses, thus, expanding the potential of Miglustat for another important target for SARS-CoV-2 infection [39]. The mechanism was not clear, as it appears to have occurred at a step following binding to the receptor. The work of Clarke et al. assessed the activity of a derivative of Miglustat, UV-4, and of Celgosivir on SARS-CoV-2-infected cells and demonstrated inhibitory activity in the micromolar range, in agreement with our work [40]. These different approaches concur in demonstrating that inhibitors of glucosidases are active in infectious assays and in in vitro assays probing Spike and ACE2 proteins. How the inhibitors are actually inhibiting the virus appears to be unrelated to binding to the receptor and, instead, to a post-binding effect.

In conclusion, this work provides in vitro evidence for the repurposing of Miglustat and for the investigational drug Celgosivir as inhibitors of SARS-CoV-2. Consideration of both drugs for clinical trials for the treatment of COVID-19 patients should carefully consider dosing, adverse side effects, and, most importantly, the initiation of treatment with respect to the progress of the disease. Alternative routes of administration, such as by aerosol, could also be envisaged for the treatment of COVID-19 patients. Inhibitors of glycosidases represent a promising class of broad-range antivirals that could represent a first line option for emerging viral infections.

Supplementary Materials: The following are available online at https://www.mdpi.com/article/10.3390/v13050808/s1, Figure S1: (A) SARS-CoV-2 infectivity, (B) Immunofluorescence assay. Figure S2: Effect of Miglustat on the mean fluorescence intensity of Spike staining in Huh7 cells. Figure S3: (A) Sequence of the SARS-CoV-2 MTG synthetic RNA, (B) Quality check of SARS-CoV-2 MTG, (C)

Definition of the linear range of amplification for the different primer sets used. Figure S4: Secretion of SARS-CoV-2 Spike RBD. Table S1: Primers and probes used for RT-qPCR.

Author Contributions: Conceptualization, A.M.; methodology, A.M., N.S.; investigation, S.R., R.M.B., L.N.A., Y.K., M.P., P.M.-O., and S.P.; writing—original draft preparation, A.M.; funding acquisition, A.M. All authors have read and agreed to the published version of the manuscript.

Funding: This research was funded by ICGEB intramural funds and by generous contributions by the Beneficentia Stiftung, the SNAM Foundation, and the Generali Foundation.

Institutional Review Board Statement: Not applicable.

Informed Consent Statement: Not applicable.

Data Availability Statement: Data are available on request from the corresponding author.

Acknowledgments: We thank Bruno Bembi for helpful suggestions.

Conflicts of Interest: Patent n. 102020000008917 "Miglustat for use in the treatment of coronavirus infections" April 2020 was filed as co-inventors with the company Biovalley Srl Italy who owns the patent. The authors declare no personal financial interests derived from the publication of this work and no influence on the representation or interpretation of reported research results.

References

1. Zhou, P.; Yang, X.L.; Wang, X.G.; Hu, B.; Zhang, L.; Zhang, W.; Si, H.R.; Zhu, Y.; Li, B.; Huang, C.L.; et al. A pneumonia outbreak associated with a new coronavirus of probable bat origin. *Nature* **2020**, *579*, 270–273. [CrossRef]
2. Wu, F.; Zhao, S.; Yu, B.; Chen, Y.M.; Wang, W.; Song, Z.G.; Hu, Y.; Tao, Z.W.; Tian, J.H.; Pei, Y.Y.; et al. A new coronavirus associated with human respiratory disease in China. *Nature* **2020**, *579*, 265–269. [CrossRef] [PubMed]
3. WHO. World Health Organization-Coronavirus Disease 2019 (COVID-19). Weekly Epidemiological Update. Available online: https://www.who.int/publications/m/item/weekly-epidemiological-update-on-covid-19---23-march-2021 (accessed on 29 April 2021).
4. V'Kovski, P.; Kratzel, A.; Steiner, S.; Stalder, H.; Thiel, V. Coronavirus biology and replication: Implications for SARS-CoV-2. *Nat. Rev. Microbiol.* **2020**. [CrossRef] [PubMed]
5. Xie, M.; Chen, Q. Insight into 2019 novel coronavirus-An updated interim review and lessons from SARS-CoV and MERS-CoV. *Int. J. Infect. Dis.* **2020**, *94*, 119–124. [CrossRef] [PubMed]
6. Tay, M.Z.; Poh, C.M.; Renia, L.; MacAry, P.A.; Ng, L.F.P. The trinity of COVID-19: Immunity, inflammation and intervention. *Nat. Rev. Immunol.* **2020**. [CrossRef]
7. Sanders, J.M.; Monogue, M.L.; Jodlowski, T.Z.; Cutrell, J.B. Pharmacologic Treatments for Coronavirus Disease 2019 (COVID-19): A Review. *JAMA* **2020**. [CrossRef]
8. Liu, Z.; VanBlargan, L.A.; Bloyet, L.M.; Rothlauf, P.W.; Chen, R.E.; Stumpf, S.; Zhao, H.; Errico, J.M.; Theel, E.S.; Liebeskind, M.J.; et al. Identification of SARS-CoV-2 spike mutations that attenuate monoclonal and serum antibody neutralization. *Cell Host. Microbe* **2021**, *29*, 477–488. [CrossRef]
9. Elbein, A.D. Glycosidase inhibitors: Inhibitors of N-linked oligosaccharide processing. *FASEB J.* **1991**, *5*, 3055–3063. [CrossRef]
10. Fischl, M.A.; Resnick, L.; Coombs, R.; Kremer, A.B.; Pottage, J.C., Jr.; Fass, R.J.; Fife, K.H.; Powderly, W.G.; Collier, A.C.; Aspinall, R.L.; et al. The safety and efficacy of combination N-butyl-deoxynojirimycin (SC-48334) and zidovudine in patients with HIV-1 infection and 200-500 CD4 cells/mm3. *J. Acquir. Immune Defic. Syndr.* **1994**, *7*, 139–147.
11. Tierney, M.; Pottage, J.; Kessler, H.; Fischl, M.; Richman, D.; Merigan, T.; Powderly, W.; Smith, S.; Karim, A.; Sherman, J.; et al. The tolerability and pharmacokinetics of N-butyl-deoxynojirimycin in patients with advanced HIV disease (ACTG 100). The AIDS Clinical Trials Group (ACTG) of the National Institute of Allergy and Infectious Diseases. *J. Acquir. Immune Defic. Syndr. Hum. Retrovirol.* **1995**, *10*, 549–553. [CrossRef]
12. Dwek, R.A.; Butters, T.D.; Platt, F.M.; Zitzmann, N. Targeting glycosylation as a therapeutic approach. *Nat. Rev. Drug Discov* **2002**, *1*, 65–75. [CrossRef] [PubMed]
13. Chang, J.; Warren, T.K.; Zhao, X.; Gill, T.; Guo, F.; Wang, L.; Comunale, M.A.; Du, Y.; Alonzi, D.S.; Yu, W.; et al. Small molecule inhibitors of ER alpha-glucosidases are active against multiple hemorrhagic fever viruses. *Antiviral. Res.* **2013**, *98*, 432–440. [CrossRef] [PubMed]
14. Wu, S.F.; Lee, C.J.; Liao, C.L.; Dwek, R.A.; Zitzmann, N.; Lin, Y.L. Antiviral effects of an iminosugar derivative on flavivirus infections. *J. Virol.* **2002**, *76*, 3596–3604. [CrossRef]
15. Platt, F.M.; d'Azzo, A.; Davidson, B.L.; Neufeld, E.F.; Tifft, C.J. Lysosomal storage diseases. *Nat. Rev. Dis. Primers* **2018**, *4*, 27. [CrossRef] [PubMed]
16. Sunkara, P.S.; Taylor, D.L.; Kang, M.S.; Bowlin, T.L.; Liu, P.S.; Tyms, A.S.; Sjoerdsma, A. Anti-HIV activity of castanospermine analogues. *Lancet* **1989**, *1*, 1206. [CrossRef]

17. Taylor, D.L.; Sunkara, P.S.; Liu, P.S.; Kang, M.S.; Bowlin, T.L.; Tyms, A.S. 6-0-butanoylcastanospermine (MDL 28,574) inhibits glycoprotein processing and the growth of HIVs. *AIDS* **1991**, *5*, 693–698. [CrossRef]
18. Durantel, D. Celgosivir, an alpha-glucosidase I inhibitor for the potential treatment of HCV infection. *Curr. Opin. Investig. Drugs* **2009**, *10*, 860–870. [PubMed]
19. Low, J.G.; Sung, C.; Wijaya, L.; Wei, Y.; Rathore, A.P.S.; Watanabe, S.; Tan, B.H.; Toh, L.; Chua, L.T.; Hou, Y.; et al. Efficacy and safety of celgosivir in patients with dengue fever (CELADEN): A phase 1b, randomised, double-blind, placebo-controlled, proof-of-concept trial. *Lancet Infect. Dis.* **2014**, *14*, 706–715. [CrossRef]
20. Watanabe, S.; Chan, K.W.; Dow, G.; Ooi, E.E.; Low, J.G.; Vasudevan, S.G. Optimizing celgosivir therapy in mouse models of dengue virus infection of serotypes 1 and 2: The search for a window for potential therapeutic efficacy. *Antiviral. Res.* **2016**, *127*, 10–19. [CrossRef]
21. Sung, C.; Wei, Y.; Watanabe, S.; Lee, H.S.; Khoo, Y.M.; Fan, L.; Rathore, A.P.; Chan, K.W.; Choy, M.M.; Kamaraj, U.S.; et al. Extended Evaluation of Virological, Immunological and Pharmacokinetic Endpoints of CELADEN: A Randomized, Placebo-Controlled Trial of Celgosivir in Dengue Fever Patients. *PLoS Negl. Trop. Dis.* **2016**, *10*, e0004851. [CrossRef]
22. Milani, M.; Donalisio, M.; Milan Bonotto, R.; Scheneider, E.; Arduino, I.; Boni, F.; Lembo, D.; Marcello, A.; Mastrangelo, E. Combined in silico docking and in vitro antiviral testing for drug repurposing identified lurasidone and elbasvir as SARS-CoV-2 and HCoV-OC43 inhibitors. *BioRxiv* **2020**. [CrossRef]
23. Licastro, D.; Rajasekharan, S.; Dal Monego, S.; Segat, L.; D'Agaro, P.; Marcello, A. Isolation and Full-Length Genome Characterization of SARS-CoV-2 from COVID-19 Cases in Northern Italy. *J. Virol.* **2020**, *94*. [CrossRef] [PubMed]
24. Stadlbauer, D.; Amanat, F.; Chromikova, V.; Jiang, K.; Strohmeier, S.; Arunkumar, G.A.; Tan, J.; Bhavsar, D.; Capuano, C.; Kirkpatrick, E.; et al. SARS-CoV-2 Seroconversion in Humans: A Detailed Protocol for a Serological Assay, Antigen Production, and Test Setup. *Curr. Protoc. Microbiol.* **2020**, *57*, e100. [CrossRef] [PubMed]
25. Marcello, A.; Civra, A.; Milan Bonotto, R.; Nascimento Alves, L.; Rajasekharan, S.; Giacobone, C.; Caccia, C.; Cavalli, R.; Adami, M.; Brambilla, P.; et al. The cholesterol metabolite 27-hydroxycholesterol inhibits SARS-CoV-2 and is markedly decreased in COVID-19 patients. *Redox. Biol.* **2020**, *36*, 101682. [CrossRef]
26. ter Meulen, J.; van den Brink, E.N.; Poon, L.L.; Marissen, W.E.; Leung, C.S.; Cox, F.; Cheung, C.Y.; Bakker, A.Q.; Bogaards, J.A.; van Deventer, E.; et al. Human monoclonal antibody combination against SARS coronavirus: Synergy and coverage of escape mutants. *PLoS Med.* **2006**, *3*, e237. [CrossRef] [PubMed]
27. Tian, X.; Li, C.; Huang, A.; Xia, S.; Lu, S.; Shi, Z.; Lu, L.; Jiang, S.; Yang, Z.; Wu, Y.; et al. Potent binding of 2019 novel coronavirus spike protein by a SARS coronavirus-specific human monoclonal antibody. *Emerg. Microbes Infect.* **2020**, *9*, 382–385. [CrossRef]
28. Petris, G.; Bestagno, M.; Arnoldi, F.; Burrone, O.R. New tags for recombinant protein detection and O-glycosylation reporters. *PLoS ONE* **2014**, *9*, e96700. [CrossRef]
29. Carletti, T.; Zakaria, M.K.; Faoro, V.; Reale, L.; Kazungu, Y.; Licastro, D.; Marcello, A. Viral priming of cell intrinsic innate antiviral signaling by the unfolded protein response. *Nat. Commun.* **2019**, *10*, 3889. [CrossRef]
30. Milani, M.; Donalisio, M.; Bonotto, R.M.; Schneider, E.; Arduino, I.; Boni, F.; Lembo, D.; Marcello, A.; Mastrangelo, E. Combined in silico and in vitro approaches identified the antipsychotic drug lurasidone and the antiviral drug elbasvir as SARS-CoV2 and HCoV-OC43 inhibitors. *Antiviral. Res.* **2021**, *189*, 105055. [CrossRef]
31. Ritchie, G.; Harvey, D.J.; Feldmann, F.; Stroeher, U.; Feldmann, H.; Royle, L.; Dwek, R.A.; Rudd, P.M. Identification of N-linked carbohydrates from severe acute respiratory syndrome (SARS) spike glycoprotein. *Virology* **2010**, *399*, 257–269. [CrossRef]
32. Fukushi, M.; Yoshinaka, Y.; Matsuoka, Y.; Hatakeyama, S.; Ishizaka, Y.; Kirikae, T.; Sasazuki, T.; Miyoshi-Akiyama, T. Monitoring of S protein maturation in the endoplasmic reticulum by calnexin is important for the infectivity of severe acute respiratory syndrome coronavirus. *J. Virol.* **2012**, *86*, 11745–11753. [CrossRef] [PubMed]
33. Yuan, M.; Wu, N.C.; Zhu, X.; Lee, C.D.; So, R.T.Y.; Lv, H.; Mok, C.K.P.; Wilson, I.A. A highly conserved cryptic epitope in the receptor binding domains of SARS-CoV-2 and SARS-CoV. *Science* **2020**, *368*, 630–633. [CrossRef] [PubMed]
34. Zakaria, M.K.; Carletti, T.; Marcello, A. Cellular Targets for the Treatment of Flavivirus Infections. *Front. Cell Infect. Microbiol.* **2018**, *8*, 398. [CrossRef]
35. Williams, S.J.; Goddard-Borger, E.D. alpha-glucosidase inhibitors as host-directed antiviral agents with potential for the treatment of COVID-19. *Biochem Soc. Trans.* **2020**, *48*, 1287–1295. [CrossRef]
36. van Giersbergen, P.L.; Dingemanse, J. Influence of food intake on the pharmacokinetics of miglustat, an inhibitor of glucosylceramide synthase. *J. Clin. Pharmacol.* **2007**, *47*, 1277–1282. [CrossRef] [PubMed]
37. Nunes-Santos, C.J.; Kuehn, H.S.; Rosenzweig, S.D. N-Glycan Modification in Covid-19 Pathophysiology: In vitro Structural Changes with Limited Functional Effects. *J. Clin. Immunol.* **2021**, *41*, 335–344. [CrossRef] [PubMed]
38. Helenius, A.; Aebi, M. Intracellular functions of N-linked glycans. *Science* **2001**, *291*, 2364–2369. [CrossRef]
39. Zhao, X.; Guo, F.; Comunale, M.A.; Mehta, A.; Sehgal, M.; Jain, P.; Cuconati, A.; Lin, H.; Block, T.M.; Chang, J.; et al. Inhibition of endoplasmic reticulum-resident glucosidases impairs severe acute respiratory syndrome coronavirus and human coronavirus NL63 spike protein-mediated entry by altering the glycan processing of angiotensin I-converting enzyme 2. *Antimicrob. Agents Chemother.* **2015**, *59*, 206–216. [CrossRef] [PubMed]
40. Clarke, E.C.; Nofchissey, R.A.; Ye, C.; Bradfute, S.B. The iminosugars celgosivir, castanospermine and UV-4 inhibit SARS-CoV-2 replication. *Glycobiology* **2020**. [CrossRef] [PubMed]